

**A PHYSICALLY BASED HYDROLOGICAL
MODEL FOR CONTINUOUS SIMULATION
OF CATCHMENT RUNOFF**

By A HOLDEN

WRC NO 183 /6/93

/

**A PHYSICALLY BASED HYDROLOGICAL MODEL FOR
CONTINUOUS SIMULATION OF CATCHMENT RUNOFF**

by

A. HOLDEN

**Water Systems Research Group
University of the Witwatersrand
Johannesburg, 2000, South Africa**

**Water Systems Research Group
Report No. 6
1992**

**Report to the Water Research Commission on the Project
" Effects of Urbanisation on Catchment Water Balance"**

**Head of Department
and Project Leader : Professor D. Stephenson**

**WRC REPORT NO. 183/6/93
ISBN 1 86845 034 1
ISBN SET NO. 1 86845 040 6**

WATER RESEARCH COMMISSION

EFFECTS OF URBANIZATION ON CATCHMENT WATER BALANCE

LIST OF REPORTS

<u>Report No.</u>	<u>Title</u>	<u>By</u>
1	Analysis of effects of urbanisation on runoff	D. Stephenson
2	Description of catchments and methodology	J.J. Lambourne T. Coleman
3	Geohydrology of Catchments	W.A.J. Paling D. Stephenson
4	A hydrometeorological data management package Wits Data Management System WITDMS	J.J. Lambourne
5	The effect of storm patterns on runoff	N. Patrick
6	Runoff Modelling	A. Holden
7	Streamflow modelling	P. Kolovopoulos
8	Runoff management modelling	T. Coleman D. Stephenson
9	Catchment water balance	J.J. Lambourne F. Sutherland
10	Urban Runoff Quality & Modelling Methods	T. Coleman
11	Compendium of papers published on the research	
12	Executive Summary	D. Stephenson

ABSTRACT

This work describes the development and application of a physically-based hydrological simulation model. Pertinent issues in physically-based modelling are addressed, including catchment discretization, numerical finite difference methods, modelling of delayed flows, parameter calibration and time increment selection.

The model follows a distributed approach with finite difference methods for routing surface runoff, soil moisture seepages and streamflows. Vertical and downslope soil moisture movements are represented with a three-layer soil sub-model, with Green-Ampt infiltration. Other model components are interception, evapotranspiration and reservoir routing. Spatial variation of rainfall is accounted for by interpolating between a number of raingauges in a catchment. The model is coded on a micro computer and is intended for continuously simulating quick flows and delayed flows in rural catchments.

Finite difference methods for solving the kinematic equations were studied and different approaches compared. The Muskingum-Cunge approach was modified for improved numerical stability and shown to resolve problems of uncontrolled numerical diffusion and parasitic waves. It also allowed for an explicit solution with savings in computation time. This approach was used for the overland and channel routing algorithms in the model.

The model was based on an unusual element approach to catchment discretization, and certain advantages of this approach over other methods were demonstrated. The concept of a variable time increment for enhancing computational efficiency was explored and successfully implemented. Various improvements to standard modelling techniques were developed for the individual hydrological processes in the model, and guidelines for evaluating model parameters were assembled.

The model was applied to a number of catchments in which simulated and recorded streamflows were compared, and was used to predict the effects of land use changes in an agricultural catchment. The role of parameter calibration in physically-based modelling was evaluated and the model was used to demonstrate advantages of a physically-based approach.

TABLE OF CONTENTS

List of figures	vi
List of plates	x
List of tables	xi
List of symbols	xii
CHAPTER 1: Introduction	1
1.1 State of the art of hydrological modelling	1
1.2 Specific areas addressed by this study	4
SECTION A: MODEL DEVELOPMENT	9
CHAPTER 2: Description of simulation model	10
2.1 Catchment discretization	10
2.2 Model structure	18
2.3 Sliding time increment	22
2.4 Program structure	23
CHAPTER 3: Finite difference studies of the kinematic equations..	27
3.1 Kinematic equations	28
3.2 Finite difference formulations of the kinematic equations	32
3.3 Generalised standard formulation	33
3.4 Muskingum-Cunge formulation	54
3.5 Weighted backward difference	65
3.6 Evaluation of finite difference formulations using measured runoff data	67
3.7 Summary and conclusions	71
CHAPTER 4: Overland routing component	73
4.1 Approaches to overland routing	73
4.2 Suitability of the kinematic equations for overland flow	75
4.3 Suitability of Manning's equation for overland flow	77
4.4 Algorithm for overland routing	79
4.5 Rill study	81
4.6 Summary	88

CHAPTER 5: Channel and reservoir routing	89
5.1 Review of channel routing methods	90
5.2 Muskingum-Cunge channel routing	93
5.3 Reservoir routing	102
5.4 Summary	106
CHAPTER 6: Subsurface processes	107
6.1 Background to model development	108
6.2 Modelling approaches	116
6.3 Model development	120
6.4 Antecedent moisture conditions	133
6.5 Summary and conclusions	135
CHAPTER 7: Vegetation-related processes	137
7.1 Evapotranspiration	138
7.2 Interception	148
7.3 Summary	153
SECTION B: MODEL APPLICATIONS	155
CHAPTER 8: Waterval catchment	156
8.1 Catchment description	156
8.2 Data collection	157
8.3 Catchment discretization and input data	163
8.4 Stormflow mechanism and antecedent moisture conditions	166
8.5 Simulation results	168
8.6 Discussion of results	173
CHAPTER 9: Eccca catchment	175
9.1 General description of the Eccca basin	175
9.2 Period simulated	179
9.3 Input data	179
9.4 Simulation results	189
9.5 Comparison with other models	192
9.6 Appraisal of the Eccca study	196

CHAPTER 10: Bethlehem catchments	198
10.1 Catchment description	198
10.2 Streamflow simulation	203
10.3 Land use changes	215
10.4 Conclusions	220
CHAPTER 11: CONCLUSIONS	221
11.1 Numerical methods	222
11.2 Development of simulation model	223
11.3 Model applications	226
11.4 Developments and further research	230
REFERENCES	232

LIST OF FIGURES

2.1 Elements of the modelling process	10
2.2 Case studies using grid approach	13
2.3 Element discretization of the Severn catchment after Jayawardena and White (1979)	15
2.4 Element discretization of the Ecca in the present study	16
2.5 Relationship between discretization framework and finite difference x-increments	19
2.6 Diagrammatic representation of model structure	19
2.7 Generalised stormflow hydrograph illustrating the principle of a variable time increment in model simulations	23
2.8 Diagrammatic representation of program structure	24
2.9 Flow diagram showing computational sequence of simulation model	25
3.1 Flood waves in a channel (after Henderson, 1966)	31
3.2 Computational cell	33
3.3 Accuracy and stability of a numerical scheme for the kinematic equations (after Constantinides, 1982)	37
3.4 Overland flow plane	37
3.5 Numerical stability test with $\theta = 0$	39
3.6 Numerical stability test with $\theta = 0.5$	39
3.7 Numerical stability test with $\theta = 1.0$	39
3.8 Stable and unstable numerical solutions for $\theta = 0.5$	40
3.9 The von Neumann criterion for numerical stability, illustrated for θ values of 0, 0.5, and 1.0	42
3.10 Relationship for θ given by equation (3.13)	43
3.11 Runoff hydrographs for $\phi = 0$, $\theta = 0.5$	45
3.12 Runoff hydrographs for $\phi = 0$, $\theta = 0$	45
3.13 Runoff hydrographs for $\phi = 0.5$, $\theta = 0.5$	46
3.14 Numerical solutions for $\phi = 0.5$ showing the effect of θ on attenuation	46
3.15 Runoff hydrographs for $\phi = 1.0$, $\theta = 0$	48
3.16 Results of variable- θ formulation with $\phi = 0$	

and for a range of grid spacings	48
3.17 Effect of Δx on hydrograph shape (using $\phi = 0.5$)	50
3.18 Parasitic waves on rising hydrograph limb for $\phi = \theta = 0.5$ and a range of $\Delta x/\Delta t$	50
3.19 Algorithm for non-iterative Muskingum-Cunge formulation	60
3.20 Algorithm for iterative Muskingum-Cunge formulation	61
3.21 Hydrographs generated using the Muskingum-Cunge formulation with $\phi = 0$ and the non-iterative algorithm	63
3.22 θ -relationship of eqn.(3.13) shown as solid curves, with θ - values generated by eqn.(3.24) superimposed as discrete points	64
3.23 Computational cell defining weighting coefficient γ for the Weighted Backward Difference	65
3.24 Standard formulation with $\phi = 0$ and variable θ compared with the data of Morgali (1970)	68
3.25 Muskingum-Cunge formulation with $\Delta x = 1.37$ m compared with the runoff data of Morgali (1970)	69
3.26 Effect of spatial resolution on Muskingum-Cunge formulation ..	69
3.27 Weighted Backward Difference with $\phi = 0$	70
4.1 Subdivision of a hillslope into elements for defining Δx and W in overland flow	80
4.2 Channelisation patterns used in rill study	84
4.3 Width-factors for parallel rills	85
5.1 Branched stream network of a catchment illustrating flow routing through a system of channels and reservoirs	89
5.2 Trapezoidal channel cross-section	95
5.3 Results of flow routing exercise	101
5.4 Rating curves generated by flow routing models	101
5.5 Diagrammatic representation of a reservoir	103
5.6 Schematic reservoir cross-sections illustrating terms in the routing equation	105
6.1 Hillslope section showing paths by which water reaches the stream	108
6.2 Horton and Dunne infiltration (after Freeze, 1980)	109

6.3	Formation of a perched water table (after Kirkby, 1978)	109
6.4	Schematic illustration of the occurrence of various runoff processes in relation to their major controls (Freeze, 1980)..	111
6.5	A time-lapse view of a basin showing expansion of the source area and channel system during a storm (Kirkby, 1978)	112
6.6	Schematic representations of (a) overland flow, (b) throughflow and (c) partial area models of hillslope hydrology (Kirkby, 1978)	112
6.7	Soil water characteristic curve	115
6.8	Variation of hydraulic conductivity with moisture content	115
6.9	Diagrammatic representation of approaches to subsurface modelling	118
6.10	Three-layer soil model	121
6.11	Computational procedure of soil model	127
6.12	Hydraulic conductivity by soil texture class after Rawls <i>et al</i> (1981)	129
6.13	Hydraulic conductivity by exponent	129
6.14	Texture chart (Soil Conservation Service, 1975)	131
7.1	Curves relating evapotranspiration to leaf area index	141
7.2	Eqns. (7.1) and (7.3) for transpiration and soil evaporation respectively	143
7.3	Effect of soil moisture stress on transpiration rate (after Doorenbos and Kassam, 1979)	143
7.4	Flow diagram of evapotranspiration model	146
7.5	Sensitivity of simulated evapotranspiration losses to leaf area index	147
7.6	Form of the interception loss curve during a shower	148
7.7	Conceptual interception store	150
7.8	Sensitivity of interception equations to (a) gross rainfall rate, (b) potential evaporation and (c) interception capacity	154
8.1	Map of Waterval catchment	156
8.2	Vegetation types of Waterval	159
8.3	Soil map showing positions of soil samples and boreholes	160
8.4	Discretization of catchment for model simulations	162
8.5	Soil moisture plots	167

8.6	Simulation without interflow	170
8.7	Simulation with interflow	172
8.8	Graphical representation of time increments used in simulation	173
9.1	Location map of the Eccca catchment	176
9.2	Relief map showing instrumentation	176
9.3	Geology map showing dip and scarp slopes after Schultz (1988)	177
9.4	Recorded rainfall and runoff for period simulated (May to August 1979)	178
9.5	Discretization of catchment into segments and elements	180
9.6	Vegetation density map (Roberts, 1978)	181
9.7	Schematic diagram of a valley cross section illustrating differences between the dip and scarp slopes	184
9.8	Soil zones used in Eccca study	187
9.9	Comparison of measured and simulated streamflow hydrographs for July and August events	190
9.10	A time-lapse view of the Eccca basin showing plots of surface water generated by the model at various stages during the event on 21 July 1979	191
9.11	Comparison of present model with models Pitr and Pith	194
9.12	Comparison of present model with the Stanford Watershed Model	195
10.1	Locality map of Bethlehem catchments	199
10.2	Nested Bethlehem catchments	199
10.3	Soil types of Bethlehem catchments (Mason-Williams, 1984)	201
10.4	Land use map (after Mason-Williams, 1984)	202
10.5	Catchment discretization for model simulations	205
10.6	Model simulations for 1981/82 season (calibration data set) ..	211
10.7	Scatter diagram for simulated and observed hydrograph peaks for 1981/82 season	212
10.8	Scatter diagram of hydrograph lags for 1981/82 season	212
10.9	Total monthly flows for 1981/82 season	213

10.10 Model simulations for 1980/81 season (verification data set)	215
10.11 Effects of changes in agricultural practices on (a) volumes and (b) peak flows	218
10.12 Effects of dam capacity on streamflow	219

LIST OF PLATES

8.1 General Waterval landscape	158
8.2 Raingauge instrumentation in the catchment	161
8.3 Measuring weir viewed from upstream side	161
8.4 Gully draining segment 10	164

LIST OF TABLES

1.1	Some prominent hydrological models	2
1.2	Summary of catchment studies	8
2.1	Summary of processes modelled	21
3.1	Overland flow parameters used in numerical stability study	38
3.2	Grid spacings used in numerical stability study	38
3.3	Summary of studies on Standard formulation	52
3.4	Data of Morgali (1970)	67
3.5	Summary of finite difference studies	70
4.1	Values of k and kFr_0^2 for a range of ground slopes and roughnesses applicable to overland flow	76
4.2	Width-factors for branched channel configuration	87
5.1	Channel routing methods used in some watershed models	91
5.2	Comparison of terms in the momentum equation (after Weinmann and Laurenson, 1979)	94
6.1	Infiltration equations	117
6.2	Soil properties defined by soil group (based on data of Rawls <i>et al</i> , 1983)	132
6.3	Input parameters for the soil model	132
6.4	Antecedent moisture criteria for ILLUDAS (after Terstriep and Stall, 1974)	135
6.5	Antecedent moisture categories for the present model	135
6.6	Main features of soil model	136
8.1	Overland and vegetation data used in the Waterval study	165
8.2	Soil data used in the Waterval study	165
8.3	Rainfall intensities (mm/h) interpolated by the simulation program from the raingauge data	169
8.4	Statistics of hydrograph fit	174

9.1	Calibrated and uncalibrated model parameters	180
9.2	Evaporation data (after Gorgens, 1983)	181
9.3	Overland and vegetation parameter values	183
9.4	Trends observed from soil samples collected by Schultz (1988)..	186
9.5	Values of soil parameters used in Ecca simulation	186
9.6	Channel properties	188
9.7	Statistics of fit between observed and simulated hydrographs ..	196
10.1	Land use division of C8M12	200
10.2	Model parameters for hillslope dams	208
10.3	Model parameters for channel dams	208
10.4	Potential evaporation (mm/day)	208
10.5	Overland and vegetation parameters	208
10.6	Monthly values of LAI	208
10.7	Soil parameters for upper two soil layers	209
10.8	Soil parameters for lower soil layer	209
10.9	Channel data	209
10.10	Initial dam levels	209
10.11	Daily coefficients of efficiency and determination for 1981/82 season	210
10.12	Parameters used in catchment management simulations	217
11.1	Role of calibration in physically-based modelling	229

LIST OF SYMBOLS

A	flow cross sectional area or reservoir surface area (m^2)
b	channel width (m)
B	breadth of water surface in open channel flow (m)
B_a	average surface width in a computational cell (m)
c	local celerity (m/s)
c_a	average celerity in a computational cell (m/s)
C	canopy vegetation parameter; spillway crest coefficient ($m^{1/2}/s$)
c_p	peak celerity at equilibrium on an overland flow plane (m/s)
$C_0 - C_3$	routing coefficients in Muskingum-Cunge routing
Cr	Courant number
d	thickness of soil layer (m)
D	diffusion coefficient (m^2/s); soil diffusivity (m^2/s)
E_L	evaporation loss from interception store (mm)
E_p	potential evaporation rate (mm/day)
E_{sa}	'actual' evaporation loss from soil surface (mm/day)
E_{sp}	potential evaporation loss from soil surface (mm/h)
Fr	Froude number
f_c	infiltration capacity (mm/h)
f_o	initial infiltration rate (mm/h)
f_∞	final (steady) infiltration rate (mm/h)
F	cumulative infiltration volume (mm)
F_c	cumulative infiltration capacity (mm)
g	acceleration due to gravity (m/s^2)
G	ground cover vegetation parameter
h	pressure head in a porous medium (m); depth of saturated soil moisture flow (m); water level in a dam or reservoir (m)
h_w	wall height of a reservoir spillway or weir (m)
i	rainfall rate (mm/h, m/s)
i_e	excess rain (mm/h, m/s)
i_n	net rainfall (mm/h, m/s)
I	reservoir or channel inflow (m^3/s); intercepted water (mm)
I_c	interception capacity (mm)
I_L	cumulative interception loss (mm)
I_s	interception loss to vegetation storage (mm)
I_t	status of interception store at time t (mm)

$I_{t-\Delta t}$	status of interception store at time $(t-\Delta t)$ (mm)
k	kinematic flow number; channelisation factor; density of plant roots; hydraulic conductivity of soil (mm/h)
K	travel time in Muskingum-Cunge routing (seconds); soil conductivity in Green and Ampt infiltration equation (mm/h)
k_L	lower conductivity or deep percolation from soil (mm/h)
k_o	proportion of the land forming catch areas for hillslope dams
k_s	saturated conductivity of soil (mm/h)
L	length of an overland flow plane (m); spillway crest length (m)
LAI	leaf area index
m	exponent in rating relationship or in expression for soil permeability
n	Manning's roughness coefficient ($\text{sm}^{-1/3}$)
n_c	Manning's coefficient for channel flow ($\text{sm}^{-1/3}$)
n_o	Manning's coefficient for overland flow ($\text{sm}^{-1/3}$)
O	reservoir or channel outflow (m^3/s)
P	wetted perimeter (m)
PAM	plant available moisture
q	flow rate per unit width (m^2/s) or per unit area (m/s)
q_a	average flow in a computational cell (m^2/s)
q_i	lateral inflow rate to a channel reach per unit length (m^2/s)
q_L	lateral soil moisture flux parallel to the ground slope (m/s)
q_v	vertical soil moisture flux (m/s)
Q	flow rate (m^3/s)
Q_a	average flow rate in a computational cell (m^3/s)
Q_i	lateral inflow rate in channel or reservoir routing (m^3/s)
R	truncation error in Taylor series; hydraulic radius (m); cumulative rainfall (mm)
R_c	cumulative rainfall when interception reaches capacity (mm)
s_o	ground or bed slope (m/m)
s_f	friction (energy) slope (m/m)
S	soil sorptivity; reservoir storage (m^3)
S_{av}	average soil suction (mm)
T_a	actual transpiration rate (mm/day)
T_p	potential transpiration rate (mm/day)
t	time (seconds)
v	flow velocity (m/s)
w	width of rills (m)

W flow width (m); weighted value of a parameter
 x longitudinal distance in flow direction (m)
 y flow depth (m); direction coordinate
 z direction coordinate

α coefficient in single-valued rating relationship
 γ weighting coefficient in Weighted Backward Difference scheme
 Δt time increment (seconds)
 Δx spatial x-increment in flow direction (m)
 θ weighting coefficient in finite difference formulation of the continuity equation
 θ_f soil moisture content at field capacity
 θ_i initial soil moisture content at the onset of infiltration
 θ_r residual soil moisture content
 θ_s saturated soil moisture content
 ϕ weighting coefficient in finite difference formulation of the continuity equation
 ξ soil porosity

Chapter 1: INTRODUCTION

1.1. State of the art of hydrological modelling

Numerous computer models for hydrological simulation currently exist, with a great diversity of approaches and mathematical rigour. Surveys of current models have been presented by Overton and Meadows (1976), Viessman *et al* (1977), Haan *et al* (1982) and ASCE (1985), and some prominent models are listed in table 1.1.

Clarke (1973) and Overton and Meadows (1976) categorised models as deterministic and stochastic, depending on their probabilistic content, and as conceptual or empirical, with the former based on an understanding of the physical processes.

Models may be further classified according to their suitability for urban or rural applications or for single event or continuous simulations, as indicated in table 1.1. Secondary limiting factors may be the catchment scale, vegetation-type or climatic zone for which a model is intended. Single event models are useful for applications such as sizing flood control facilities, and continuous simulations over extended periods for synthetic streamflow generation and record patching. In continuous simulation, evapotranspiration processes and the regeneration of infiltration rates are important.

The manner in which the spatial variability of catchment parameters is accounted for determines whether a model may be classified as a lumped or distributed parameter model. Lumped models in table 1.1 treat a catchment as a single entity without subdivision into smaller zones. Distributed or semi-distributed models generally employ either sub-areas, a rectangular grid superimposed on a catchment, or elements, which are narrow strips of land parallel to the topographical contours.

Modelling approaches vary from simple empirical relations to rigorous numerical solutions of the differential equations governing surface and

Table 1.1: Some prominent hydrological models.

Model	Reference	Processes modelled								Urban/ Rural	Single event/ Continuous	Method of discretization	Modelling approach
		surface runoff	conduit routing	infiltration	subsurface flows	interception	evapotrans- piration	reservoir routing					
SWM*	Crawford & Linsley (1966)	yes	yes	yes	yes	yes	yes	yes	U/R	C	sub-areas	conceptual stores	
TR-20	Soil Conservation Service (1972)	yes	yes	yes	yes	no	no	yes	U/R	S	sub-areas	SCS curve number and unit hydrographs	
USGS	Carrigan (1973)	yes	yes	yes	yes	no	yes	no	R	S/C	lumped	time-area routing	
HYMO	Williams & Hann (1973)	yes	yes	yes	no	no	no	yes	U/R	S	sub-areas	SCS curve number and unit hydrographs	
HEC-1	U.S. Army Corps (1973)	yes	yes	yes	yes	no	no	yes	U/R	S	sub-areas	time-area theory and unit hydrographs	
ILLUDAS	Terstriep & Stall (1974)	yes	yes	yes	no	no	no	yes	U	S	sub-areas	time-area routing	
USDAHL	Holtan <i>et al</i> (1975)	yes	yes	yes	yes	no	no	no	R	C	sub-areas	empirical relationships with fitted & measurable parameters	
SSARR	Rockwood (1975)	yes	yes	yes	yes	no	yes	yes	U/R	C	sub-areas	empirical relationships with fitted parameters	
HYDROCOMP	Crawford <i>et al</i> (1976)	yes	yes	yes	yes	yes	yes	yes	U/R	C	sub-areas	based on Stanford Watershed Model	
PITMAN	Pitman (1977)	yes	yes	yes	yes	yes	yes	yes	R	S	lumped	conceptual stores	
ANSWERS	Beasley <i>et al</i> (1977)	yes	yes	yes	yes	yes	yes	no	U/R	S	grid	physically-based model using kinematic wave surface routing	
IHCM**	Eeles (1978)	yes	yes	yes	yes	yes	yes	no	R	C	lumped	conceptual stores	
RUNOFF	Jayawardena & White (1979)	yes	no	yes	yes	yes	no	no	R	S	elements	finite element solution of flow equations	
CREAMS	Knisel (1980)	yes	yes	yes	yes	no	yes	no	R	C	lumped	SCS method with physically-based soil functions	
SWMM	Huber <i>et al</i> (1982)	yes	yes	yes	no	no	no	yes	U	S/C	sub-areas	numerical solutions of flow equations	
KINE 2	Constantinides (1983)	yes	yes	yes	no	no	no	no	R	S	grid	kinematic model	
HSPF	Johanson <i>et al</i> (1984)	yes	yes	yes	yes	yes	yes	yes	U/R	C	sub-areas	derivative of Stanford Watershed Model	
ACRU	Schulze (1984)	yes	yes	yes	yes	yes	yes	no	R	C	sub-areas	SCS curve number & unit hydrographs	
IIDM***	Institute of hydrology (1984)	yes	yes	yes	yes	yes	yes	no	R	S	sub-areas	numerical solutions of surface & subsurface flow eqns	
WITWAT	Green (1984)	yes	yes	yes	no	no	no	yes	U	S	sub-areas	kinematic wave approximation for surface flows	
SHE	Abbot <i>et al</i> (1986 b)	yes	yes	yes	yes	yes	yes	no	R	S	grid	diffusion wave surface routing, 3-D subsurface eqns	
MDOR	Villeneuve <i>et al</i> (1986)	yes	yes	yes	yes	no	yes	yes	R	C	grid	automatic self-calibrating model	
WITSKM	Stephenson (1989a)	yes	yes	yes	yes	no	no	yes	U/R	S	sub-areas	kinematic wave approximation to flow eqns	
Present study		yes	yes	yes	yes	yes	yes	yes	R	S/C	elements	diffusion & kinematic wave approximations to flow eqns	

* Stanford Watershed Model

** Institute of Hydrology Conceptual Model

*** Institute of Hydrology Distributed Model

subsurface flows in one, two or three dimensions. Moisture stores representing surface runoff, interflow and ground water flow have been successfully employed in a large number of models since Crawford and Linsley's (1966) Stanford Watershed Model. Such an approach depends on calibration of input parameters against measured streamflow records, and has proved particularly useful in applications such as streamflow record patching (Middleton *et al*, 1981). The SCS method, unit hydrographs and time-area theory (isochronal techniques) have also been encoded in computer models. In recent years there has been an increasing awareness of the value of physically-based modelling in which the input parameters are measurable quantities with a physical interpretation. Numerical solutions of the kinematic equations for overland and channel flow became widely accepted in the 1970's and '80's (Ponce, 1986) following early studies by Lighthill and Whitham (1955) and Woolhiser and Liggett (1967). The use of the more rigorous diffusion wave approximation of the hydrodynamic equations has been adopted in a few models, notably the European model SHE (Abbot *et al*, 1986b). Modelling below-ground moisture conditions has progressed from the Hortonian concept of considering infiltration as a loss from the system, to modelling subsurface moisture seepages using either empirical moisture-budgeting procedures or physically-based numerical solutions of the subsurface flow equations. The recognition of the importance of source areas has resulted in many models attempting to account for their influence on streamflow generation (for example Bernier, 1985 and Beven and Kirkby, 1979).

The time increments used by models vary with the type of model and application. Short time increments of a few minutes are typically used where the dynamics of catchment response during a storm are being modelled. Daily and monthly time increment models are used for simulations over longer periods. Time increments may be user-specified as in SWMM (Huber *et al*, 1982) and WITWAT (Green, 1984), or fixed by the program as in the Pitman (1977) model.

Advancing computer technology has had an impact on hydrological modelling. Greater data handling capacities and computation speed have facilitated finer catchment discretization, more rigorous numerical solutions, and longer simulation periods. Increasing use has also been

made of micro computers for simulation programs. Green (1984) lists some advantages of micro computer models over mainframe models.

The present study describes the development and application of a physically-based hydrological simulation model. It is a distributed model using an element approach for catchment discretization, and is intended for general application to a range of rural catchment types and sizes. It is coded on a micro computer, and utilises a variable time increment controlled by the user. The model is intended for continuous simulation of catchment streamflows, but may also be used for simulating single events.

1.2. Specific areas addressed by this study

Abbot *et al* (1986a) emphasised a number of advantages of physically-based, distributed modelling: (1) the effects of land-use changes on runoff can be predicted, (2) ungauged catchments can be modelled, and (3) spatial variability of catchment inputs and outputs facilitate more detailed analysis of study areas. While these factors strongly favour this type of model, the inconclusiveness of recent model studies (Beven, 1989) indicates the necessity for ongoing research in this field. Pertinent issues are addressed by the model and its applications presented in the present study.

Many physically-based models are based on a grid approach to catchment discretization. The element approach has been less extensively used (Jayawardena and White, 1979; Bernier, 1985) although it has certain advantages such as greater flexibility in representing the physical features of a catchment, greater computing economy and reduced computational complexity. In the present study, the element approach is used in the simulation program in order to explore further its potential in hydrological modelling. Different approaches to catchment discretization are discussed in detail in chapter 2 and compared with the element approach.

The kinematic equations (kinematic wave approximation to the Saint Venant equations) are widely used for overland and channel routing in

hydrological modelling. Five of the models listed in table 1.1 utilise numerical solutions of the kinematic equations. Numerous different finite difference schemes for these equations are reported in the literature, incorporating many variants of implicit, explicit, backward and forward differences, leaving the modeller with a bewildering choice of alternatives. Previous studies comparing different schemes (Woolhiser and Liggett, 1967 and Constantinides, 1982) are limited in their application, and a rigorous and comprehensive analysis is needed. Furthermore, early studies of the writer have indicated that finite difference methods currently used for the kinematic equations may be in error (Holden and Stephenson, 1988). An in-depth study of finite difference modelling of the kinematic equations is therefore presented in chapter 3, analysing the convergence, accuracy and stability criteria of different families of schemes, and showing up inadequacies in many of the schemes commonly used. The results of this study are intended to enhance current understanding of this subject, as well as to provide a sound theoretical basis for finite difference schemes used for the various hydrological processes in the present simulation model. In particular a suitable numerical scheme is sought for overland and channel routing.

The subject of model calibration is given considerable attention in this study. Abbot *et al* (1986a) pointed out that although in principle calibration of a physically-based model should not be required, it is necessary because of inadequate representation of hydrologic processes and insufficient data. Beven (1989) argued that calibration is undesirable in physically-based models as it defeats the purpose of physically-based modelling. He pointed out that the inter-dependence of many parameters in a physically-based model makes physical reasoning difficult to apply when adjusting parameters on a trial-and-error basis, and the large number of parameters that generally characterise such models renders them unsuitable for calibration using optimisation techniques. The following questions are addressed in the present study:

1. Are good results possible without calibration of input parameters?
2. To what extent is calibration necessary in a physically-based model?
3. How does catchment scale affect calibration?

These issues are addressed in the model applications presented in chapters 8, 9 and 10.

One of the advantages of physically-based models is their suitability for evaluating the effects of land-use changes on runoff. Since the model parameters have a physical meaning, they can be adjusted to represent natural or man-made changes in vegetation, crops, erosion patterns and channel conditions. Such an exercise is carried out here on a large agricultural catchment, in which the effects of land-use and catchment management changes on streamflow are assessed.

In order to avoid unnecessary computation effort and voluminous output during continuous simulations, a larger time increment should be used during dry periods than during wet. This problem is typically overcome by switching from a small time increment during rainy periods to a larger one (such as one day) during dry periods (for example Gorgens, 1983). This is taken a step further in the present study by implementing a sliding time increment. Short time steps of the order of minutes used during intense rain may be increased somewhat on the falling limb of a hydrograph, and further increased up to a few hours for baseflows and a number of days during dry periods. In this way the time increment may be tailored to prevailing conditions, enhancing optimum model performance. A method of accomplishing this is investigated here.

The processes included in the present model are overland and channel flow routing, reservoir routing, interception, evapotranspiration, infiltration, soil moisture movements and ground water flow. Improved methods for modelling the various processes have been sought. This is reflected in the modified finite difference schemes used for overland, channel and reservoir routing; the development of a rill factor to account for the effect of rills and channelisation on overland flow; the approach to modelling soil moistures and delayed flows; the evapotranspiration sub-model assembled from the literature; and the equations for interception loss based on a dynamic store.

The model is intended to be comprehensive in the processes incorporated, and flexible in application to different climatic, topographic and vege-

tation conditions. Limitations imposed on the model are that it is intended for rural and not urban applications, and snow-melt and water quality modelling are not included. Nevertheless it could be extended to incorporate these items, and the basic principles of physically-based modelling developed here are more widely applicable.

Since physically-based modelling depends largely on measurable parameters, the quality of model output relies on well-assessed parameter values. Data evaluation has therefore been given considerable attention, with comprehensive guidelines for assessing the various input parameters, assembled from various sources.

The objectives of this study may be summarised as the development and application of a physically-based hydrological model with a view to:

- o adapting and developing the element approach for catchment discretization;
- o developing improved numerical methods for finite difference solutions of the kinematic equations;
- o developing a model capable of reproducing all the components of streamflow (quickflow as well as interflow and baseflow) in continuous simulations, and able to represent source areas and other streamflow producing mechanisms of a catchment; and
- o developing the concept of a sliding time increment.

Secondary objectives include:

- o where appropriate, developing improved methods for modelling individual hydrological or hydraulic processes;
- o investigating the role of calibration in physically-based modelling;
- o demonstrating the use of a physically-based model to evaluate land use changes on runoff; and
- o providing comprehensive guidelines for the evaluation of input parameters.

Volume 1 of this report is organised into two main parts. Section A describes the model and all the component processes, and Section B presents

the results of field applications. The three case studies dealt with in Section B are summarised in table 1.2, showing a range of catchment sizes and types. In these case studies, simulated streamflows are compared with measured flows and model performance is compared with that of other models. The Appendices (volume 2) include a user's manual, guidelines for parameter evaluation, equation derivations, catchment data and program listings.

Table 1.2: Summary of catchment studies.

Catchment	Area	Location	Climate & land use	Source of data	Features of study
Waternal	0.75 km ²	Central Transvaal	temperate grassland	Collected in the present study	Simulation of surface runoff and interflow in a multiple-peak event.
Ecca	9.1 km ²	Eastern Cape	semi-arid bushveld	HRU, Rhodes University	Continuous simulation and comparison with Pitman and Stanford Watershed Models.
Bethlehem*	83 - 372 km ²	Orange Freestate	temperate agricultural	Department of Water Affairs	Continuous simulation with studies of the affects of land use changes on runoff.

* Nested catchments

Chapter 2: DESCRIPTION OF SIMULATION MODEL

Catchment modelling may be seen as comprising two conceptual steps as illustrated in fig. 2.1. The first is the replacement of the physical catchment with a representation that preserves the important physical features and provides a framework for the model equations. This is the process of catchment discretization. The second step is the use of mathematical techniques to model the hydrological processes.

This chapter gives an overview of the simulation model developed in the present study, and reflects the elements of the modelling process identified above. Common approaches to catchment discretization are discussed and the approach used in the present study is motivated. The model structure used for accommodating the various hydrological processes is described, and the use of variable time increments and the structure of the computer program are dealt with.

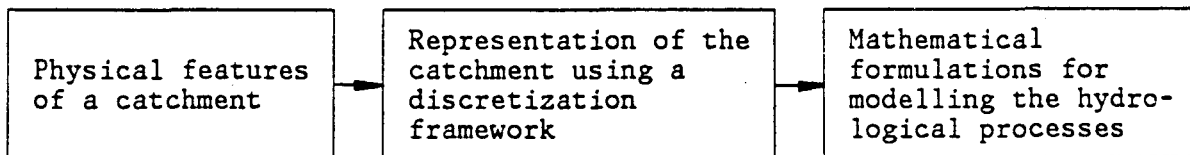


Figure 2.1: Elements of the modelling process.

2.1. CATCHMENT DISCRETIZATION

Discretization of a catchment into smaller units facilitates distributed modelling of spatially variable quantities such as soil moistures and overland flows, and enables variations in topography, land-use and soil types to be catered for. The smaller the size of the sub-units relative to the whole catchment, the finer is said to be the level of discretization (James and Robinson, 1981). Stephenson (1989b) studied the effects of using a coarse or fine level of discretization on model

calibration and output. In motivating the approach to catchment discretization adopted for the present model, common modelling approaches are discussed below.

2.1.1. Approaches to catchment discretization

(i) Sub-catchment approach

A commonly used approach in distributed or semi-distributed models is the subdivision of a catchment into a number of sub-areas or sub-catchments drained by a channel network. Input parameters are specified separately for each sub-catchment, affectively treating each sub-catchment as homogenous with respect to ground slope, land-use and soil characteristics. Stormflows are computed for each sub-catchment and then routed through the channel network to the catchment outlet. Examples of models using this approach are the urban drainage models SWMM (Huber *et al*, 1982) and WITWAT (Green, 1984), and the widely-used Stanford Watershed Model (Crawford and Linsley, 1966). These three models all utilise one-dimensional kinematic overland routing.

The sub-catchment approach has a number of shortcomings:

1. Spatial variations of quantities such as infiltration rates and soil moistures over a hillslope are not modelled unless a very fine level of discretization is used.
2. The assumption of homogeneity of slope, land-use and soil type within a sub-catchment may not be an accurate representation of reality.
3. Models using a flow-resistance equation for surface runoff require the specification of an overland flow length for each sub-catchment. This input parameter is intended to represent the average length of drainage channels or flow routes in a sub-catchment. Effectively the use of an overland flow length replaces a sub-catchment with a rectangular plane of dimensions such that one-dimensional sheet flow on the plane will produce the same runoff as that of the physical sub-catchment. Since a sub-catchment is rarely rectangular, the overland flow length can become merely a calibration parameter and not a

physical dimension, which is contrary to the purposes of physically-based modelling.

4. When finite difference methods are used to solve the surface flow equations, the use of an overland flow length leads to poor performance of the finite difference algorithms, as will be shown in chapter 3. A hillslope should be subdivided onto smaller sections for the best numerical results.
5. An assumption sometimes made in models that follow the sub-catchment approach, is that surface runoff from each sub-catchment is assumed to enter the drainage channel at a node, whereas lateral inflow into streams is more realistic in many cases.

Undeniably, models using the sub-catchment approach have been shown to produce good results when calibrated against observed runoff hydrographs, despite the above factors. However, the increasing use of methods such as the grid approach in distributed models indicates a trend towards a finer level of discretization in pursuit of improved modelling techniques.

(ii) Grid approach

Models following this approach utilise a rectangular grid superimposed on a catchment. Examples are KINE2 (Constantinides, 1982), SHE (Abbot *et al*, 1986 a, b) and ANSWERS (Beasley *et al*, 1977). Sample applications of grid models to two catchments are shown in fig. 2.2. In models such as KINE2 and SHE, the grid constitutes a finite difference grid for two-dimensional overland routing, using either kinematic routing as in KINE2 or diffusion routing as in SHE. The ANSWERS model treats each cell in the rectangular grid as having an average slope and slope direction, and uses one-dimensional kinematic routing to route overland flow from one cell to the next.

The grid approach can be a powerful technique for two-dimensional routing of overland flow. However, unless a very fine grid is used, topography and rivers can be poorly detailed. For example the crest of a hill may lie in the middle of a grid cell, not conveniently on the boundary between two cells. Similarly a stream or a river may lie right across a cell,

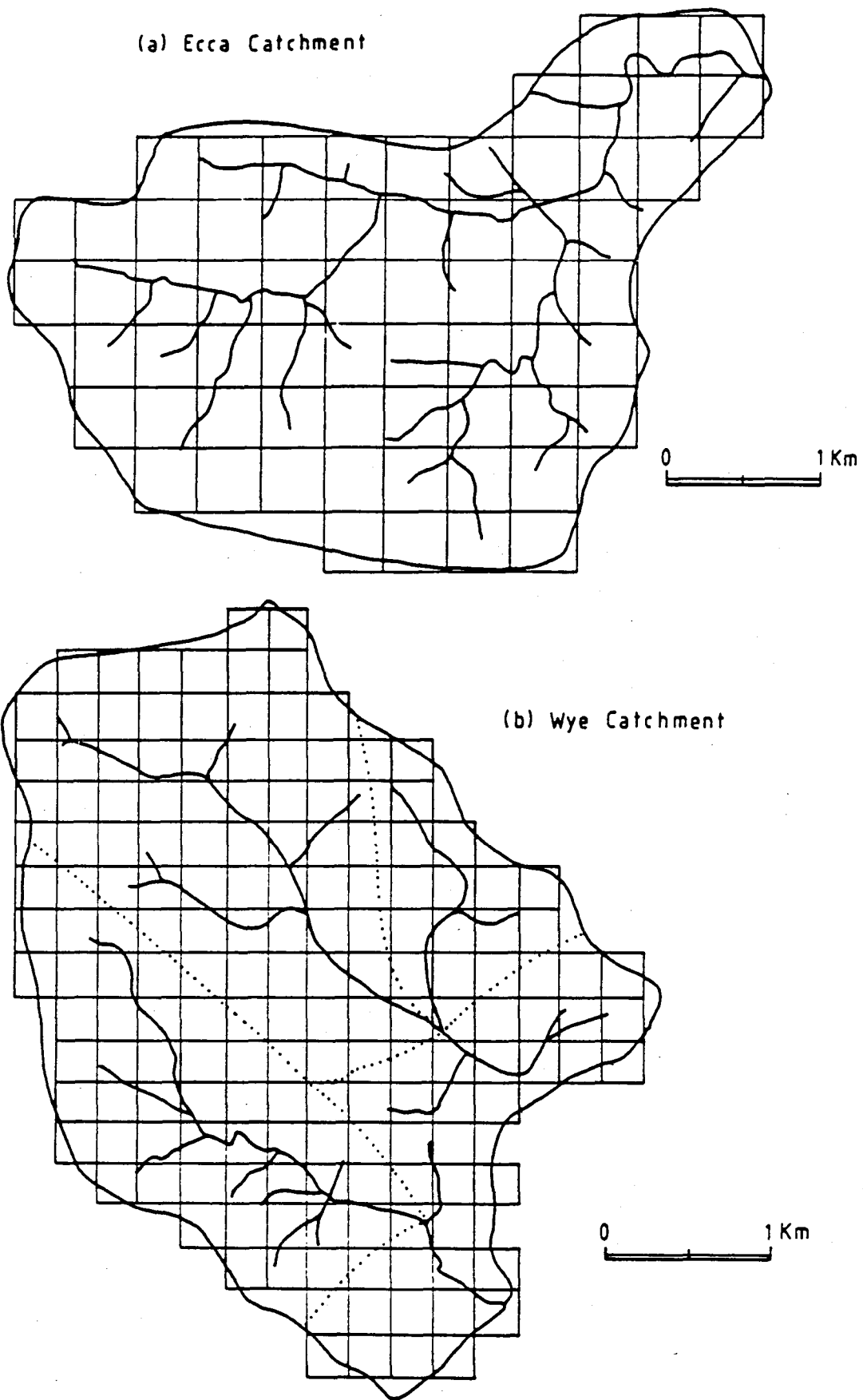


Figure 2.2: Case studies using the grid approach.

(a) ANSWERS model applied to Ecca catchment, Eastern Cape (Schultz, 1988).

(b) SHE model applied to the Wye, United Kingdom (Bathurst, 1986).

confusing slopes and slope direction. These problems are evident in the examples in fig. 2.2. A fine grid would overcome these problems, but at the expense of greatly increased computation time. Also, if a fine grid was used it could be argued that a fine computational mesh may be incompatible with the relatively coarse level of detail of available soil, vegetation and rainfall data.

Notwithstanding these drawbacks, the grid approach can be an effective tool in runoff models because of its versatility and its distributed nature, as evidenced by the number of leading models that successfully employ this approach.

(iii) Element approach

This approach is illustrated in fig. 2.3. Assuming flow to be normal to the topographical contours, a catchment is divided into segments with boundaries along convenient flow lines. Each segment is further divided into a number of elements parallel to the topographical contours and to the stream at the bottom of the hillslope, and one-dimensional flow routing is used down each hillslope. The dimension normal to the assumed flow direction is accounted for by the variable width of a segment. This approach has been used in the models VSAS2 (Bernier, 1985) and RUNOFF1 (Jayawardena and White, 1979). The Variable Source Area Simulator VSAS2 uses a finite difference solution for routing flows down each hillslope, and RUNOFF1 uses finite element techniques for solving the surface and subsurface flow equations.

The element approach uses a simplified one-dimensional solution to represent a complex two-dimensional problem. The use of one-dimensional equations for overland and subsurface flows is naturally less complex than a two-dimensional solution, which can be a computational advantage provided accuracy and versatility are not sacrificed. According to Jayawardena and White (1979), the one-dimensional element solution "can give quite meaningful information about general (catchment) behaviour with only a reasonably modest effort." However, the large number of elements previously used in this approach as shown in fig. 2.3 would have to be reduced for the full computational advantages to be utilised. An-

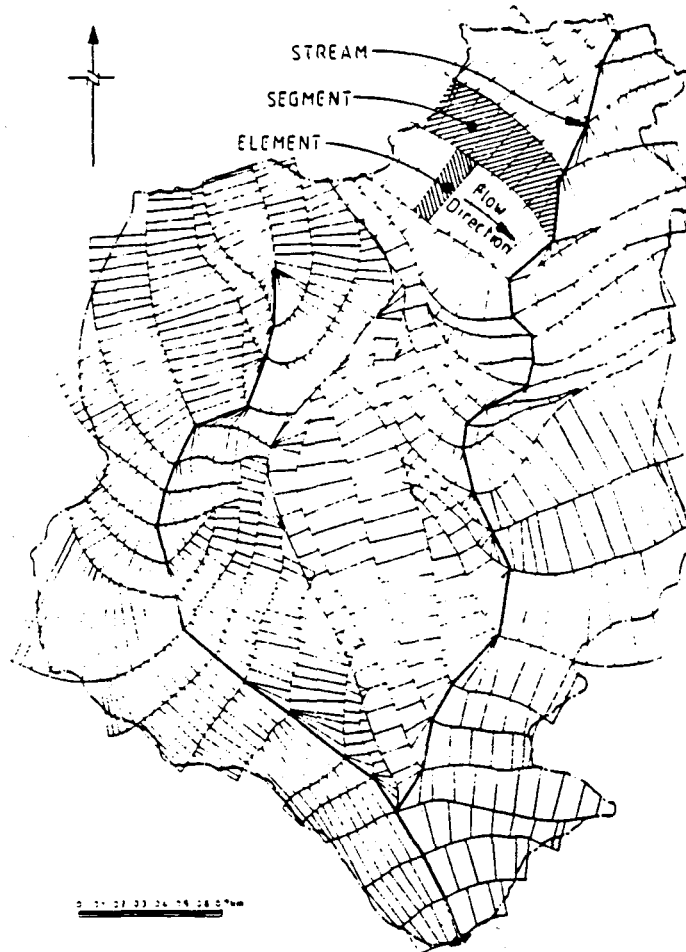


Figure 2.3: Element discretization of the Severn catchment, after Jayawardena and White (1979).

other possible drawback of this method is the effort involved in setting up the element network and entering information on slopes, areas and dimensions for all the elements into a computer data file.

2.1.2. Catchment discretization in the present study

The catchment discretization adopted for the present simulation model is based on the element approach described above. A number of advantages of this approach may be illustrated by comparing an element discretization of the Ecca catchment shown in fig. 2.4 with the grid approach on the same catchment in fig. 2.2(a):

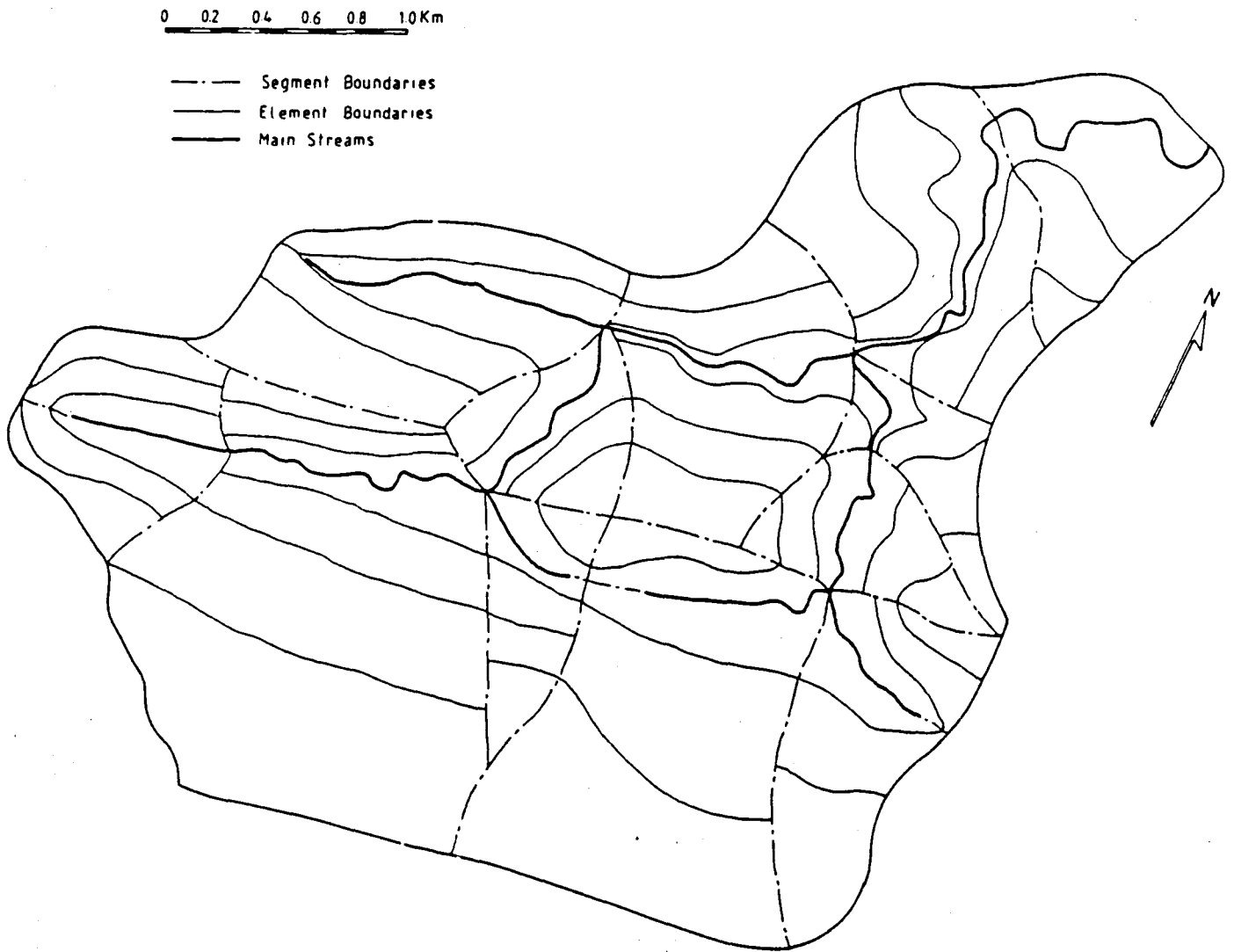


Figure 2.4: Element discretization of the Ecca in the present study.

1. In the element approach, the shape and size of the elements can be tailored to fit in with topography, the watershed shape and the lie of rivers and streams. The grid approach necessitates a linear or zig-zag approximation of these features.
2. The size of elements can be varied for optimum computing economy. Regions of rapidly changing topography or variable source areas can be represented with small elements, while in other areas the element size can be increased considerably. The grid approach does not have this flexibility because the grid is uniform over the catchment.

3. The element discretization of the Ecca shown in fig. 2.4 has 69 elements, and the grid discretization in fig. 2.2(a) has 66 grid cells - a similar number of cells or elements and therefore a similar level of discretization. However, comparison of these two studies shows a better representation of topographic and stream details by the element approach. For the grid study to represent the catchment details with the same resolution, at least twice the number of cells used in fig. 2.2(a) would be required. Thus for the same number of elements or cells, the element approach facilitates a better representation of a catchment than the grid approach; or conversely, fewer elements are required in the element approach for the same effectiveness of discretization. This has obvious advantages in terms of computation time and computer storage requirements.

Other advantages of the element approach are:

- o Each element has its own width and flow length, obviating the need for an overland flow length and average width as in the sub-catchment approach.
- o The local value of ground slope is used in each element, which is a better representation of reality than an average subcatchment slope.
- o Lateral inflow to streams is easily catered for.
- o The division of a hillslope into elements is ideal for modelling interflow, spatially variable soil moistures and dynamic source areas.
- o Subdivision of a hillslope into elements facilitates optimum functioning of the finite difference methods, as will be shown in chapter 3.

Another reason for using the element approach in the present study is that the grid approach has been well explored and utilised elsewhere, whereas the element approach has limited application in the literature. Research using the element approach can therefore be valuable in exploring its potential in hydrological modelling.

The practical problems associated with using a large number of small elements are overcome in the present study by increasing the size of the

individual elements, as can be seen by comparing figs. 2.3 and 2.4. Furthermore the large amount of effort in setting up the elements is streamlined by employing digitised entry of element data in the simulation program.

2.2. MODEL STRUCTURE

Flows in streams, over land and through the soil are governed by the continuity equation for one-dimensional flow, which can be written

$$\frac{\partial Q}{\partial x} + \frac{\partial A}{\partial t} = q_i \quad (2.1)$$

where Q is flow rate, A is cross-sectional area of flow, x is distance in the flow direction, t is time and q_i is an inflow term. In the finite difference formulations of this equation, ∂t becomes Δt , the time increment of the model, and ∂x becomes Δx , the spatial increment in the flow direction. Fig. 2.5 shows how the finite difference formulations are related to the discretization framework of elements. When applying the model to a catchment, individual channel reaches are defined by nodes in the stream network. The length of each channel reach between two nodes corresponds to the spatial increment Δx in the finite difference formulation for channel routing. The element flow length Δx is used in the finite difference formulations for overland and subsurface flow routing. The channel and element flow lengths shown in fig. 2.5 provide the link between the second and third blocks in fig. 2.1, i.e. the relationship between the discretization framework and the mathematical formulations.

Fig. 2.6 represents diagrammatically the model structure and segment connectivity. Each segment may have up to 5 elements, and may flow to another segment, a reach or a node. Flow to a channel reach constitutes lateral inflow along the length of the reach, and flow to a node is useful at the head of streams.

The cut-away portion in fig. 2.6 illustrates the processes modelled in each element. Incident rainfall is passed through an interception store, and the net rain after interception abstractions is added to the ponded water. This water is available for infiltration and surface runoff.

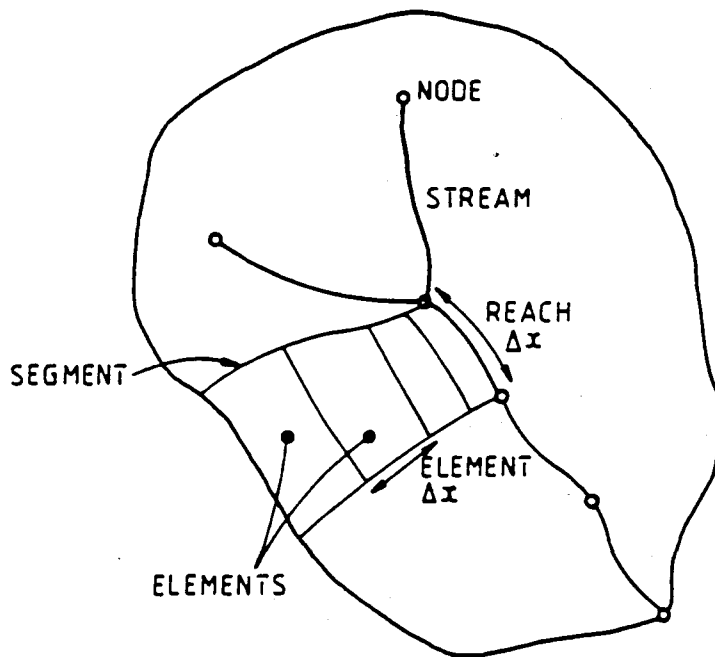


Figure 2.5: Relationship between discretization framework and finite difference x-increments.

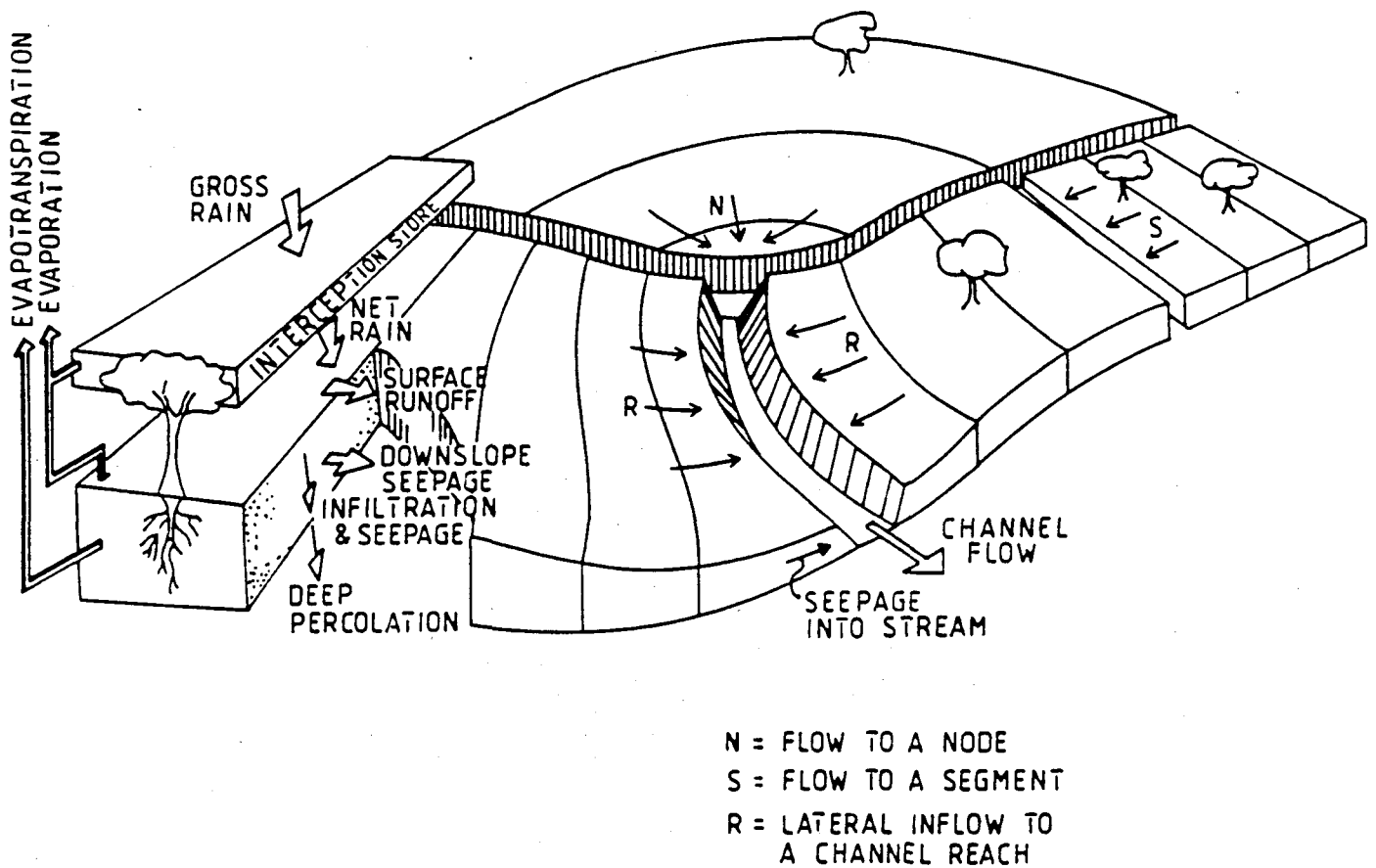


Figure 2.6: Diagrammatic representation of model structure.

Overland flow is routed from one element to the next towards the stream. Infiltrating water constitutes input for the soil sub-model, which represents the subsurface environment by means of three soil layers. The upper two layers have variable moisture contents and the lowest layer accommodates ground water or a perched water table. Moisture in each soil layer is subject to both vertical and downslope seepage. Vertical seepage determines the soil moisture distribution in the soil profile, and downslope seepage is routed from one element to the next. The lowest element in a hillslope seeps into the stream. Evaporation occurs from the interception store and from the soil surface, and evapotranspiration losses from the soil are determined by the vegetation leaf area and the root density in each soil layer. Stream flows are routed down the channel network, and flows may be routed through a dam or reservoir at any node. Spatial variation of rainfall is accounted for by using a number of raingauges in a catchment and interpolating between them at each time step during a simulation, using the method of Patrick (1988).

The hydrological processes are dealt with individually in the chapters following this one. The modelling approach and input parameters for each process are summarised in table 2.1 together with the parameter symbols generally used in the text.

Topographical data and element boundaries are entered by means of a digitiser. Ground slopes, element widths, areas and Δx 's are all inferred from the digitised data. This facilitates screen graphics and also reduces the effort involved in data entry, rendering the element approach more practical. Model parameters are specified separately either for each segment or each element.

Table 2.1: Summary of processes modelled.

Process	Computation method	Input parameters
Overland routing (chapter 4)	One-dimensional, Muskingum-Cunge finite difference solution of the kinematic equations.	Manning's coefficient (n) Channelisation factor (k) Connectivity: segment, node or channel collecting outflow Element Δx , width, plan area and ground slope (digitised data)
Channel flow (chapter 5)	Muskingum-Cunge routing with provision for looped or single-valued rating relationships.	Manning's coefficient (n) Bed slope (s_b) Channel width (b) Bank-slope Connectivity: inflow and outflow nodes
Infiltration & soil model (chapter 6)	Green & Ampt infil. with vertical & horizontal soil moisture seepage in a 3-layer soil model.	Soil depth and thickness of soil layers Soil texture/group* Saturated conductivity (k_s) Deep percolation (k_L)
Evapo-transpiration (chapter 7)	Soil evaporation & plant transpiration based on leaf area index.	Monthly or daily potential evaporation Leaf area index (LAI) Root distribution in soil layers
Interception (chapter 7)	Dynamic interception store.	Interception capacity (I_c)
Reservoir routing (chapter 5)	Modified Storage-indication approach	Crest coefficient Storage/stage relationship Position in channel network
Spatial rainfall	Interpolation between raingauges.	Digitised coordinates of each raingauge Digitised coordinates of centroid of each segment Rainfall data in raingauge files

* The soil group determines the values of saturated moisture content (θ_s), residual moisture content (θ_r), field capacity (θ_f) and soil suction (S_{av}).

2.3. SLIDING TIME INCREMENT

A constant time increment is usually used in hydrological simulation models, either user-specified or fixed, for example hourly, daily or monthly models. Some continuous simulation models use a small time increment during rainy periods and switch to a larger time increment for dry periods and recession flows. An example of this dual time increment system is the Pitman suite used by Gorgens (1983) with hourly time increments during flood events and daily time increments during dry periods.

For the modelling methodologies used in the present study, small time increments are required during a storm in order to model the rapidly changing infiltration rates and surface water conditions. Typically a time increment of 5 to 15 minutes is required for small and medium sized catchments, although this can be relaxed somewhat during periods of light rain. On the recession limb of a hydrograph, progressively larger time increments can be used as the flow recedes. Short-term interflow responds more slowly than surface runoff and can be modelled using time increments of the order of a few hours. Ground water flows have an even slower response, and daily time increments may be appropriate for the days following a storm. During long dry periods the time increment can be increased to a few days or a week for computing soil evapotranspiration losses, small water table fluctuations and low baseflows. This variation of time increment with hydrograph shape is illustrated in fig. 2.7.

The use of a variable time increment in a continuous simulation model would have substantial benefits both in terms of computation efficiency and modelling accuracy, and would be preferable to a rigid dual time increment system. The present model has been structured for a sliding time increment that can vary according to catchment response and be tailored by the user to factors such as catchment size, rainfall conditions and the required resolution of model output. After experimenting unsuccessfully with various methods by which the program selects appropriate time increments as a simulation proceeds, the approach finally adopted was to use a user-specified set of time increments covering the full duration of the simulation and stored in a file dedicated to this purpose. The time increment file is set up by the user before commencing a simulation,

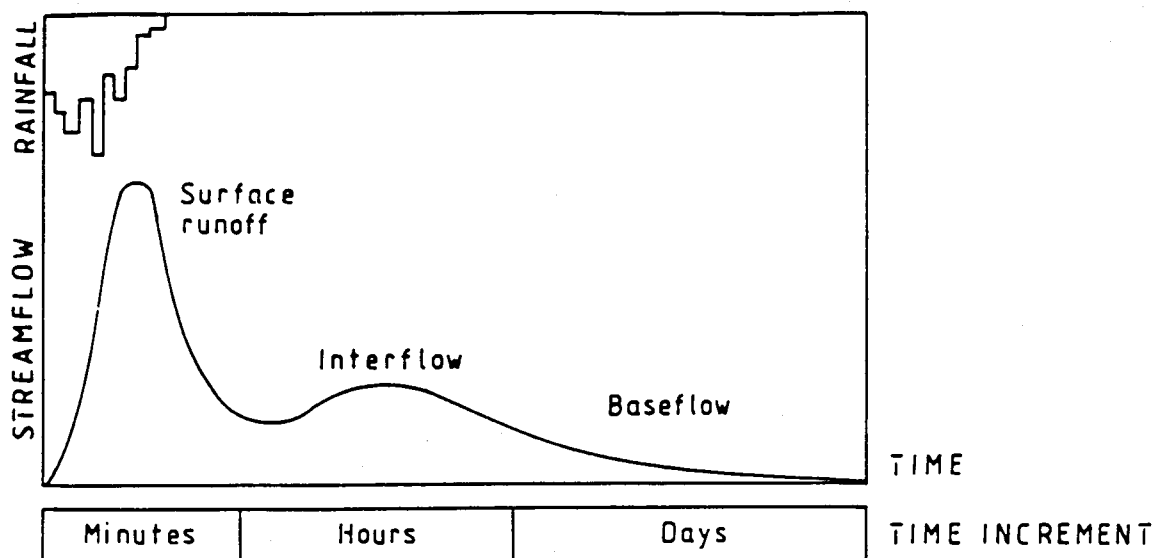


Figure 2.7: Generalised stormflow hydrograph illustrating the principle of a variable time increment in model simulations.

and specifies the time increments to be used at every stage during the simulation. This file is read by the program together with the rainfall files at the beginning of each time step. Setting up this file necessitates consulting the rainfall record and (if available) the flow record for the period under consideration. Expertise in setting up time increment files was found to improve with experience, and the time increments used in different case studies are given in Part B.

2.4. PROGRAM STRUCTURE

The computer program developed in this study incorporates the simulation model as well as routines for handling data and presentation of output. The overall structure of the program is illustrated in fig. 2.8. The user can pass between two environments. The data processing environment facilitates loading, storing, creating and editing data files; editing or processing raingauge and time increment files; and plotting hydrographs from the simulation output files. The simulation environment is for running and monitoring simulations. In both environments, specific tasks are performed by subprograms while a main controlling program controls the loading of subprograms into computer memory and the flow of variables.

The program is coded on a Hewlett-Packard 9816 micro computer and the whole system constitutes a total of 350 kilobytes of coding. The matrices and variables occupy a further 152 kilobytes of memory. The coding is listed in Appendix F.

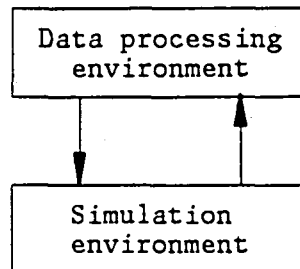


Figure 2.8: Diagrammatic representation of program structure.

The computational procedure of the simulation model is shown in fig. 2.9. Each hydrological process is treated as a sub-model. At the beginning of each time step, the length of the next time increment is read from the time increment file and used to update the current date and time which are displayed as computation proceeds. The amount of rain falling in this time increment is then read from each raingauge file and converted into an intensity. The rainfall interpolation procedure assigns a weighted rainfall intensity to each segment. Interception losses are abstracted, and the infiltration, soil moistures, subsurface seepages and surface runoffs are computed for each element. Connectivity matrices determine the sequence of computations such that computation always proceeds down-slope to ensure that the upstream flow conditions are known for each element. Computation then proceeds downstream through the channel network towards the outlet. Channel flows at the outlet are stored in output files together with the current date and time before proceeding to the next time step.

Primary output consists of simulated flow records which can be accessed at any date and time for plotting hydrographs. Secondary output includes maps of soil moisture and surface water which may be plotted at any stage during a simulation.

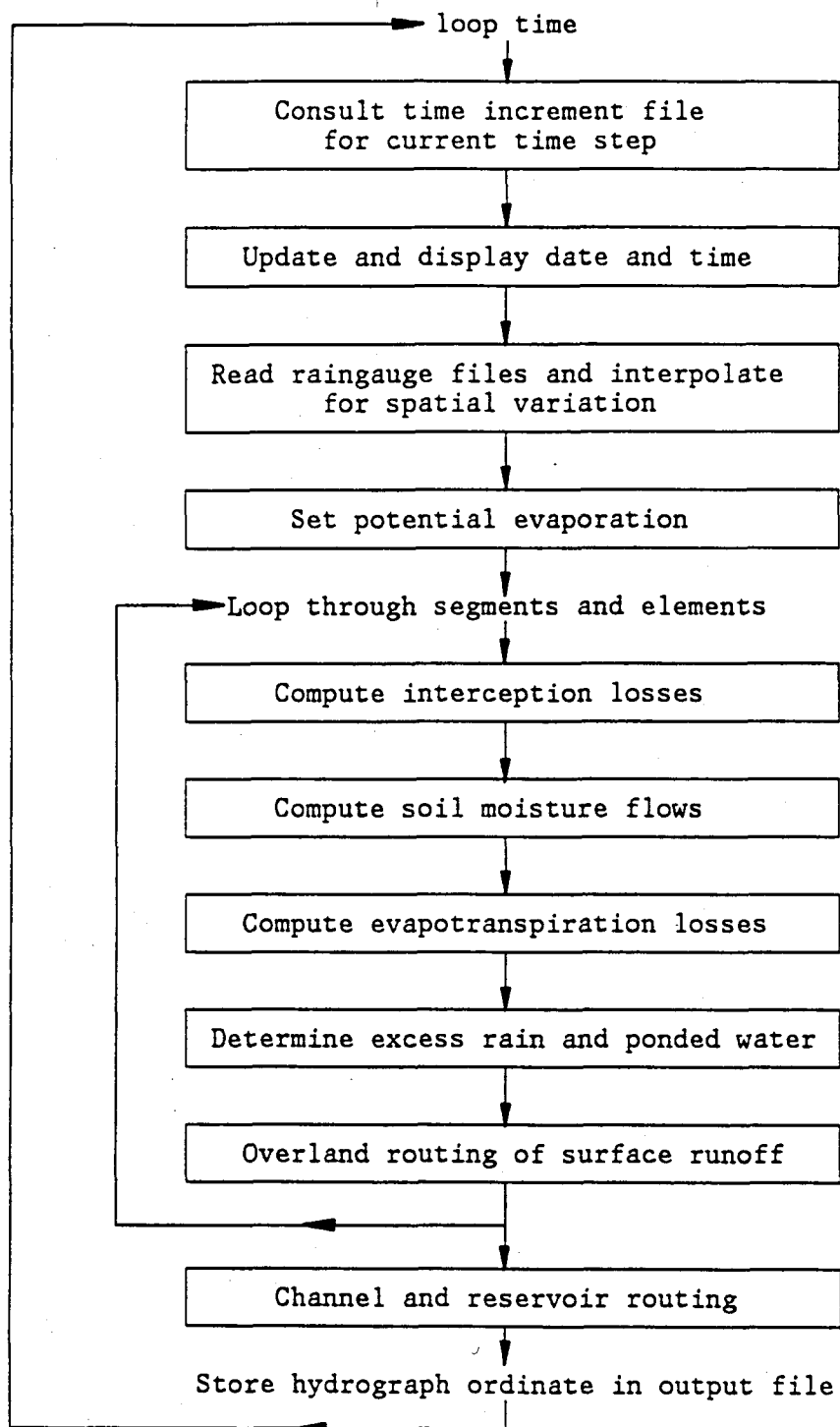


Figure 2.9: Flow diagram showing computational sequence of simulation model.

The rainfall data for the raingauges used in a study is stored in separate files on disk. The format of these files accommodates break-point as well as fixed time increment rainfall data (such as hourly or daily rainfall), and the time increments used in the simulation are independent of those in which the data is stored. The format of the raingauge, time increment and output files was devised for optimum storage efficiency and is described in Appendix E.

Detailed guidelines on the use of the program are given in the user's manual in Appendix A. The theoretical development of the modelling procedures for each hydrological process is presented in the chapters following this one.

Chapter 3: FINITE DIFFERENCE STUDIES OF THE KINEMATIC EQUATIONS

Finite differences are used extensively in the present simulation model to solve the differential equations governing various physical processes. In particular, the kinematic equations are used in finite difference formulations for overland and channel routing. Many finite difference formulations for the kinematic equations are reported in the literature, but there is no unified treatment of the subject showing how specific formulations are related and how their properties can be predicted and explained. There is a need for a lucid explanation of the accuracy and stability characteristics of different schemes or families of schemes.

Presented here is a study of various approaches to finite difference solutions of the kinematic equations, using algorithms for overland routing to illustrate their behaviour and properties. Although of particular relevance to overland flow, the principles developed in this chapter are also of relevance to other finite difference applications presented later in this work, such as the selection and development of a suitable finite difference formulation for channel routing, and ensuring numerical stability in reservoir routing and soil moisture seepages.

3.1. KINEMATIC EQUATIONS

3.1.1. Kinematic approximation to hydrodynamic equations

The Saint Venant (full hydrodynamic) equations for one-dimensional flow consist of the continuity and momentum equations, which are derived in Appendix B. The continuity equation describes conservation of mass, and for overland flow it can be written:

$$\frac{\partial q}{\partial x} + \frac{\partial y}{\partial t} = i_e \quad (3.1)$$

with q = flow rate per unit width [L^2T^{-1}]
 y = flow depth [L]
 x = longitudinal distance in flow direction [L]
 t = time [T]
 i_e = excess rain [LT^{-1}]

The momentum equation, expressing conservation of momentum, has the following form for a rectangular channel and for overland flow:

$$s_f = s_o - \frac{\partial y}{\partial x} - \frac{v}{g} \frac{\partial v}{\partial x} - \frac{1}{g} \frac{\partial v}{\partial t} \quad (3.2)$$

where s_f = energy (friction) slope [L/L]
 s_o = bed slope [L/L]
 v = depth-averaged velocity [LT^{-1}]
 g = acceleration due to gravity [L^2T^{-1}]

Eqn.(3.2) represents non-uniform, unsteady flow. Omitting smaller order terms (as will be discussed in more detail in chapters 4 and 5 on overland and channel routing) gives the relationship $s_f \approx s_o$, which is the kinematic approximation. This will be shown in chapter 4 to be a good approximation for overland routing. It implies the use of a single-valued rating relationship or friction equation which for overland flow has the general form:

$$q = \alpha y^m \quad (3.3)$$

in which y represents the flow depth and α and m are constants. For Manning's equation, $\alpha = s_0^{1/2}/n$ where n is Manning's roughness coefficient, and $m = 5/3$. Eqn.(3.3) also represents a general equation for other flow problems. For saturated Darcian flow through soil parallel to the ground surface, α is the product of the soil permeability and the ground slope, and $m = 1.0$. For flow over a weir, α is the crest coefficient and $m = 3/2$.

Eqns.(3.1) and (3.3) constitute the kinematic equations for overland flow. Analytical solutions are limited to particular geometries, rainfall patterns and initial and boundary conditions, and so the use of numerical finite difference solutions is generally resorted to in hydrological simulation models. This constitutes a physically-based modelling approach which is flexible in the geometry and rainfall input that can be modelled. Before discussing finite difference schemes for the kinematic equations, we will take a brief look at the kinematic flow behaviour that is implied by the kinematic approximation.

3.1.2. Kinematic behaviour

The following terms are defined for the sake of clarity:

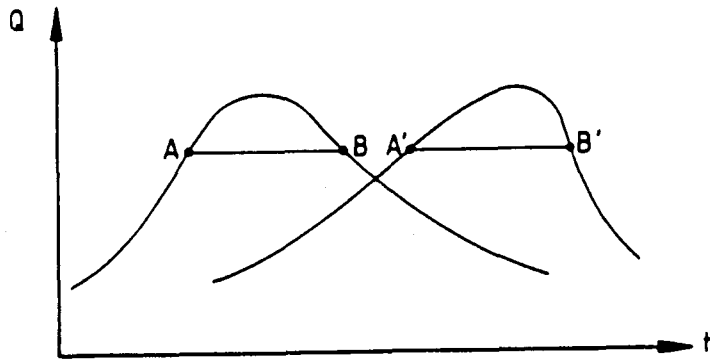
- o *Waves* are of two kinds. A *flood wave* describes the progress of a flood as it travels down a catchment or through a channel reach. Small surface disturbances are also referred to as waves, propagating upstream and downstream at characteristic speeds known as *wave celerity*. These wavelets transmit information regarding flow conditions upstream or downstream of a particular point.
- o *Subsidence, attenuation and diffusion* all refer to the reduction in peak of a flood wave as it travels down a catchment or channel reach. *Physical diffusion* is the natural process by which this phenomenon occurs and it is caused by storage. *Numerical diffusion* is an artificial attenuation of a flood wave by virtue of the finite difference scheme used to model the routing equations. Unless measures are taken to match the numerical diffusion of the finite difference scheme to

the physical diffusion, they will be unrelated and the numerical diffusion is said to be *uncontrolled*.

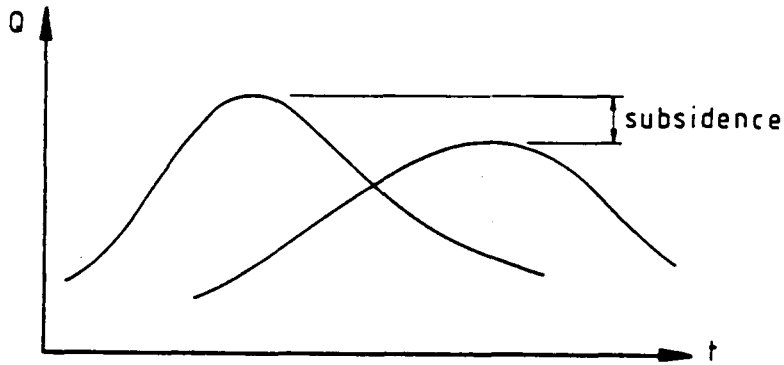
- o *Dispersion* is a lateral spreading of a hydrograph as a flood wave proceeds down a catchment or a channel reach.

It is implicit in kinematic theory that a flood wave modelled by the kinematic equations exhibits no diffusion or dispersion. This has been shown mathematically by Henderson (1966) and Stephenson and Meadows (1986). Kinematic behaviour or a kinematic wave describes a flood wave that does not attenuate and is therefore perfectly modelled by kinematic theory. The difference between kinematic and non-kinematic waves is illustrated in fig. 3.1 (after Henderson, 1966). It is illustrated here by considering a flood wave passing down a channel, since a visible flood wave is not so obvious in overland flow (Constantinides, 1982). The first curve in fig. 3.1(a) represents a hydrograph at some point in a channel reach, and the second curve is the hydrograph at a point downstream of the first. It exhibits no subsidence and hence is purely kinematic. There is also no dispersion which would be seen as an increase in the length of the cord AB. Thus a kinematic wave only undergoes a shift in time and a change of shape, which can be seen in fig. 3.1(a) as a steepening of the downstream face. Fig. 3.1(b) shows a non-kinematic wave in which attenuation and dispersion of the hydrograph are clearly evident.

Since real flows do exhibit attenuation, the kinematic approximation should be used with caution. It can be shown (chapter 4) that the kinematic approximation generally holds for overland flow, and it is therefore commonly used for overland routing with substantial advantages gained in terms of reduced computational complexity. The kinematic equations may also be used for channel routing as a refinement of time shift routing, or with a modification to incorporate attenuation. Overland routing will be used in this chapter in the studies of finite difference formulations of the kinematic equations.



(a) Kinematic waves



(b) Non-kinematic waves

Figure 3.1: Flood waves in a channel (after Henderson, 1966).

3.2. FINITE DIFFERENCE FORMULATIONS OF THE KINEMATIC EQUATIONS

The kinematic equations can be solved numerically using four approaches (Constantinides, 1982):

- finite elements
- method of characteristics
- explicit finite differences
- implicit finite differences

Finite element solutions are not generally used for the kinematic equations since, according to Constantinides (1982), computation can be excessive and accuracy and stability criteria can become tedious to apply. The characteristic method is hard to apply in hydrological models because of the changing x-t grid, and is not suitable for the present application in which Δx is pre-determined by the catchment discretization. The discussion here is therefore directed at explicit and implicit finite difference methods.

Woolhiser and Liggett (1967) compared a number of explicit and implicit finite difference schemes for the kinematic equations. Constantinides (1982) compared various explicit schemes on the basis of stability and accuracy by comparing them with the analytical solution for overland flow on a sloping rectangular plain.

This present study considers three categories of finite difference schemes:

- (1) Generalised Standard formulation (Preissmann "box" scheme)
- (2) Muskingum-Cunge formulation
- (3) Weighted Backward Difference

Many of the traditional finite difference approaches are incorporated in the first category by using a generalised Preissmann scheme. The interaction between the temporal and spatial weighting coefficients (θ and ϕ) and $\Delta x/\Delta t$ is studied with respect to accuracy and numerical stability. The Muskingum-Cunge formulation is introduced as the second category, and finally the Weighted Backward Difference scheme that breaks away from the

Preissmann box. Each category is dealt with separately and then measured overland flow data is used to compare and evaluate their accuracy.

3.3. GENERALISED STANDARD FORMULATION

3.3.1. Preissmann box

Preissmann (1961) suggested a scheme for the hydrodynamic equations in which eqn. (3.1) is expressed in finite differences as:

$$\frac{\phi(q_3 - q_1) + (1 - \phi)(q_4 - q_2)}{\Delta x} + \frac{\theta(y_2 - y_1) + (1 - \theta)(y_4 - y_3)}{\Delta t} = i_e \quad (3.4)$$

ϕ and θ are weighting coefficients defined in fig. 3.2, with numerical values between 0 and 1.0. Fig. 3.2 represents a "computational cell" on the x-t grid. For simplicity, subscripts 1, 2, 3 and 4 are used to represent the conditions at the corners of the computational cell. With this notation q_1 is the flow at $(x - \Delta x, t - \Delta t)$, q_2 at $(x - \Delta x, t)$, etc.

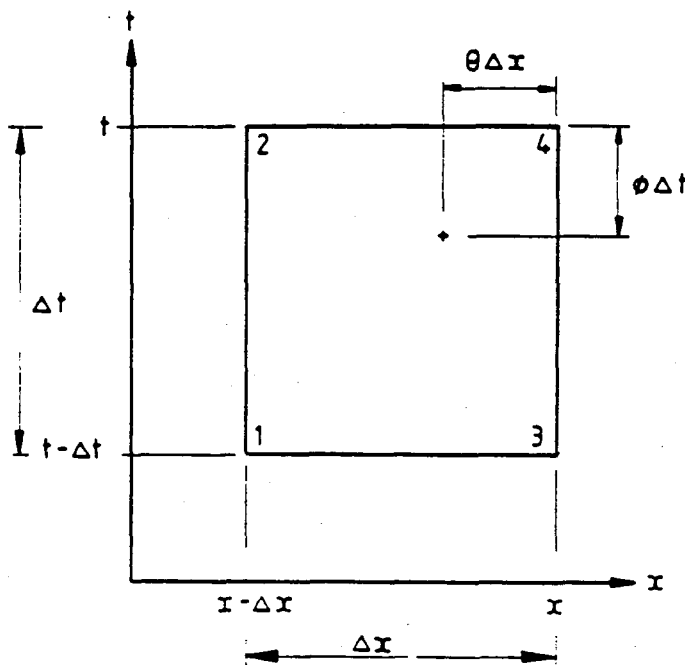


Figure 3.2: Computational cell

Eqn. (3.4) is a useful generalised treatment because it encompasses many schemes that are used for the kinematic equations. For example if $\theta = 0$, eqn. (3.4) reduces to a backward difference, and $\theta = 1.0$ to a forward difference. Some sources promote the use of a backward difference ($\theta = 0$) arguing that the kinematic equations imply information propagation in the flow direction only (Constantinides, 1982). An explicit formulation corresponds to $\phi = 1.0$ in eqn. (3.4), while lower values of ϕ result in an implicit formulation. $\phi = 0$ and 0.5 are common choices for implicit schemes. If θ and ϕ are both equal to 0.5 then eqn. (3.4) becomes a central difference. Some of the well-established schemes can be expressed as special cases of the Preissmann scheme. For example the leap-frog scheme is a central difference scheme similar to a Preissmann box with $\theta = \phi = 0.5$. Similarly the Crank-Nicholson scheme reduces to a Preissmann scheme with $\theta = 0.5$ and ϕ left variable, if the Δx in the Preissmann equivalent is set at twice the Δx in the Crank-Nicholson scheme.

A means of solving the Preissmann scheme is now developed, as it will be used extensively in this chapter. Solving equation (3.4) for y_4 gives the following equation:

$$(1-\theta)y_4 = i_e \Delta t + y_3(1-\theta) + \theta(y_1 - y_2) - [\phi(q_3 - q_1) + (1-\phi)(q_4 - q_2)]\Delta t/\Delta x \quad (3.5)$$

Expressing flow rate q in terms of depth y by using eqn. (3.3), and writing eqn. (3.5) as a function of y_4 denoted $f(y_4)$, we obtain:

$$f(y_4) = i_e \Delta t + (1-\theta)(y_3 - y_4) + \theta(y_1 - y_2) - \alpha[\phi(y_3^m - y_1^m) + (1-\phi)(y_4^m - y_2^m)]\Delta t/\Delta x \quad (3.6)$$

Eqn. (3.6) is implicit in y_4 which is the only unknown if computation proceeds downstream and marches forward in time. Unless $\phi = 1.0$ (explicit scheme), eqn. (3.6) must be solved iteratively for y_4 . Eqn. (3.6) lends itself to a Newton-Raphson solution in which:

$$y^{i+1} = y^i - f(y^i)/f'(y^i) \quad (3.7)$$

where y^i represents an estimate of y_4 in the i^{th} iteration, and y^{i+1} is the improved value of y_4 to be used in the next $(i+1)^{\text{th}}$ iteration.

$f(y^i)$ is evaluated using eqn. (3.6), and $f'(y^i)$ is obtained by differentiating eqn. (3.6) with respect to the unknown y_k :

$$f'(y_k) = -(1-\theta) - (\Delta t/\Delta x)(1-\phi)\alpha m y_k^{m-1} \quad (3.8)$$

Eqns. (3.6) to (3.8) constitute a finite difference formulation of the kinematic equations based on the Preissmann box (fig. 3.2), and will be referred to in this study as the "Preissmann formulation" or the "Generalised Standard formulation" because this is the most common approach.

3.3.2. Numerical stability

The Preissmann formulation can be used for a generalised study of numerical stability in finite difference formulations of the kinematic equations. There are two criteria for numerical stability which will be discussed in turn.

(i) Grid spacing criterion

Implicit solutions to the full hydrodynamic equations (i.e. $\phi = 0.5$ or less) are generally favoured over explicit solutions ($\phi = 1.0$) because of greater numerical stability. The same is true for the kinematic equations. An explicit scheme goes unstable at low values of grid spacing (grid spacing being the ratio $\Delta x/\Delta t$). This is illustrated in fig. 3.3 after Constantinides (1982) showing a critical value of $\Delta x/\Delta t$ below which the scheme goes unstable. This critical grid spacing is given by the Courant criterion after Courant *et al* (1928) which states that:

$$(\Delta x/\Delta t)_{\text{crit}} = c \quad (3.9)$$

where c is the celerity. Defining the Courant number as $c/(\Delta x/\Delta t)$, eqn. (3.9) is equivalent to the Courant number equal to unity. Eqn. (3.9) holds for explicit schemes, i.e. those based on $\phi = 1.0$, but for lower values of ϕ the critical grid spacing is relaxed, until for some value of ϕ , $(\Delta x/\Delta t)_{\text{crit}} = 0$, i.e. unconditional numerical stability. The var-

iation of critical grid spacing with ϕ is illustrated below using numerical experiments.

Consider a rectangular plane sloping in its longitudinal direction with a slope of s_0 , subject to a steady uniform excess rain (i_e) of 50 mm/h (fig. 3.4). The plane is 100 m long by 20 m wide and is divided into increments Δx in the x-direction for modelling one-dimensional overland flow. The initial condition is a dry plane at time $t = 0$ (i.e. $y = 0$, $q = 0$ for all x), the upstream boundary condition is $y = 0$, $q = 0$ at $x = 0$ for all t , and the downstream boundary condition is uniform flow at $x = L$. After 10 minutes the rain is stopped and i_e is set equal to zero.

The Standard formulation of the kinematic equations (eqns. (3.6) to (3.8)) was used to generate runoff hydrographs for this problem, using a bed slope s_0 of 0.1 and a Manning's roughness coefficient of 0.01. The pertinent parameters are summarised in table 3.1. Three values of ϕ were considered: 0, 0.5 and 1.0. For each value of ϕ , hydrographs were generated using various values of $\Delta x/\Delta t$ obtained by holding Δx constant and varying Δt . θ was held constant at 0.5, except for the $\phi = 1.0$ case in which θ was set equal to 0. (It will be seen in the following section that this is a necessary secondary condition for stability.) The Δx and Δt values that were used are shown in table 3.2. The grid spacing is expressed in a dimensionless form as $(\Delta x/\Delta t)/c_p$ where c_p is the peak celerity at equilibrium. $(\Delta x/\Delta t)/c_p$ is equivalent to the inverse of the Courant number and hence the notation $1/Cr$ will be used for convenience.

The runoff hydrographs are shown in figs. 3.5, 3.6 and 3.7 in which the numerical instability is seen as oscillations. For $\phi = 0$ (fig. 3.5) there is no instability, irrespective of $\Delta x/\Delta t$, only a change in shape of the hydrograph as grid spacing varies (this influence of grid spacing on hydrograph shape will be examined later on). The opposite extreme occurs when $\phi = 1.0$, large oscillations being evident in fig. 3.7. In this figure it can be seen that instability sets in at $1/Cr$ around unity, which accords with the Courant criterion (eqn. (3.9)), and oscillations increase in severity the further the solution lies in the unstable zone.

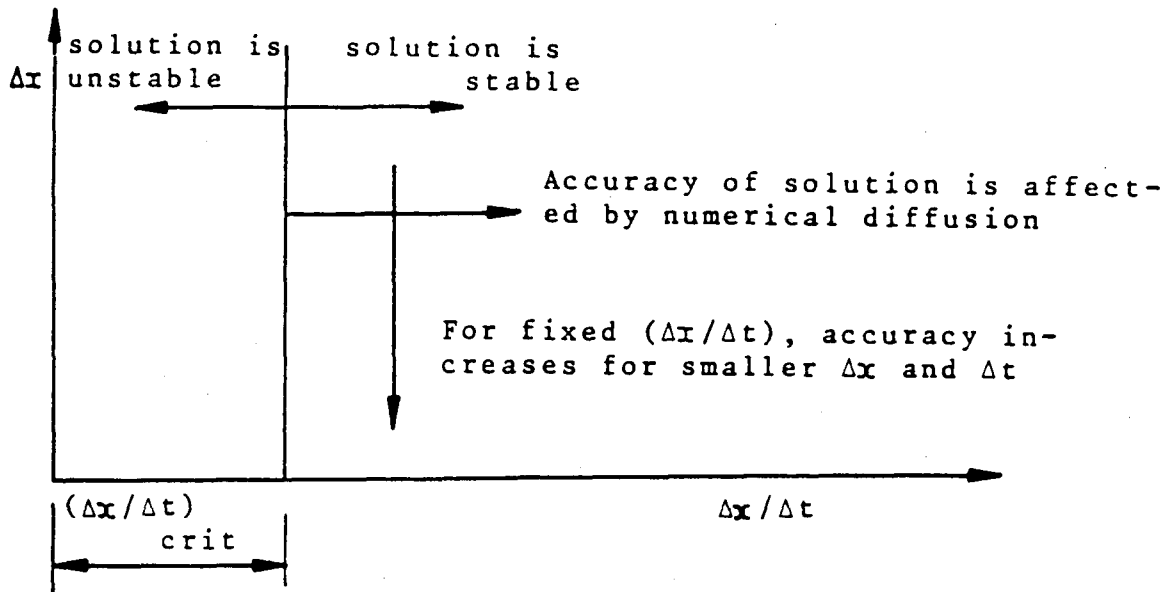


Figure 3.3: Accuracy and stability of a numerical scheme for the kinematic equations (after Constantinides, 1982).

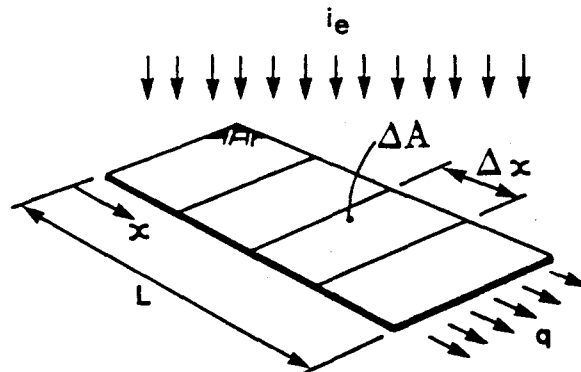


Figure 3.4: Overland flow plane.

Fig. 3.6 shows considerably smaller oscillations for the $\phi = 0.5$ case than for $\phi = 1.0$. Clearly the critical grid spacing lies at $1/Cr < 1.0$, i.e. a lower grid spacing than that predicted by the Courant criterion. This was further investigated over a range of slopes and hydraulic roughnesses, and the results are shown in fig. 3.8. The Muskingum-Cunge formulation (to be described later) was used because parasitic waves in the Standard formulation were found to obscure the results. In fig. 3.8, stable and unstable solutions are represented by solid and open points respectively,

Table 3.1: Overland flow parameters used in numerical stability study.

Parameter	Value
plane length L	100 m
plane width W	20 m
slope s_0	0.10
Manning's n	0.01
rainfall i_e	50 mm/h
storm duration	10 mins

Table 3.2: Grid spacings used in numerical stability study.

Δx (m)	Δt (secs)	1/Cr
10	30	0.35
10	20	0.50
10	17.5	0.60
10	13	0.80
10	8.5	1.24

indicating that for $\phi = 0.5$ and $\theta = 0.5$ the critical grid spacing lies at $1/Cr = 0.5$, i.e. half that predicted by the Courant criterion. It was found that using θ less than 0.5 with $\phi = 0.5$ seemed to reduce the critical grid spacing further, presumably because a lower θ suppresses oscillations.

These results confirm that as ϕ decreases from 1.0 to zero, the grid spacing criterion for numerical stability is relaxed and the instability problem decreases in severity. This is in agreement with the results of Brakensiek (1967). It now remains to ascertain the value of ϕ at which $(\Delta x/\Delta t)_{crit}$ equals zero.

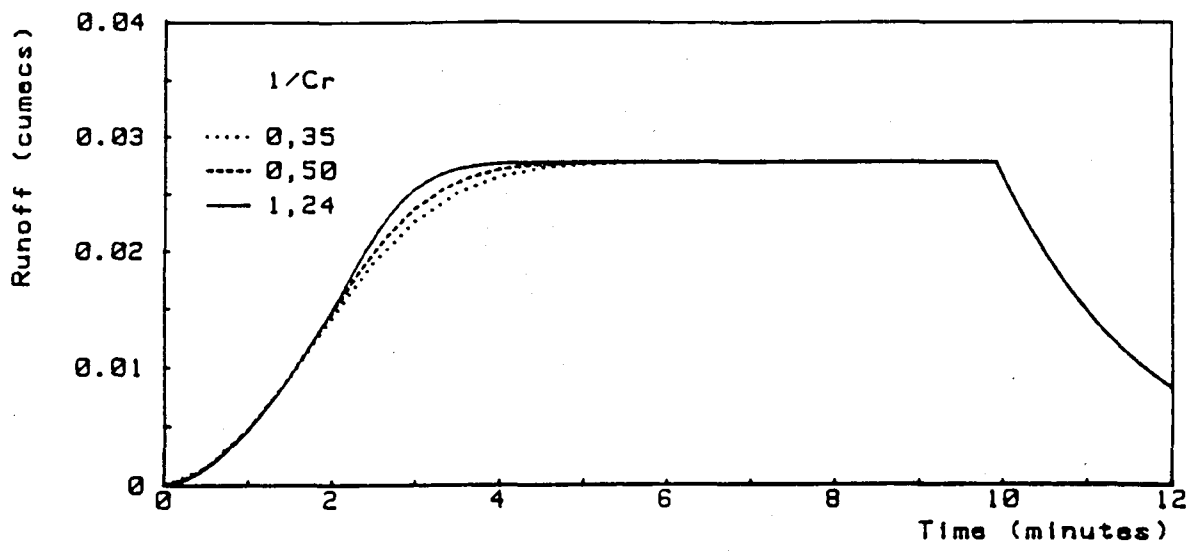


Figure 3.5: Numerical stability test with $\phi = 0$.

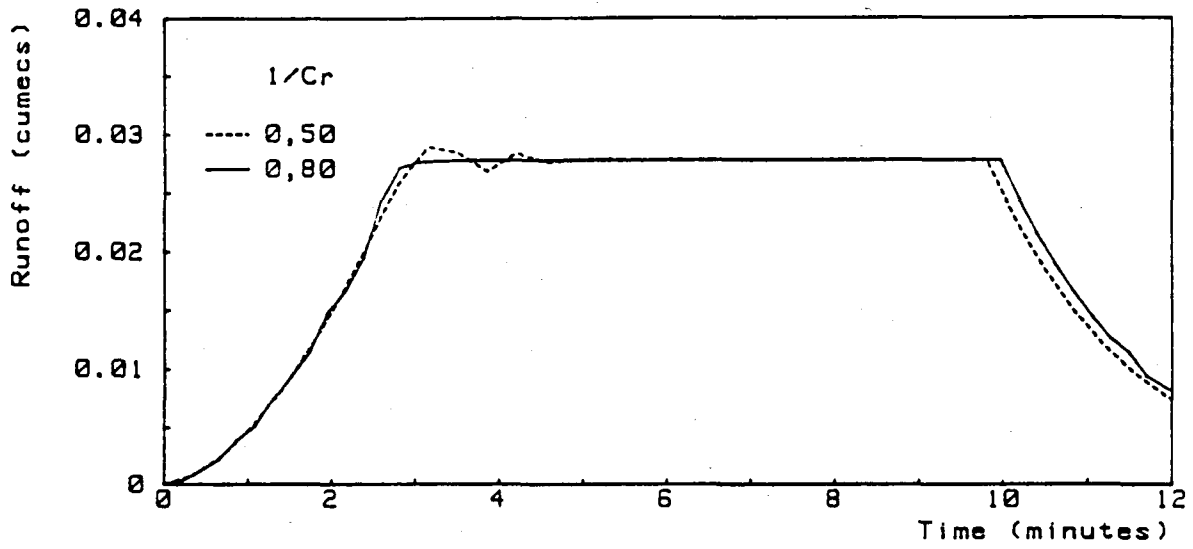


Figure 3.6: Numerical stability test with $\phi = 0.5$.

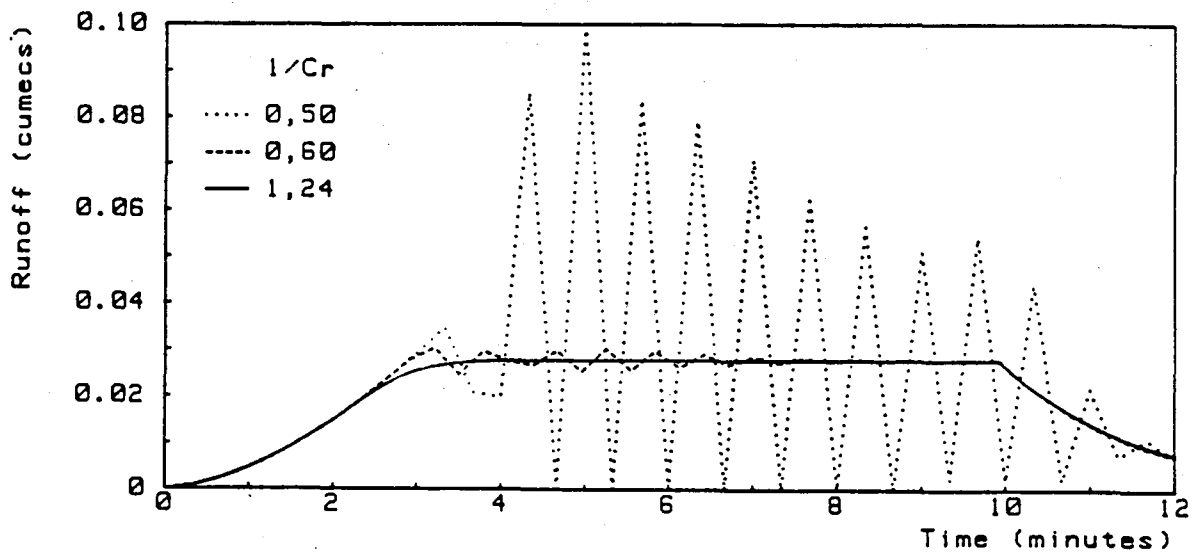


Figure 3.7: Numerical stability test with $\phi = 1.0$.

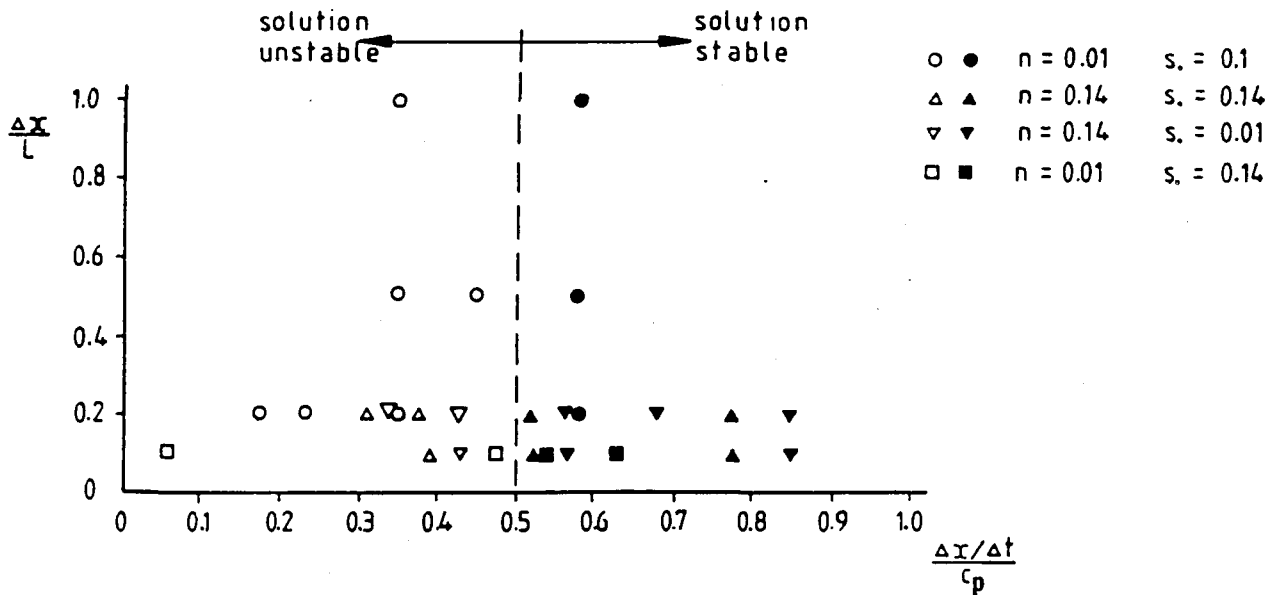


Figure 3.8: Stable and unstable numerical solutions for $\phi = 0.5$.

Theoretically, unconditional numerical stability should be possible with schemes based on $\phi = 0.5$, provided θ is not greater than 0.5 (Ponce, Chen and Simons, 1979; and Lynn and Goodwin, 1987). Such stability analyses are based on a Fourier series of a linearised form of the problem. However, numerical solutions of the hydrodynamic equations and of the kinematic equations have shown that instability is possible at low grid spacings for $\phi = 0.5$ or smaller, and only $\phi = 0$ will ensure unconditional stability (Brakensiek, 1967 and Kolovopoulos, 1988). This has been confirmed by the writer's experience. The work of Brakensiek (1967) in numerical flood routing with the kinematic equations indicates that as ϕ decreases from 1.0 to 0, the criteria for numerical stability are relaxed. This was confirmed by Kolovopoulos (1988) who showed that instability can occur in a numerical solution of the hydrodynamic equations when $\theta = 0.5$ and ϕ lies between zero and 0.5. ϕ -values in the region of 0.34 to 0.40 had to be used in many flood routing problems, and he demonstrated that $\phi = 0$ results in the most stable scheme.

Clearly only $\phi = 0$ is unconditionally stable. This is an important consideration when setting up and using finite difference schemes, and will be used later in this work when developing finite difference schemes for various hydrological processes.

(ii) von Neumann criterion

The ϕ -dependent grid spacing criterion described above is a *necessary* but not a *sufficient* condition for numerical stability (Grijsen, 1986). A second condition relates to the allowable value of θ for a given value of ϕ . It is given by the von Neumann criterion (Lyn and Goodwin, 1987) obtained from a Fourier analysis, which can be expressed as:

$$\theta \leq \frac{1}{2} - Cr(\phi - \frac{1}{2}) \quad (3.10)$$

This relationship is shown in fig. 3.9 for three values of ϕ . θ is plotted here as a function of $1/Cr$ so that grid spacing variations can be easily visualised. The inequality relationship in eqn. (3.10) is indicated by shading in fig. 3.9 such that a solution is unstable for a given grid spacing if θ lies in the shaded zone.

The grid spacing criterion places a lower limit on $\Delta x/\Delta t$ for a scheme with a given value of ϕ , and the von Neumann criterion places an upper limit on the value of θ for a given ϕ and a particular Cr . This Cr is a function of the local value of the celerity, which changes throughout a numerical solution as the flow conditions change. Both the grid spacing and von Neumann criteria must be satisfied for a solution to be stable.

3.3.3. Numerical diffusion analysis

An error analysis of a finite difference scheme can be carried out using a Taylor series expansion of the difference equation. Such analyses have been carried out by Cunge (1969) and Ponce, Chen and Simons (1979) on a Preissmann-type scheme. Expanding eqn. (3.4) around the point $(x-\Delta x, t-\Delta t)$ with a Taylor series, the approximation error R is obtained as:

$$R = |[(\theta - \frac{1}{2}) + Cr(\phi - \frac{1}{2})]| |\partial^2 Q / \partial x^2| \Delta x + \dots \text{ (terms in } \Delta x^2 \text{ and higher orders)} \quad (3.11)$$

If the first term in eqn. (3.11) is zero, then R is a function of terms in Δx^2 and smaller and the scheme is of second order accuracy. For the first term to be zero we require

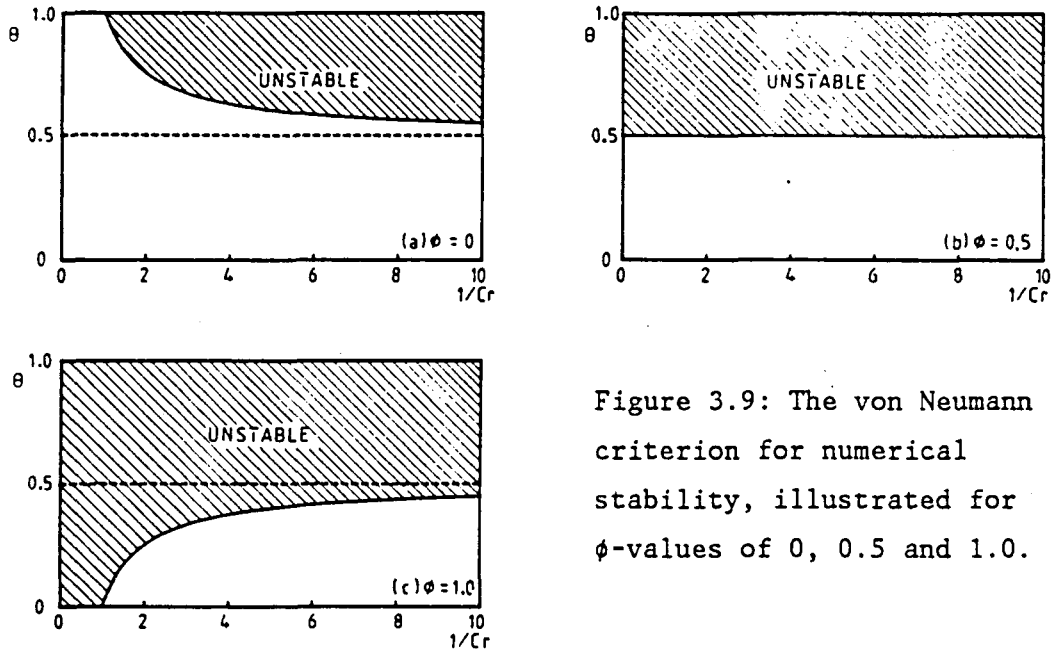


Figure 3.9: The von Neumann criterion for numerical stability, illustrated for ϕ -values of 0, 0.5 and 1.0.

$$(\theta - \frac{1}{2}) + Cr(\phi - \frac{1}{2}) = 0. \quad (3.12)$$

Solving for θ gives

$$\theta = \frac{1}{2} - Cr(\phi - \frac{1}{2}). \quad (3.13)$$

This analysis shows that for a scheme based on a Preissmann box to acquire second order accuracy, θ must vary in accordance with eqn. (3.13). Note that this equation is the same as the upper bound to θ given by the von Neumann criterion for numerical stability (eqn. 3.10), obtained by a Fourier stability analysis.

Eqn. (3.13) is plotted in fig. 3.10 for various values of ϕ , observing the limits (+1, -1) on θ . It can now be seen that a difference scheme with a given value of ϕ should satisfy three criteria, two for stability and one for accuracy:

1. For stability, $\Delta x/\Delta t$ must be greater than the critical grid spacing (which is $c\phi$ for $\phi = 0, 0.5$ and 1.0).
2. For stability, θ must lie below the relevant curve in fig. 3.10.
3. For accuracy, θ should lie close to the relevant curve in fig. 3.10.

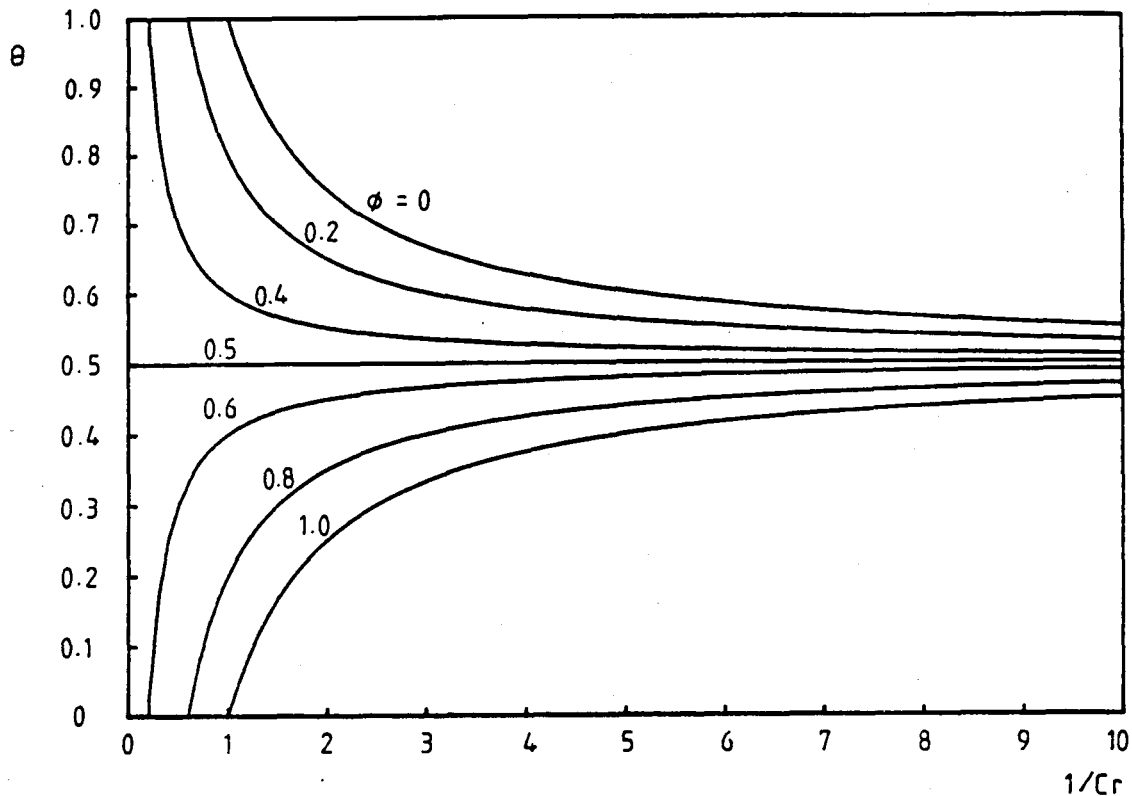


Figure 3.10: Relationship for θ given by eqn. (3.13).

Consider now a scheme using a constant θ , satisfying conditions (1) and (2) above but not necessarily condition (3). We shall apply the numerical scheme set forth in eqns. (3.6) to (3.8) to the overland flow plane problem defined in section 3.3.2 and fig. 3.4. As before the plane has length $L = 100$ m and width $W = 20$ m and is subject to an excess rain of 50 mm/h. It was found that the behaviour of the numerical scheme was the same over a range of slopes s_0 and Manning's coefficients and so the results presented below are presented as dimensionless hydrographs with the time dimension expressed at t/t_d (where t_d is storm duration), and the ordinate as $q/i_e L$ where $i_e L$ is the peak (equilibrium) runoff. As in the numerical stability study, three values of ϕ will be considered: 0, 0.5 and 1.0.

(i) *Implicit scheme, $\phi = 0$*

Using eqns. (3.6) to (3.8) with $\phi = 0$ gives a fully implicit scheme. From fig. 3.9 it is clear that if a constant θ is used, this θ must not be greater than 0.5 for the scheme to satisfy the von Neumann stability

criterion over a wide range of grid spacings. θ -values of 0.5 and 0 are considered here.

Fig. 3.11 shows runoff hydrographs generated using θ fixed at 0.5 with Δx equal to the plane length ($\Delta x/L = 1$). Hydrographs are shown that were generated using different values of $\Delta x/\Delta t$, obtained by keeping Δx constant and changing Δt in order to eliminate the effect on accuracy of changing Δx , and to isolate the effect of grid spacing on numerical diffusion, as illustrated qualitatively in fig. 3.3. Grid spacing in fig. 3.11 is expressed in a dimensionless form as $(\Delta x/\Delta t)/c_p$ where c_p is the peak celerity at equilibrium.

The results in fig. 3.11 show that different values of $\Delta x/\Delta t$ result in different numerical solutions. This phenomenon will be referred to as *numerical diffusion dependent on grid spacing*, and can be explained with reference to fig. 3.10. For solutions using a low grid spacing ($1/Cr$ close to 1.0), the correct value of θ given by the $\phi = 0$ curve in fig. 3.10 is considerably larger than the chosen value of $\theta = 0.5$ used here. Hence the error (eqn. (3.11)) is large, evident as high numerical diffusion or an over-attenuated hydrograph. As higher values of $\Delta x/\Delta t$ are used, the θ -curve in fig. 3.10 approaches the chosen θ -value of 0.5 and the amount of numerical diffusion in the generated hydrographs decreases, so that they converge on the true solution. Obviously such uncontrolled numerical diffusion is undesirable in a numerical scheme.

Fig. 3.12 shows results using $\phi = 0$ and $\theta = 0$. The same numerical diffusion is apparent. It can be seen from figs. 3.11 and 3.12 and from the above discussion that for a constant- θ scheme with $\phi = 0$, accuracy of the numerical solution improves as grid spacing is increased.

(ii) *Central spatial derivative, $\phi = 0.5$.*

Using eqns. (3.6) - (3.8) with $\phi = 0.5$ gives a scheme with a centred spatial derivative. Observing the von Neumann stability criterion, θ -values of 0.5, 0.25, and 0 were used with various Δx 's, and sample results are shown in fig. 3.13 for $\theta = 0.5$ with $\Delta x/L = 1.0$. In this figure the hydrographs generated using different grid spacings all coincide on

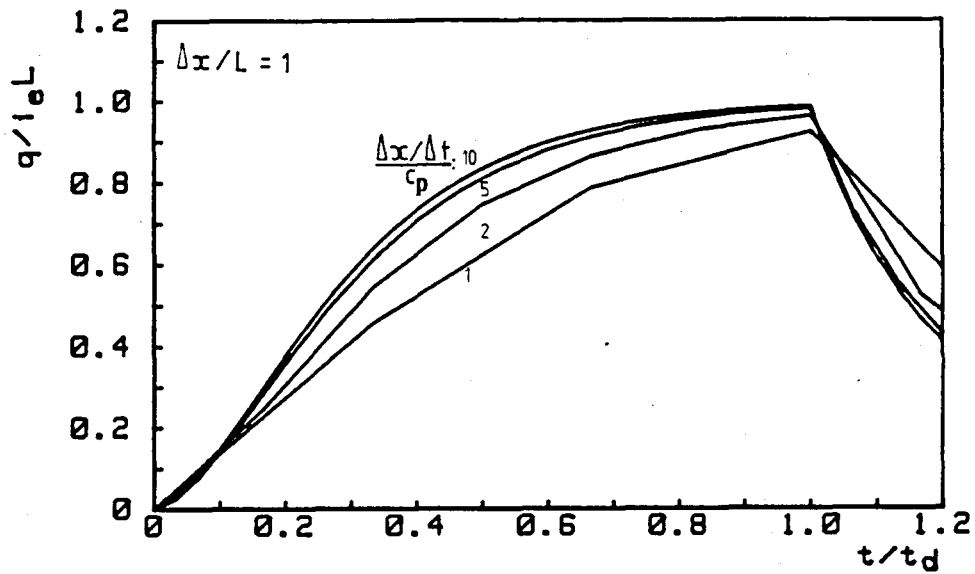


Figure 3.11: Runoff hydrographs for $\phi = 0$, $\theta = 0.5$.

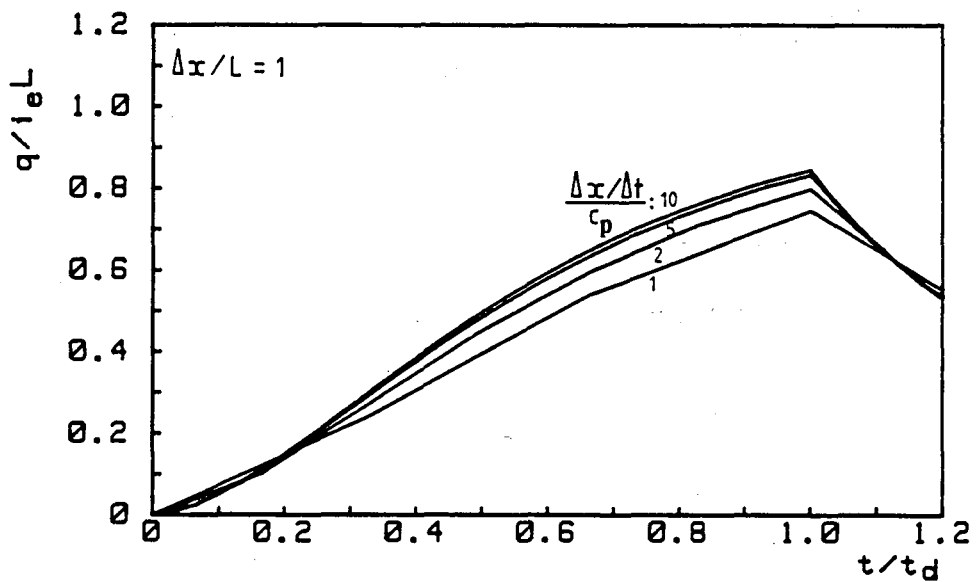


Figure 3.12: Runoff hydrographs for $\phi = 0$, $\theta = 0$.

the same curve. Thus there is an absence of the grid spacing dependant numerical diffusion that was observed for $\phi = 0$. This can again be explained in the light of fig. 3.10, in which for $\phi = 0.5$, θ is shown constant at 0.5 for all grid spacings. $\phi = 0.5$ is the only case for which θ should be constant.

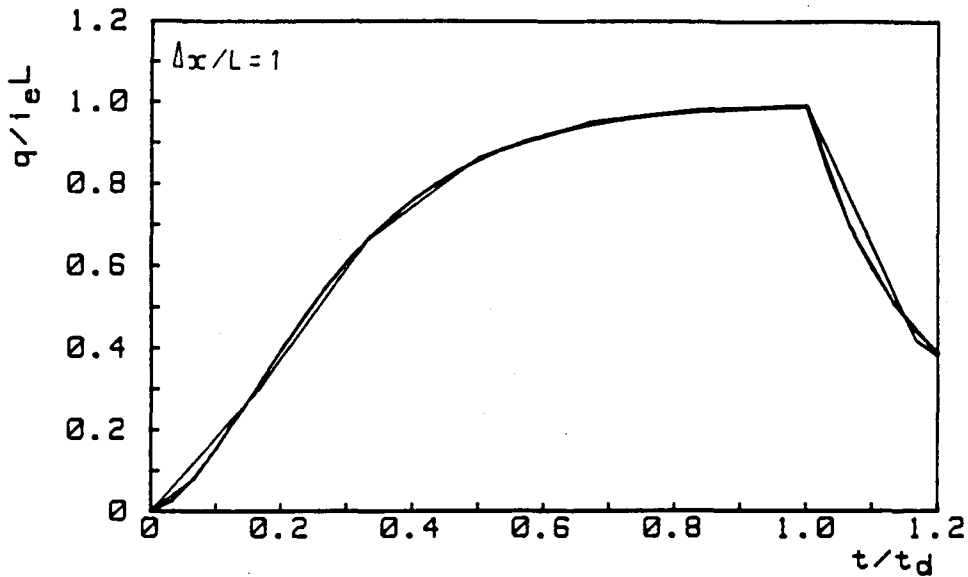


Figure 3.13: Runoff hydrographs for $\phi = 0.5$, $\theta = 0.5$.

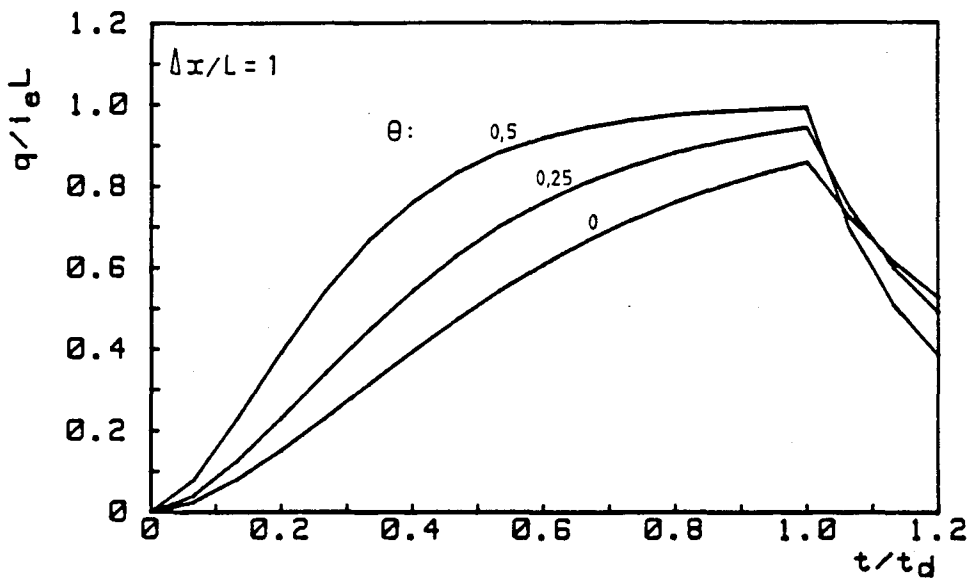


Figure 3.14: Numerical solutions for $\phi = 0.5$ showing the effect of θ on attenuation.

An absence of grid spacing dependant numerical diffusion does not necessarily imply an absence of numerical diffusion altogether. Because $\theta = 0.5$ is the correct choice when $\phi = 0.5$ according to fig. 3.10, any value of θ less than 0.5 will result in a certain amount of numerical diffusion being introduced into the solution. This numerical diffusion will be

invariant with grid spacing as discussed above and illustrated in fig. 3.13, but will depend on the value of θ .

The effect of θ on the numerical solution is illustrated in fig. 3.14 where runoff hydrographs generated using 3 values of θ are shown. According to eqn. (3.13), $\theta = 0.5$ allows no numerical diffusion, but as θ is decreased, numerical diffusion is introduced into the solution in increasing amounts, attenuating the hydrograph. This is an important result which will be used later for modelling attenuation by adjusting θ to control the numerical diffusion. In their review of flood routing methods, Weinmann and Laurenson (1979) discussed the effect of $\theta = 0.5$ and $\theta = 0$ on a $\phi = 0.5$ scheme. They stated that $\theta = 0.5$ (central difference) models a true kinematic wave, i.e. pure translation and no attenuation, and they described $\theta = 0$ as "reservoir-type action" in which large numerical diffusion results in significant attenuation of an inflow hydrograph.

(iii) *Explicit scheme, $\phi = 1.0$*

An explicit formation is obtained by using eqns. (3.6) to (3.8) with $\phi = 1.0$. To satisfy the von Neumann criterion, only $\theta = 0$ can be used in a constant- θ scheme. Fig. 3.15 shows grid spacing dependent numerical diffusion for this solution. For $\phi = 0$, the numerical diffusion was seen in fig. 3.11 to decrease with increasing grid spacing; here the reverse occurs, fig. 3.15 showing numerical diffusion to *increase* as progressively larger grid spacings are used, seen as an increase in hydrograph subsidence at $\Delta x/\Delta t$ increases. The reason is because the correct value for θ corresponding to the $\phi = 1.0$ curve in fig. 3.10, diverges from the constant $\theta = 0$ as grid spacing increases. Thus a $\phi = 1.0$, $\theta = 0$ formation will only be accurate at low grid spacings ($1/Cr$ close to 1.0).

(iv) *Scheme with variable θ*

The effect of varying θ in accordance with fig. 3.10 and eqn. (3.13) is now demonstrated. For a given value of ϕ , θ depends on Δx , Δt and celerity. Δx and Δt are fixed for a particular simulation, but the celerity constantly changes at each point on the overland flow plane and

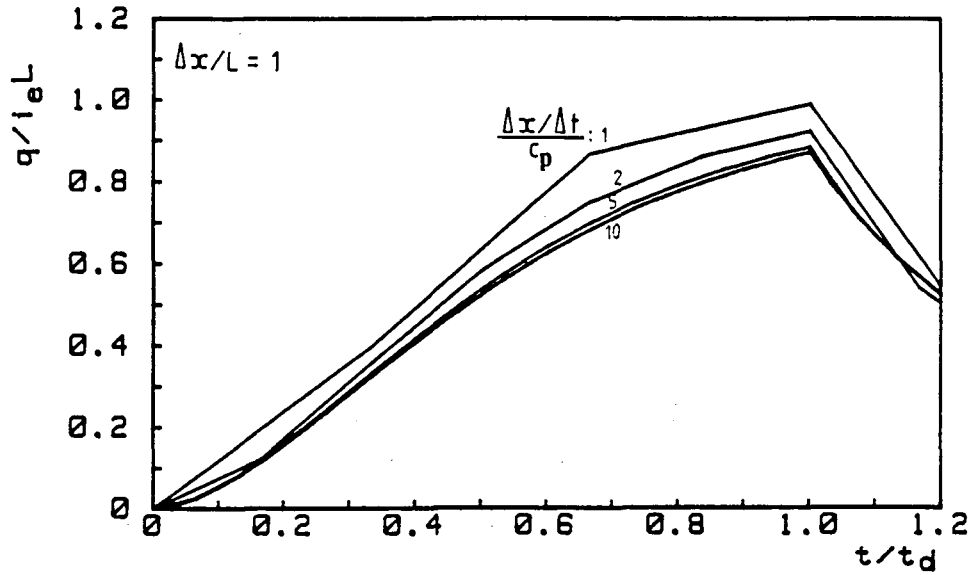


Figure 3.15: Runoff hydrographs for $\phi = 1.0$, $\theta = 0$.

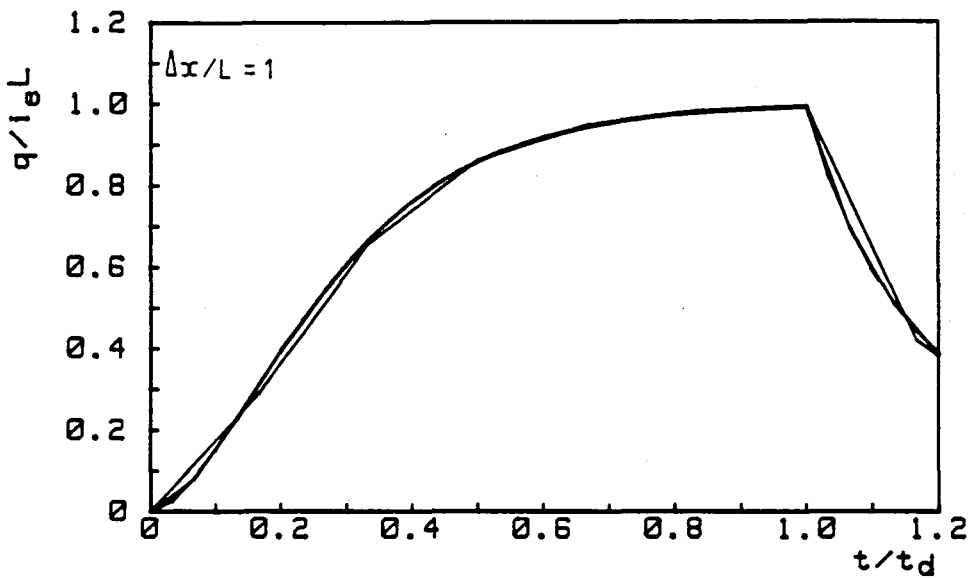


Figure 3.16: Results of variable- θ formulation with $\phi = 0$ for a range of grid spacings.

at each time increment. Therefore θ should change for each computational cell. In a numerical solution, θ can be calculated for each computational cell using eqn. (3.13) with the celerity evaluated as the arithmetic average of the celerities at the four corners of the computational cell (grid points 1, 2, 3 and 4 in fig. 3.2).

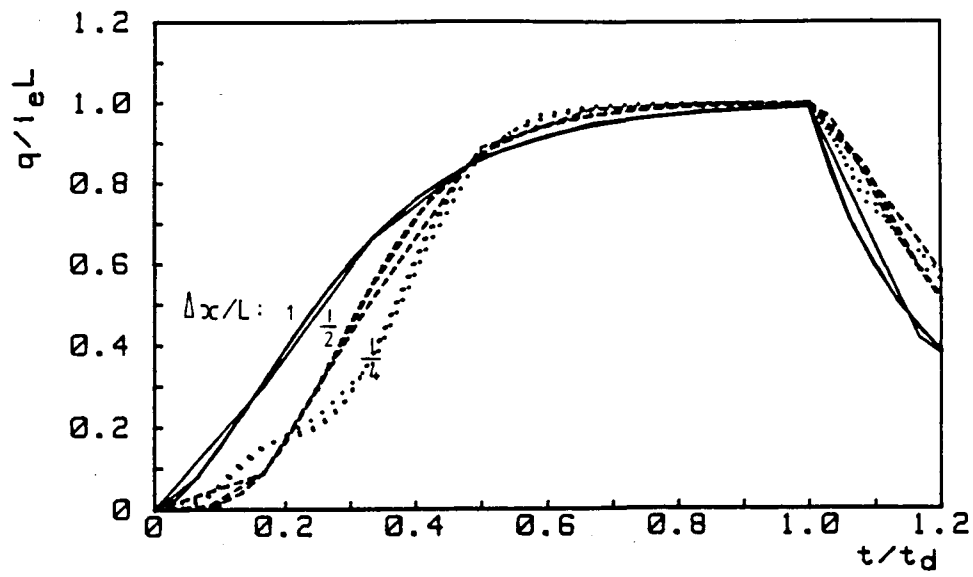
Using this approach, numerical solutions with a varying θ were generated for various values of ϕ and Δx , and representative results for $\phi = 0$ and $\Delta x/L = 1$ are shown in fig. 3.16. The curves for different $\Delta x/\Delta t$ all coincide, showing that the use of a varying θ in accordance with fig. 3.10 eliminates grid spacing dependent numerical diffusion. The accuracy of the numerical solution is thus independent of grid spacing. This constitutes a true kinematic solution (i.e. non-diffusive).

(v) *Parasitic waves and effect of Δx*

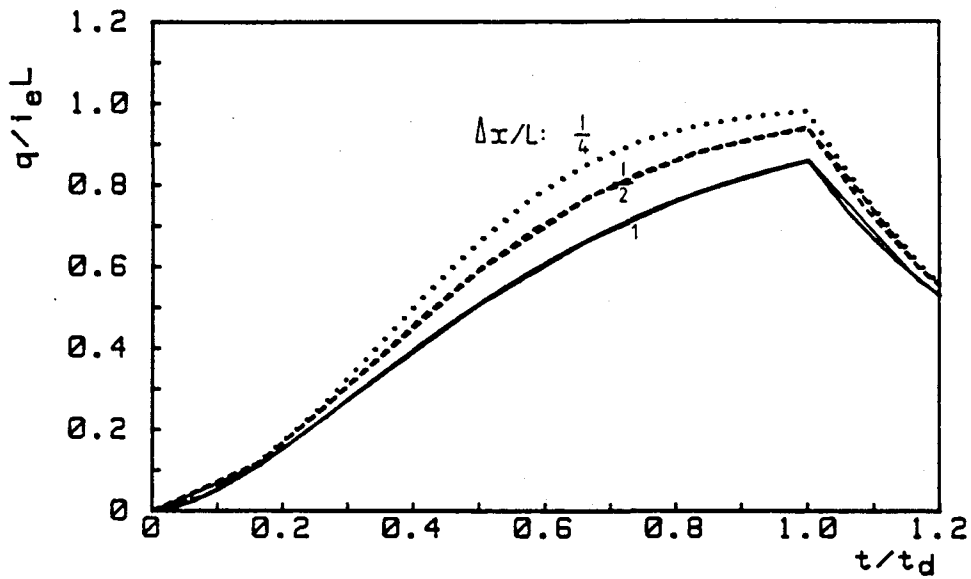
To complete this evaluation of the Preissmann-based formulation, effects of parasite waves and of the value of Δx will be considered.

The magnitudes of Δx and Δt determine the resolution of a numerical scheme, and a converging finite difference scheme converges on the true solution as Δx and Δt are decreased. The magnitude of Δt is not critical provided enough time increments are allowed for the shape of the rising hydrograph limb to be adequately represented - generally at least 4 to 5 points to the peak. Δx can however affect the solution noticeably as illustrated in fig. 3.17 which shows changes in hydrograph shape with decreasing Δx . This has relevance to hydrological modelling because it relates to the level of catchment discretization and its effect on accuracy. For a converging scheme the solution should be more accurate for smaller Δx (as indicated in fig. 3.3), and this will be illustrated in section 3.6 where numerical solutions are compared with measured runoff data.

Apart from affecting the hydrograph shape, the value of $\Delta x/L$ has other implications in the scheme presently being studied. It was found during numerical experiments that the use of more than 2 Δx -increments on the overland flow plane resulted in uneven water surface profiles and waviness on the rising limb of the runoff hydrograph. This is illustrated by the curve for $\Delta x/L = \frac{1}{4}$ (four Δx -increments) in fig. 3.17(a), which is reproduced in fig. 3.18 for clarity. This phenomenon appears to be a weakness inherent in this type of formulation, and is caused by the term $\theta(y_1 - y_2)$ in eqn. (3.6), which is negative if the water level is rising.



(a) $\theta = 0.5$



(b) $\theta = 0$

Figure 3.17: Effect of Δx on hydrograph shape (using $\phi = 0.5$).

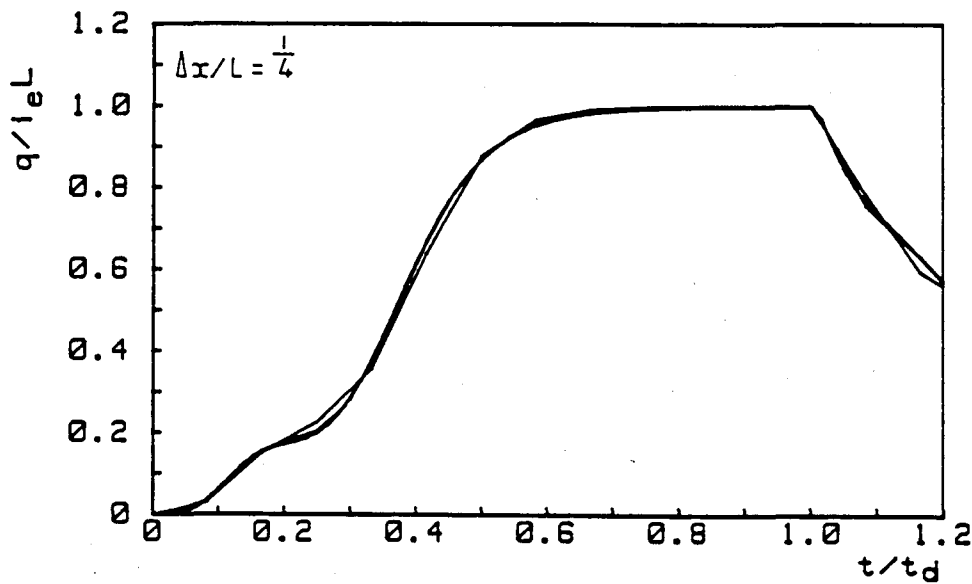


Figure 3.18: Parasitic waves on rising hydrograph limb for $\phi = \theta = 0.5$ and a range of $\Delta x/\Delta t$.

It was found that small values of θ dampen out the wavelets, as can be seen by the smooth hydrographs in fig. 3.17(b) for $\theta = 0$.

(vi) *Summary*

The hydrographs in this section (figs. 3.11 - 3.18) reflect typical behaviour of the Preissmann-based formulation for particular conditions. A comprehensive range of tests was conducted including $\Delta x/L = 1, \frac{1}{2}$ and $\frac{1}{4}$ for each value of θ and ϕ , and only sample results have been shown here in order to avoid repetition. The results of the larger data set and the findings discussed in this section are summarised in table 3.3.

3.3.4. Finite difference schemes in the literature

Finite difference schemes for the kinematic equations reported in the literature generally follow the approach of a constant θ , possibly the only exception being the Muskingum-Cunge scheme (which will be dealt with later in this chapter). Many finite difference schemes reported in the literature can be evaluated in the light of the numerical diffusion and stability analysis presented above, and 3 examples are cited below.

(i) *Overland routing in SWMM*

The overland routing algorithm in the well-known Storm Water Management Model (SWMM, described by Huber *et al*, 1982) is equivalent to a Preissmann scheme with $\phi = 0.5$ and $\theta = 0$. From the present discussions the following predictions can be made for this scheme:

- o The von Neumann criterion for numerical stability is satisfied by using $\theta = 0$. However, the grid spacing criterion will dictate lower limits on Δx and upper limits on Δt for numerical stability, imposing constraints on the user of the model.
- o Because $\phi = 0.5$ requires a constant- θ formulation, runoff predictions will be invariant with grid spacing, so that the choice of $\Delta x/\Delta t$ will not affect the solution. The developers of SWMM probably chose this formulation with this advantage in mind.

Table 3.3: Summary of studies on Standard formulation.

ϕ	θ	parasitic waves present			Numerical diffusion
		$\Delta x/L=1$	$\Delta x/L=\frac{1}{2}$	$\Delta x/L=\frac{1}{4}$	
0	0.5	no	no	yes	Numerical diffusion is present as a function of grid spacing. Accuracy improves as grid spacing increases.
0	0	no	no	no	
0.5	0.5	no	no	yes	No numerical diffusion.
0.5	0.25	no	no	no	Numerical diffusion is present, but is invariant with grid spacing.
0.5	0	no	no	no	Numerical diffusion is present ("reservoir action"), but is invariant with grid spacing.
1.0	0	no	no	no	Numerical diffusion is present as a function of grid spacing. Accuracy decreases as grid spacing increases.
0	variable	no	no	yes	No numerical diffusion in the solution.
1	variable	no	no	no	

- o The low value of θ will result in large numerical diffusion with a well-attenuated runoff hydrograph, corresponding to the "reservoir action" described by Weinmann and Laurenson (1979). Therefore the runoff component of SWMM is not a true kinematic solution but should exhibit somewhat dampened peaks.

(ii) *Explicit overland formulation in KINE2*

For an explicit scheme ($\phi = 1.0$), only a backward difference ($\theta = 0$) can be used in a constant- θ scheme because of the von Neumann criterion.

Constantinides (1982) used an explicit backward difference for overland routing in the two-dimensional runoff model KINE2, and the various behavioural patterns that he reported for this scheme all agree with and can be explained by the present study. He found it to be unstable for $1/Cr < 1.0$, which accords with the grid spacing stability criterion (section 3.3.2). He also found that accuracy declined with increasing grid spacing, and that optimum accuracy was obtained at $1/Cr$ close to 1.0. This is explained by the $\phi = 1$ curve in fig. 3.10, where θ increases above zero with increasing grid spacing, resulting in a loss of accuracy if $\theta = 0$ is used at large grid spacings. Optimum accuracy is obtained close to where the curve intersects the line $\theta = 0$, which is at $1/Cr = 1.0$.

(iii) Channel flood routing of Huang (1978)

The third example is the finite difference kinematic formulation of Huang (1978) for channel routing, based on $\phi = 0$ and $\theta = 0$. Huang reported unconditional stability which accords with the observations in section 3.3.2 (critical grid spacing is zero when $\phi = 0$). From fig. 3.10 we can predict a grid spacing dependent solution as a result of using $\theta = 0$. Huang (1978) noted that small time increments (i.e. large $\Delta x/\Delta t$) were required to maintain accuracy. This is explained by the $\phi = 0$ curve in fig. 3.10 where it can be seen that $\theta = 0$ is a better approximation for large grid spacings than for small.

3.4. MUSKINGUM-CUNGE FORMULATION

The second type of finite difference scheme to be studied is the Muskingum-Cunge approach. The traditional Muskingum-Cunge equations are presented below as a finite difference formulation of the continuity equation based on $\phi = 0.5$, and then re-derived using $\phi = 0$. Algorithms are presented for overland flow and finally the performance of the various Muskingum-Cunge derivatives is discussed.

3.4.1. The Muskingum-Cunge equations

Weinmann and Laurenson (1979) derived the Muskingum-Cunge equations from a Preissmann expression of the continuity equation. Eqn. (3.1) can be written as

$$\frac{\partial Q}{\partial x} + \frac{\partial A}{\partial t} = q_i \quad (3.14)$$

where q_i is lateral inflow per unit length in the flow direction [L^2T^{-1}], Q is flow rate and A is cross-sectional flow area. Eqn. (3.14) is equivalent to

$$\frac{\partial Q}{\partial x} + \frac{dA}{dQ} \frac{\partial Q}{\partial t} = q_i \quad (3.15)$$

Wave celerity is defined (Henderson, 1966) by

$$c = dQ/dA \quad (3.16)$$

and hence eqn. (3.15) can be written

$$\frac{\partial Q}{\partial x} + \frac{1}{c} \frac{\partial Q}{\partial t} = q_i \quad (3.17)$$

which as a Preissmann finite difference scheme is

$$\frac{\phi(Q_3 - Q_1) + (1-\phi)(Q_4 - Q_2)}{\Delta x} + \frac{\theta(Q_2 - Q_1) + (1-\theta)(Q_4 - Q_3)}{c_a \Delta t} = q_i \quad (3.18)$$

where θ and ϕ are the weighting coefficients defined previously (fig. 3.2), and subscripts 1 to 4 correspond to the corners of a computational cell as shown in fig. 3.2. c_a is the average celerity in a computational cell.

Setting $\phi = 0.5$ in eqn. (3.18) and solving for Q_4 gives the Muskingum routing equation:

$$Q_4 = C_1 Q_1 + C_2 Q_2 + C_3 Q_3 + C_0 q_i \Delta x \quad (3.19)$$

with the routing coefficients defined by

$$C_0 = \frac{2\Delta t}{\Delta t + 2K(1 - \theta)} \quad (3.20a)$$

$$C_1 = \frac{\Delta t + 2K\theta}{\Delta t + 2K(1 - \theta)} \quad (3.20b)$$

$$C_2 = \frac{\Delta t - 2K\theta}{\Delta t + 2K(1 - \theta)} \quad (3.20c)$$

$$C_3 = \frac{2K(1 - \theta) - \Delta t}{\Delta t + 2K(1 - \theta)} \quad (3.20d)$$

The sum of C_1 , C_2 and C_3 is always unity. K is the travel constant, approximately equal to the travel time of a flood wave through a distance Δx , and is given by

$$K = \Delta x / c_a \quad (3.21)$$

Eqns. (3.19) to (3.21) are identical to the well-known Muskingum river routing equations (documented by Chow, 1964 and Henderson, 1966). In classical Muskingum routing, eqns. (3.19) to (3.21) are derived from a linear storage relationship, and K and θ are constants which may be determined for a particular reach by calibration using measured inflow and outflow flood hydrographs.

Cunge (1969) showed that the Muskingum equations constitute a finite difference formulation of the kinematic equations (as in the above derivation), and this is the basis for their use in the present study. Cunge

(1969) showed that this approach approximates diffusion routing if θ is calculated for each computational cell using

$$\theta = \frac{1}{2}(1 - Q/Bc\Delta x s_f). \quad (3.22)$$

Eqns. (3.19) to (3.22) constitute Muskingum-Cunge routing. The derivation above shows that the difference between this and the Standard formulation (section 3.3) is in the use of the celerity in eqn. (3.18), allowing the continuity equation to be solved explicitly for the unknown Q_4 . Q_1 , Q_2 and Q_3 are known in each computational cell if computation proceeds downstream.

A brief outline follows of the development of Muskingum-Cunge routing since Cunge's (1969) refinement.

Ponce and Yevjevich (1978) showed that K and θ can be allowed to vary in time and space in a simulation, evaluating the "variable parameter" Muskingum-Cunge method by using it to route a sinusoidal hydrograph down a channel with good results. Ponce (1979) showed that lateral inflow along the length of a reach can be accounted for (i.e. the term $C_0 q_1 \Delta x$ in eqn. (3.19)). Ponce and Theurer (1982) analysed accuracy criteria for the Muskingum-Cunge formulation, and Hjelmfelt (1985) examined the generation of negative flows in Muskingum-Cunge routing. Ponce (1986) was the first to apply Muskingum-Cunge routing to overland flow. He also discussed how the Muskingum-Cunge approach models the attenuation of a flood wave by means of the variable θ .

The use of approximate methods for flood routing can be valuable because of the ease of solution of the equations. An example of the application of Muskingum-Cunge routing in a hydrological model is given by Price (1978) who used a variable-parameter Muskingum-Cunge approach for channel routing in a catchment model, and reported good predictions of flood peaks and of hydrograph shapes.

None of the work summarised above deviates from the $\phi = 0.5$ based routing coefficients (eqns. (3.20)). From the derivation of these equations outlined above it is evident that Muskingum-Cunge routing can be viewed

as an *approach* to finite difference formulations of the kinematic equations. Any value of ϕ could be inserted in eqn. (3.18) provided an appropriate choice is made for θ . Because of the numerical stability limitations associated with using $\phi > 0.5$, only $\phi = 0$ will be considered here.

3.4.2. $\phi = 0$ Muskingum-Cunge formulation

Using $\phi = 0$ has distinct advantages in terms of unconditional numerical stability. A Muskingum-Cunge formulation based on $\phi = 0$ is obtained by solving eqn. (3.18) for Q_4 with ϕ set to zero. This yields the same routing eqn. (3.19) but different coefficients as follows:

$$C_0 = \frac{\Delta t}{\Delta t + K(1 - \theta)} \quad (3.23a)$$

$$C_1 = \frac{K\theta}{\Delta t + K(1 - \theta)} \quad (3.23b)$$

$$C_2 = \frac{\Delta t - K\theta}{\Delta t + K(1 - \theta)} \quad (3.23c)$$

$$C_3 = \frac{K(1 - \theta)}{\Delta t + K(1 - \theta)} \quad (3.23d)$$

K is defined as before. These coefficients are similar to the original coefficients but a comparison shows that there are significant differences.

The expression for θ must now be re-evaluated. Using the Taylor series analysis described previously for the Standard formulation, θ would be defined by eqn. (3.13) and fig. 3.10, eliminating numerical diffusion and ensuring that accuracy does not change with grid spacing. This would be a perfectly acceptable solution, comparable to the variable- θ formulation dealt with in the previous section. However, the Muskingum-Cunge approach takes this one step further. Instead of equating the first term of the

error eqn. (3.11) to zero, it is equated with the diffusion term in the diffusion equation, which for a rectangular channel is

$$\frac{-Q}{2Bcs_f} = \frac{\partial^2 Q}{\partial x^2}$$

in which s_f is the energy slope and B is the breadth. Equating gives

$$[(\theta - \frac{1}{2}) + Cr(\phi - \frac{1}{2})]\Delta x = -Q/2Bcs_f$$

and solving for θ gives

$$\theta = \frac{1}{2}[1 - 2Cr(\phi - \frac{1}{2}) - Q/B\Delta xcs_f]. \quad (3.24)$$

Putting $\phi = 0.5$ in eqn. (3.24) results in the conventional expression for θ in Muskingum-Cunge routing (eqn. (3.22)). The terms $\frac{1}{2}[1 - 2Cr(\phi - \frac{1}{2})]$ eliminate grid spacing dependant numerical diffusion (equivalent to eqn. (3.13)) and the term $-Q/2B\Delta xcs_f$ refines the solution by matching numerical diffusion to the physical attenuation (Ponce, 1986). This allows for the modelling of attenuation in channel routing applications. Although not as important in overland routing, this term will be retained here as a refinement of a purely kinematic approach. Setting $\phi = 0$ in eqn. (3.24) and using terms appropriate to overland routing, the expression for θ becomes

$$\theta = \frac{1}{2}(1 + Cr - q/\Delta xcs_o). \quad (3.25)$$

3.4.3. Algorithms for Muskingum-Cunge formulation

Before applying the Muskingum-Cunge approach to the overland flow plane problem, algorithms will be developed employing iterative and non-iterative solutions methods.

q_a and c_a must be assessed as average values for a computational cell. Ponce and Yevjevich (1978) evaluated 3 means of determining c_a and q_a :

1. A 2-point average of the values at grid points 1 and 3 (referring to fig. 3.2 for definition of grid points).

2. A 3-point average of the values at grid points 1, 2 and 3.
3. A 4-point average of the values at grid points 1, 2, 3 and 4.

The first two methods result in non-iterative formulations and the third method in an implicit formulation, since conditions are unknown at grid point 4 and known at points 1 to 3 as computation proceeds from one computational cell to the next in a downstream direction. Ponce and Yevjevich (1978) found methods (2) and (3) to be preferable to method (1), and there to be little difference between the results obtained using the 3- and 4-point methods. The 3-point and 4-point methods were adopted here.

For the 3-point (non-iterative) algorithm, the arithmetic averages can be expressed as follows, with subscripts 1, 2 and 3 referring to conditions at grid points 1, 2 and 3 respectively in the computational cell (fig. 3.2):

$$q_a = \frac{1}{4}(q_1 + q_2 + 2q_3) \quad (3.26)$$

$$c_a = \frac{1}{4}(c_1 + c_2 + 2c_3) \quad (3.27)$$

A weighted average in favour of grid point 3 compensates for the missing flow and celerity at point 4. q_i in eqn. (3.26) ($i = 1, 2, 3$) is simply the flow per unit width:

$$q_i = Q_i/W. \quad (3.28)$$

The celerity c_i in eqn. (3.27) is evaluated by differentiating the rating relationship eqn.(3.3):

$$c_i = dq_i/dy_i = \alpha m y_i^{m-1}. \quad (3.29)$$

Substituting eqn. (3.29) into eqn. (3.27) yields

$$c_a = \frac{1}{4}\alpha m (y_1^{m-1} + y_2^{m-1} + 2y_3^{m-1}). \quad (3.30)$$

Similarly eqn. (3.26) becomes

$$q_a = \frac{1}{4}\alpha (y_1^m + y_2^m + 2y_3^m). \quad (3.31)$$

The flow depths y_1 , y_2 and y_3 can be evaluated from the known flows Q_1 , Q_2 and Q_3 using the rating relationship eqn. (3.3) in the form:

$$y_i = (q_i/\alpha)^{1/m} = (Q_i/W\alpha)^{1/m}. \quad (i = 1, 2, 3) \quad (3.32)$$

The 4-point iterative algorithm follows the same approach but with q_a and c_a defined as

$$q_a = \frac{1}{4}(q_1 + q_2 + q_3 + q_4) \quad (3.33)$$

$$\text{and } c_a = \frac{1}{4}(c_1 + c_2 + c_3 + c_4). \quad (3.34)$$

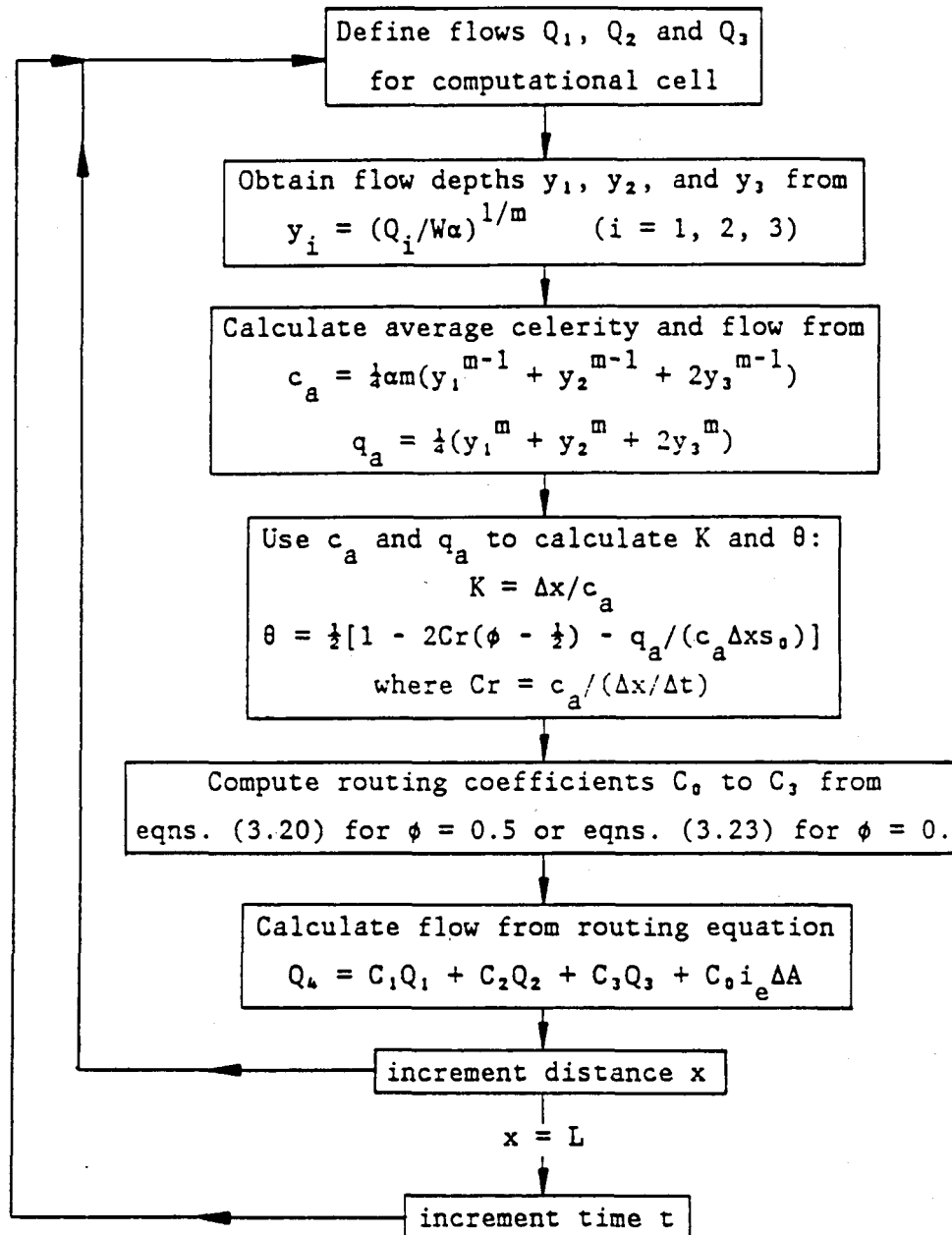


Figure 3.19: Algorithm for non-iterative Muskingum-Cunge formulation.

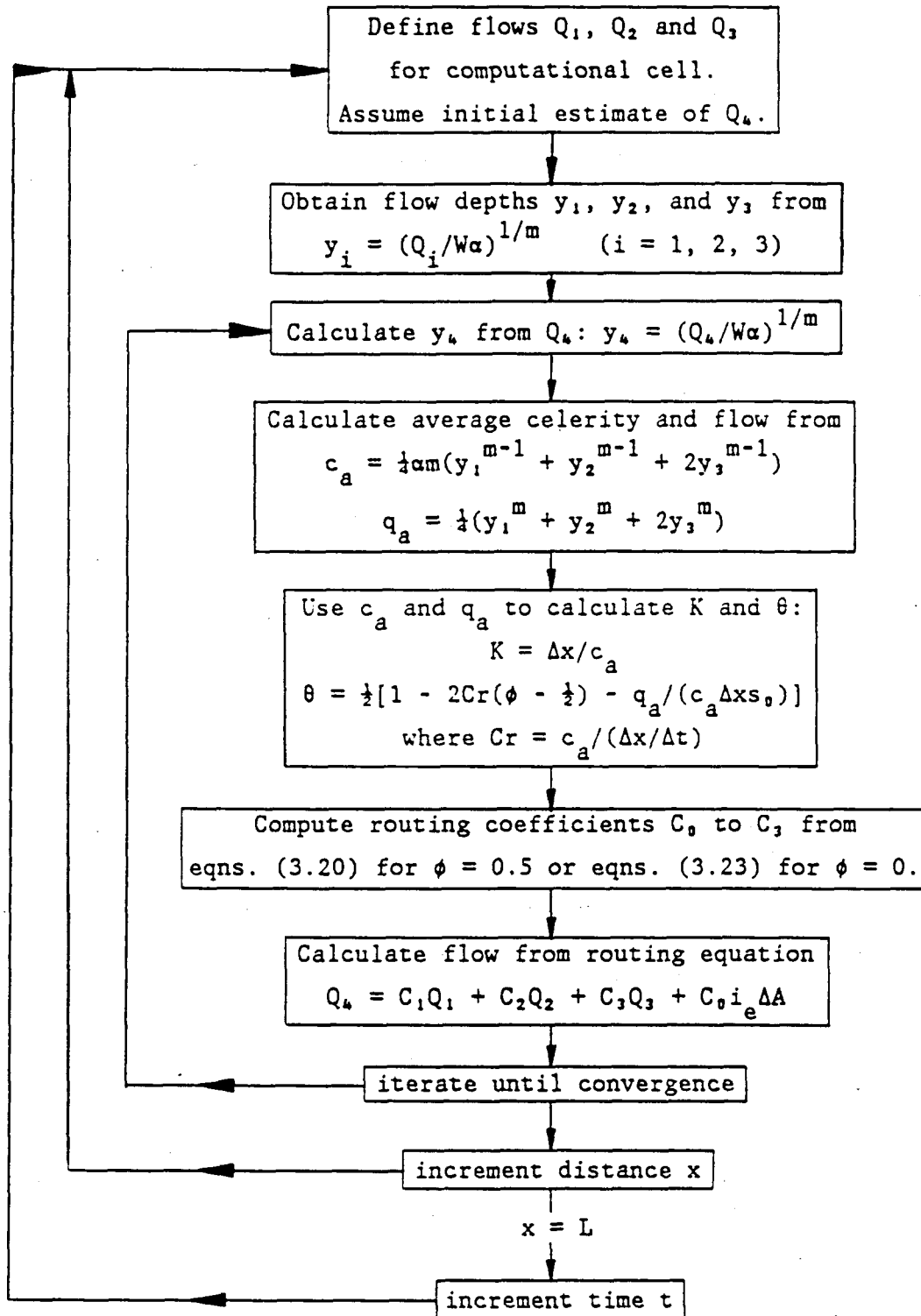


Figure 3.20: Algorithm for iterative Muskingum-Cunge formulation.

Eqns. (3.30) and (3.31) therefore become

$$c_a = \frac{1}{2} \alpha m (y_1^{m-1} + y_2^{m-1} + y_3^{m-1} + y_4^{m-1}) \quad (3.35)$$

$$\text{and } q_a = \frac{1}{2} \alpha (y_1^m + y_2^m + y_3^m + y_4^m). \quad (3.36)$$

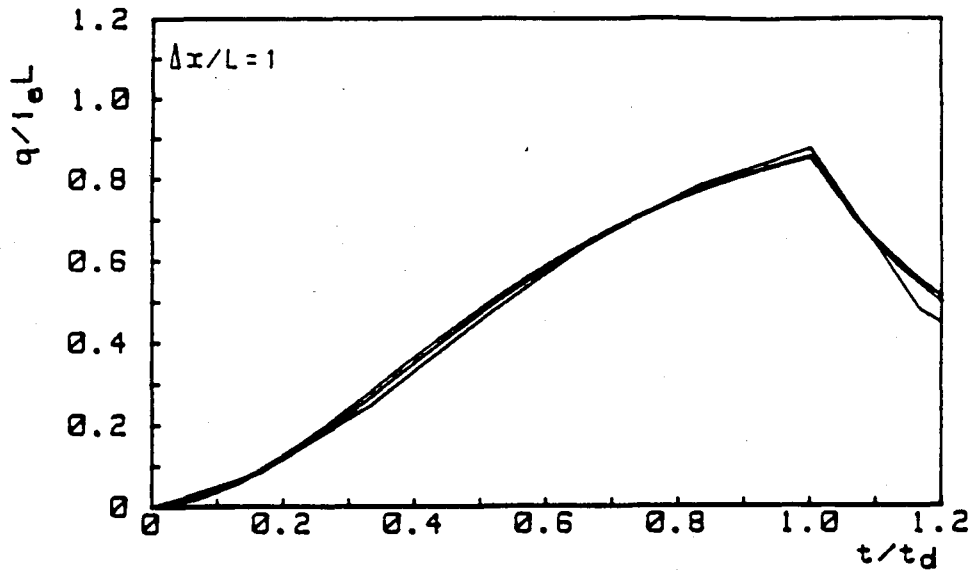
The computational algorithms are shown in figs. 3.19 and 3.20 for the non-iterative and iterative solutions respectively. Computation proceeds downstream and marches forward in time.

For the overland flow plane problem y_1 and y_3 are zero at the start of a simulation because the plain is initially dry. In addition y_1 and y_2 are always zero at $x = 0$. Therefore to avoid computational problems, the non-iterative solution uses the iterative algorithm for the first time step.

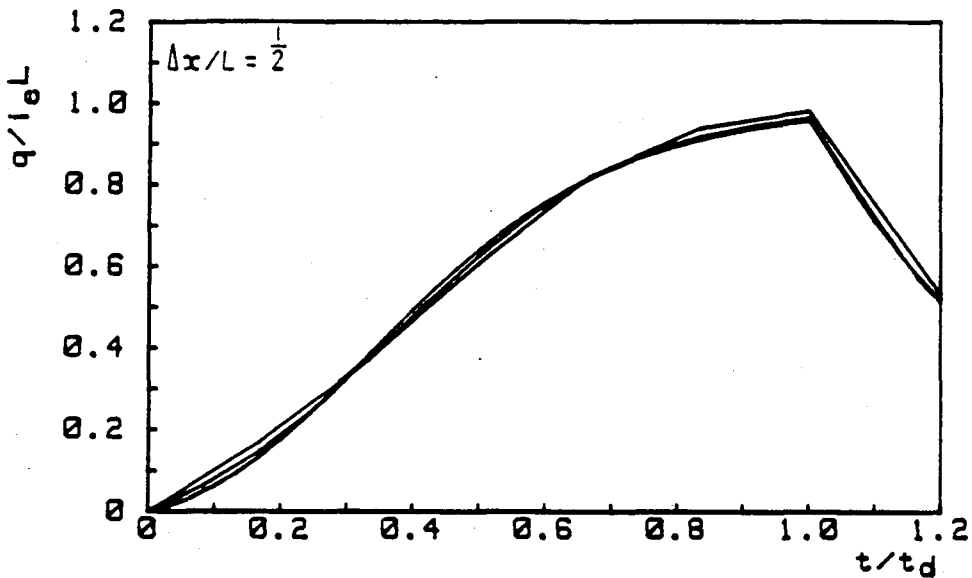
For overland routing the lateral inflow term in eqn. (3.19) becomes $C_e i \Delta A$ where ΔA is the plan area $W \Delta x$ (fig. 3.4).

3.4.4. Results of numerical experiments

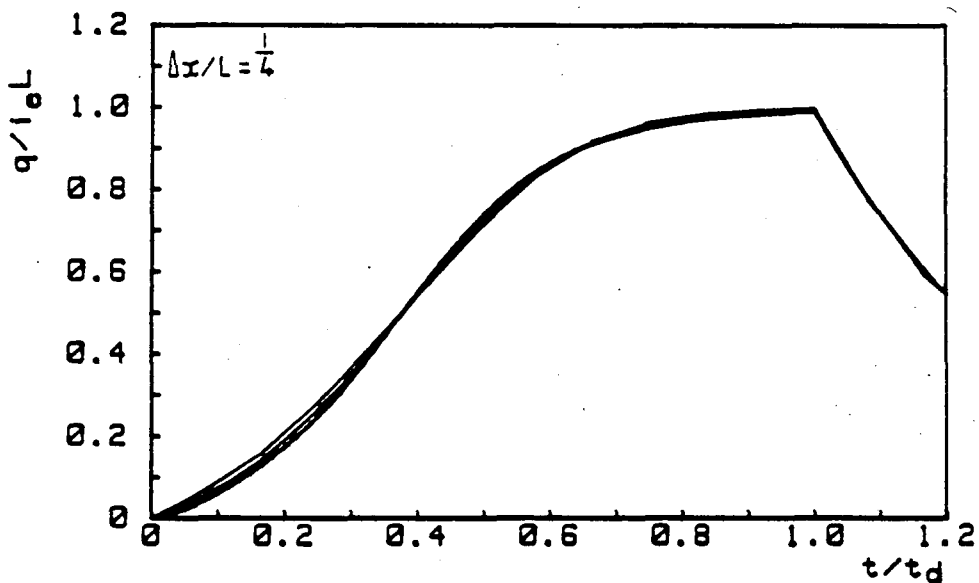
Four different Muskingum-Cunge formulations were tested on the overland flow plane problem: the $\phi = 0.5$ and $\phi = 0$ formulations presented above, each with an iterative and a non-iterative algorithm. It was found that the $\phi = 0$ and $\phi = 0.5$ solutions yielded the same numerical results, with the $\phi = 0$ solution carrying the advantage of unconditional stability. The iterative algorithm did not show any noticeable improvement over the non-iterative one. The results were all virtually the same, and hydrographs generated using the $\phi = 0$, non-iterative algorithm are shown in fig. 3.21 for three levels of spatial discretization. The curves for different grid spacings are seen here to coincide, and the parasitic waves are not present in this formulation.



(a) $\Delta x = 100$ m



(b) $\Delta x = 50$ m



(c) $\Delta x = 25$ m

Figure 3.21: Hydrographs generated using the Muskingum-Cunge formulation with $\phi = 0$ and the non-iterative algorithm.

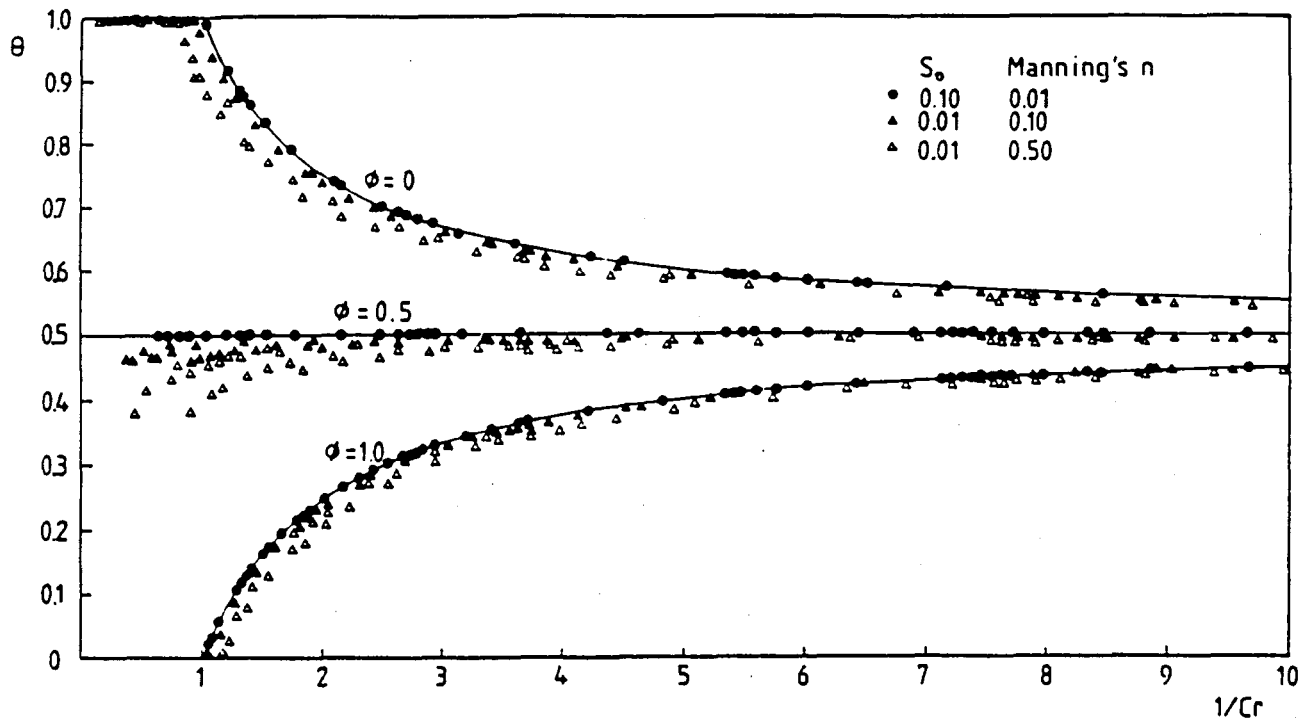


Figure 3.22: θ -relationship of eqn. (3.13) shown as solid curves, with θ -values generated by eqn. (3.24) superimposed as discrete points.

Before closing the Muskingum-Cunge finite difference study an observation will be made regarding the necessity of the last term in eqn. (3.24) in overland routing applications. Fig. 3.22 shows values of θ generated by eqn. (3.24) in modelling planes of various slopes and roughnesses. The plotted values of θ hardly deviate from the curves given by eqn. (3.13), indicating that a kinematic wave is generally satisfactory for overland flow. Only for rough surfaces with gentle slopes does attenuation start becoming important and under these circumstances the Muskingum-Cunge approach of eqn. (3.24) provides a refinement.

3.5. WEIGHTED BACKWARD DIFFERENCE

The third type of formulation to be studied will be referred to as the Weighted Backward Difference formulation. It can be argued that a finite difference scheme propagating information in the direction of flow should be used for the kinematic equations, because of the single, forward characteristic that is implied by the kinematic characteristic equations (Constantinides, 1982). Such a finite difference scheme does not fit into either of the previous categories because it breaks away from the Preissmann "box".

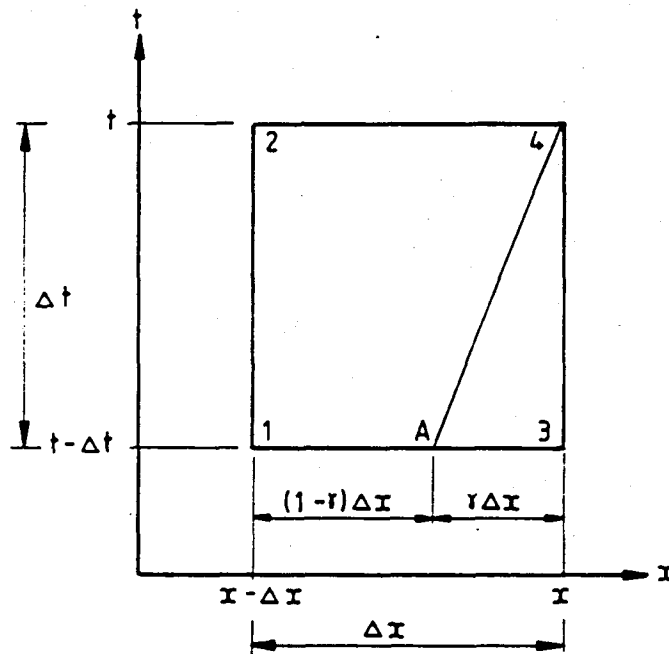


Figure 3.23: Computational cell defining weighting coefficient γ for the Weighted Backward Difference.

Fig. 3.23 illustrates the means of determining the temporal derivative ($\partial y / \partial x$) in the continuity equation using a forward characteristic. Flow depth at point 4 is obtained from the flow depth at point A such that the slope of line AB is the same as the slope of the characteristic. Taking the flow depth at A as a weighted average of depths at points 1 and 3 with γ as the weighting coefficient, line AB will match the characteristic if γ is given by

$$\gamma = \frac{c}{\Delta x / \Delta t} = Cr. \quad (3.37)$$

Using this approach for the temporal derivative and the conventional treatment of the spatial derivative, the finite difference formulation is given by

$$\frac{\phi(q_3 - q_1) + (1 - \phi)(q_4 - q_2)}{\Delta x} + \frac{y_4 - [\gamma y_1 + (1 - \gamma)y_3]}{\Delta t} = i_e \quad (3.38)$$

Note that point 2 in the computational cell does not appear in the expression for the temporal derivative. Solving for y_4 gives

$$y_4 = i_e \Delta t + \gamma y_1 + (1 - \gamma)y_3 - [\phi(q_3 - q_1) + (1 - \phi)(q_4 - q_2)] \Delta t / \Delta x \quad (3.39)$$

which is solved by Newton Raphson as described previously for the Standard formulation. This scheme will be evaluated in the next section using measured runoff data.

3.6. EVALUATION OF FINITE DIFFERENCE FORMULATIONS USING MEASURED RUNOFF DATA

The accuracy of the 3 basic approaches to finite difference formulations for the kinematic equations is now evaluated using measured overland flow data. The recorded runoff hydrograph of Morgali (1970) is used, for a turf plane 22 m long subject to a uniform simulated rain for 28 minutes. The pertinent parameters are listed in table 3.4.

Table 3.4: Data of Morgali (1970).

Parameter	Value
length L	21.95 m
slope s_0	0.01
Manning's n	0.39
rainfall i_e	96.8 mm/h
rainfall duration	28 mins

In preceding sections the effects of varying $\Delta x/\Delta t$ for a constant Δx have been studied in order to isolate the influence of grid spacing on numerical diffusion from the effect of Δx on accuracy. For application to hydrological modelling it is of interest to see the effect of various levels of catchment discretization on accuracy, which corresponds to $\Delta x/L$ in the present routing exercise. A modeller needs to know how finely a hillslope should be discretized in order to ensure accurate and realistic results. Consequently the results presented below were obtained by keeping Δt fixed (at 84 seconds) and varying Δx .

Standard formulation

The Standard formulation was applied to the above problem with ϕ set at zero and using a variable θ for optimum accuracy. The results obtained using various values of Δx are shown in fig. 3.24 together with the data of Morgali (1970). It can be seen that the value of Δx chosen for a simulation affects the hydrograph shape although the peak at equilibrium remains the same. The numerical solution approaches the measured data

points as Δx is decreased, which is consistent with a converging formulation. Using more than 2 Δx 's results in the parasitic waves identified previously. Using 1 or 2 Δx 's gives a smooth solution but at the expense of accuracy, resulting in over-predicted runoffs on the rising hydrograph limb.

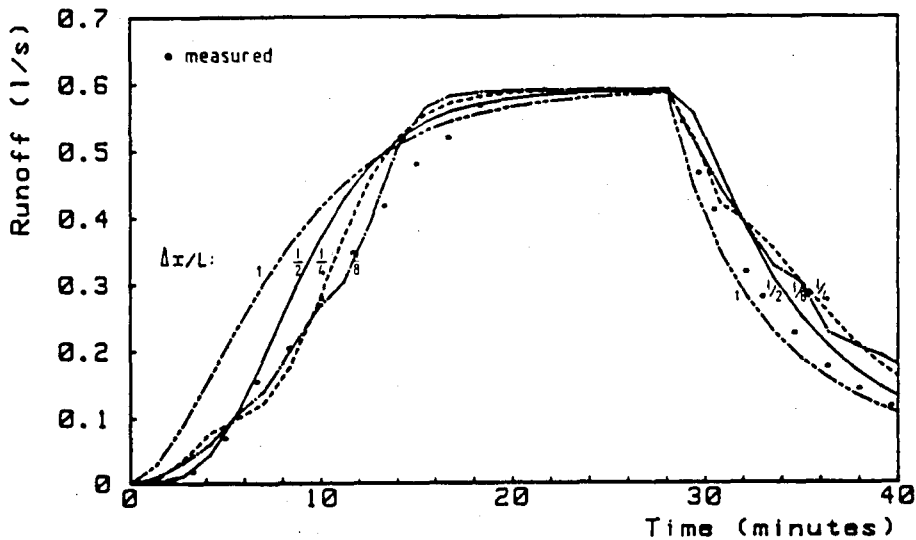


Figure 3.24: Standard formulation with $\phi = 0$ and variable θ compared with the data of Morgali (1970).

Muskingum-Cunge formulation

Fig. 3.25 shows the results obtained using the Muskingum-Cunge formulation with the data points of Morgali (1970) superimposed. The non-iterative formulation with coefficients based on $\phi = 0$ was used here, with $\Delta x = 1.37\text{m}$ ($\Delta x/L = 1/16$). The good fit with the measured hydrograph shows that Muskingum-Cunge routing can produce accurate results. The slight over-prediction on the falling limb and at the base of the rising limb of the hydrograph is because of lamina effects. According to Morgali (1970) lamina flow occurs in these regions whereas the resistance equation $q = \alpha y^{5/3}$ models turbulent flow.

The effect of Δx on the solution is shown in fig. 3.26. In the Standard formulation (fig. 3.24) the solution approached the rising limb of the hydrograph from the left; the Muskingum-Cunge formulation is seen here to approach it from below, converging on the true solution as Δx decreases. At least 4 Δx 's are required for an accurate solution.

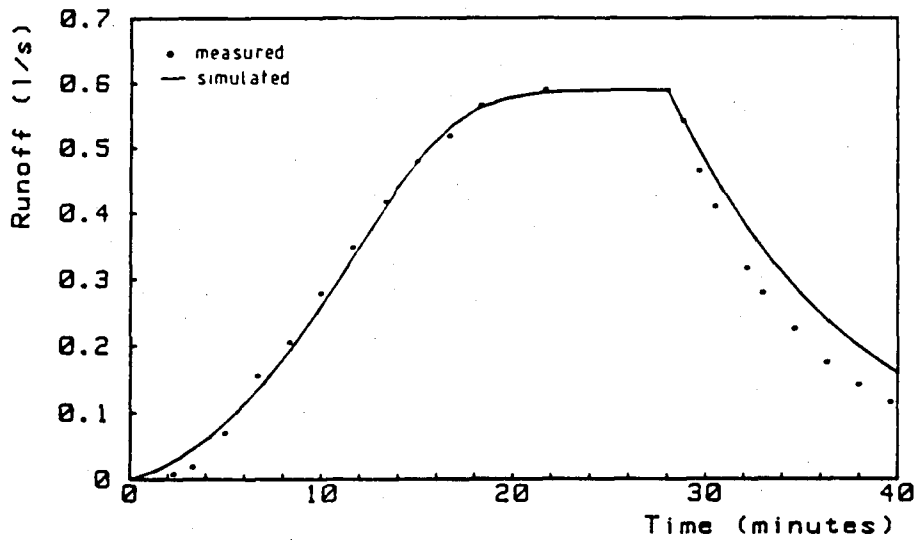


Figure 3.25: Muskingum-Cunge formulation with $\Delta x = 1.37$ m compared with the runoff data of Morgali (1970).

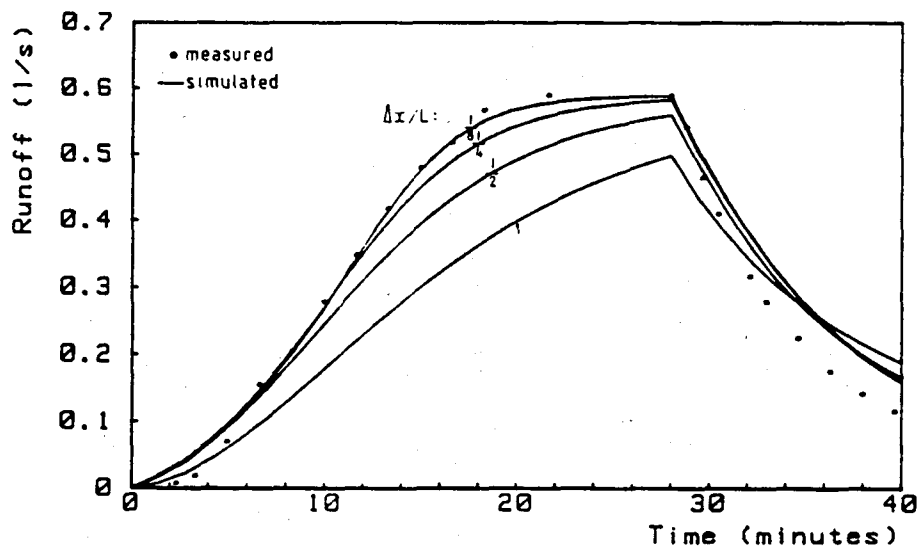


Figure 3.26: Effect of spatial resolution on Muskingum-Cunge formulation.

Weighted backward difference

This formulation was found to converge on a solution that greatly under-predicts the runoffs. This is illustrated in fig. 3.27 using $\phi = 0$, where the predicted equilibrium runoff is about half the true runoff. This is consistent with the findings of Constantinides (1982) who observed the same behaviour with an explicit ($\phi = 1.0$) formulation. This property of the scheme renders it unsuitable for modelling purposes.

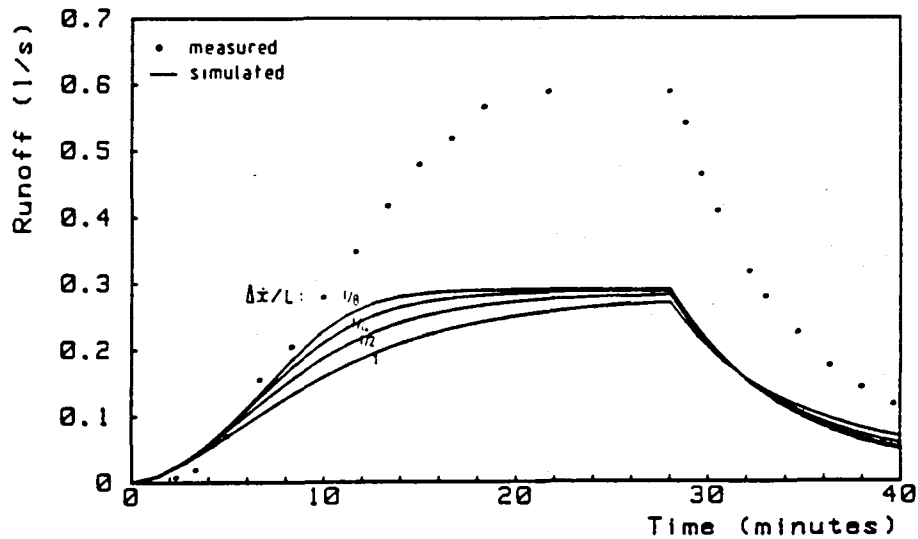


Figure 3.27: Weighted Backward Difference with $\phi = 0$.

Table 3.5: Summary of finite difference studies.

Formulation	Convergence	Parasitic waves	Numerical diffusion (N.D.)
Standard formulation	converges as Δx decreases	present for $\Delta x/L < \frac{1}{2}$	Uncontrolled N.D. is present except for $\theta = \phi = 0.5$.
Standard formulation, variable θ	converges as Δx decreases	present for $\Delta x/L < \frac{1}{2}$	No N.D., i.e. true kinematic solution.
Muskingum-Cunge	converges as Δx decreases	not present	Controlled N.D. used to model attenuation.
Weighted backward difference	non-convergent	not present	Uncontrolled N.D. renders the solution invalid.

3.7. SUMMARY AND CONCLUSIONS

The generalised treatment presented in this chapter for finite difference modelling of the kinematic equations is intended to enhance current understanding of this subject, with conclusions that have specific relevance to the development of the hydrological simulation model in the present study.

The two necessary criteria for numerical stability were identified, namely a grid-spacing criterion and the von Neumann criterion. The latter limits the upper-value of θ , depending on the grid spacing, the celerity and the value of ϕ . It is illustrated in fig. 3.9.

The grid-spacing criterion corresponds to the Courant criterion for explicit schemes ($\phi = 1.0$) but the critical grid spacing was shown to decrease as ϕ decreases. An argument was presented showing that only when $\phi = 0$ is a formulation unconditionally stable. Consideration will be given extensively to this factor throughout this work when developing finite difference schemes for various hydrological processes. A variable time increment is used in this model because of the advantages in terms of computing economy. Therefore to ensure numerical stability over a wide range of time increments, finite difference schemes for overland, channel, reservoir and soil moisture routing will all be based on $\phi = 0$.

The diagram for θ was introduced showing curves for θ as a function of grid spacing for various values of ϕ (fig. 3.10). It was shown that a scheme based on the Preissmann box should use a θ that varies in accordance with this diagram, since this eliminates uncontrolled numerical diffusion. Schemes reported in the literature are generally based on a constant θ . In the light of fig. 3.10, a scheme can be evaluated and its accuracy and behaviour at various grid spacings can be predicted, as illustrated in section 3.3.4.

Three approaches to finite difference formulations were studied, namely the Standard formulation, the Muskingum-Cunge formulation and a Weighted Backward Difference, and the findings are summarised in table 3.5. The Muskingum-Cunge approach was found to be the most acceptable. The weak-

ness of the Standard formulation is the generation of parasitic waves, affecting the water surface profile and the hydrograph shape, and the Weighted Backward scheme severely under-predicts runoff. The Muskingum-Cunge scheme is convergent, is not susceptible to parasitic waves, and has the additional advantage of *an explicit formulation being possible for any ϕ -value*, with savings in computation time. For these reasons the Muskingum-Cunge approach was adopted for both overland and channel routing in the simulation model as will be discussed further in the relevant chapters.

Some runoff models (such as SWMM, Huber *et al*, 1982) base computations on the assumption that Δx equals the "overland flow length", i.e. $\Delta x/L = 1$. The results of the study in section 3.6 show that this yields inaccurate runoff predictions, and that a hillslope should be divided into a number of elements Δx for modelling purposes. This supports the division of subcatchments into smaller elements as done in the element approach to catchment discretization in the present work.

Chapter 4: OVERLAND ROUTING COMPONENT

The overland routing component of the hydrological simulation model is for routing surface runoff that results from excess rain. In this chapter a brief overview is given of common approaches to overland flow routing, followed by discussions on the suitability of the kinematic equations and of Manning's equation to overland flow. The Muskingum-Cunge algorithm used in the model is then described, and finally a means of accounting for the effect of rilling and channelisation on runoff is presented.

4.1. APPROACHES TO OVERLAND ROUTING

Techniques for overland flow computations in hydrological models consist mainly of isochronal methods and physically-based kinematic and diffusion methods.

Isochronal techniques include the rational method, unit hydrographs, linear reservoirs and time-area routing. They are generally suited to manual flood computations, but have been used extensively in computer simulation models. Many of the early hydrological models were merely computer codings of manual computation techniques in use at the time.

Isochronal "coefficient" methods for predicting peak storm water runoffs were the first attempts at storm water calculations. The most well-known of these is the rational method (Kuichling, 1889) in which all losses are lumped into the rational coefficient.

The unit hydrograph was reported by Sherman (1932). It is based on the assumption that for a given duration of rain and a constant land use, the same unit response will result for a given catchment. Nash (1957) developed the linear reservoir concept in which a catchment flow system is conceptualised as a series of linear storage elements.

Time-area routing makes use of isochrones to subdivide a catchment into zones with the same travel time to the outlet. The runoff from each zone is routed to the outlet using discrete time increments.

Isochronal techniques have been successfully used in hydrological models, for example unit hydrographs in CELMOD (Diskin, 1984) and time-area routing in ILLUDAS (Terstriep and Stall, 1974). However, in the 1970's there was a trend towards physically-based kinematic routing, which has since gained general acceptance among hydrologists as a runoff computation tool (Hromadka *et al*, 1987; Ponce, 1986). It involves a finite difference solution of the kinematic equations as described in chapter 3. Meadows (1984) compared kinematic and isochronal methods and concluded that models using kinematic theory for overland routing are among the most reliable. Authors such as Green (1984) and Stephenson and Meadows (1986) believed kinematic routing to be superior to isochronal techniques because of its physical basis.

Kinematic routing has several distinct advantages over isochronal methods. The latter are all based on assumptions of linearity, whereas kinematic routing accounts for the non-linearity of runoff by using a flow resistance equation to relate flow rate to flow depth. Kinematic routing can also cater easily for spatial variations in catchment characteristics, and both spatial and temporal variations in rainfall intensity. Cascading planes can be modelled easily. One of the greatest advantages of kinematic routing is that the parameters have a physical interpretation because of the physical basis of the approach.

A few recent physically-based models have used a diffusion routing algorithm for overland flow, for example the SHE model (Abbot *et al*, 1986 b). Hromadka *et al* (1987) compared kinematic and diffusion routing for overland flow predictions, and found them to produce almost identical results except at very gentle slopes (less than about 0.2 to 0.4%) where diffusion affects are important. Both kinematic and diffusion routing are physically-based, and for the present simulation model to be comparable with the state of the art physically-based models, a finite difference formulation of a suitable approximation to the hydrodynamic equations

must be used. In this study the kinematic approximation is used with a refinement for diffusion.

4.2. SUITABILITY OF THE KINEMATIC EQUATIONS FOR OVERLAND FLOW

Kinematic theory was introduced by Lighthill and Whitham (1955) and was used by Henderson and Wooding (1964) to study the runoff hydrograph resulting from excess rain on a sloping plane. Woolhiser and Liggett (1967) investigated the conditions under which the kinematic approximation holds for overland flow. Analytical solutions to the equations have been obtained for planes of various geometries and specific rainfall patterns (for example Hjelmfelt, 1981). Constantinides (1982) outlines the development of models using numerical solutions to the kinematic equations.

A consideration of the momentum equation is useful for defining various levels of approximation of flow routing methodologies:

$$s_f = s_0 - \frac{\partial y}{\partial x} - \frac{v}{g} \frac{\partial v}{\partial x} - \frac{1}{g} \frac{\partial v}{\partial t} \quad (4.1)$$

Henderson (1966) showed that the last two terms (acceleration terms) are generally an order of magnitude smaller than $\partial y/\partial x$. Stephenson and Meadows (1986) demonstrated by manipulating the terms in eqn. (4.1) that the acceleration terms are often either insignificant or cancel one another out. Neglecting them results in the diffusion approximation in which the term $\partial y/\partial x$ accounts for changes in the water profile. In the kinematic approximation, the diffusion term is omitted as well, giving the simplified equation $s_f = s_0$. Dynamic flood routing models include all the terms. In overland flow the term $\partial y/\partial x$ is generally at least an order of magnitude smaller than the ground slope s_0 (Stephenson, 1981) and the kinematic approximation is valid. In a catchment the depth of overland flow might typically vary by a few millimetres over a length of

100 m, whereas the elevation can vary by a meter or more over the same length.

The validity of the kinematic approximation for overland flow was examined by Woolhiser and Liggett (1967) who developed a dimensionless kinematic flow number:

$$k = \frac{s_0 L}{y_0 Fr_0} \quad (4.2)$$

where s_0 and L are the slope and length of a uniform rectangular plane subject to steady rainfall, y_0 is the flow depth at the downstream end of the plane at equilibrium, and Fr_0 is the corresponding Froude number. A k -value approaching infinity corresponds to the analytical solution of the kinematic equations being an exact solution. Woolhiser and Liggett (1967) found that for $k > 10$ the kinematic equations provide a good approximation to the full hydrodynamic equations. Morris and Woolhiser (1980) extended this to $kFr_0^2 > 0.5$. Table 4.1 shows values of k and kFr_0^2 for a plane of length 100 m with excess rain 50 mm/h, for ranges of slope s_0 and roughness (Manning's n) typically encountered in overland flow applications. Clearly both conditions are easily fulfilled, supporting the validity of the kinematic equations for overland routing.

Table 4.1: Values of k and kFr_0^2 for a range of ground slopes and roughness applicable to overland flow.

slope s_0	Manning's n	k	kFr_0^2
0.01 (1%)	0.10	1 900	52
	0.40	10 000	23
	0.70	20 000	16
0.10 (10%)	0.10	4 800	1034
	0.40	25 100	450
	0.70	49 200	320

Qualitatively, the kinematic equations approximate the flow well at large values of the kinematic number (eqn. 4.2) which correspond to steep bed

slopes (s_0) and small flow depths (y_0), both of which are true for overland flow. The same conclusions can be made from criteria developed by Ponce *et al* (1978) for the selection of kinematic and diffusion models.

Ross *et al* (1979) gives an extensive list of investigators who have verified the applicability of the kinematic approximation for overland flow. Ponce (1986) commented on the common use of the kinematic equations for simulation of overland flow, pointing out that they generally lead to physically realistic solutions without the computational complexities of full dynamic formulations.

Fig. 3.22 in chapter 3 illustrates that for most overland flow situations, physical diffusion is negligible, and it only becomes important for gently sloping, very rough surfaces. The weighting coefficient θ in the Muskingum-Cunge finite difference formulation of the kinematic equations can be adjusted by eqn. 3.25 to cater for such diffusive properties, constituting a refinement of kinematic routing.

4.3. SUITABILITY OF MANNING'S EQUATION FOR OVERLAND FLOW

Physically-based diffusion or kinematic routing of overland flow necessitates the use of a friction equation together with the continuity equation. There are various factors that complicate overland flow, such as raindrop impact, laminar and turbulent flow regimes, spacing of roughness elements, and the effect of rainfall intensity on the roughness coefficient. Chen (1976) presents a comprehensive review of these aspects of overland flow. The simple single-coefficient equations such as those of Manning and Chezy were originally developed for channel flow and need critical appraisal for application to overland routing.

Many researchers have developed complex models and relationships for overland flow, such as Kouwen and Li (1980) who tried to model physical characteristics of the stiffness and spacing of individual vegetation elements, and Rovey *et al* (1977) who used a two-stage friction law for overland flow that switches from laminar to turbulent flow. Chen (1976) considered the effect of raindrop impact on the roughness coefficient.

Most researchers agree that laminar, turbulent and transitional flow regimes are encountered in overland flow (Engman, 1986). Generally flow changes from laminar to turbulent and back to laminar through the rise and recession of a hydrograph. However, Overton (1971) points out that the critical Reynold's number between laminar and turbulent flow is difficult to assess, and the situation is made more complex by the fact that the transition from laminar to turbulent flow varies both in time and space on an overland flow plane. Such considerations discourage the use of complex models for overland flow routing.

Research has shown that although the friction factor varies at the low Reynolds numbers encountered in overland flow, friction equations with a constant roughness coefficient (such as Manning's 'n' and Chezy's 'C') representing average conditions over the rise and fall of a hydrograph, are adequate for practical applications. Podmore and Huggins (1980) attempted to describe surface roughness by means of a description of micro-topography, using spectral analysis, amplitude separation techniques and area/wetted-perimeter methods. The resulting models were complex and Podmore and Huggins (1980) concluded that the results from the complex models were not much better than single parameter models (Manning and Chezy) for modelling field situations. Foster *et al* (1968) found that a constant roughness coefficient gives results that are equally as good as a variable coefficient accounting for the effects of changing flow regimes. Engman (1986) concluded that the simple one-parameter models such as Manning and Chezy using a constant roughness coefficient appear to work well in field situations.

The present study therefore uses Manning's equation without any special modifications, with the roughness coefficient user-specified according to land use. Engman (1986) observed that the roughness coefficient is actually an effective coefficient that includes the effects of raindrop impact, flow channelisation, frictional drag over the surface, erosion and transportation of sediment, and obstacles such as litter, crop ridges, rocks and tillage roughness. A comprehensive set of Manning's n values reported in the literature for various natural and agricultural surfaces is presented in Appendix A.

4.4. ALGORITHM FOR OVERLAND ROUTING

Chapter 3 presented an in-depth study into finite difference schemes for the kinematic equations, using overland flow problems to illustrate the properties of different numerical schemes. Of the schemes studied it was found that the Muskingum-Cunge scheme was preferable to the Standard formulation and the Weighted Backward difference for the following reasons:

1. The Muskingum-Cunge formulation is not prone to the parasitic waves inherent in the Standard formulation.
2. The Muskingum-Cunge formulation converges on the true solution as Δx is decreased, whereas the Weighted Backward difference is non-convergent.
3. An explicit (non-iterative) algorithm is possible with the Muskingum-Cunge approach, greatly reducing computation time.

Consequently the Muskingum-Cunge algorithm based on $\phi = 0$ described in section 3.4 was adopted for the overland routing component of the model. It was found in chapter 3 to under-predict peak runoffs if only one or two Δx -increments were used to model a plane, but this does not pose a problem in the present application since each hillslope is divided into a number of elements as shown in fig. 4.1. For each element, Δx is the average length of the overland flow path perpendicular to the topographical contours, and the width W is the average element width. In the simulation program this information is obtained from the digitised topographical input data.

The $\phi = 0$ algorithm was found to be necessary to prevent numerical instability when using the small Δx 's shown in fig. 4.1. The Muskingum-Cunge algorithm was found to be computationally fast and provides a kinematic solution with a refinement for diffusive properties of the flow, namely the term $-q/\Delta xcs$, in the expression for θ , which matches numerical diffusion to physical diffusion. This is not true diffusion routing because a single-valued rating relationship is used, but according to the discussion in section 4.2 above, it is adequate for overland flow computations.

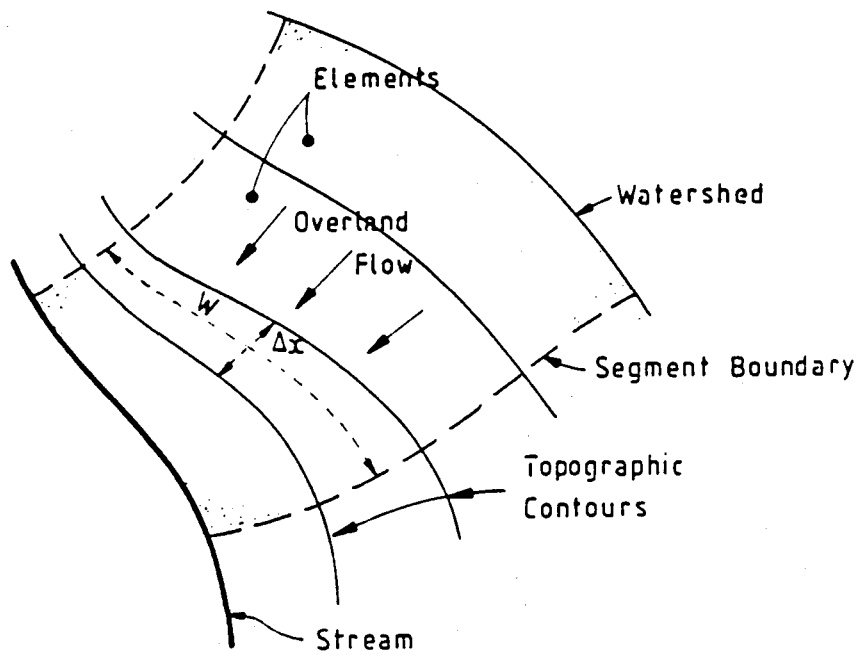


Figure 4.1: Subdivision of a hillslope into elements for defining Δx and W in overland flow.

Muskingum-Cunge routing has a well-known tendency to generate negative flows during low-flow conditions at the base of a hydrograph (Weinmann and Laurenson, 1979; Hjelmfelt, 1985). A check was incorporated into the program coding to prevent this occurrence without loss of accuracy. It was found that setting Q_u equal to $C_e i_e W \Delta x$ on the generation of negative flows, was preferable to setting $Q_u = 0$, the former resulting in more realistic hydrograph shapes.

In the program coding, interception and infiltration losses are abstracted as follows before calling the overland routing subprogram:

$$\text{net rain } (i_n) = \text{gross rain} - \text{interception loss}$$

$$\text{excess rain } (i_e) = \text{net rain} - \text{infiltration loss}$$

Interception loss is described in chapter 7. Ponding in surface depressions on the ground can be catered for by incorporating the ponding depth into the foliage interception capacity. Infiltration losses are

computed using Green and Ampt infiltration which is described in chapter 6 on subsurface processes.

4.5. RILL STUDY

4.5.1. Channelisation of overland flow

An assumption implicit in kinematic or diffusion routing of overland flow is that surface runoff occurs in a thin sheet of water such that the flow depth in a lateral cross-section is uniform over the width of the flow plane. However in reality such a sheet of water rarely occurs because surface runoff generally collects in rivulets or rills. Cook (1946) described the sequence of events that occur during overland flow, which may be summarised as follows:

- (1) A thin layer of water forms on the surface and downslope surface flow is initiated.
- (2) The flowing water collects in surface depressions.
- (3) When full, these depressions begin to overflow.
- (4) The overland flow enters micro-channels, which combine to form rills, which in turn combine to form rivulets, which discharge into major drainage channels.
- (5) Along each collecting micro-channel, lateral inflow from the land surface takes place.

Surface runoff thus has a micro-channel flow component and can be conceptualised as a combination of sheetwash and channel flow (Foster, 1982). Some kind of adjustment should therefore be made to the overland routing component of a simulation model if the presence of rills is to be taken into consideration.

The small channels in which overland flow concentrates are generally referred to as *rills* and *gullies*, rills being somewhat smaller than gullies. Foster (1982) gives a distinguishing criterion which states that a rill becomes a gully if its depth exceeds 300 mm.

Conditions favouring the formation of rills and gullies include agricultural practises such as tillage, concentration of runoff from a field by

topography, the presence of foot-paths and cattle-tracks, erodable soils, and poor vegetation cover. Rills are typically studied in the context of erosion and sedimentation models rather than in runoff quantity models. The present study, however, focuses on the influence of rills on generated runoff hydrographs. The following discussion relies on a visual assessment by the modeller of the extent of rilling in a study-area, not on dynamic modelling of the erosion and sedimentation processes affecting the occurrence and size of rills. The discussion is also applicable on a larger scale to lumped subcatchments drained by a number of streams but represented by a single segment for computing economy.

4.5.2. Accounting for channelisation by width-adjustment

One way of artificially altering runoff hydrographs is by adjusting the width of the overland flow plane. If a *reduced* width is used in the overland routing equations to relate total discharge to unit-width discharge, and the *true* width is used for computing incident rainfall ($i_e W \Delta x$), then the water levels will be increased. These increased flow depths result in less attenuation and hence a reduced time to equilibrium. In this way a width-adjustment can be used to alter the shape of a runoff hydrograph.

Such an approach was used here to account for the effect of channelisation on overland flow. Let the width-factor k be defined as the ratio of the adjusted width of an overland flow element to its physical width. The modified overland flow depth resulting from the width-adjustment can be viewed as an equivalent depth giving the same runoff as the combination of the overland and rill flows on the rilled surface. The width-factor k was incorporated as an input parameter in the simulation program. The actual ground surface areas are used in the program to compute rainfall input and infiltration loss, but the adjusted width of each element is used in the overland routing equations, replacing the width W in equation (3.32) with kW .

The user-specified values of the width-factor k must be judiciously chosen according to the degree of rilling on a rilled surface. Guidelines for choosing appropriate values of k were developed experimentally by study-

ing two cases, namely parallel and branched rills as illustrated in fig. 4.2. These two land segments were finely discretized and the overland and channel flows resulting from incident rainfall were modelled by the simulation program. Runoff hydrographs obtained in this way were compared with the hydrographs obtained assuming a simple overland flow plane with no rills or channels, and k-values were chosen for the latter by trial such that the generated hydrographs matched. In all the experiments a constant excess rainfall intensity of 50 mm/h was used, and the results checked at higher intensities to verify their consistency. The results of parallel and branched rill studies are presented separately below.

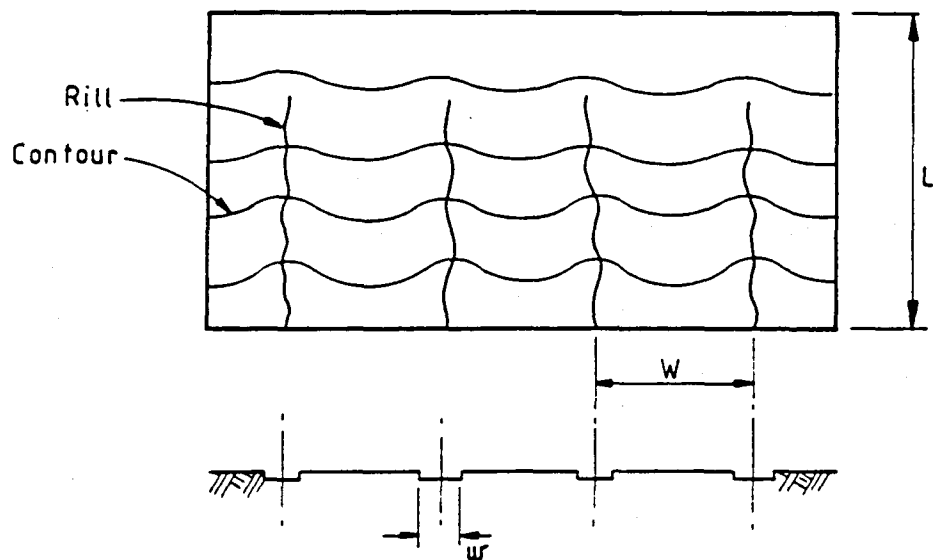
4.5.3. Parallel rills

The land segment shown in fig. 4.2(a) was used with the length L set at 100 m, the rill spacing W set at 60 m, and the rill width w variable. The factors affecting the width-ratio k are the rill or channel dimensions and the hydraulic roughness of the rill relative to that of the overland flow. k-values were therefore determined for a range of values of the ratio w/W , and for different ratios of Manning's n in the channel to Manning's n for overland flow (n_c/n_o). The results are presented in fig. 4.3.

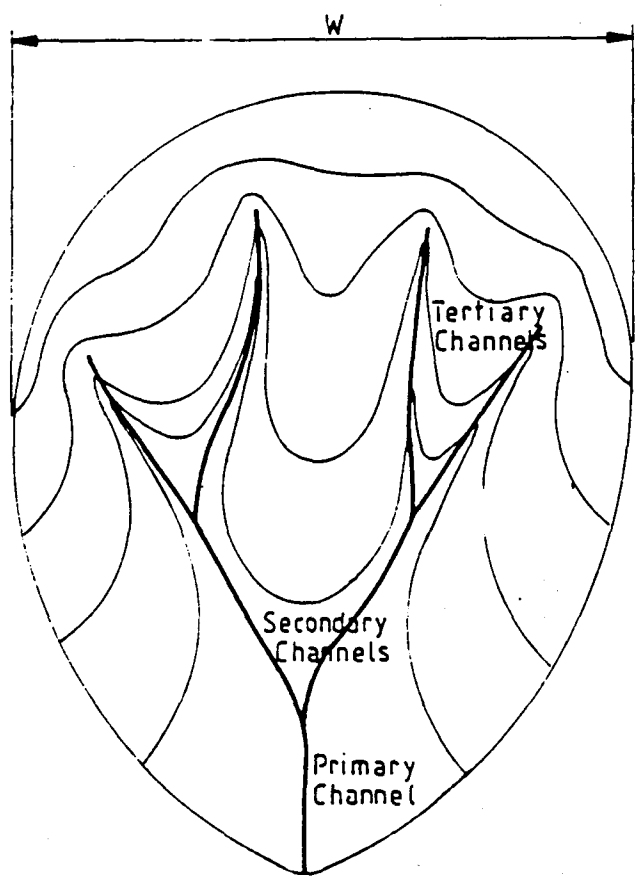
The curve for $n_c/n_o = 1.0$ shows increasing k-values as the ratio w/W increases. As w/W approaches 1.0 the k value approaches unity, implying no width modification if the rill occupies the full width of the land segment, in which case pure overland flow occurs with no channelisation.

The k-values in fig. 4.3 generally reflect a very good fit between the runoff hydrographs generated using rigorous modelling of the rilled surface, and those generated using pure overland flow with a width adjustment. For very smooth rills (n_c/n_o around 0.05) the fit was not as good but still acceptable.

The use of the dimensionless parameter w/W means that fig. 4.3 can be used for any size of subcatchment to obtain a value of the width-factor k. For small subcatchments the user of the model needs to assess the average rill size (w) and spacing (W), and select a k-value according to the hy-



(a) Parallel rills



(b) Branched rills

Figure 4.2: Channelisation patterns used in rill study.

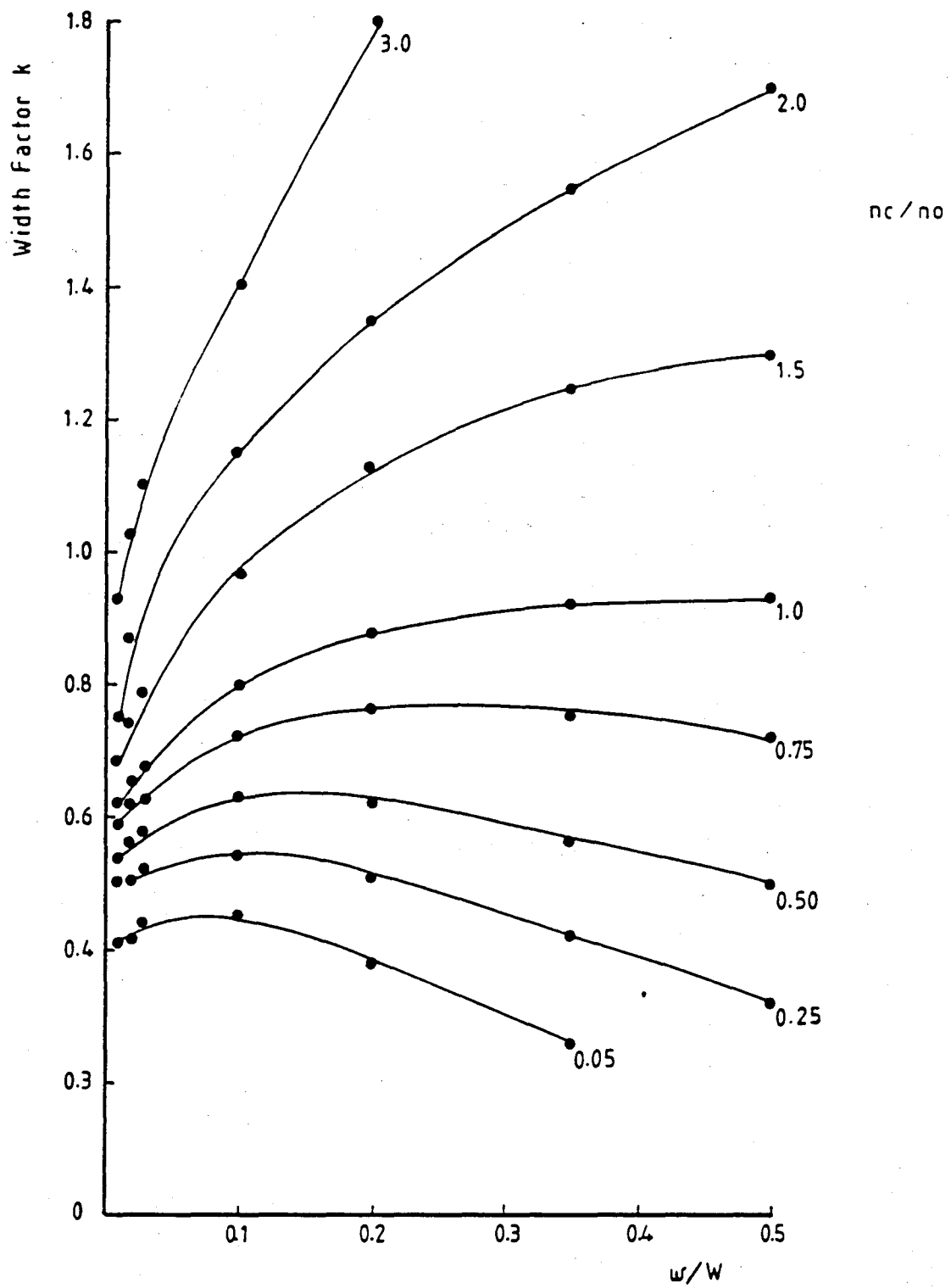


Figure 4.3: Width-factors for parallel rills.

draulic roughness of the rills relative to the overland (interrill) roughness. (The Manning's coefficient for interrill conditions (n_o) corresponds to the model input parameter for overland flow.) For larger subcatchments, w and W become the average stream width and spacing respectively.

4.5.4. Branched rills

The branched rill problem is more complex to analyse than parallel rills because of the large number of possibilities with regard to subcatchment shape and the configuration of the rill network. Since an exhaustive study of different shapes and configurations would be beyond the scope of this study, a representative case as shown in fig. 4.2(b) was used to develop the guidelines for width-factors in branched rill or channel systems. A land segment of width 10 m (W) and area 100 m² was used, with the channel widths increasing from $w/2$ in their upper reaches to w at the outfall. The value of w was varied from 100 mm to 1 m and the roughness ratio n_c/n_o was varied from 0.10 to 1.50. The k -factors found by this procedure were scaled up to obtain the results shown in table 4.2. The validity of these results was checked at larger catchment scales and at higher rainfall intensities. Since width W is dependant on the shape of a watershed, the subcatchment area is included in the first column of the table as an indication of the scale. For a given problem the appropriate size category is selected and then a k -value chosen according to prevailing rill or stream conditions, interpolating between the values listed in the table if necessary. Hydrograph fits were generally excellent except for those otherwise indicated with an asterisk.

For both the parallel and branched rill cases it was found that hydrograph shape is not sensitive to small changes in the k -value, and a 10 - 15% uncertainty in the estimation of k is acceptable.

Table 4.2: Width-factors for branched channel configuration.

Subcatch size category	Channel type and size	n(channel)/n(overland)			
		0.10	0.50	1.0	1.5
Width 10m, area 100m ²	Small rills, 100 - 150 mm wide	0.11	0.42	0.95	1.40
	Large rills, 300 - 500 mm wide	0.13	0.46	0.92	1.45
	Gullies 800 - 1000 mm wide	0.19	0.66	1.26	1.90
Width 100m, area 10000m ² (1ha)	Small deep rills, 100-150mm wide	0.27*			
	Large rills, 300-500mm wide	0.14	0.60*		
	Gullies, 1m wide	0.10	0.43	1.00*	1.40**
	Streamlets, 5m wide	0.15	0.50	0.97	1.50
	Large streams, 10m wide	0.20	0.70	1.35	2.00
Width 1km, area 1km ²	Deeply incised streamlets, 1m wide	0.30*			
	Streams 5m wide	0.12	0.58*		
	Large streams 10m wide	0.10	0.43	1.00*	1.40**
	Small rivers 20m wide	0.11	0.40	0.85	1.40
	Large rivers 60m wide	0.16	0.54	1.03	1.60
	Large rivers 100m wide	0.20	0.70	1.35	2.00
Width 10km, area 100 km ²	Deep streams 10m wide	0.30*			
	Small rivers 20m wide	0.22*			
	Large rivers 60m wide	0.11	0.53*		
	Large rivers 100m wide	0.10	0.43	1.00*	1.40**
Width 50km, area 5000km ²	Rivers 60m wide	0.30*			
	Rivers 100m wide	0.22			

* Hydrograph fit is acceptable but not exact.

** Recommended k-value, but fit is poor.

Note: Channel sizes refer to primary and secondary rills or streams.

4.6. SUMMARY

The overland routing component of the simulation model comprises a non-iterative Muskingum-Cunge finite difference algorithm together with the width-adjustment for rilling and channelisation. Features unique to this study are the width-adjustment procedure and the use of Muskingum-Cunge routing coefficients based on the weighting coefficient $\phi = 0$. The latter is important for ensuring numerical stability over a range of time increments, and because of the small values of the length increment Δx resulting from subdividing subcatchments into elements. These small Δx 's would result in numerical instability if a numerical scheme with ϕ greater than zero was used. The algorithm was found in the present application to constitute a computationally fast approach predicting physically realistic flows.

Chapter 5: CHANNEL AND RESERVOIR ROUTING

Flood routing is the process whereby the spatial and temporal variations of a flood wave are predicted as it travels down the stream network of a catchment. Any ponds, lakes or man-made reservoirs occurring in the channel network must be included in the routing process. Channel routing is a major component of the present hydrological simulation model since the channels collect all the surface runoff and convey it to the catchment outlet. Reservoir routing through small dams and ponds is included in the model as illustrated in fig. 5.1, which shows a channel system with reservoirs located at some of the nodes.

Channel routing methods are briefly reviewed below and the Muskingum-Cunge routing method developed for the simulation program is described. An algorithm for reservoir routing is then presented.

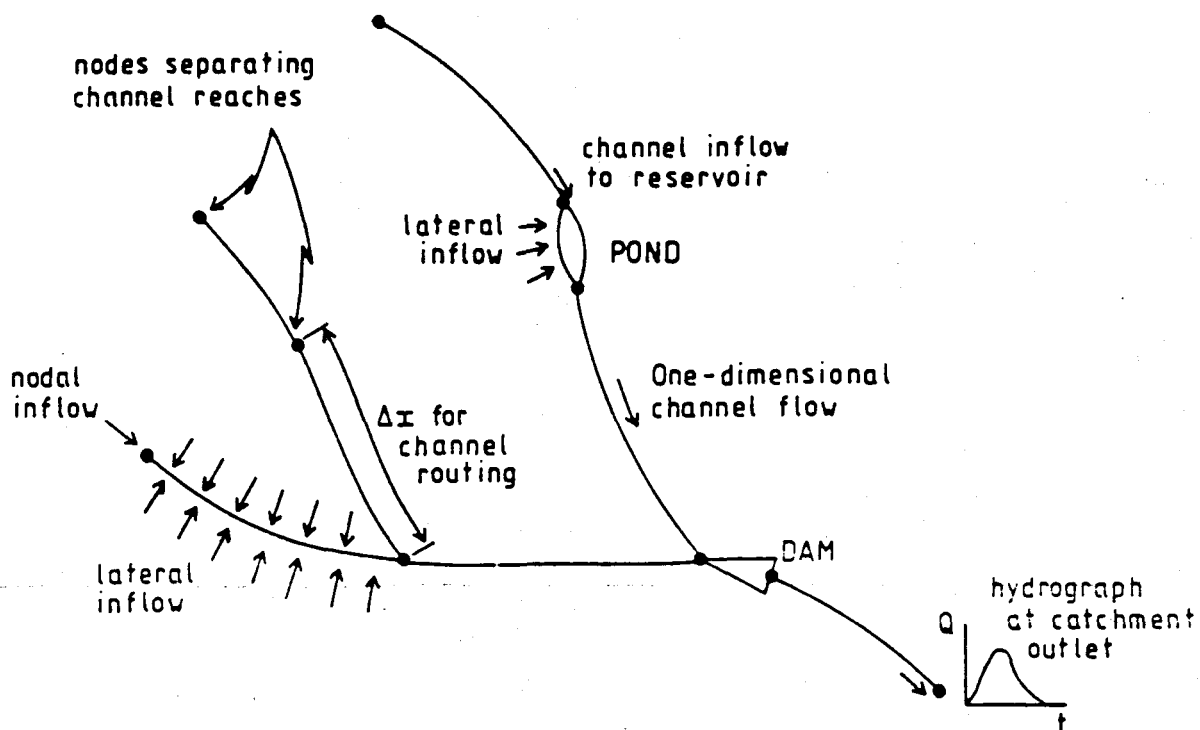


Figure 5.1: Branched stream network of a catchment illustrating flow routing through a system of channels and reservoirs.

5.1. REVIEW OF CHANNEL ROUTING METHODS

Channel routing methods may be categorised as hydraulic or hydrologic. Hydraulic methods attempt to model the actual physical processes with the continuity and momentum equations, while hydrologic models are based on continuity with some means of relating storage to discharge. Channel routing methods used in a number of watershed models are listed in table 5.1.

A well-known hydrologic river routing method is Muskingum routing (Chow, 1964) in which the routing equation is derived from a linear relationship between flow and storage, and the travel time and attenuation parameter are obtained by calibration on observed flood hydrographs. Other hydrologic methods include the Variable Storage Coefficient method, the Modified Puls and the Working R and D methods, which are described by Viessman *et al* (1977). Keefer and McQuivey (1974) compared a number of convolution models, which are simple routing models derived assuming time-averaged values of celerity and dispersion during a flood event. The time shift technique (Constantinides, 1983) lags a hydrograph down a conduit without attenuation using a representative flow velocity to determine the lag time. Variants exist such as the Progressive and Successive Average Lag methods used in HEC-1 (U.S. Army Corps of Engineers, 1973) in which subsets of consecutive inflow rates are averaged before lagging.

Hydraulic routing models employ dynamic, diffusion and kinematic methods, which have been compared by Kolovopoulos (1988). Dynamic models utilising all the terms in the momentum equation are the most rigorous channel routing methods. The momentum and continuity equations are solved simultaneously for flow depth or discharge using explicit or implicit finite difference formulations on a rectangular x-t grid or a characteristic grid. A friction equation such as that of Manning or Chezy relates energy slope to the flow rate and the channel characteristics. Weinmann and Laurenson (1979) point out that the complexity of a full dynamic solution does not necessarily guarantee accurate modelling, because it is still subject to the validity of the assumptions made in the derivation of the

Table 5.1: Channel routing methods used in some watershed models.

Model	Reference	Channel routing method
Stanford Watershed Model	Crawford & Linsley (1966)	hydraulic storage coefficient method
TR-20	SCS (1972)	convex method
HEC-1	US Army Corps of Engineers (1973)	Muskingum, time shift and storage coefficient methods
USGS	Carrigan (1973)	time shift
HYMO	Williams & Hann (1973)	variable storage coefficient
Hydrocomp	Crawford <i>et al</i> (1976)	kinematic method
SWMM	Huber <i>et al</i> (1982)	kinematic method
VSAS2	Bernier (1985)	time shift
WITWAT	Green (1984)	time shift and kinematic
SHE	Abbot <i>et al</i> (1986b)	diffusion wave method
WITSKM	Stephenson (1989a)	kinematic method

Saint-Venant equations, and irregularities in natural channels have to be catered for empirically in the roughness coefficient. Dynamic models place large demands on computer resources as well as on the quantity and quality of input data, prompting modellers to seek approximate hydraulic models based on diffusion and kinematic approximations to the momentum equation (eqn. 4.1).

Models based on the diffusion approximation generally either solve a non-linear system of equations using the same numerical methods as used for a complete dynamic model, or utilise an equation of the convective diffusion type as follows:

$$\frac{\partial Q}{\partial t} + c \frac{\partial Q}{\partial x} - D \frac{\partial^2 Q}{\partial x^2} = cq_i \quad (5.1)$$

c is the wave celerity, q_i is the lateral inflow rate, D is the diffusion coefficient, and Q , x and t are flow rate, distance and time respectively. Eqn. 5.1 is obtained by combining the continuity equation and the diffusion approximation of the momentum equation. It is referred to as a

diffusion analogy because it is of the same form as that describing convective diffusion of a pollutant. If the coefficients are fitted to observed hydrographs then the diffusion coefficient can account for effects of channel irregularities and flood plain storage. The diffusion term $D(\partial^2Q/\partial x^2)$ is responsible for the attenuation of a flood wave (Henderson, 1966) and allows for a looped rating curve.

Kinematic models employ the simplest approximation to the momentum equation, equating the energy slope to the bed slope and omitting all smaller order terms. This implies the use of a single-valued rating relationship. Kinematic models therefore allow for a shift in time and a change in shape of an inflow hydrograph, but not attenuation (although random attenuation may be introduced by uncontrolled numerical diffusion as discussed in chapter 3). The term *kinematic* is used because the models are based on concepts of water movement as embodied in the continuity equation, but neglect consideration of the forces causing the movement, which are embodied in the momentum equation. Although kinematic routing does not account for attenuation, its popular use in watershed models can probably be ascribed to the relative simplicity and physical basis of the approach as well as the rise in popularity of the kinematic equations for overland routing.

Muskingum-Cunge routing was shown by Weinmann and Laurenson (1979) to be a general approach encompassing a number of approximate hydraulic models, and was recommended as one of the best approximate methods short of using a full dynamic solution. Although derived from the kinematic equations, Muskingum-Cunge routing is more general than a kinematic model because attenuation is accounted for through the numerical methods used. As such it constitutes a second order approximation to the diffusion analogy (Cunge, 1969) and can even be upgraded to a diffusion wave model by employing a looped rating relationship.

Weinmann and Laurenson (1979) studied the relative magnitude of the terms in the momentum equation and showed that a diffusion wave approximation is sufficient for a wide range of channel flow applications. This is because the acceleration terms are typically small in magnitude and tend

to cancel each other out, as illustrated in table 5.2. These observations were verified by Henderson (1966) in an analytical study of the equation.

While a kinematic wave model may be satisfactory for overland flow (as argued in section 4.2 of chapter 4), a diffusion model is more appropriate for channel routing where more gentle slopes are encountered and attenuation effects can be significant. Clearly a diffusion model which caters for attenuation would be preferable to a kinematic model while avoiding the rigour and complexity of a full dynamic solution.

The Muskingum-Cunge approach was chosen for the channel routing component of the present simulation program. It lends itself to conduit routing in a watershed model because, unlike the conventional diffusion model, it does not require a downstream boundary condition. For this reason Price (1978) used a Muskingum-Cunge approach in preference to a diffusion model for flood routing in rivers, finding the Muskingum-Cunge method to be computationally fast and to give good predictions of flood peak attenuation and hydrograph shape. The Muskingum-Cunge algorithm developed in the present study has the option of being used with either a single-valued or a looped rating relationship. Development of the routing algorithm is presented below.

5.2. MUSKINGUM-CUNGE CHANNEL ROUTING

5.2.1. Routing equations

The Muskingum-Cunge routing equations were derived in chapter 3 using a Preissmann finite difference formulation of the continuity equation with the spatial weighting coefficient ϕ set at 0 or 0.5 and the temporal weighting coefficient θ left variable. The scheme based on $\phi = 0$ is used here because of its advantages in terms of numerical stability. The routing equation is

$$Q_4 = C_1 Q_1 + C_2 Q_2 + C_3 Q_3 + C_0 Q_i \quad (5.2)$$

and the routing coefficients C_0 to C_3 are given by equations (3.23). Q_i is the total lateral inflow along the length Δx of a channel reach, and

Table 5.2: Comparison of terms in the momentum equation*
(after Weinmann and Laurenson, 1979).

Terms	Channel type 1	Channel type 2
bed slope	0.002	0.000 2
diffusion term	-0.000 06	-0.000 17
local acceleration	0.000 025	0.000 014
convective acceleration	-0.000 023	-0.000 013

* Computed for a point midway on the rising limb of a hydrograph routed through a prismatic channel with a Manning's coefficient of 0.04 and a length of 40 km.

constitutes overland runoff and soil moisture seepage from adjacent land segments as shown in fig. 5.1. Q_1 and Q_2 are inflows at the upstream node of each reach, and may come from an upstream channel, reservoir or segment. Computation proceeds downstream along the channel network at every time increment such that Q_a is the only unknown in each reach and can be calculated directly using eqn. (5.2).

For channel routing the expression for θ is given by eqn. (3.24). With $\phi = 0$ this equation becomes:

$$\theta = \frac{1}{2} [1 + c_a \Delta t / \Delta x - Q_a / (B_a c_a \Delta x s_f)] \quad (5.3)$$

in which the subscript 'a' indicates average values for the computational cell, and B is the surface width of the water. The other symbols are as previously defined.

In seeking a suitable means of evaluating the average celerity c_a , two methods were investigated, one explicit and the other implicit. In the following discussion a single-valued rating relationship is assumed initially and provision for a looped rating curve is dealt with further on.

5.2.2. Explicit algorithm

In outlining the explicit algorithm below, the channel sectional properties are first defined, an expression for evaluating the celerity is then derived, and finally the computational procedure is presented.

For convenience of collecting and entering channel data and ease of computation, the simulation model allows for the specification of channel dimensions (width and bank slope) rather than a table relating flow area to stage, which would require detailed surveying of channel cross-sections. The algorithm is not limited to rectangular channels but allows for trapezoidal cross-sections with sloping river banks. Manning's equation is used with the sectional properties calculated as follows:

$$A = y(b + ky) \quad (5.4)$$

$$B = b + 2ky \quad (5.5)$$

$$P = b + 2y(k^2 + 1)^{\frac{1}{2}} \quad (5.6)$$

A, B and P are the flow cross-sectional area, surface width and wetted perimeter respectively as indicated in fig. 5.2. y is flow depth, b is the bottom channel width and k represents the bank slope (1 vertical to k horizontal units).

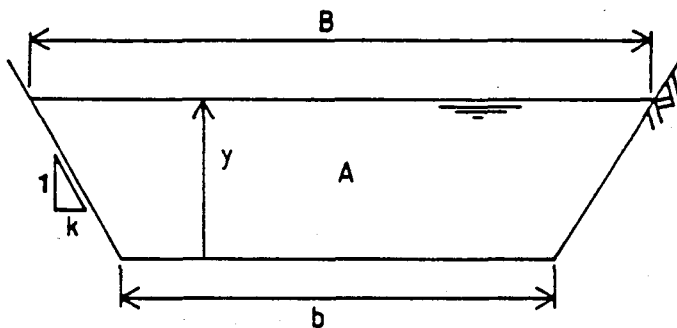


Figure 5.2: Trapezoidal channel cross-section.

In the explicit algorithm, c_a in eqn. (5.3) is evaluated as an average of the celerities at grid points 1, 2 and 3 in a computational cell (fig.

3.2.). Manning's equation is employed below to obtain an analytical relationship with which the celerity at each grid point may be calculated.

Celerity is defined as dQ/dA which can be written using the chain rule as

$$c = dQ/dA = (dQ/dy)(dy/dA). \quad (5.7)$$

Manning's equation may be expressed as

$$Q = \alpha AR^{m-1} \quad (5.8)$$

where $\alpha = s_0^{1/2}/n$, n is Manning's roughness coefficient, R is the hydraulic radius equal to A/P , and m is a constant with a value of $5/3$ for turbulent flow. Differentiating (5.8) with respect to area A , combining with eqn. (5.7) and using equations (5.4) to (5.6) gives an expression relating celerity to channel and flow properties:

$$c = \alpha R^{m-1} [m - 2(m - 1)R(k^2 + 1)^{1/2} B^{-1}]. \quad (5.9)$$

Eqn. (5.9) reduces to the equation for a wide channel or overland flow, $c = \alpha m y^{m-1}$, if y is substituted for R , and B approaches infinity.

The derivation of eqn. (5.9) relies on a single-valued rating relationship (eqn. (5.8)) and therefore neglects the effects of the term $\partial y/\partial x$. Koussis (1976) maintained that this is an acceptable approximation for the computation of celerity since only the increments in Q and A are required, not the actual values.

In the explicit Muskingum-Cunge algorithm, c_a , Q_a and B_a are evaluated as follows for use in eqn. (5.3):

$$c_a = \frac{1}{4}(c_1 + c_2 + 2c_3) \quad (5.10)$$

$$Q_a = \frac{1}{4}(Q_1 + Q_2 + 2Q_3) \quad (5.11)$$

$$B_a = \frac{1}{4}(B_1 + B_2 + 2B_3) \quad (5.12)$$

where c_1 , c_2 and c_3 are calculated using eqn. (5.9).

The computational procedure for each channel reach is as follows:

1. Lateral inflow Q_i is defined from adjacent segments, and upstream inflows Q_1 and Q_2 are defined and used to calculate y_1 and y_2 from a rating relationship. Q_3 and y_3 are known from the previous time step.
2. Eqn. (5.5) is used to calculate B_1 , B_2 and B_3 .
3. c_a , Q_a and B_a are evaluated from eqns. (5.10) to (5.12) with eqn. (5.9) to calculate the celerities.
4. θ is evaluated using eqn. (5.3) with the bed slope in place of s_f .
5. The routing coefficients are calculated from eqns. (3.21) and (3.23).
6. Q_4 is calculated using eqn. (5.2).
7. The corresponding flow depth y_4 is calculated by solving eqn. (5.8) using a Newton-Raphson iterative procedure.

This constitutes an explicit algorithm in which Q_4 can be solved for directly. Iterative solution is only required when conditions in a channel are initially dry ($Q_1 = Q_2 = y_1 = y_2 = 0$), in which case the flow conditions at grid point 4 are included in equations (5.10) to (5.12), and steps 1 to 7 above are repeated a few times until the algorithm converges on a value of Q_4 .

5.2.3. Implicit algorithm

Using finite differences to represent dQ/dA , an expression for the average celerity in a computational cell c_a' can be defined as follows:

$$\begin{aligned} c_a' &= \frac{1}{2} [(\Delta Q/\Delta A)_{x-\Delta x} + (\Delta Q/\Delta A)_x] \\ &= \frac{1}{2} [(Q_2 - Q_1)/(A_2 - A_1) + (Q_4 - Q_3)/(A_4 - A_3)]. \end{aligned} \quad (5.13)$$

Since eqn. (5.13) includes the unknown flow Q_4 , iteration is required to solve the Muskingum-Cunge system of equations for Q_4 . In keeping with an implicit solution, Q_a and B_a for use in eqn. (5.3) are now expressed as

$$Q_a = \frac{1}{4}(Q_1 + Q_2 + Q_3 + Q_4) \quad (5.14)$$

$$B_a = \frac{1}{4}(B_1 + B_2 + B_3 + B_4) \quad (5.15)$$

The computational steps 3 to 7 outlined above are repeated in an iterative loop until convergence is satisfied, using eqns. (5.13) to (5.15) in place of eqns. (5.9) to (5.12).

5.2.4. Algorithm used in simulation program

It was found that the explicit and implicit algorithms gave virtually the same results when applied to routing problems, although the computation time was about 20% longer when using the implicit algorithm. This increased to 45% when using the looped rating relationship described below. Since there appears to be no advantage in using the implicit algorithm, the explicit algorithm was adopted for use in the model.

5.2.5. Looped rating relationship

Only a single-valued rating relationship (eqn. (5.8)) has been considered in the above discussions. A looped relationship provides greater accuracy when modelling mildly sloping streams or slow flowing rivers. Weinmann and Laurenson (1979) and Koussis (1976) successfully used looped rating relationships in conjunction with Muskingum-Cunge routing models. Koussis (1976), Williams (1975) and Henderson (1966) describe looped rating relationships for use with approximate hydraulic models. The method presented below is based in part on the approach of Koussis (1976).

Combining the diffusion approximation of the momentum equation with Manning's friction equation gives the expression

$$Q = n^{-1} AR^{m-1} (s_0 - \partial y / \partial x)^{\frac{1}{2}}. \quad (5.16)$$

Following the approach of Koussis (1976) the term $\partial y / \partial x$ can be written as

$$\frac{\partial y}{\partial x} = \frac{\partial y}{\partial t} \frac{dt}{dx} = - \frac{1}{c} \frac{\partial y}{\partial t}. \quad (5.17)$$

Substituting eqn. (5.17) into eqn. (5.16) gives

$$Q = n^{-1} AR^{m-1} [s_0 + (1/c)(\partial y / \partial t)]^{\frac{1}{2}}. \quad (5.18)$$

The celerity c in eqn. (5.18) is evaluated in the present study using a finite difference form of dQ/dA , and eqn. (5.18) is solved in the form:

$$Q_4 = n^{-1} A_4 R_4^{m-1} s_f^{\frac{1}{2}} \quad (5.19)$$

where

$$s_f = s_0 + \frac{(A_4 - A_3)(y_4 - y_3)}{(Q_4 - Q_3)\Delta t} \quad (5.20)$$

Subscripts 3 and 4 refer to corners of the computation cell as before. Eqns. (5.19) and (5.20) are used to obtain the flow depth y_4 corresponding to the flow Q_4 generated by the Muskingum-Cunge routing algorithm. Q_3 , Q_4 , A_3 and y_3 are known, and A_4 and R_4 are functions of the unknown y_4 . An iterative solution is therefore required, and a Newton-Raphson technique is used for rapid convergence. With this method the estimate of y_4 in the i 'th iteration is calculated from

$$y_4^i = y_4^{i-1} - f(y_4^{i-1})/f'(y_4^{i-1}) \quad (5.21)$$

in which y_4^{i-1} is the value of y_4 in the previous $(i-1)$ 'th iteration, and $f(y_4^{i-1})$ and $f'(y_4^{i-1})$ are the function and its derivative evaluated using y_4^{i-1} . $f(y_4)$ is given by eqn. (5.19) in the form

$$f(y_4) = Q_4 - n^{-1} A_4 R_4^{m-1} s_f^{\frac{1}{2}} \quad (5.22)$$

Differentiating (5.22) with respect to y_4 gives an expression for $f'(y_4)$:

$$f'(y_4) = \frac{-B_4 n^{-1} R_4^{m-1} [m - 2(m-1)R_4(k^2 + 1)^{\frac{1}{2}} B_4^{-1}] A_4 R_4^{m-1} [A_4 - A_3 + (y_4 - y_3)B_4]}{2ns_f^{\frac{1}{2}} \Delta t (Q_4 - Q_3)} \quad (5.23)$$

in which s_f is given by eqn. (5.20). Eqns. (5.21) to (5.23) constitute the looped rating relationship used with the Muskingum-Cunge algorithm. Measures are taken in the coding to prevent instabilities near the tip of a rating curve. The energy slope s_f for use in eqn. (5.3) can only be evaluated once y_4 has been calculated using the rating relationship, and so the Muskingum-Cunge algorithm is repeated once with this value of s_f so as to obtain an improved value of Q_4 .

5.2.6. Application of channel routing algorithm

Performance of the Muskingum-Cunge algorithm presented above is illustrated using a channel routing exercise described by Viessman *et al* (1977) and repeated by Kolovopoulos (1988). Both obtained the same results when routing a triangular hydrograph down a 3.2 km channel reach using rigorous numerical solutions of the hydrodynamic equations. The channel was rectangular in cross-section with a width of 6.1 m, a slope of 0.0015 and a Manning's roughness coefficient of 0.020. The Muskingum-Cunge explicit algorithm described above was applied to the same routing exercise, using the looped rating relationship to relate flow rates to flow depths. Three different values of Δx and a 5-minute time increment were used. The routed hydrograph is shown in fig. 5.3 along with the results of the rigorous dynamic models. The peak flow is slightly over-estimated by the Muskingum-Cunge model, which can probably be ascribed to the dynamic effects that are omitted from the Muskingum-Cunge solution. However the hydrograph shape is well-predicted and the number of sub-reaches (Δx) hardly affects the solution. The corresponding looped rating curves are shown in fig. 5.4. The rating curve generated by the approximate model deviates slightly from the rigorous solution but the general form is maintained.

This comparison of the Muskingum-Cunge algorithm with a rigorous numerical solution of considerably greater complexity indicates that the Muskingum-Cunge formulation gives consistent results that approximate to a dynamic solution. In a watershed modelling application, any errors introduced by using an approximate hydraulic model such as the Muskingum-Cunge approach are offset by uncertainties in estimating channel dimensions, slopes and roughnesses.

Although the use of $\phi = 0$ ensures no lower limit to grid spacing for numerical stability, it was found that there is a constraint on the upper limit. If grid spacing is too large then oscillations are introduced into the routed hydrograph, which are related to the well-known tendency of Muskingum routing to generate negative flows under certain conditions (Hjelmfelt, 1985). It was found that problems occur at large values of

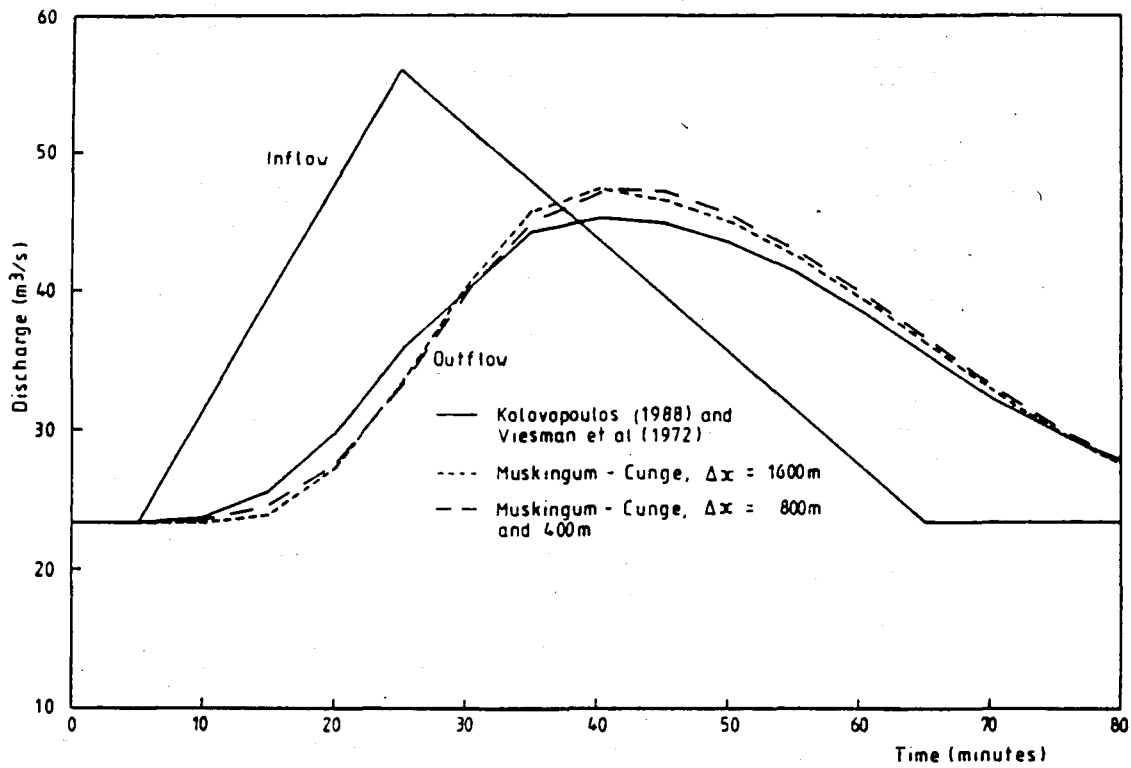


Figure 5.3: Results of flow routing exercise.

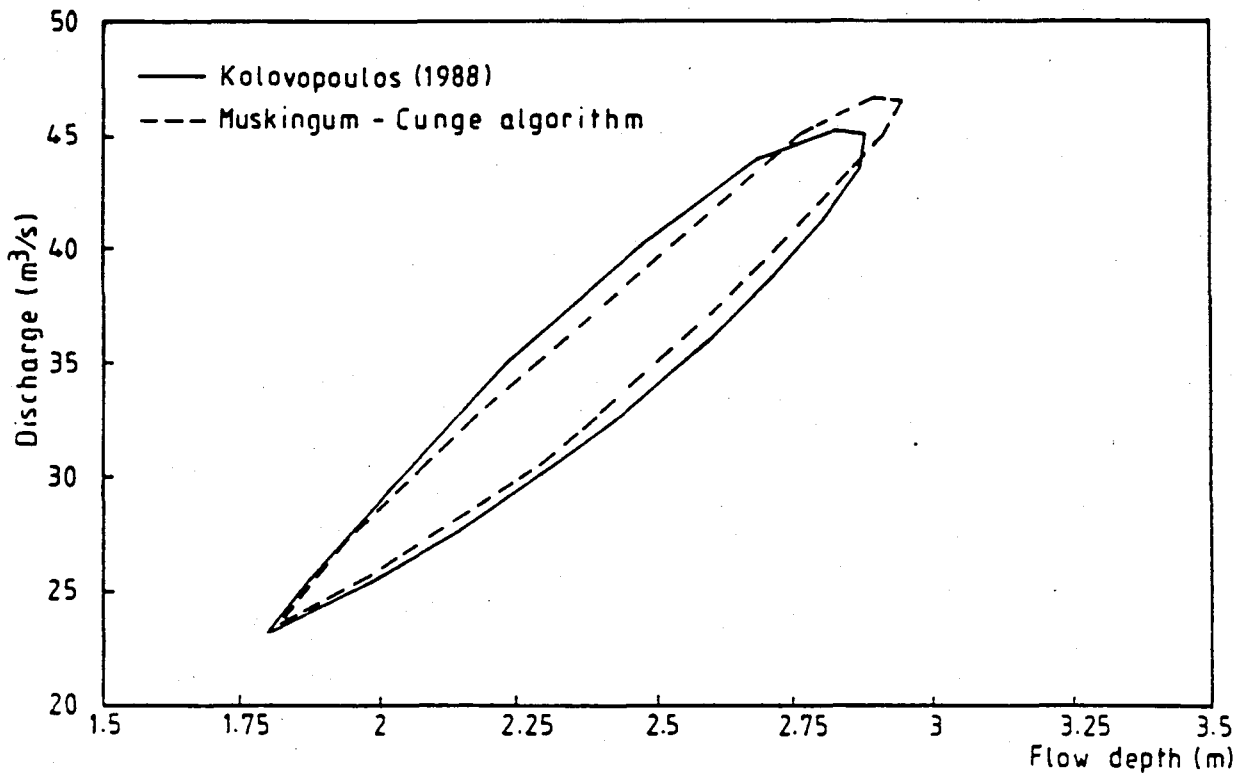


Figure 5.4: Rating curves generated by flow routing models.

$\Delta x/\Delta t/c$ which correspond to long channel reaches at small time increments and low celerity, i.e. primarily the base of the rising hydrograph limb. It was found that with sensible choices of Δx and Δt according to the catchment scale, instability was not encountered. However, this shortcoming should be addressed in future research.

5.3. RESERVOIR ROUTING

As with channel routing, reservoir routing methods may be classified as hydraulic or hydrologic. Hydraulic methods involve a solution of the Saint Venant equations or a suitable approximation, using reservoir cross-sections and hydraulic flow resistance properties as input data. Hydrologic methods such as the storage indication method are considerably simpler, involving the solution of the continuity equation together with the storage/head characteristics of the reservoir and the weir or spillway outflow relationship.

Storage is the cause of attenuation in both channels and reservoirs. Hydraulic methods are preferable for channel routing because of the influence of flow resistance on storage, but in reservoirs the downstream control at the weir or outfall is the dominating control and hydrologic routing methods may be used. The term "level pool" routing is sometimes used because of the assumption that storage from inflowing water is distributed uniformly over the surface area of the reservoir.

The algorithm presented below is based on the widely-used hydrologic storage-indication method (Viessman *et al*, 1977), which has been used in a number of watershed models for their reservoir routing component, for example HEC-1 (U.S. Army Corps of Engineers, 1973), HYMO (Williams and Hann, 1973) and TR-20 (Soil Conservation Service, 1972). For the purpose of the present study, the storage-indication routing equation is re-defined below using $\phi = 0$ for enhanced numerical stability.

Applying a volumetric balance to the element indicated in fig. 5.5 gives the basic relationship from which a routing equation may be derived:

$$Qdt + q_i dxdt - (Q + \partial Q)dt = \partial S . \quad (5.24)$$

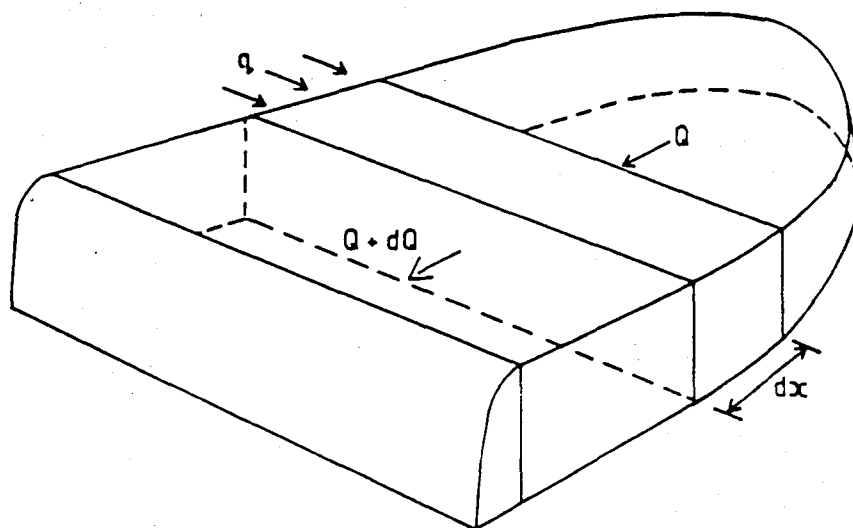


Figure 5.5: Diagrammatic representation of a reservoir.

In this equation q_i includes lateral inflow from creeks along the banks of the reservoir as well as rain incident on the water surface, and ∂S is the incremental increase in storage in a time dt . Manipulating gives the continuity equation in the form:

$$\frac{\partial Q}{\partial x} + \frac{1}{dx} \frac{\partial S}{\partial t} = q_i. \quad (5.25)$$

Expressing the derivatives as finite differences and multiplying throughout by Δx gives:

$$\Delta Q + \frac{\Delta S}{\Delta t} = Q_i. \quad (5.26)$$

If eqn. (5.26) is applied to the reservoir as a whole then the terms take on global values, i.e. Q_i is the total lateral inflow and ΔS is the change in total storage of the reservoir. Eqn. (5.26) may be written in a general finite difference form as follows:

$$\phi(Q_3 - Q_1) + (1 - \phi)(Q_4 - Q_2) + \frac{\theta(S_2 - S_1) + (1 - \theta)(S_4 - S_3)}{\Delta t} = Q_i \quad (5.27)$$

where subscripts 1 to 4 refer to the corners of a computational cell as defined previously in overland and channel routing, and θ and ϕ are the

weighting coefficients used previously in a Preissmann scheme (section 3.1.1 of chapter 3).

From eqn. (5.27) it can be shown that commonly used hydrologic reservoir routing methods implicitly make assumptions regarding θ and ϕ . The basic equation used in the storage-indication method (Viessman *et al*, 1977) is:

$$\frac{1}{2}(I_A + I_B) - \frac{1}{2}(O_A + O_B) = \Delta S/\Delta t \quad (5.28)$$

where I and O represent inflows and outflows respectively, and subscripts A and B refer to the beginning and the end of a time interval Δt . Using symbols compatible with the present study, eqn. (5.28) can be written as

$$\frac{1}{2}(Q_1 + Q_2) - \frac{1}{2}(Q_3 + Q_4) = \Delta S/\Delta t. \quad (5.29)$$

Comparison with eqn. (5.27) shows that $\phi = 0.5$ has been assumed in eqn. (5.29). Furthermore, the use of storage/head and outflow/head relationships imply downstream control, i.e. $\theta = 0$. Weinmann and Laurenson (1979) referred to the use of $\theta = 0$ as "reservoir action" in finite difference schemes because of the large numerical diffusion associated with it.

Although methods as widely used as the storage-indication approach are based on $\phi = 0.5$, the algorithm could be re-defined to advantage using $\phi = 0$ ensuring unconditional numerical stability. Substituting $\phi = 0$ and $\theta = 0$ in eqn. (5.27) and re-arranging terms results in the expression:

$$Q_4\Delta t + S_4 = Q_1\Delta t + S_3 + Q_2\Delta t. \quad (5.30)$$

In this form of the routing equation the unknowns at the end of the current time step are grouped on the left hand side, since S_3 is known from the stage at the previous time step, and Q_2 is the known inflow from the upstream channel reach. The terms are illustrated in fig. 5.6 for clarity. Rainfall, lateral inflow and evaporation loss can be included in Q_1 . Q_4 and S_4 can be related to stage using expressions of the form

$$Q = a_1(h - h_w)^{b_1} \quad (5.31)$$

$$S = a_2h^{b_2} \quad (5.32)$$

in which h is the water stage above the base of the weir, h_w is the height of the overflow weir or spillway, and a_1 , a_2 , b_1 and b_2 are constants. For an overflow spillway, the exponent b_1 is 1.5 and a_1 is the crest coefficient. The constants a_2 and b_2 can be obtained from surveyed profiles or known surface area/stage relationships. b_2 lies between 1.0 and 3.0 depending on the shape of the reservoir basin. The constants in eqns. (5.31) and (5.32) are input parameters for each reservoir in the model.

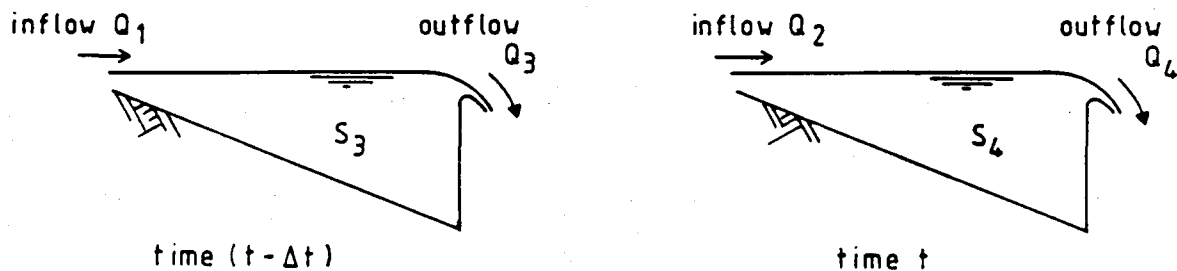


Figure 5.6: Schematic reservoir cross-sections illustrating terms in the routing equation.

The routing algorithm simply evaluates the right hand side of eqn. (5.30) at each time step, and then using eqns. (5.31) and (5.32) for Q_4 and S_4 , solves for h with an iterative Newton-Raphson procedure. For specific applications, different forms of eqn. (5.31) could be used to cater for particular spillway features.

The algorithm based on $\phi = 0$ was found to be more consistently stable than the conventional approach based on $\phi = 0.5$, which gave erratic results at large values of Δt . The algorithm based on $\phi = 0$ forms the reservoir routing component of the simulation model.

5.4. SUMMARY

The Muskingum-Cunge channel routing methodology presented in this chapter constitutes a second order approximation to diffusion routing, and is equivalent to a diffusion model if used in conjunction with a looped rating relationship. The explicit algorithm described in section 5.2.2 forms the channel routing component of the hydrological simulation model, with the user-defined option of using either a single-valued or looped rating relationship. Values of Manning's roughness coefficient for different channel conditions are given in Appendix A.

It was shown that the storage-indication method of reservoir routing is based on a Preissmann-type finite difference scheme with $\phi = 0.5$ and $\theta = 0$. The routing equation was re-derived using $\phi = 0$ with improved numerical stability. This algorithm is used in two of the case studies in Section B: a small weir controlling outflow from the Waterval catchment, and farm dams in the Bethlehem agricultural catchments.

Chapter 6: SUBSURFACE PROCESSES

Subsurface processes in the present context refer to all the hydrological processes occurring beneath the soil surface, including infiltration, soil moisture seepage, interflow and baseflow. Modelling these processes has received considerable attention in hydrological literature because of their importance in the hydrological cycle. Infiltration rates determine the quantity and the time-distribution of surface runoff. Interflow can contribute significantly to streamflows and may even result in a second peak to the runoff hydrograph as observed by Diskin and Green (1985) and Burt and Butcher (1984). In continuous simulations, soil moisture seepages after a rainy period are important for determining soil moisture conditions and hence infiltration rates when rain re-occurs, and baseflows must be accounted for if streamflows are to be modelled during recession periods.

In developing a suitable soil sub-model for the hydrological simulation model, three conceptual steps were followed:

1. Establishing an understanding of pertinent physical processes and basic theory of soil moisture movement.
2. Studying current modelling approaches and techniques.
3. Development of a suitable model by matching its mathematical and computational rigour to the availability of data and model requirements.

These stages in the model development process are reflected in this chapter. A descriptive treatment of the subject and a brief presentation of pertinent theory are followed by an outline of current modelling approaches. The soil model developed in the present study is described and the determination of input parameters is discussed. Finally a means of evaluating antecedent moisture conditions for single event modelling is presented.

6.1. BACKGROUND TO MODEL DEVELOPMENT

6.1.1. Components of hillslope hydrology

The components of hillslope discharge are represented in fig. 6.1. Early hydrological models simply considered infiltration as a loss from the system, whereas more rigorous physically-based modelling approaches attempt to account for soil moisture movements in order to simulate inter-flow and baseflows. An understanding of the mechanisms governing soil water movement and streamflow generation is therefore essential for effective modelling of these components when following a physically-based approach.

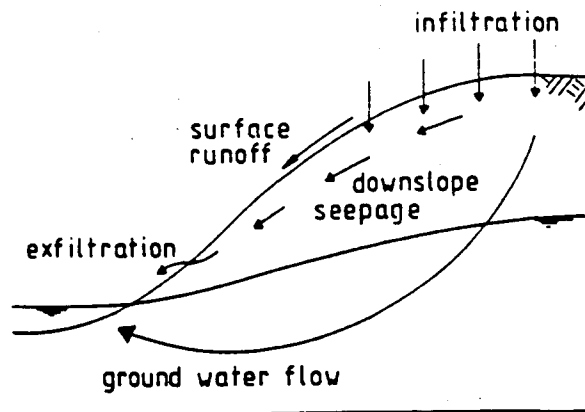


Figure 6.1: Hillslope section showing paths by which water reaches the stream.

The concept of infiltration as an advanced wetting front is well-established in hydrological circles (for example Kirkby, 1978; Haan *et al*, 1982). Pre- and post-ponding conditions have been described by Mein and Larson (1973) and form the basis of infiltration equations such as the Green and Ampt (1911) equation. Dunne (1978) described another mechanism of infiltration that is characterised by a rising saturated layer rather than a downward advancing wetting front. It occurs when a water table is initially near the soil surface and surface saturation is caused by the rise of the water table (Dunne, 1978; Freeze, 1980), or when the soil profile fills up above a flow restricting layer in the soil

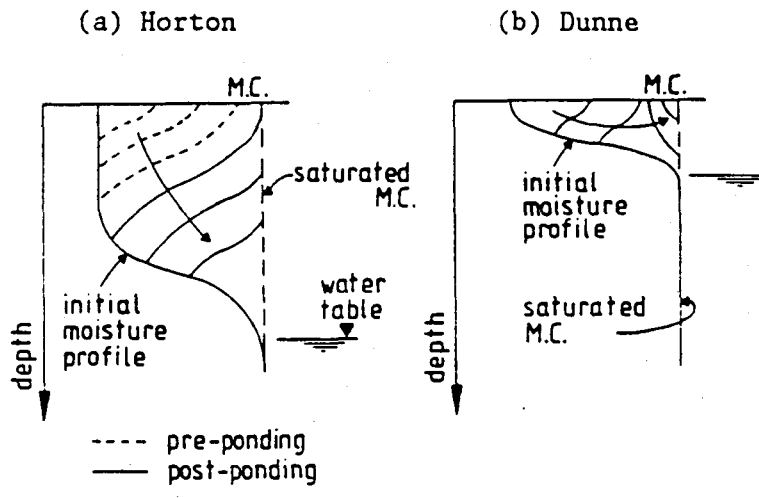


Figure 6.2: Horton and Dunne infiltration (after Freeze, 1980).

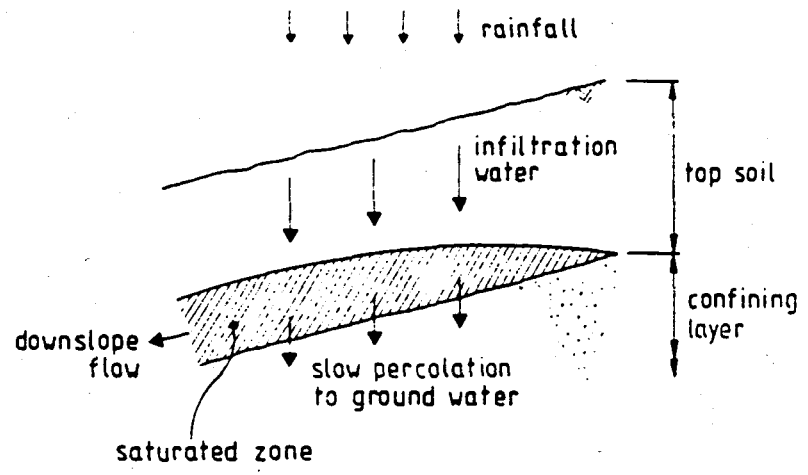


Figure 6.3: Formation of a perched water table (after Kirkby, 1978).

(Smith and Hebbert, 1983). Fig. 6.2 illustrates the difference between the advancing wetting front model (termed "Horton infiltration" after Horton, 1933) and the Dunne mechanism. According to Smith and Hebbert (1983), Dunne-type infiltration is enhanced by shallow soils, convergent topography and extended periods of rainfall.

Interflow is associated with saturated or unsaturated downslope seepage or a perched water table. Conditions favouring interflow include soil layering, piping and microtopographic features forcing soil water to the surface. The mechanism of interflow has been described by Kirkby (1978) as the formation of a saturated zone above a layer of low-permeability soil or where permeability decreases with depth. This induces downslope flow as illustrated in fig. 6.3.

Kirkby (1978) listed the components of hillslope discharge in order of decreasing rapidity of response to rain:

1. *Infiltration excess overland flow.* When the rainfall intensity exceeds the infiltration capacity of the soil, overland flow occurs and dominates the hydrograph peak. This is associated with Horton infiltration.
2. *Saturation overland flow.* This arises from areas in a catchment where the surface has become saturated through the Dunne infiltration mechanism. Response times are slower than for infiltration excess overland flow because of the time taken to saturate the surface before runoff is initiated.
3. *Interflow.* Flow through the soil matrix is significantly slower than surface runoff, but can contribute volumetrically to stormflow hydrographs and may continue providing sustained flows after an event.
4. *Ground water flow.* The saturated flow below a water table may contribute to low flow stream discharge for prolonged periods after the occurrence of rain.

The relative significance of these components in different types of catchments is represented in fig. 6.4 after Freeze (1980), based on the results of numerical model studies. Delayed flows (interflow and ground water) are seen here to give the greatest contributions to storm flow in humid climates, which also favour saturation (Dunne) overland flow. Infiltration excess (Horton) overland flow dominates in other climates. Another major factor influencing stormflow generation is the occurrence of source areas which are discussed in the following section.

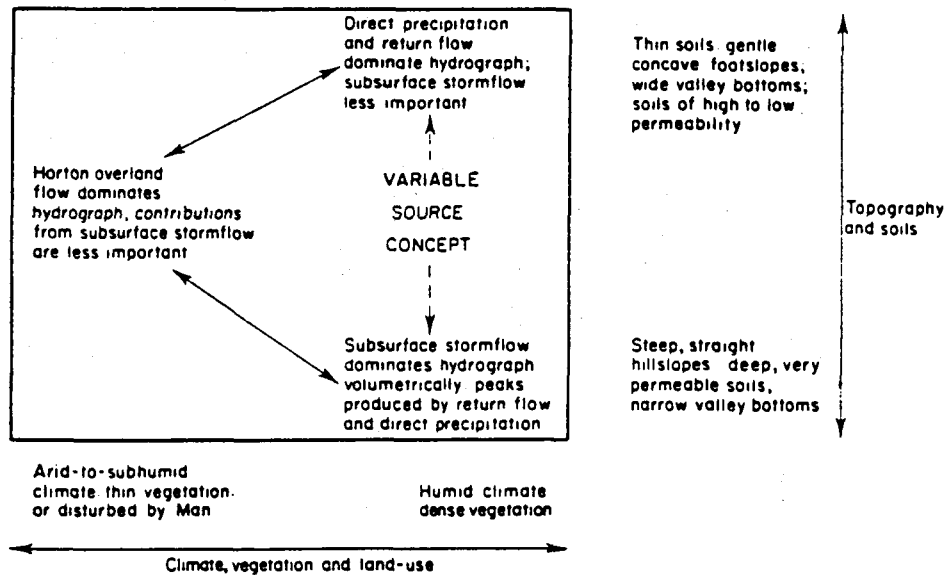


Figure 6.4: Schematic illustration of the occurrence of various runoff processes in relation to their major controls (Freeze, 1980).

6.1.2. Source area concept

The Hortonian concept of infiltration views it as a loss from the system, and runoff is calculated from rainfall less infiltration over the full area of the catchment. However, workers such as Kirkby and Chorley (1967) found that this approach produces linear errors that could be explained by assuming that only the rainfall on a small part of the catchment contributes to runoff during the hydrograph peak. This has led to the contributing source area concept (also referred to as the expanding source area or partial area concept).

Even when vegetation and soil conditions are homogenous, infiltration rates are generally not spatially uniform over a catchment. In areas such as valleys, hollows and narrow regions adjacent to streams, soil moisture accumulates due to throughflow during and after rainy periods. Downslope seepage of soil moisture creates a gradient of increasing soil moisture with primed zones near the streams for a rapid response to rain. The source area concept proposes that these areas provide the main contribution to surface runoff during a storm and collectively constitute the contributing source area. The area may expand upslope during the progress

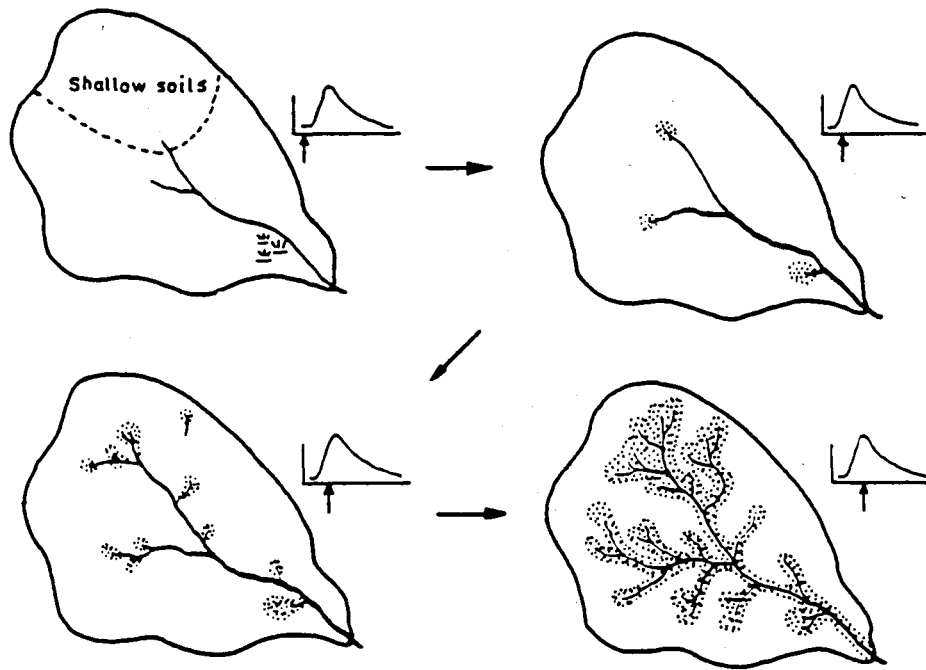


Figure 6.5: A time-lapse view of a basin showing expansion of the source area and channel system during a storm (Kirkby, 1978).

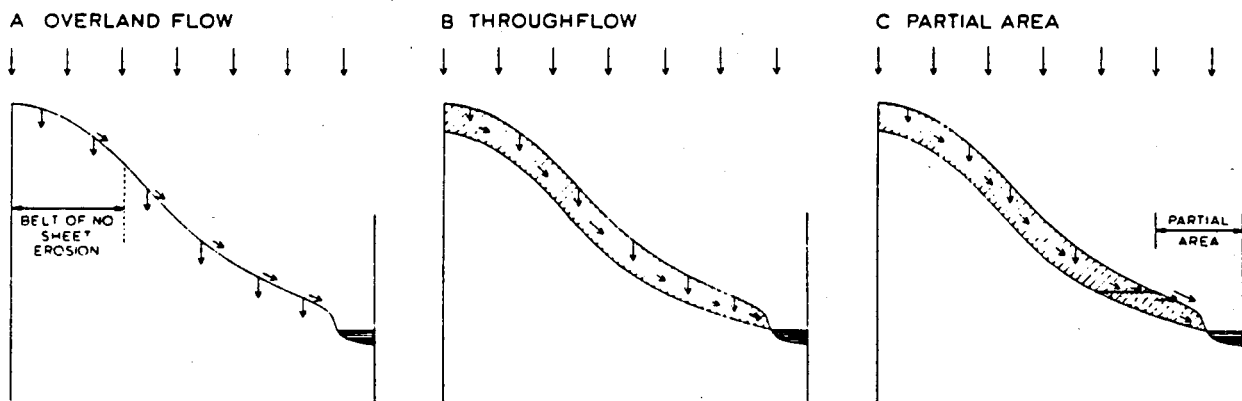


Figure 6.6: Schematic representations of (A) overland flow, (B) throughflow and (C) partial area models of hillslope hydrology (Kirkby, 1978).

of a storm or a rainy season as the zone of saturation expands. Fig. 6.5 shows the growth of a source area during a storm, and fig. 6.6 illustrates the source area as compared with other models of hillslope hydrology.

The validity of the source area concept has substantial support. Hewlett (1961) showed that the lower parts of slopes could be expected to generate runoff early in a storm while infiltration was still occurring on the higher areas. Betson (1964) studied various basins ranging from 4.5 ha to 85 km² in size, and found that only a portion of each catchment contributed to runoff. For his study catchments the contributing area lay between 5% and 86% of the land area, the lower percentages being the norm and higher percentages only occurring during extreme events.

Tischendorf (1969) described the source area as a dynamic region that shrinks and expands in response to rain. Dunne (1978) observed that a source area may vary in extent from season to season and even during a storm. Zaslavsky and Sinai (1981 a) used regions of enhanced vegetative growth to identify contributing source areas. Moore *et al* (1983) studied a rural catchment in which there was believed to be rapid subsurface flow, and concluded that its hydrological behaviour could be well described by the source area concept. Rajendran and Mein (1986) applied a simulation model to eleven different catchments in Australia, and found their results to be consistent with the source area concept.

The extent to which a source area will influence streamflow generation will vary for different catchments, depending on factors such as climate, soils and topography. As seen in some of the case studies in Section B, a source area need not only arise from downslope soil moisture seepages but also from areas of clay with low infiltration rates alongside streams. The present model allows for the occurrence and expansion of source areas by allowing for different soil moistures and properties in each element comprising a hillslope.

6.1.3. Basic concepts of soil physics

The theory of soil physics is treated in detail by Campbell (1985) and Amerman and Naney (1982). Basic concepts that are relevant to the present study are briefly reviewed below.

The subsurface environment consists of an arrangement of porous materials in which water moves within the pores between the soil grains. Darcy's law is the basic relationship describing water movement in a porous medium:

$$q = -k\partial H/\partial s \quad (6.1)$$

where q is the flux or flow rate per unit area in the s -direction, k is the proportionality constant equal to the hydraulic conductivity, H is the total head and $\partial H/\partial s$ is the head gradient providing the driving force for flow. H is made up of a number of components, but the important components in soil physics are the pressure head and the elevation head.

The pressure head h is related to the moisture content θ in the soil as illustrated in fig. 6.7. (The symbol ψ is sometimes used for h in soil physics literature.) The pressure head is positive for a saturated soil (θ equal to the saturated moisture content θ_s), but takes on negative values as the soil drains, resulting in soil suction.

The relationship between the conductivity k in eqn. (6.1) and moisture content is shown in fig. 6.8. In an unsaturated soil mass, water moves primarily in small pores and through films around particles. As moisture content decreases below saturation, conductivity rapidly decreases as the cross-sectional area of the films diminishes and the flow paths become more limited. The k - θ curve for a particular soil may be determined from laboratory tests, and predictive relationships have been presented by Brooks and Corey (1966), Campbell (1974) and Lambourne and Stephenson (1986). The relationship given by Campbell (1974) is used in this study:

$$k = k_s (\theta/\theta_s)^m \quad (6.2)$$

where k_s is the saturated hydraulic conductivity and m is a constant dependent on soil texture. Campbell (1985) suggested evaluating m as $(2b + 2)$ or $(2b + 3)$ where b is the slope of the $\log_e(h)$ versus $\log_e(\theta)$ curve.

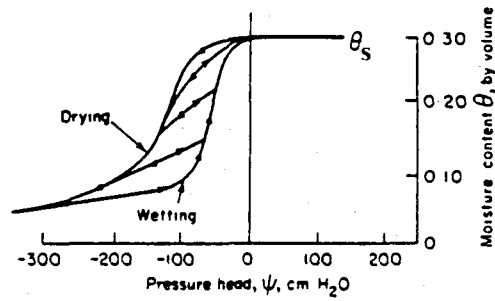


Figure 6.7: Soil water characteristic curve.

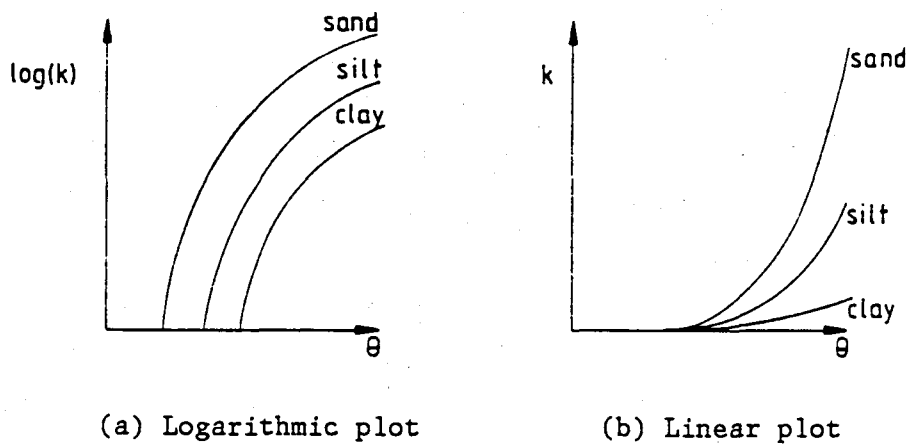


Figure 6.8: Variation of hydraulic conductivity with moisture content.

A knowledge of the $h-\theta$ and $k-\theta$ relationships for a particular soil is required in order to solve the transient differential equation for unsteady flow in a porous medium. The equation is attributed to Richards (1931) and is derived from a combination of the continuity equation and Darcy's law, and may be written

$$\frac{\partial \theta}{\partial t} = - \frac{\partial q}{\partial x} - \frac{\partial q}{\partial y} - \frac{\partial q}{\partial z} \quad (6.3a)$$

$$= \frac{\partial}{\partial x} \left(k \frac{\partial h}{\partial x} \right) + \frac{\partial}{\partial y} \left(k \frac{\partial h}{\partial y} \right) + \frac{\partial}{\partial z} \left(k \frac{\partial h}{\partial z} \right) - \frac{\partial k}{\partial z} \quad (6.3b)$$

x, y and z are orthogonal direction coordinates with z corresponding to depth vertically below the soil surface. The equation may be expressed as a function of h or θ as the only independent variable as shown in the derivation in Appendix B. The equation describes both saturated and unsaturated conditions, and reduces to the Laplace equation (Childs, 1969) when saturation prevails. Jacob (1950) derived a similar equation for unsteady flow in a confined aquifer. The Richards equation forms the basis of many soil models using rigorous or approximate numerical solutions to simulate subsurface seepages.

6.2. MODELLING APPROACHES

The literature abounds in soil and infiltration models with a diversity of applications and approaches. The examples cited below are intended to illustrate primary modelling approaches.

Table 6.1 summarises some prominent infiltration equations in use over the years. Early equations were empirically-based such as those of Kostiaikov (1932) and Horton (1933). A move towards physically-based equations such as the Philip (1957) equation followed the recognition of an advancing wetting front by Bodman and Coleman (1944). Davidoff and Selim (1986) compared a number of simple infiltration equations. The work of Mein and Larson (1973) facilitated the evaluation of the parameters in the Green and Ampt (1911) infiltration model, which are related to soil properties. This model has since become widely used because of its physical basis.

More recent infiltration equations include those of Morel-Seytoux (1984) and Tolikas *et al* (1983) who presented equations for calculating the ponding time and moisture profiles during rainfall. Germann and Beven (1985) discussed the modelling of subsurface flow through macropores arising from shrinkage cracks, root and animal channels, and presented a theory using a kinematic wave approximation for modelling the infiltration into such soils. One-dimensional forms of the Richards equation for vertical downward seepage have been used to model infiltration and redistribution of rainfall, such as the approximate solution of Pingoud (1982).

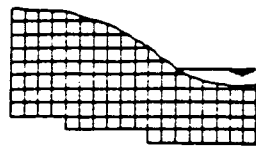
Table 6.1: Infiltration equations.

Reference	Equation
Kostiakov (1932)	$f_c = C_k t^{-\alpha}$
Horton (1933)	$f_c = f_{\infty} + (f_o - f_{\infty})e^{-\beta t}$
Philip (1957)	$f_c = \frac{1}{2} S t^{-\frac{1}{2}} + b$
Holtan (1961)	$f_c = f_{\infty} + a(F_c - F)^{1.4}$
Green and Ampt (1911), Mein and Larson (1973)	$f_c = K[1 + S_{av}(\theta_s - \theta_i)/F]$

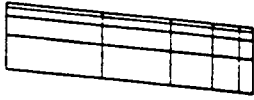
Parameter definitions

f_c = infiltration capacity	K = soil conductivity
f_o = initial infiltration capacity	S = sorptivity
f_{∞} = equilibrium infiltration rate	S_{av} = average suction
F = cumulative infiltration	θ_s = saturated moisture content
F_c = ultimate infiltrated volume	θ_i = initial moisture content
t = time after the start of infiltration	
C_k, α, β, a, b = constants evaluated experimentally	

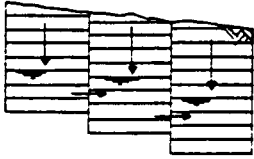
Different types of soil and ground water models are illustrated in fig. 6.9 showing common approaches to discretizing the subsurface environment. Two- or three-dimensional grids representing a hillslope profile (fig. 6.9(a)) form the basis of finite difference or finite element solutions to the Richards equation for saturated and unsaturated flows. A classic model of this type is the pioneering work of Freeze (1971), coupling a three-dimensional subsurface hillslope model with one-dimensional channel flow. Rovey and Richardson (1975) developed one of the first general watershed models incorporating physically-based simulation of subsurface flows using a three-dimensional numerical solution of the Richards equation. The European watershed model SHE (Abbot *et al*, 1986 b) utilises a grid representation of the subsurface system for modelling aquifer flows. Bernier (1985) used an irregular finite difference grid parallel to the ground surface to model seepage down a hillslope (fig. 6.9(b)).



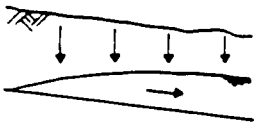
(a) Rectangular finite difference grid, eg. SHE (Abbot *et al*, 1986b) and Freeze (1971).



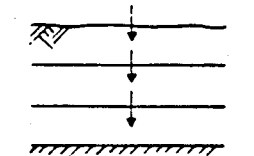
(b) Variable grid parallel to the ground surface (Bernier, 1985).



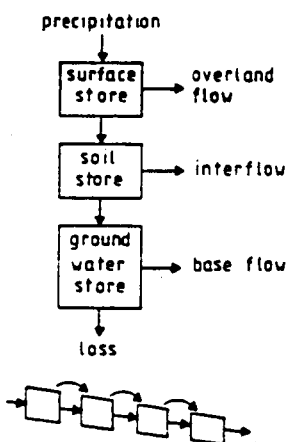
(c) One-dimensional finite difference grid (Hillel and Hornberger, 1979).



(d) One-dimensional flow vertically to water table and horizontally with hillslope, eg. Smith and Hebbert (1983).



(e) Layered soil model such as in ACRU (Schulze, 1984).



(f) Store approach.

(g) Hillslope model of Burt and Butcher (1984).

Figure 6.9: Diagrammatic representation of approaches to subsurface modelling.

A simplified approach is to employ one-dimensional finite difference schemes to model the primary components of subsurface flows. Hillel and Hornberger (1979) used an approximate solution of the Richards equation to model downward percolation of infiltrating water and horizontal flow in the saturated zone below the water table, as shown in fig. 6.9(c). Smith and Hebbert (1983) used a kinematic wave approximation for one-

dimensional vertical percolation of infiltrating water and for lateral seepage under a perched water table (fig. 6.9(d)).

An approach used in many watershed models is to employ simplified subsurface routing through a number of conceptual stores, often with empirical relationships that require calibration on recorded streamflows. Fig. 6.9(e) shows the 3-layer approach used in the ACRU model (Schulze, 1984), in which each soil layer is treated as a store with daily moisture budgeting to determine moisture contents. Fig. 6.9(f) illustrates the typical structure of such models in which the soil profile is represented by a series of stores stacked vertically. Examples of this approach include the model of Beven and Kirkby (1979) that utilises stores for interception, infiltration and a saturated soil zone; and Brendecke *et al* (1985) who used a three-tier model in which a subsurface reservoir can exfiltrate via an upper soil store or percolate to a ground water reservoir and ground water is lost to a sink or routed to baseflow as a function of the level of ground water storage. The well-known Pitman model (Pitman, 1977; Pitman and Basson, 1979) and Stanford Watershed Model (Crawford and Linsley, 1966) both utilise store approaches. Burt and Butcher (1984) used a "leaky bottle" storage model in which a hillslope is conceptualised as a series of stores linked laterally in a downslope direction as indicated in fig. 6.9(g). Downslope flow is calculated using the slope gradient, moisture content and hydraulic conductivity in each store.

Another category of subsurface models is those utilising stochastic approaches. A synthetic time series is generated that preserves the statistics of the real time series used for calibration, as in the models of Fiering and Jackson (1971). Bathala *et al* (1976) coupled a finite difference model of the transient flow aquifer equation with stochastic inputs, and used this to evaluate a regional aquifer.

A rigorous numerical solution of the Richards equation requires detailed knowledge of system geometry, distribution of hydraulic properties within the system, and boundary conditions (Amerman and Naney, 1982). Even with all this data, a certain amount of calibration is required. Soil parameters such as soil depth, permeability, porosity and suction are highly

variable in the field, even in a relatively small area. Detailed soil data is therefore costly to collect in a catchment study, and the modeller generally has to rely on approximate, average values of soil properties that are representative of field conditions, obtained either from selective sampling or the results of field surveys and soil classifications conducted by a soil scientist. For a general watershed model, the computational effect of a rigorous numerical subsurface model is therefore incompatible with the availability of data, and an approximate solution with modest data requirements would be preferable.

A physically-based rather than an empirical approach was followed in the present study in order to predict soil moisture conditions based on measurable or estimated soil properties. The soil model presented below is based on a three-layer representation of the soil profile, in which vertical and downslope seepages are calculated using a simplified form of the Richards equation. The approach can be seen either as a coarse two-dimensional finite difference grid or as a series of soil moisture stores with physically-based relations governing inflows and outflows.

6.3. MODEL DEVELOPMENT

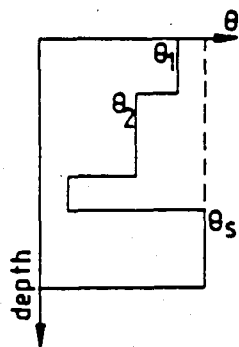
6.3.1. Structure of soil model

A soil model should be able to account for the following important characteristics of soil moisture movements:

- o Infiltration as a function of soil properties and of soil moisture content near the surface.
- o Vertical redistributions of moisture within the soil profile.
- o Downslope saturated and unsaturated seepages associated with interflow and ground water flow.

In the present study, the spatial variations of soil properties and moisture conditions over a catchment are accounted for by the element discretization of a catchment. The other dimension, namely depth below the surface, is represented by means of three soil layers as illustrated in fig. 6.10. The upper two layers represent the A and B soil horizons

(a) Moisture profile



LEGEND

- \dashrightarrow inflow from upslope element
- \rightarrow downslope seepage
- \downarrow vertical percolation

(b) Element cross-section

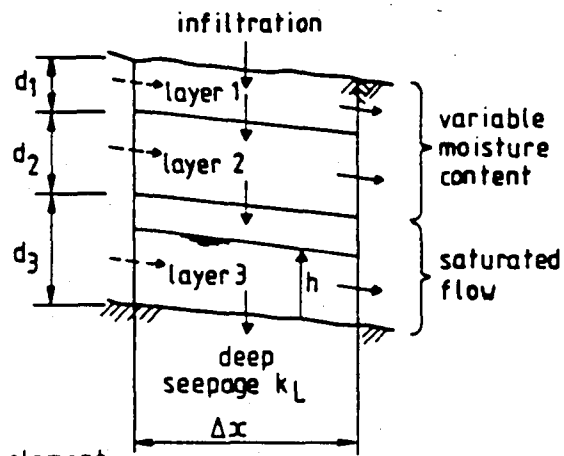


Figure 6.10: Three-layer soil model.

or the hydrologically active topsoil. The first layer receives infiltrating water calculated using the Green and Ampt (1911) equation, and lateral and vertical seepages are modelled using Darcy's law. The lower layer represents saturated flow beneath a water table or perched water table, with input being moisture seepage from layer 2. Deep percolation into the underlying soil or rock stratum is represented as a constant loss k_L . Lateral seepage from each of the three soil layers enters the corresponding layer in the downslope element, and the lowest element in a hillslope seeps into the stream. Exfiltration occurs if an element saturates to the surface, allowing for the possibility of Dunne-type infiltration.

Soil properties such as permeability and texture may be specified separately for each layer in each element. This creates a high degree of flexibility in model applications in which features such as layered soils and varying soil depths may be accounted for. The use of three soil layers also facilitates the distribution of evapotranspiration losses in the soil profile according to root densities (dealt with in chapter 7).

In the following sections, the soil sub-model is described dealing firstly with the method of computing infiltration into the upper soil layer,

followed by descriptions of the finite difference schemes for unsaturated flow in the upper two soil layers and saturated downslope flow in the lower soil layer.

6.3.2. Infiltration

The Green and Ampt (1911) and Mein and Larson (1973) infiltration model is a physically-based approach that has gained wide acceptance in hydrological modelling applications. Rajendran and Mein (1986) give a list of investigators who have used the model and demonstrated its suitability in watershed models. Although originally derived for uniform, homogenous soils, it has been found to yield good results for layered soils, partially sealed surfaces and non-uniform initial moisture conditions (Haan *et al*, 1982).

The equation makes it possible to predict infiltration rate at the soil surface as a function of rainfall history and soil properties. It may be derived from an approximate solution of Darcy's equation for vertical flow in the wetted zone above the wetting front, and is written

$$f_c = K[1 + S_{av}(\theta_s - \theta_i)/F] \quad (6.4)$$

with the symbols as defined in table 6.1. The equation is derived in Appendix B.

Research has shown that the soil in the transmission zone above the wetting front is not fully saturated because of trapped air, and consequently the conductivity K in eqn. (6.4) is less than the saturated conductivity k_s . Using available data, Bouwer (1969) found K to be of the order of $0.4k_s$ to $0.6k_s$, and used $0.5k_s$ as his estimate. Rawls *et al* (1983) also assumed a value of $0.5k_s$. Studies such as those of Slack (1978) have evaluated K from an assumed moisture content in the transmission zone, suggesting values in the region of $0.1k_s$ - $0.3k_s$. In this study a compromise value of $k_s/3$ was adopted after Rajendran and Mein (1986).

Infiltration into the upper soil layer is assessed under the three conditions identified by Mein and Larson (1973):

1. $i \leq K$. If the rainfall rate i is less than the conductivity K , all the rain infiltrates, raising the moisture content of the upper soil layer (θ_1). This corresponds to light rain or drizzle soaking into the soil.
2. $K < i < f_c$. These are pre-ponding conditions under which all the rain infiltrates, i.e. $f = i$.
3. $i \geq f_c$. The post-ponding infiltration rate is given by eqn. (6.4). Rainfall as well as ponded water are available for infiltration.

f_c is evaluated using eqn. (6.4) in the form

$$f_c = \frac{k_s}{3} \left[1 + \frac{S_{av}(\theta_s - \theta_i)}{d_1(\theta_1 - \theta_i)} \right] \quad (\theta_1 \neq \theta_i) \quad (6.5)$$

with θ_1 given by the average moisture content in soil layer 1 during the current time interval. θ_1 and d_1 are defined in fig. 6.10. Eqn. (6.5) is obtained by substituting $F = (\theta_1 - \theta_i)d_1$ in eqn. (6.4). In this way the advance of the wetting front is represented as a rise in the moisture content of the upper soil layer. This approach avoids introducing another variable into the model to account for the depth of the wetting front, as well as the complexities that would arise with multiple soil moisture profiles resulting from alternating periods of wetting front formation and moisture redistribution during wet and dry periods.

If the top soil layer saturates during infiltration, the process is transferred to the second layer, using d_2 and θ_2 in place of d_1 and θ_1 in eqn. (6.5). On the onset of rain after a dry period, θ_1 is equal to θ_i . This value is retained during intermittent rain and updated after a dry period. When $\theta_1 = \theta_i$, f_c given by eqn. (6.5) is infinitely large, in which case f_c is assumed equal to the rainfall rate for one time step.

6.3.3. Finite difference scheme for upper two soil layers

The upper two soil layers may be considered as cells in which the moisture content is increased by inflows and depleted by outflows. Infiltration, vertical moisture re-distribution and downslope seepages constitute the inflows and outflows. The finite difference scheme may be derived by considering a water balance on one such cell:

$$(\theta_t - \theta_{t-\Delta t})Wd\Delta x = (q_{vi} - q_{vo})W\Delta x\Delta t + (q_{Li} - q_{Lo})Wd\Delta t \quad (6.6)$$

where θ_t = moisture content of cell at end of time interval

$\theta_{t-\Delta t}$ = moisture content of cell at beginning of time interval

W = width of element normal to the flow direction

x = flow direction

d = thickness of soil layer (c.f. d_1 and d_2 in fig. 6.10)

q_{vi} = vertical inflow

q_{vo} = vertical outflow

q_{Li} = lateral inflow

q_{Lo} = lateral outflow

q_{vi} and q_{vo} represent vertical moisture seepages (per unit area), and q_{Li} and q_{Lo} are flows parallel to the ground surface. Eqn. (6.6) could also be derived from a Preissmann finite difference formulation of the continuity equation, with the weighting coefficient θ set at zero. It was not considered necessary to incorporate a variable θ because the uncertainties in estimating soil properties render a high level of accuracy impossible.

Solving eqn. (6.6) for the unknown θ_t gives

$$\theta_t = \theta_{t-\Delta t} + (q_{vi} - q_{vo})\Delta t/d + (q_{Li} - q_{Lo})\Delta t/\Delta x. \quad (6.7)$$

The vertical and lateral flows are Darcian flows related to moisture content (except q_{vi} in the top soil layer which is equal to the infiltration rate). Considering vertical soil moisture seepage in eqns. (6.3) and the component of downslope flow parallel to the soil surface, it can be shown (for mild slopes) that

$$q_v = k(\theta) - D\partial\theta/\partial z \quad (6.8)$$

$$\text{and } q_L = k(\theta)s_0 - D\partial\theta/\partial x. \quad (6.9)$$

Here, x is the direction coordinate for downslope seepage and s_0 is the ground slope. The diffusivity D is defined as $k(\theta)dh/d\theta$ and $k(\theta)$ denotes permeability as a function of moisture content.

Seepage thus has a gravity component related to $k(\theta)$ and a diffusion component related to the moisture gradient in the flow direction. Attempts were made at including both the gravity and diffusion components in the finite difference scheme. However, this meant that a number of sweeps down a hillslope were required at each time interval in order to evaluate the moisture gradients, increasing computation time considerably. Convergence problems were also encountered because of the coarse finite difference grid which results in large moisture gradients between the soil layers. Furthermore the model was difficult to calibrate because the effect of moisture gradients on subsurface flows made the response of the model to changes in input parameters unpredictable. Determining soil properties such as the soil water characteristic for evaluating diffusivity D was also found to be difficult in field applications, and attempts to define parameter values based on trends related to soil texture were unsuccessful.

The diffusivity component was therefore omitted and the following relationships adopted:

$$q_V = k(\theta) \quad (6.10)$$

$$\text{and } q_L = k(\theta)s_0. \quad (6.11)$$

Beven (1981, 1982) showed that this is equivalent to a kinematic approximation of the subsurface flow equations. He studied the conditions under which the approximation holds and concluded that it is useful for a range of cases of practical interest, and that models based on this approach can produce good results in field situations with only a modest computational effort. Zaslavsky and Sinai (1981 b) verified the use of eqn. (6.11) as a close approximation for the flow component parallel to the ground surface.

The flows in eqn. (6.7) are calculated using moisture conditions at the end of each time interval which is equivalent to a $\phi = 0$ finite difference scheme. Using eqns. (6.10) and (6.11), eqn. (6.7) may be written

$$\theta_t = \theta_{t-\Delta t} + [q_{vi} - k(\theta_t)]\Delta t/d + [q_{Li} - k(\theta_t)S_0]\Delta t/\Delta x \quad (6.12)$$

Inflows q_{vi} and q_{Li} are known for each cell since computation proceeds downslope. The equation of Campbell (1974) (eqn. 6.2) is used for evaluating $k(\theta)$. The only unknown in eqn. (6.12) is θ_t , which is solved for in each cell using an iterative Newton-Raphson procedure which generally converges rapidly in two to three iterations.

6.3.4. Saturated flow in lower soil layer

Saturated flow under the water table or perched water table in the third soil layer is routed downslope from one element to the next. The continuity equation for one-dimensional flow through a porous medium is

$$\frac{\partial Q}{\partial x} + \xi \frac{\partial A}{\partial t} = q_i \quad (6.13)$$

where ξ is the porosity of the medium. The inflow term q_i includes percolation from the soil layer above (q_v^{23}) and deep seepage to the underlying strata (k_L):

$$q_i = q_v^{23} - k_L \quad (6.14)$$

Retaining a kinematic solution, downslope flow is given by eqn. (6.11). For saturated flow, $k(\theta)$ in eqn. (6.11) is replaced with k_s , and the flow rate is given by

$$Q = Whk_s s_0 \quad (6.15)$$

where h is the depth of flow (fig. 6.10). Combining eqns. (6.13) - (6.15) and writing in finite differences with $A = Wh$, using the subscripts 1 to 4 previously defined for the corners of a computational cell, setting $\theta = \phi = 0$ and solving for h_4 gives:

$$h_4 = \frac{(q_v^{23} - k_L)\Delta x \Delta t + q_2 \Delta t + (\theta_s - \theta_f)\Delta x h_3}{k_s S_0 \Delta t + (\theta_s - \theta_f)\Delta x} \quad (6.16)$$

q_2 is inflow from the upslope element and θ_f is moisture content at field capacity. This formulation assumes zero travel time for seepage from soil layer 2 to reach the water table. This assumption was tolerated because of the additional complexities of modelling moisture movements above the

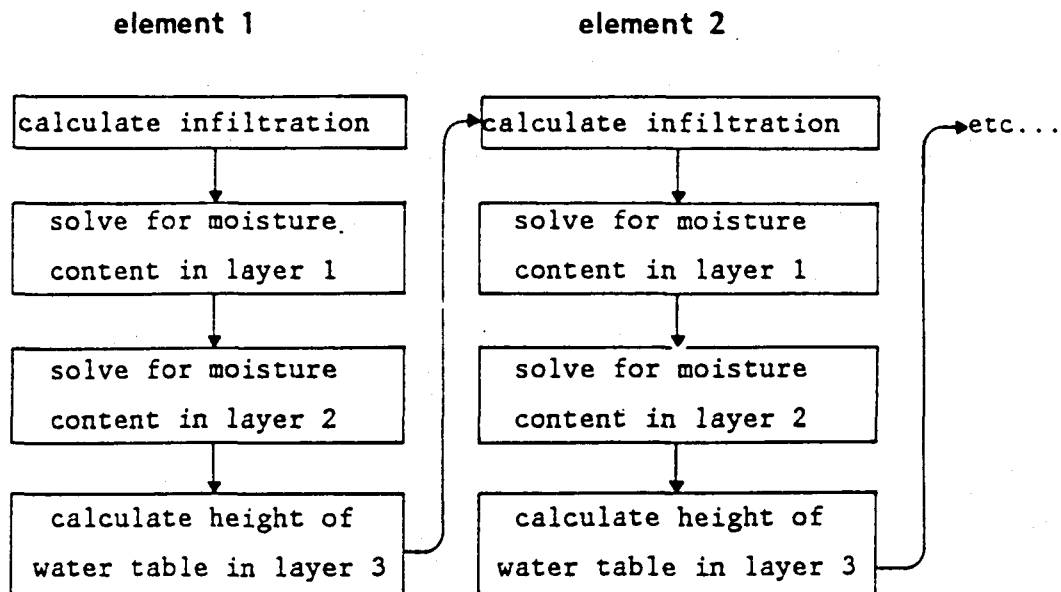


Figure 6.11: Computational procedure of soil model. Element numbers refer to consecutive hillslope elements in a downslope direction.

water table in layer 3, and because the travel times of vertical flow are orders of magnitude smaller than those of nearly horizontal flow. The use of field capacity θ_f in eqn. (6.16) assumes that a rising water table rises in a zone where the moisture content is at field capacity, which is probable if unsaturated flow is trickling down to a water table. A θ -value of zero is used because of the low celerities typical of downslope seepage, resulting in values of θ close to zero.

Eqn. (6.16) is used to calculate the height of the water table in each element at each time step, with computation proceeding downslope so that inflows are known for each element.

The overall computational procedure for the soil model is illustrated in fig. 6.11.

6.3.5. Evaluating soil parameters

The input parameters for the soil model described above are:

- k_s saturated conductivity (mm/h) for infiltration into top soil layer and Darcian flow in all three soil layers

S_{av}	average suction on wetting front (mm) in infiltration equation
k_L	deep seepage loss from third soil layer (mm/h)
d	thickness of each soil layer (mm)
θ_r	residual moisture content
θ_s	saturated moisture content
m	exponent in equation for $k(\theta)$
s_0	ground slope (m/m)
Δx	element length in flow direction (m)
W	element width (m)

s_0 , Δx and W are obtained from digitised topographic data, and are the same as for overland routing as discussed previously (chapters 3 and 4). The other parameters are discussed below.

The k - θ curves presented by Rawls *et al* (1981) were used here to evaluate to exponent m in eqn. (6.2). The curves are shown in fig. 6.12 and represent a large amount of soil data processed by Rawls *et al* (1981, 1983). Re-plotting the curves on a linear basis as shown in fig. 6.13, values of m between 6.7 and 9.2 were obtained by curve fitting. No trend that could be correlated with soil texture was evident, and an average value of $m = 8.0$ for all soil types was adopted and coded in the simulation program.

Values of the saturated hydraulic conductivity k_s are obtainable from laboratory tests on soil samples or from field studies in which soil flows are collected in troughs and measured. However, these methods are costly and time-consuming, and the values obtained in this way may still need to be calibrated when applying the model to a field situation because of the inhomogeneities in the soil and the simplified representation of the subsurface environment in the model. The use of published values of soil permeability was therefore resorted to for the case studies in Section B of this work.

Various analytical relationships have been proposed for evaluating k_s . Scheidegger (1960) reviewed a number of equations relating k_s to pore size distribution. Childs and Collis-George (1950) and Marshall (1958) re-

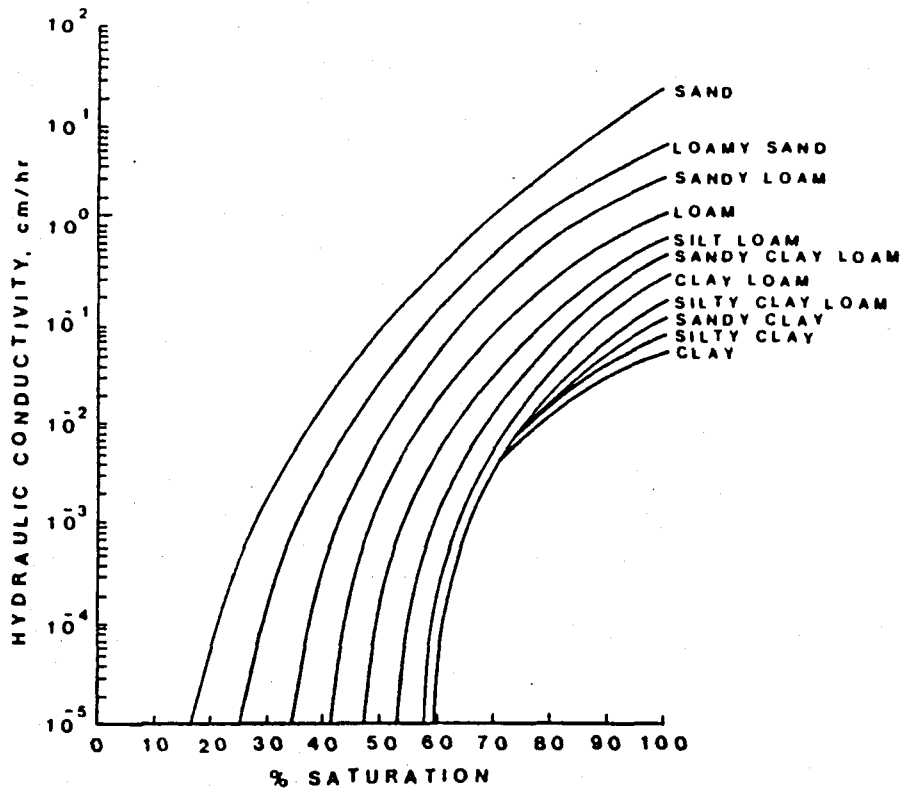


Figure 6.12: Hydraulic conductivity by soil texture class (Rawls *et al*, 1981).

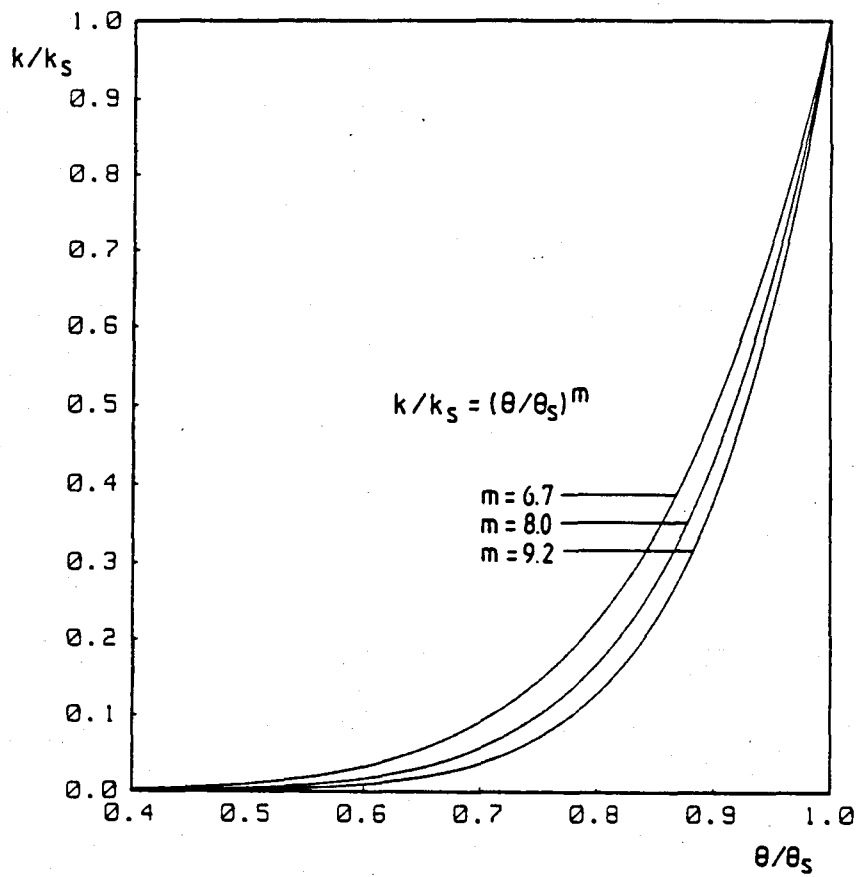


Figure 6.13: Hydraulic conductivity by exponent.

lated k_s to soil and water properties. Studies such as those of Bloemen (1980) have related k_s to properties of the particle size distribution function, indicating that k_s can be related to soil texture. Campbell (1985) developed predictive relationships for k_s by correlating conductivity data with the silt and clay content of the soil.

Mean values of saturated conductivity for different soil textures are listed by Rawls *et al* (1981) based on experimentally measured values on a wide range of soils. Beven (1989) warned against the use of such published data because of the large discrepancies possible in the field. Structural defects such as cracks, worm holes and root channels can also significantly alter the conductivity. Bearing these factors in mind, published data is used in the present study only as a *guideline* for model calibration. In the case studies in Section B, probable ranges of k_s are evaluated according to the soil textures identified in each catchment, and these are used as a guide for model calibration. The conductivity data of Rawls *et al* (1981) is given in Appendix A.

Porosity and residual moisture content may also be related to soil texture (Rawls *et al*, 1983; Schulze, 1983). Simulated streamflows were found here to be relatively insensitive to these parameters, and therefore model input was simplified by requiring only the *soil texture* to be specified by the user, and the program allocates values of θ_r and θ_s from the values listed in table 6.2. The eleven soil groups are defined according to their sand, silt and clay content in the soil texture triangle shown in fig. 6.14. The values of soil suction S_{av} shown in table 6.2 are also automatically assigned by the program since it was found that infiltration rates could be adequately calibrated by adjusting the soil conductivity k_s . The parameters θ_s , θ_r and k_s are therefore represented in the simulation program by a single input parameter, namely the soil group number in table 6.2.

Thicknesses of the soil layers can be defined from sampling pits dug in field studies. The values used represent average soil depth over an area, and the greater the variation in soil depth or the less data is available, the more this variable has to be calibrated. Generally, experience with a particular catchment will develop a knowledge of how soil depths are

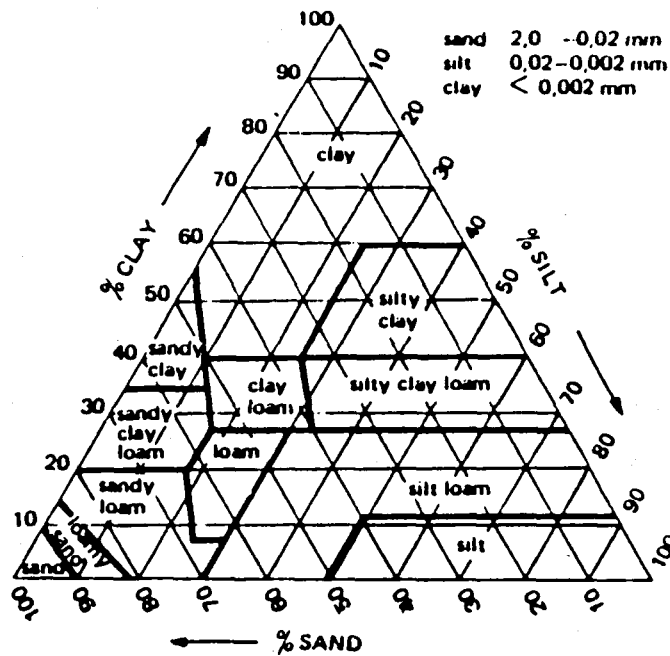


Figure 6.14: Texture chart (Soil Conservation Service, 1975).

typically related to topography, geology or locations such as hill tops, hill slopes and areas adjacent to streams. South African soils are generally relatively shallow, and the layer thicknesses for the upper two layers are typically in the range of 100 - 300 mm in the case studies in Section B. The third layer may be thicker, up to a few meters.

With experience in using the model it was found that the downslope (lateral) seepage in the upper two soil layers made calibration complicated and difficult, and that interflow as well as ground water flow could be well modelled with downslope saturated flow in the lower soil layer only. In the Bethlehem case study (chapter 10), the allowance for lateral seepage in the upper two layers was disabled, and only the third layer was used for lateral flows. Under these circumstances the third soil layer may become a conceptual layer rather than a physical zone. Its thickness (d_3) then represents a quantity sufficient to prevent saturation of the layer to its full depth, as in the Ecca study (chapter 9), and not a physical depth measurable in the field.

Table 6.2: Soil properties defined by soil group. (Based on data of Rawls *et al*, 1983.)

soil group	θ_r	θ_s	S_{av} (mm)
1 Sand	0.02	0.44	50
2 Loamy sand	0.035	0.44	60
3 Sandy loam	0.04	0.45	100
4 Silt loam	0.02	0.46	150
5 Loam	0.03	0.46	80
6 Sandy clay loam	0.07	0.46	200
7 Clay loam	0.075	0.46	180
8 Silty clay loam	0.04	0.47	230
9 Sandy clay	0.10	0.46	210
10 Silty clay	0.06	0.48	250
11 Clay	0.09	0.48	270

Table 6.3: Input parameters for the soil model.

Parameter	Possible sources of data
soil group	Analysis of soil samples; soil classifications from field surveys.
k_s	Published data based on soil texture; analysis of soil samples collected in the field; field tests.
layer thicknesses	Field studies supplemented with knowledge of typical profiles that are associated with particular soil types or topographic features.
k_L	Generally requires calibration.

Another modification that proved useful was to create a user-defined option regarding the downstream boundary condition for lateral subsurface flow in each hillslope. This option allows the user to specify either free outflow from the stream-side elements into the streams, or to suppress the outflow. The latter results in a region of saturation developing adjacent to streams, representing a source area for surface runoff.

The deep percolation loss k_L from the lower soil layer may be evaluated as the saturated conductivity of the underlying stratum, assuming that the confining layer saturates before a perched water table can form above it. Generally this quantity is difficult to measure and has to be calibrated, although in the Waterval study (chapter 8) it is estimated using borehole data. As a calibration parameter, k_L determines how rapidly the lower soil layer drains, and can be used to adjust the shape of the delayed flow hydrographs or recession flows.

The user-specified input parameters are summarised in table 6.3 along with suggested means of evaluation.

6.4. ANTECEDENT MOISTURE CONDITIONS

Soil moisture conditions are one of the prime factors that influence infiltration and surface runoff during a rainfall event. A means of evaluating antecedent moistures is necessary for single-event modelling as well as at the start of a continuous simulation if a "warm up" period or pre-run is not used to generate soil moisture conditions.

Lambourne and Stephenson (1986) reviewed current methods for determining antecedent moistures. The most common approach is to define an antecedent moisture index related to the degree of wetness of the soil or the antecedent rainfall and evaporation. Examples of indices based on rainfall history are the SCS method (Soil Conservation Service, 1972) in which the curve number is adjusted according to a soil wetness index, and the ILLUDAS approach (Terstriep and Stall, 1974) which employs the antecedent moisture indices shown in table 6.4 to determine the initial infiltration rate in Horton's equation. More advanced methods incorporate the evaporation as well as rainfall history, such as the Hawkins (1978) method that

replaced the standard SCS indices with a continuous range of antecedent moisture values, and the Flood Studies Report (NERC, 1975) in which a catchment Wetness Index is determined using a moisture accounting procedure. Lambourne and Stephenson (1986) developed an antecedent moisture model that estimates the antecedent moisture for use in a hydrological simulation model, using a moisture budgeting procedure incorporating daily rainfall and evaporation.

Consideration of the source area concept shows that soil moisture conditions are not uniform over a catchment but vary spatially. The approach adopted here accounts for spatial variations and is based on the analysis of Beven and Kirkby (1979) and Beven and Wood (1983). They showed that the soil moisture at a particular point on a hillslope is proportional to $\ln(a/s)$ where a is the upslope area draining to the point under consideration per unit length of topographic contour, s is the local ground slope and \ln is the natural logarithm. Beven and Kirkby (1979) presented a map showing zones of similar values of $\ln(a/s)$ for a small catchment, which compared well with observed patterns of source areas.

The antecedent moisture routine in the present model initialises the moisture conditions in each element prior to a simulation by calculating the value of $\ln(a/s)$ relative to its value in the lowest element of a hillslope. Moisture content is calculated using

$$\theta = \frac{[\theta_r + k(\theta_s - \theta_r)]\ln(a/s)}{\ln(a_0/s_0)} \quad (6.17)$$

Each hillslope is considered separately with a_0 and s_0 calculated for the streamside element, and a and s for each of the other elements in turn. In this way soil moisture decreases up each hillslope and is greater in areas of gently sloping topography. k is a factor evaluated by the user of the model according to the degree of wetness of a catchment as shown in table 6.5. If $k = 1.0$ (antecedent moisture condition class I) then the streamside elements are saturated, and if $k = 0$ (class V) the soil is set at residual moisture content θ_r . The antecedent moisture category may be estimated by judgement taking the climate and season of year into account, or evaluated by considering the rainfall and evaporation for a few months prior to the period to be simulated.

Table 6.4: Antecedent moisture criteria for ILLUDAS (after Terstriep and Stall, 1974).

A. M. C. class	Total 5-day antecedent rainfall (mm)	Description
1	0	bone dry
2	0 - 12.7	rather dry
3	12.7 - 25.4	rather wet
4	> 25.4	saturated

Table 6.5: Antecedent moisture categories for the present model.

A. M. C. category	k
I saturated	1.0
II wet	0.75
III moist	0.5
IV dry	0.25
V arid	0

6.5. SUMMARY AND CONCLUSIONS

The main features of the soil sub-model described in this chapter are summarised in table 6.6. The three-layer approach facilitates the modelling of vertical as well as downslope seepages, and permits variations of soil properties with depth. The numerical methods used to solve for soil moisture movements consist of a two-dimensional kinematic finite difference scheme for vertical and lateral flows in the upper two soil layers, and a one-dimensional kinematic approximation for saturated flow in the third soil layer. The difference schemes are based on a ϕ -value

Table 6.6: Main features of soil model.

Model aspect	Details
Infiltration	Green and Ampt infiltration equation.
Upper two soil layers	Variable moisture content with vertical soil moisture redistribution and downslope seepage (eqn. 6.12).
Lower soil layer	Saturated flow beneath a water table or perched water table (eqn. 6.16).
Variables	θ_1, θ_2 : moisture content of upper two soil layers h : depth of saturated flow in layer 3 θ_i : initial moisture content in top soil layer during infiltration
Input parameters	Soil texture, saturated conductivity, soil depths and deep seepage.

of zero (for numerical stability) and a θ -value of zero (because of low celerities).

Features such as source areas, interflow and baseflow flow are modelled in the various case studies in Section B. Source areas may be represented by elements of differing soil moisture and permeability; interflow is modelled by means of downslope seepages; exfiltration occurs when an element saturates to the surface; and ground water flows may be modelled by saturated flow in the third soil layer.

Difficulties in modelling soil conditions arise from the inherent heterogeneous nature of soils, the expense of collecting detailed soil data in the field, and the necessity of using a simplified representation of the complex subsurface environment. Because of these factors, soil parameters are likely to require more calibration than the above-ground parameters for overland and channel processes. The extent of calibration required for the soil parameters is investigated in the model studies in Section B.

Chapter 7: VEGETATION-RELATED PROCESSES

Vegetation in a catchment affects the friction coefficient for overland flow, influences soil erosion and the formation of rills, and maintains the infiltration capacity of the soil. Vegetation is also responsible for two important losses from the hydrological system being modelled, namely interception and evapotranspiration, which are the focus of this chapter.

Evapotranspiration, sometimes referred to as *total evaporation* (De Jager and Van Zyl, 1989), is the loss of water from a vegetated surface by direct evaporation from the soil surface and transpiration loss from the foliage. Transpiration is the process whereby soil water that has been absorbed by plant roots is lost to the atmosphere by evaporation from the leaf surfaces. Modelling evapotranspiration losses is important in continuous watershed simulations because they determine soil moisture conditions which significantly influence infiltration rates and surface runoff. Evapotranspiration can constitute a significant loss from the system being modelled, and 65 - 70% of the total global annual rainfall is believed to be returned to the atmosphere by evapotranspiration (Schulze, 1983).

Interception loss is the portion of rainfall that is retained on the surface of vegetation and subsequently evaporated. Interception losses can vary from almost negligible amounts in sparsely vegetated areas to significant amounts of up to 25% of gross rainfall in humid forested regions (Linsley *et al*, 1949). Fleming (1975) maintains that no model structure is complete without the process.

The evapotranspiration and interception components of the simulation model are described below.

7.1. EVAPOTRANSPIRATION

Saxton and McGuinness (1982) presented an in-depth discussion of the evapotranspiration processes. The main factors influencing evapotranspiration losses can be summarised as follows:

- *Climatic factors.* Solar radiation, wind and humidity determine the potential energy available for drawing moisture out of the soil and vegetation. Climatic factors may be represented by the potential evaporation rate.
- *Above-ground factors.* The extent of the vegetation canopy determines the amount of intercepted solar radiation and the surface area available for evaporation from the stomata. The canopy also determines the degree of shading of the soil which limits the evaporation occurring directly from the soil surface. Phenological development of plants also affects transpiration rates, and has been studied with particular reference to crops where the need for water and the ability to transpire alter as a crop matures.
- *Below-ground factors.* Water-uptake of plants is determined by the root system and the available moisture in the soil. When soil moisture is depleted and plants cannot absorb water at a rate to meet demand, plant stress sets in with plants transpiring at less than their potential rate.

Current approaches to modelling evapotranspiration generally separate plant transpiration and soil evaporation, estimating losses using semi-empirical relations to account for above- and below-ground factors. A research emphasis on agricultural crops has resulted in many relationships based on crop behaviour, with models varying from simple to complex. Simple models consist of an equation relating evapotranspiration loss to potential evaporation and variables representing canopy and soil moisture conditions, for example the equation of Holtan *et al* (1975) and England (1975). The Penman (1948) equation is a well-known model based on climatic data. Complex models such as that of Saxton *et al* (1974) calculate daily evapotranspiration losses from incoming potential energy, account-

ing for factors such as canopy characteristics, plant phenology, seasonal root distribution and soil moisture status.

The evapotranspiration component of the simulation model is described below and accounts for the important above- and below-ground factors without extensive input data requirements. Evapotranspiration losses are calculated at each time interval from potential evaporation using a sequence of operations relating soil and plant evaporation to parameters representing canopy, root and soil moisture conditions, substantiated by research findings and modelling approaches reported in the literature.

The soil evaporation and plant transpiration losses are computed separately. Climatic factors are represented by potential evaporation, from which actual evapotranspiration losses are estimated taking above- and below-ground factors into account in the following sequence:

Solar energy represented
by potential evaporation.

↓

Calculate ET rates assuming
unlimited soil moisture.
('Potential' ET rates based
on above-ground factors.)

↓

Calculate 'actual' ET rates taking
soil moisture conditions and
root distribution into account
(below-ground factors).

7.1.1. Potential evaporation

Potential evaporation is the rate at which water will be lost to the atmosphere from an open body of water such as a lake. Models for predicting potential evaporation have been grouped by Schulze (1983) and Saxton and McGuinness (1982) into a number of categories. Energy budget methods are based on a vertical energy budget over a vegetated surface. Temperature-based methods use mean air temperatures to predict daily or

monthly potential evaporation rates, such as the Blaney-Criddle (1966) and Linacre (1977) models. Aerodynamic profile methods require the measurement of wind velocities above the evaporating foliage, as well as air temperature, vapour pressure and humidity. Combination methods such as the Penman (1948) equation and its modifications by Monteith (1965) and Maaren (1978) combine the energy budget and aerodynamic profile methods.

Data from evaporation pans may also be used to assess daily or monthly potential evaporation amounts, the two standard types being the Symons pan and the American A-class pan. A pan factor must be applied to correct for the difference between the measured pan evaporation and that which would occur from a large body of water.

In the present model, potential evaporation is not calculated by the program from climatic data but is supplied by the user as an input parameter. It may be specified on a daily or monthly basis and may be based on evaporation pan data as in the Waterval and Eccla studies in chapters 8 and 9, or calculated from predictive equations as in the Bethlehem study in chapter 10.

7.1.2. Canopy effects

Two parameters commonly used to account for the effect of canopy on evapotranspiration are crop coefficients and leaf area index. Crop coefficients have been developed for irrigation evapotranspiration predictions on crops, and are simply the ratio of transpiration loss to potential evaporation assuming no soil water stress. They may be expressed as average seasonal values or as seasonal distributions.

Leaf area index (LAI) is the ratio of leaf surface area to projected ground area beneath the canopy. Ritchie and Burnett (1971) and Kristensen (1974) presented similar curves relating evapotranspiration to LAI for a number of different crops as shown in fig. 7.1. In most studies on LAI this ratio has been found to approach 1.0 as LAI approaches 3.0 (Saxton and McGuinness, 1982). For higher values of LAI, the transpiration ratio is greater than unity, reaching a steady state in which the transpiration

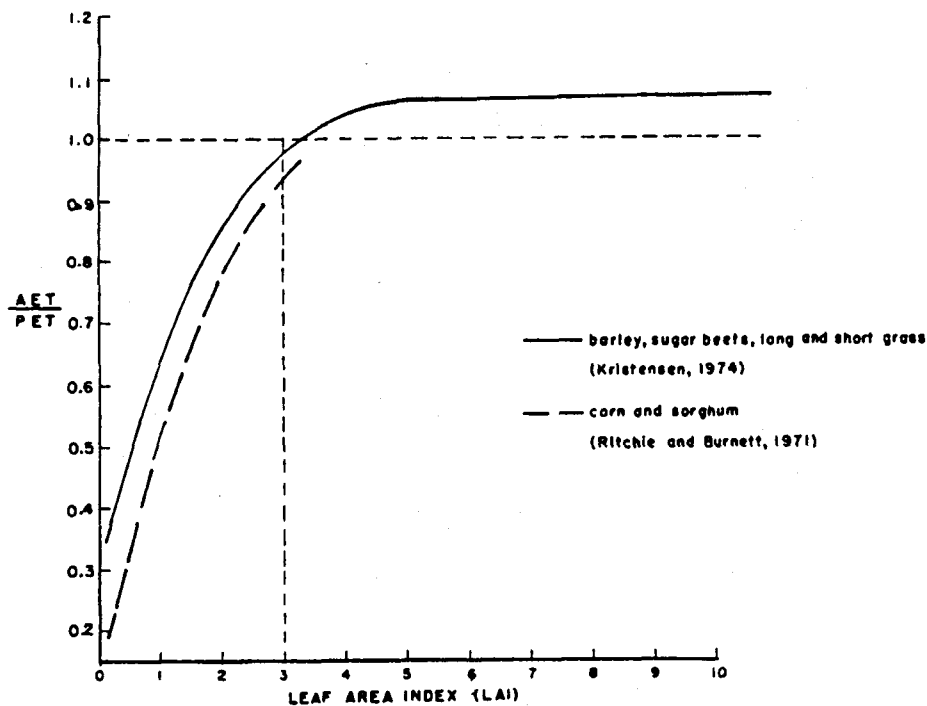


Figure 7.1: Empirical curves relating evapotranspiration to leaf area index.

loss exceeds the potential evaporation because of the large leaf area. Forests and full-canopy crops operate in this regime (Schulze, 1984).

In the present model, leaf area index is used to represent the effects of canopy on evapotranspiration and to divide potential evaporation into soil and plant components. In the absence of an established relationship for generalised application in the literature, an exponential curve was assumed of the form

$$T_p/E_p = 1.06(1 - e^{-kLAI}) \quad (7.1)$$

where T_p and E_p are the potential transpiration and evaporation rates respectively, and k is a constant. T_p is referred to here as the *potential* transpiration rate because soil moisture is assumed not to be limiting. The constant 1.06 was obtained by fitting the equation to Kristensen's (1974) data, which also gave the constant k close to unity.

Since leaf area index represents the degree of shading, it may also be used to estimate the proportion of solar radiation available for evaporation of moisture from the soil surface. Al-Soufi (1987) described an evapotranspiration model in which soil evaporation was calculated using a parameter representing the penetration of net radiation through the vegetation canopy, expressed as a function of LAI. Horticulturalists use an exponential relationship of the form

$$E = E_0 e^{-\alpha \text{LAI}} \quad (7.2)$$

to relate solar energy below the canopy (E) to that radiant above the canopy (E_0), with α a constant (Monsi and Saeki, 1953).

Since soil evaporation decreases with increasing canopy coverage, a mirror image of eqn. (7.1) may be expected, of the same form as eqn. (7.2). Given that the soil evaporation should be equal to the potential evaporation rate when LAI = 0, and taking the constant k in eqn. (7.1) equal to unity, the relationship assumed for soil evaporation is

$$E_{\text{sp}}/E_{\text{p}} = e^{-\text{LAI}} \quad (7.3)$$

E_{sp} is the potential evaporation from the soil surface, again assuming unlimited water supply. Eqns. (7.1) and (7.3) are represented graphically in fig. 7.2.

7.1.3. Below-ground factors

Evaporation from the soil and leaves depletes the moisture reservoir in the soil. Evaporation and transpiration proceed at their potential rates given by equations (7.1) and (7.3) until the water in the reservoir drops below a certain limiting value, whereafter the available soil moisture limits the evapotranspiration loss, and actual losses may be assumed to decrease linearly as soil moisture decreases (Schulze, 1983; Saxton *et al*, 1974). The classical literature of the past two decades has frequently attributed differences in observed values of the limiting soil moisture to textural soil properties (Schulze, 1983). Others, notably irrigation modellers, maintain that plant stress sets in at a fixed

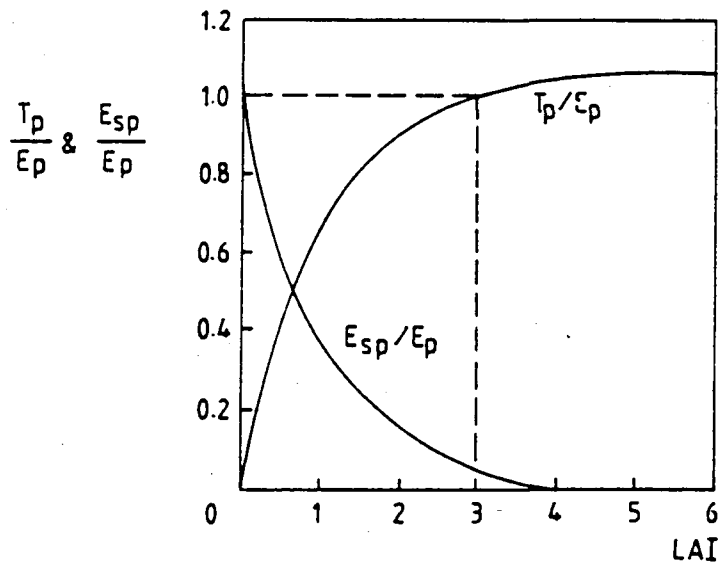


Figure 7.2: Equations (7.1) and (7.3) for transpiration and soil evaporation respectively.

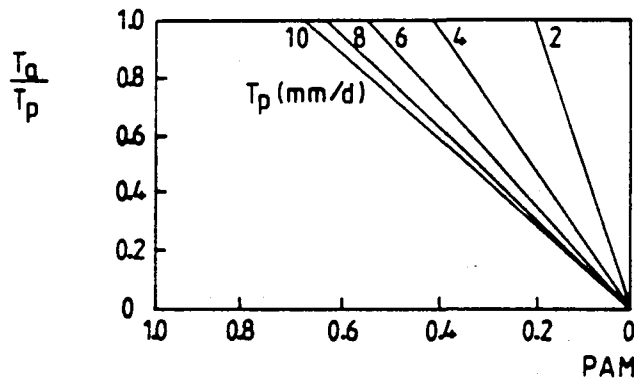


Figure 7.3: Effect of soil moisture stress on transpiration rate (after Doorenbos and Kassam, 1979).

moisture content such as 0.5 of the plant available water. Meyer and Green (1980) found that a value of 0.3 was more applicable for wheat in Southern Africa, and Slabbers (1980) showed that the limiting soil moisture for crops may vary with atmospheric demand and the hardness of the crop in drought situations.

In the present study, separate relations are used to assess the affects of moisture stress on soil evaporation and plant transpiration. For transpiration, a relationship of Doorenbos and Kassam (1979) was adopted,

in which the point at which plant stress sets in is related to the potential transpiration rate T_p . The relationship is shown in fig. 7.3 where T_a is the actual transpiration rate and PAM is the plant available moisture. In the upper two soil layers PAM is given by $(\theta - \theta_r)/(\theta_s - \theta_r)$ where θ is the current moisture content of the layer, and θ_r and θ_s are the residual and saturated moisture contents respectively. If there are roots in the lower (third) soil layer, then PAM is given by the ratio of the water table depth to the layer thickness (h/d).

The distribution of roots in the soil profile is taken into consideration by introducing another input parameter giving the proportion of roots occurring in each of the three soil layers in the model. The moisture in the i'th soil layer is depleted at a rate $T_a k_i$ where T_a is obtained from the relationship shown in fig. 7.3 and k_i is the proportion of roots in the i'th layer (i = 1, 2 or 3).

As for transpiration, the evaporation from the soil surface occurs at its potential rate E_{sp} until the limiting moisture content is reached. As the loss of water increases further, moisture has to rise from deeper below the surface. The hydraulic conductivity of the soil decreases as it dries out and consequently evaporation is limited. The relationship between evaporation and available soil moisture is referred to here as the soil extraction function and a relationship of the same form as the transpiration relationship in fig. 7.3 is used, with the limiting moisture content given by the field capacity θ_f . Field capacity is not a separate input parameter in the model but is set in the program according to soil texture, using the trends given by Schulze (1983). The actual soil evaporation calculated in this way is given the symbol E_{sa} . Soil evaporation does not continue to an indefinite depth but ceases once the soil has dried out down to a certain limiting depth below the surface, which may range from about 150 mm in sand to 500 mm in clay (Scholes, 1989). In the present model the top soil layer only is depleted by soil evaporation.

Water loss from the three soil layers is therefore calculated as follows:

$$\text{layer 1: ET loss} = E_{sa} + T_a k_1 \quad (7.4a)$$

$$\text{layer 2: ET loss} = T_a k_2 \quad (7.4b)$$

$$\text{layer 3: ET loss} = T_a k_3 \quad (7.4c)$$

7.1.4. Suppression by intercepted and ponded water

Blake (1975) noted that transpiration is suppressed during rain because of the intercepted water as well as reduced solar energy, and evaporation of intercepted rain water on foliage proceeds at the expense of transpiration. Similarly the evaporation of water from the soil is suppressed by ponded water on the surface. During and following a shower, evapotranspiration losses are suppressed using a linear relationship after Al-Soufi (1987), in which the losses given by equations (7.4) above are reduced by $(1 - I/I_c)$ where I/I_c is the ratio of intercepted water to interception capacity as dealt with in the next section. The same relationship is used for the suppression of soil evaporation by ponded water.

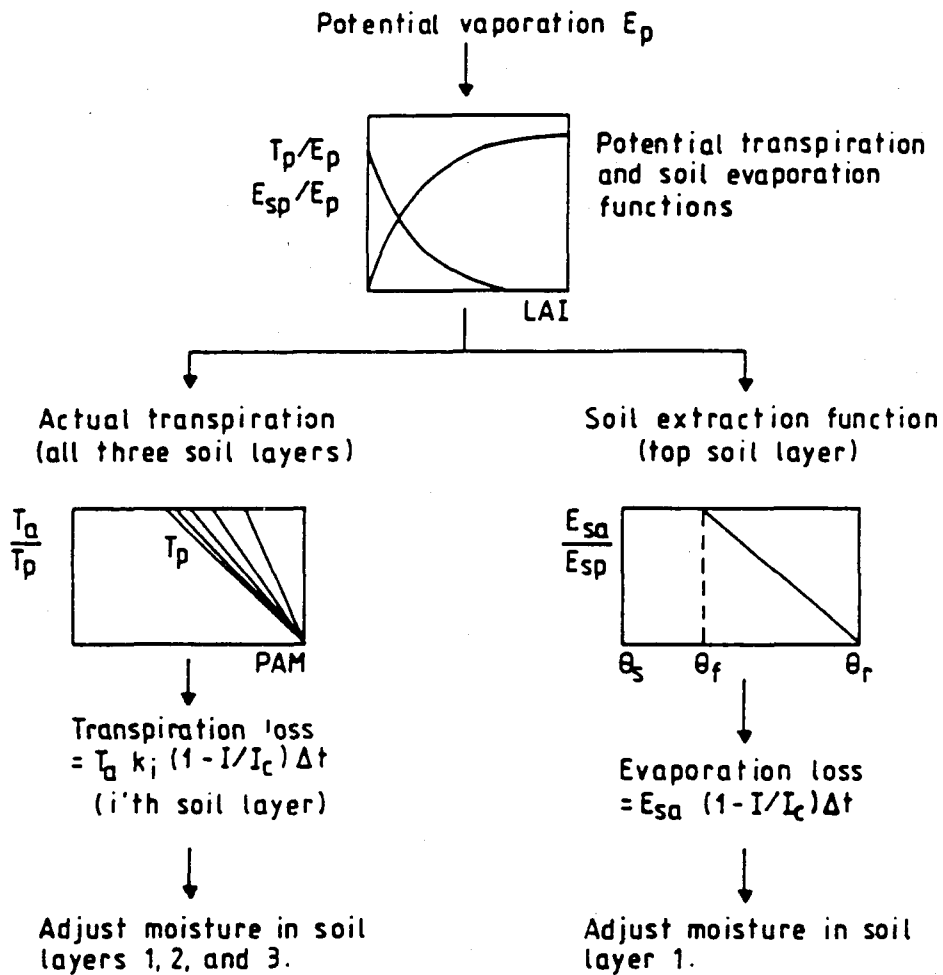
Total evapotranspiration loss in the current time interval Δt is the sum of the losses in the three layers given by

$$\text{Total ET loss} = (E_{sa} + T_a k_1 + T_a k_2 + T_a k_3)(1 - I/I_c)\Delta t. \quad (7.5)$$

7.1.5. Operation of evapotranspiration model

The component processes and sequence of computation are shown in fig. 7.4. The input parameters consist of potential evaporation rate E_p , the leaf area index and the root distribution. Potential evaporation may be assessed using predictive equations or pan evaporation records. LAI depends on plant growth stage, vegetation type and the season of the year. LAI for a particular vegetation type may be measured using radiation-detecting instruments or by measuring sample leaf surfaces, but this is costly in a catchment study and published values may be resorted to as given in Appendix A. For agricultural crops at different growth stages, crop coefficients published by Green (1985) may be used to calculate values of LAI from equation (7.1). LAI typically ranges from less than 1.0 for sparse vegetation cover to more than 3.0 for forests and full canopy crops. In the Bethlehem case study in chapter 10, the seasonal variations in vegetation cover of crops and grasses are taken into account by employing monthly values of LAI.

Figure 7.4: Flow diagram of evapotranspiration model.



Symbols:

- | | | | |
|------------|---|-------|------------------------------|
| E_p | potential evaporation rate | T_a | actual transpiration loss |
| E_{sp} | potential soil evaporation rate | T_p | potential transpiration rate |
| E_{sa} | actual soil evaporation rate | I | intercepted water |
| PAM | plant available moisture | I_c | interception capacity |
| LAI | leaf area index | k | root density |
| Δt | current time interval in simulation program | | |
| θ_s | saturated moisture content of soil | | |
| θ_f | field capacity of soil | | |
| θ_r | residual moisture content of soil | | |

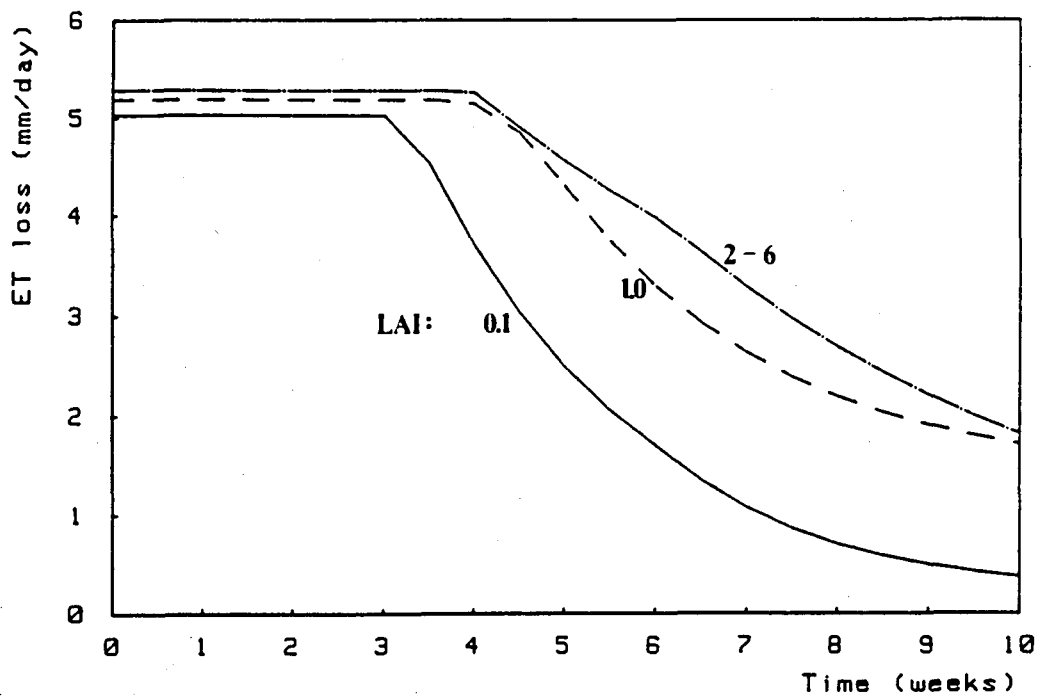


Figure 7.5: Sensitivity of simulated evapotranspiration losses to leaf area index.

Rooting depths vary from less than a metre for small crops and grasses to about 1.5 m for grassland and 4.0 m for forests (Scholes, 1989). Green (1985) gives rooting depths for all agricultural crops grown in Southern Africa, and Schulze (1984) presents guidelines for estimating root distributions for natural vegetation.

Fig. 7.5 shows curves generated by this model showing the effect of LAI on total evapotranspiration loss for a 1 m thick soil mantle with 60 % of the roots in the top 500 mm and a potential evaporation rate of 5 mm/day. The curves fall away sharply when plant stress sets in, and evapotranspiration losses are higher for larger LAI-values because of a more extensive transpiring surface. In the simulation program the evapotranspiration sub-model is evoked immediately after the soil sub-model to adjust soil moistures at every time step.

7.2. INTERCEPTION

7.2.1 The interception process

As described by Gorgens (1978), there are two phases in the interception process during a shower of rain. The first involves the build-up of intercepted water on the vegetation until capacity is reached. Water collects in droplets and films on the surfaces of leaves, stems and branches. If the shower continues long enough, the second phase will be entered when the maximum surface storage capacity of the vegetation is exceeded and the only interception loss is that required to balance evaporation loss from the leaf surfaces. This process is represented by the interception loss curve shown in fig. 7.6.

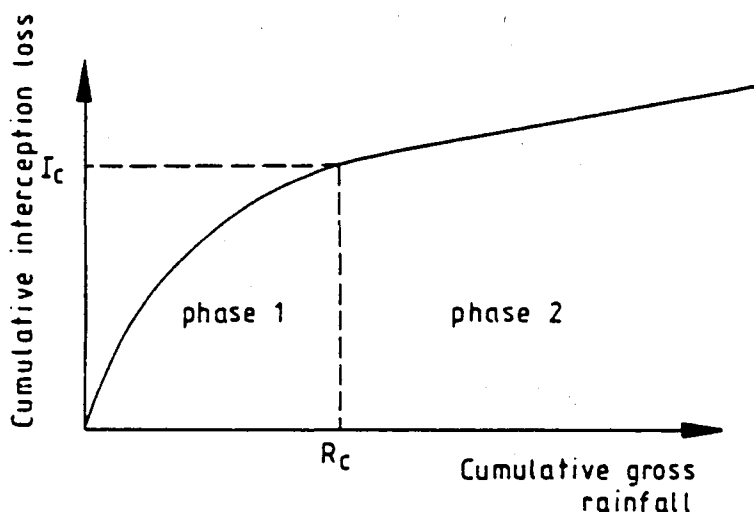


Figure 7.6: Form of the interception loss curve during a shower.

7.2.2. Predicting interception loss

The variables on which interception loss depends during a shower include rainfall intensity, storm duration, evaporation, and vegetation type and density. Current approaches to predicting interception losses can be summarised as follows:

(i) *Average daily interception amounts*

The simplest means of accounting for interception loss is to use average daily values (mm lost/day) which depend on vegetation type and climate. Typical values of daily interception losses for crops and natural vegetation have been published by de Villiers (1975) and Schulze (1984). The ACRU (Schulze, 1984) and Pitman (Pitman, 1977) daily time increment models are among those using this approach.

(ii) *Regression correlations*

Horton (1919) published a set of regression equations relating interception loss to gross rainfall for various vegetation types, and numerous studies have since used this approach. The relationships are generally either linear or logarithmic and often exhibit large amounts of scatter. Jackson (1975) presented a correlation for a tropical rain forest in East Africa, and showed that the data could be better represented as an interception/storm-duration/rainfall-intensity diagram.

(iii) *Models incorporating meteorological and vegetation data*

Models in this category aim at reproducing the details of the interception process, using meteorological data and vegetation characteristics. Two well-known examples are the models of Rutter *et al* (1971) and Gash (1979) which can reproduce measured interception amounts accurately but have a large number of parameters requiring measurement or calibration.

In the present study, rainfall input consists of break-point data, and time increments much smaller than one day are used to model short-term, time-dependent processes such as infiltration and overland flow. Within this context, a dynamic modelling of the interception process is clearly preferable to the daily interception and regression approaches described above. Schulze *et al* (1978) maintained that interception storage is of sufficient importance in the water balance to warrant the use of interception models in preference to gross daily interception amounts.

In this study a single dynamic interception store was adopted in preference to the data-intensive Rutter- and Gash-type models. The model described below is simple with easily-assessed parameters, but represents the essential time-dependent aspects of the interception process. The

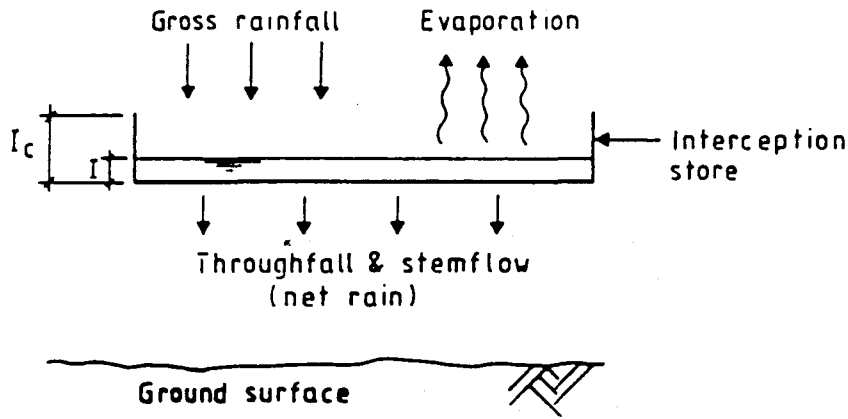


Figure 7.7: Conceptual interception store.

use of a store is no less physically-based than models such as that of Rutter *et al* (1971) which also employs interception stores.

7.2.3. Development of interception equations for the present study

The interception component of the simulation model is conceptually based on a leaky tank analogy as illustrated in fig. 7.7. Input to the store is rainfall, and the contents are constantly depleted by evaporation, throughfall and stemflow. Evaporation is lost from the system, and throughfall and stemflow constitute net rainfall. The store starts filling up at the beginning of a shower until it is full (phase 1) whereafter the evaporation rate determines the interception loss (phase 2). The depth of water in the store represents the amount of water currently retained on the vegetation, and the interception capacity I_c corresponds to the capacity of the canopy to retain water.

Linsley *et al* (1949) considered interception loss to consist of two components, namely that required to satisfy the surface storage of the vegetation, and that which evaporates during the period of rainfall. This can be expressed as

$$I_L = I_s + E_L \quad (7.6)$$

where I_L is cumulative interception loss, and I_s and E_L are cumulative losses to vegetation storage and evaporation respectively. I_s corresponds to the water level in the store. Linsley *et al* (1949) further suggested an exponential relationship for the cumulative interception

loss. Following this approach for the storage component I_s , eqn. (7.6) can be written as

$$I_L = I_c (1 - e^{-kR/R_c}) + E_L \quad (7.7)$$

in which R is cumulative rainfall, R_c is the cumulative rain when the store reaches capacity, and k is a dimensionless constant. In evaluating the constant k , Linsley *et al* (1949) reasoned that for very short storms, the interception should approach the rainfall, the limiting condition being dI/dR equal to unity for $R = 0$. Differentiating eqn. (7.7) with respect to R gives

$$dI_L/dR = (I_c k/R_c) e^{-kR/R_c} + dE_L/dR. \quad (7.8)$$

Taking discrete time steps Δt , with the evaporation from the leaf surface equal to the potential evaporation, the derivative dE_L/dR can be expressed as $(E_p \Delta t)/(i \Delta t)$ or simply E_p/i . Setting $dI_L/dR = 1.0$ and $R = 0$ in eqn. (7.8) gives an expression for k as follows:

$$k = (R_c/I_c)(1 - E_p/i). \quad (7.9)$$

Eliminating R/R_c from eqns. (7.7) and (7.8) and making use of eqns. (7.6) and (7.9) gives

$$dI_L/dR = (1 - I_s/I_c)(1 - E_p/i) + E_p/i. \quad (7.10)$$

Eqn. (7.10) can be used to evaluate the incremental interception loss ΔI_L by multiplying by the incremental rainfall ΔR falling in a time increment Δt (i.e. $\Delta R = i \Delta t$):

$$\begin{aligned} \Delta I_L &= (dI_L/dR) \Delta R \\ &= (1 - I_s/I_c)(1 - E_p/i) i \Delta t + E_p \Delta t \end{aligned} \quad (7.11)$$

Eqn. (7.11) facilitates the computation of incremental interception loss during any time increment, using the current status of the interception store (I_s/I_c), the gross rainfall rate and the potential evaporation. Note that during phase 2 interception when $I_s = I_c$, eqn. (7.11) gives the interception loss as $E_p \Delta t$ as expected.

For continuity, the status of the interception store at the current time interval (I_t) is related to the status at the previous time interval ($I_{t-\Delta t}$) by

$$I_t = I_{t-\Delta t} + \Delta I_L - \Delta E_L \quad (7.12)$$

where ΔE_L is the evaporation loss during the current time increment, equal to $E_p \Delta t$. Combining eqns. (7.11) and (7.12), setting $I_s = I_t$ (equivalent to $\phi = 0$ in a Preissmann finite difference scheme), and solving for I_t results in the following expression:

$$I_t = \frac{I_{t-\Delta t} + \Delta t(i - E_p)}{1 + (i - E_p)\Delta t/I_c} \quad (7.13)$$

At equilibrium (phase 2 interception), it is expected that $I_t = I_{t-\Delta t} = I_c$. Substituting I_t for $I_{t-\Delta t}$ reduces eqn. (7.13) to $I_t = I_c$ as expected.

Net rainfall intensity is calculated from

$$i_n = i - \Delta I_L / \Delta t \quad (7.14)$$

where i is the gross rainfall intensity measured by raingauges.

When $i = 0$, eqn. (7.11) is undefined. It is also not applicable at very low rainfall rates when $i < E_p$, since the derivation is based on the assumption that there is sufficient rain to be divided between interception storage and evaporation. Under these conditions therefore the following relationships are used in place of eqns. (7.11) and (7.13):

$$\Delta I_L = i\Delta t \quad (7.15)$$

$$I_t = I_{t-\Delta t} + \Delta t(i - E_p) \quad (i < E_p \text{ or } i = 0) \quad (7.16)$$

Eqns. (7.11) to (7.16) constitute the interception model used in the hydrological simulation program. Any approximations introduced by deriving eqn. (7.11) from a theoretical relationship are outweighed by uncertainties in interception capacity, evaporation rate and measured rainfall.

7.2.4. Application of interception model

Fig. 7.8 shows rainfall curves obtained using equations (7.11) to (7.14) with constant rainfall and evaporation rates and assumed values of interception capacity. Fig. 7.8(a) shows that the higher the rainfall intensity, the shorter is the duration of phase 1 interception, because the interception store fills more quickly. It also illustrates that interception is a more significant loss for low intensity rain than for heavy storms. Fig. 7.8(b) and (c) show that the model is more sensitive to interception capacity than to potential evaporation.

The interception capacity (I_c) differs from one species of vegetation to the next and also varies seasonally. De Villiers (1978) published interception capacities ranging from 0.15 to 0.8 mm for a number of crops at various growth stages. Interception capacities for grass are typically 1.0 to 1.2 mm (Chow, 1964) and for South African savanna about 1.25 mm (de Villiers, 1982). Trees vary widely, with values of I_c commonly in the range of 0.5 to 2.0 mm, although values of up to 6 or 8 mm have been reported for mature, dense stands of trees and tropical forests (Zinke, 1967; Jackson, 1975; Horton, 1919). In Southern Africa, I_c varies typically from about 0.3 mm for sparse vegetation to 2.0 mm for dense vegetation. Guidelines for estimating interception capacities for different vegetation types are given in the User's Manual (Appendix A).

7.3. SUMMARY

The routines used for computing evapotranspiration and interception losses at each time step in the simulation program have been described. The evapotranspiration component is based on canopy leaf area with adjustments for root distributions and limiting soil moisture conditions. The equations used for calculating interception losses were derived using continuity and an exponential relationship for cumulative interception loss.

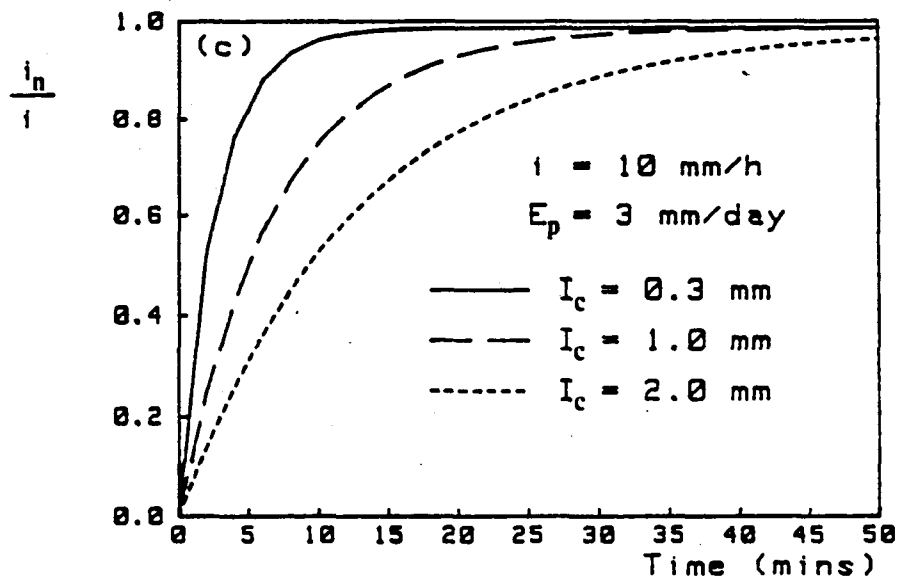
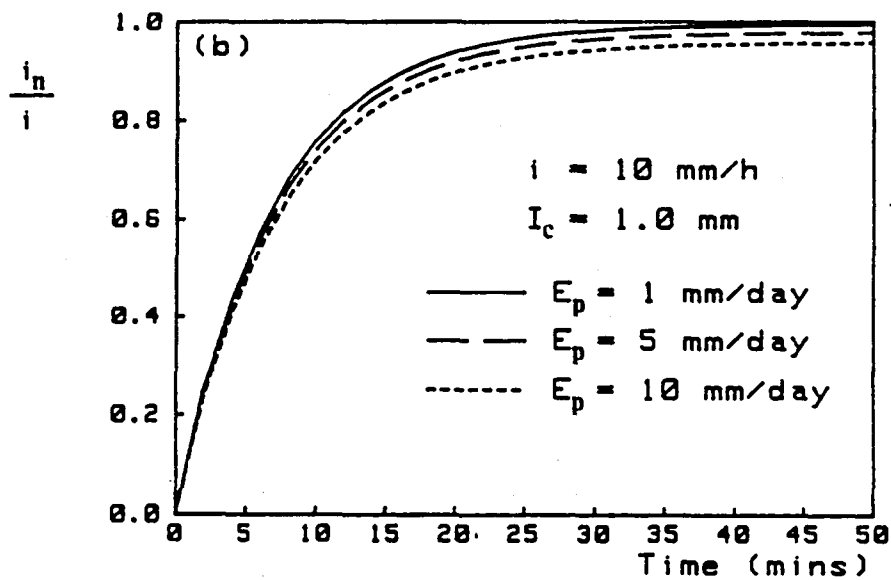
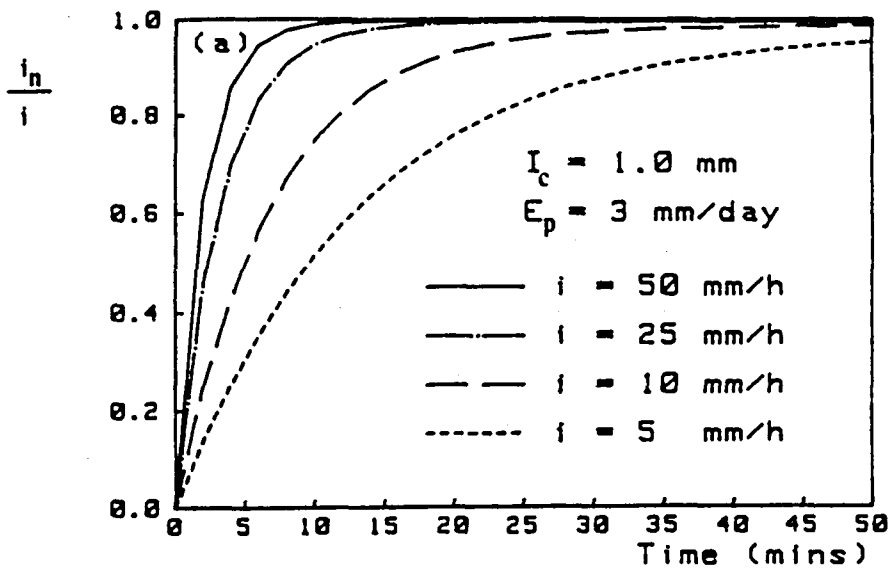


Figure 7.8: Sensitivity of interception equations to (a) gross rainfall rate, (b) potential evaporation and (c) interception capacity.

8.1. CATCHMENT DESCRIPTION

Waterval is a small research catchment, 75 ha in extent, situated on a farm on the northern border of the Johannesburg metropolitan area. Vegetation is open grassland (veld) and scattered to dense clusters of trees, mainly bluegums. A small amount of grazing is allowed, but the land is generally unused. A few houses and an electrical substation on the watershed encroach on the catchment, but the area covered by them is small and does not detract from the rural nature of the area.

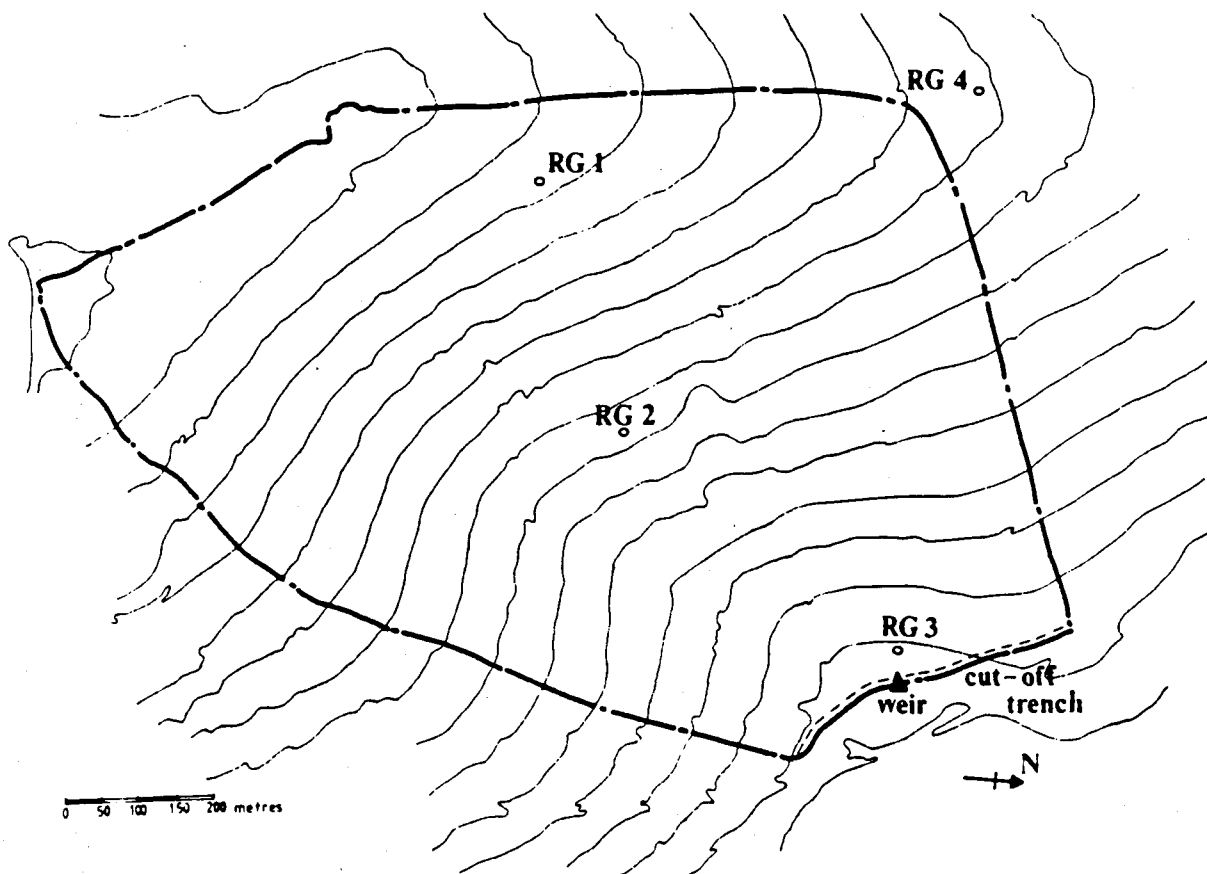


Figure 8.1: Map of Waterval catchment.

There are no streams in the catchment, but as can be seen in fig. 8.1, the ground slopes fairly uniformly down to a cut-off trench at the bottom of the hillslope, which converges the storm runoff into a gauging weir where flow is measured and channelled out of the catchment. Ground slopes are about 5%. The underlying rock is granite, with soils of decomposed granite overlain in places by transported soil of a higher clay content.

Waterval lies in a temperate climate with a mean annual precipitation of 740 mm. Most of the rainfall occurs in the summer months and is characterised by sudden, sharp thunder storms. This, coupled with the high infiltration rates of the sandy soils, results in low, sporadic runoffs. Consequently the catchment is more suited to event modelling than continuous modelling. The focus of this study is a 2-day, multiple event occurring during the wet season of 1987. Features of particular interest are rilling and interflow. Also illustrated in this study is the spatial variation of rain on a small catchment.

8.2. DATA COLLECTION

The Waterval catchment is monitored by the Water Systems Research Group, and rainfall and runoff data was obtained for the present study from this data bank. Vegetation and soil data was collected for the present study as described below.

The vegetation map in fig. 8.2 was compiled from aerial photographs and site surveys. The northern part of the catchment is open veld with occasional rock outcrops and localised clusters of heather bushes. The remainder of the land has tree and grass cover with some dense groves of trees, as seen in plate 8.1.

Soil profiles were studied from existing borehole data, and in addition a soil survey was carried out to ascertain the soil textures of the topsoil. Seventeen soil samples were taken from different locations scattered over the catchment at depths up to 500 mm, and were analysed using hydrometer and sieve tests to obtain their particle size distributions and hence the soil textures. Details of the test results and locations of the soil samples are given in Appendix D along with the



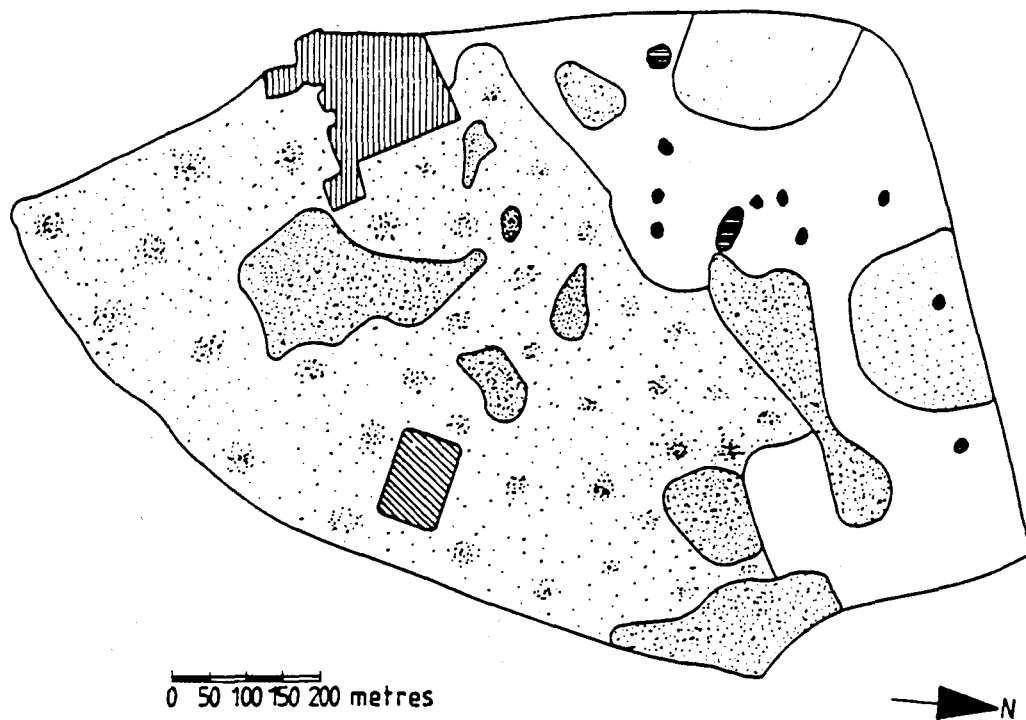
Plate 8.1: General Waterval landscape.

borehole profiles. Most of the catchment was found to be loamy sand as shown in fig. 8.3, with a small zone of very clayey soil around the gauging weir. This clay layer could be seen from the borehole profiles to penetrate about 4.5 m below the ground surface.

Borehole profiles and electrical soundings revealed soil depths of 3.5 to 4.0 m in the western and southern portions of the catchment, deepening to 20 or 30 m in the central and northern parts. A perennial water table lies well below the soil surface.

The monitoring instrumentation includes four tipping-bucket raingauges to measure precipitation (plate 8.2) and a pressure transducer which measures the water depth behind the gauging weir. The data is stored on electronic data loggers and transferred via EPROMS to a microcomputer data base. The locations of the raingauges and weir are shown in fig. 8.1.

The use of this data in the present study necessitated processing of the raw data for the chosen simulation period, viz. screening, filtering and re-formatting. A program was developed for re-formatting the rainfall



- 0 50 100 150 200 metres
- LEGEND
-  Open veld
 -  Veld with scattered heather bushes
 -  Thick grass with scattered trees
 -  Dense trees with sparse grass
 -  Rock outcrops
 -  Lawn playing field
 -  Roads and buildings

Figure 8.2: Vegetation types of Waterval.

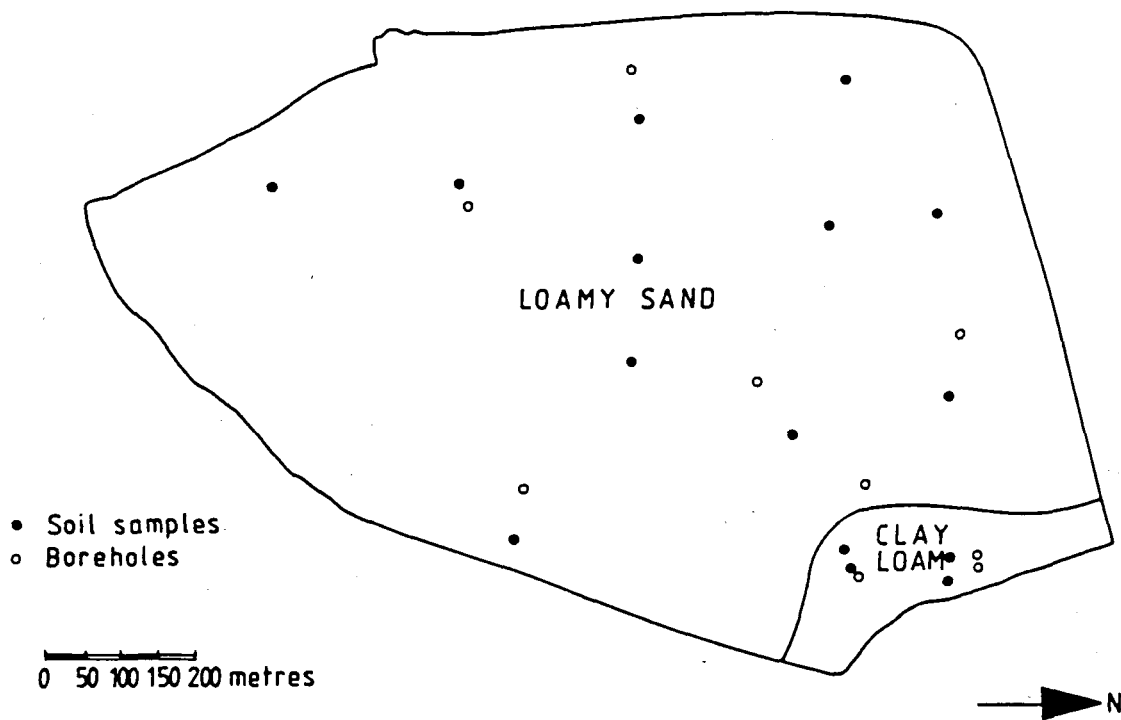


Figure 8.3: Soil map showing positions of soil samples and boreholes.

data in the format required by the simulation program, and is listed in Appendix F.

The weir for measuring runoff at the catchment outlet is shown in plate 8.3. It consists of a V-notch for low flows surmounted by a portion with vertical sides for higher flows. Using the guidelines of Ackers *et al* (1978), the rating relationship for this configuration was established as:

$$Q = 2.766 h^{2.5} \quad \text{for } h < 0.373 \text{ m} \quad (8.1)$$

$$Q = 2.766 (h^{2.5} - (h - 0.373)^{2.5}) \quad \text{for } h \geq 0.373 \text{ m} \quad (8.2)$$

where h is the height of water above the bottom of the V (in metres) and Q is the flow rate (in m^3/s). A substantial pool of water can form behind the weir during heavy rains, and so it was necessary to use the reservoir routing facility of the simulation program to route runoffs through the

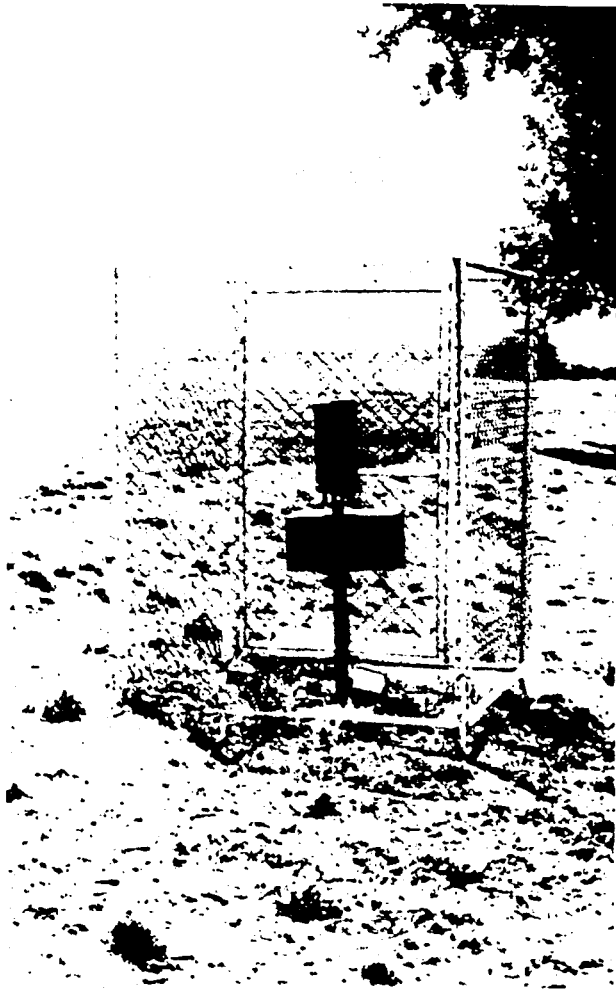


Plate 8.2:
Raingauge instrumentation
in the catchment.

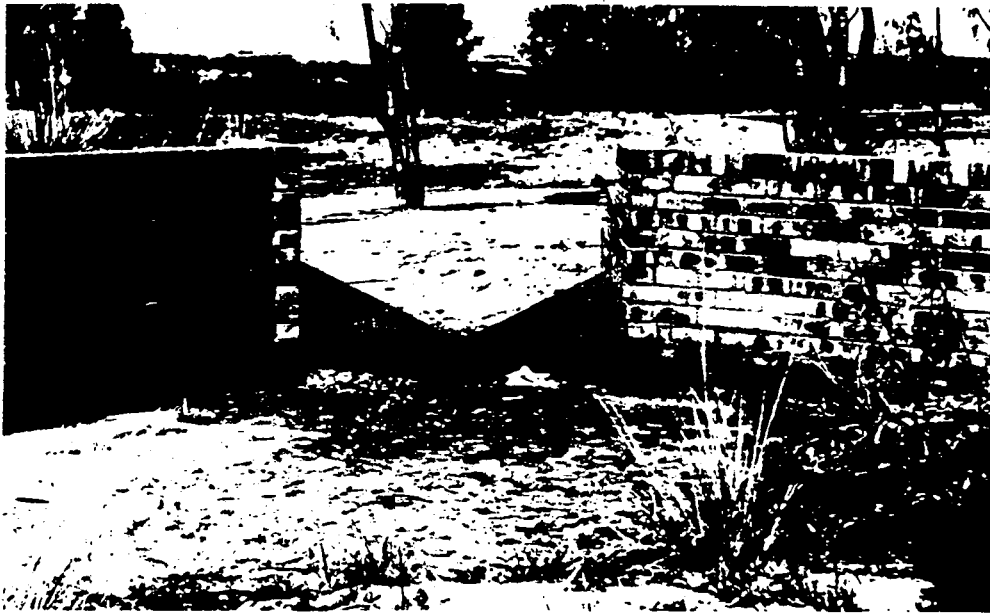


Plate 8.3: Measuring weir viewed from upstream side.

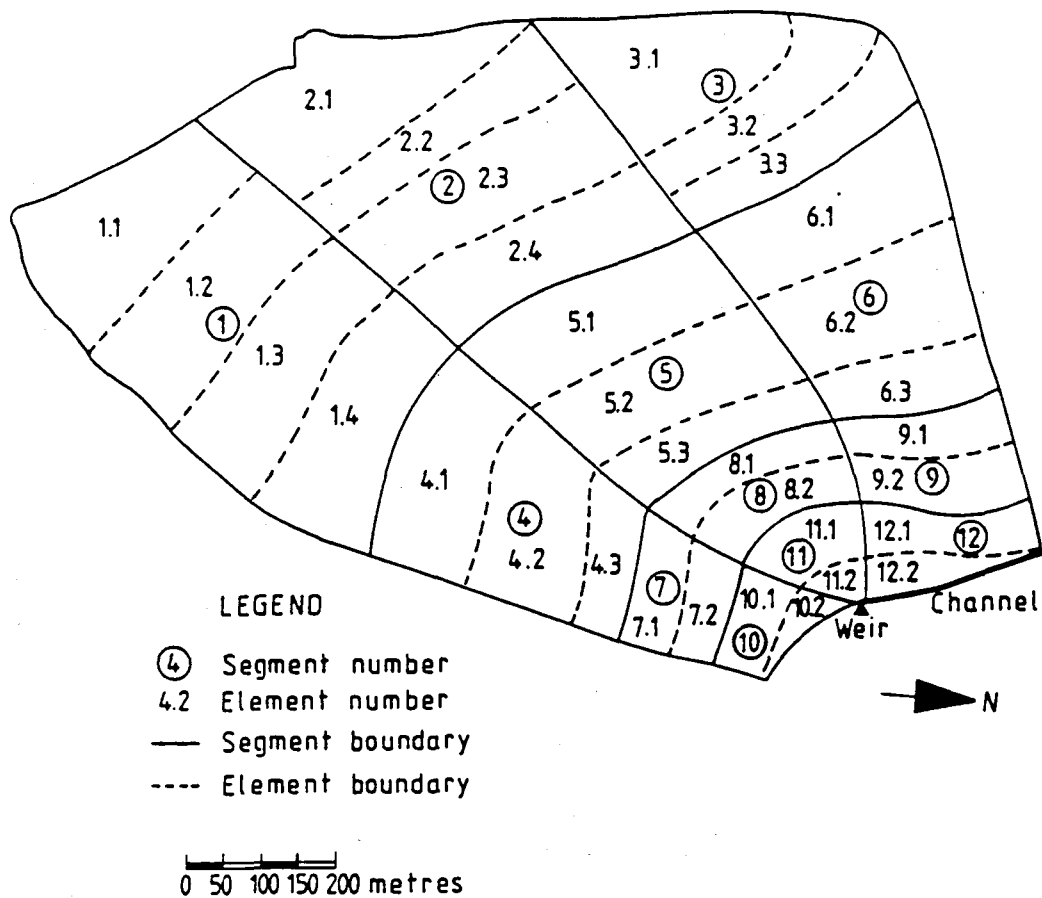


Figure 8.4: Discretization of catchment for model simulations.

storage behind the weir. The following storage/stage relationship was obtained by surveying the area prone to flooding behind the weir:

$$S = 62.1 h^{2.5} \quad (8.3)$$

for storage S in m^3 and h in meters.

Waternal has generally yielded low runoffs since its establishment as a research catchment, but a large event was recorded in October 1987 which was selected for this study. It constitutes a 2-day period of intermittent rain with sharp peak runoffs and low baseflows.

8.3. CATCHMENT DISCRETIZATION AND INPUT DATA

For application to the simulation program the catchment was discretized into segments and elements as shown in fig. 8.4. Element boundaries follow topographic contours and each of the segments 1 to 9 cascades onto its respective downslope segment. Segments 10 and 11 have nodal outflows onto the weir, and runoff from segment 12 flows laterally into the cut-off trench which is modelled as a small trapezoidal channel. Ground slopes and areas were digitised together with the element and segment boundaries from a topographical map.

Overland and vegetation input data were estimated by visual assessment of the catchment and are tabulated in table 8.1. The Manning's roughness coefficient of 0.15 for overland flow is the mean value recommended for prairie or veld in Appendix A. Significant branched rilling occurs in segment 11, and a large gully fed by rills drains segment 10 as shown in plate 8.4. Using the guidelines developed in the rill study in chapter 4, width factors of 0.40 and 0.60 were selected for segments 10 and 11 respectively. The remainder of the catchment shows minor rilling for which a width factor of 0.85 was used as shown in table 8.1. Interception capacities of 1.25 and 1.0 mm were used for tree-cover and open grassland respectively.

Table 8.2 shows the input soil data used in model simulations. Results of geophysical investigations of Waterval (Antoine, 1989) showed that about the top 250 mm of the soil governs the short-term response to rain. Accordingly the top two soil layers in the model were set to a total thickness of 250 mm representing the hydrologically active topsoil. The lower soil layer was set at 1.0 m thick to accommodate saturated flow without saturating to the surface. The clay region (segments 10 to 12) were treated slightly differently as shown in table 8.2.

Soil groups were based on the results of the soil survey and correspond to the soils shown in fig. 8.3. Hydraulic conductivity values of 60 and 2.3 mm/h were taken from the soil data of Rawls *et al* (1981) and correspond to mean values for loamy sand and clay loam respectively. The deep seepage was estimated by consulting records of water table levels for four



Plate 8.4: Gully draining segment 10.

boreholes in the catchment. Assessing the rise and drop of the water table during wet and dry periods, the percolation of infiltrated water to the water table was estimated for the four boreholes as 0.55 mm/h, 0.61 mm/h, 0.62 mm/h and 0.68 mm/h respectively. An average value of 0.60 mm/h was therefore assumed as deep seepage from the lower soil layer.

Evapotranspiration was not modelled in this study because of the relatively short duration of the simulation. Potential evaporation for the interception store was taken from regional monthly records, and allowing for a reduction due to cloud cover was set at 2 mm/day.

The data shown in tables 8.1 and 8.2 was used to generate the results presented below without adjustment or calibration.

Table 8.1: Overland and vegetation data used in the Waterval study.

Segment	Manning's n	Width factor	Interception capacity (mm)
1	0.15	0.85	1.25
2	0.15	0.85	1.25
3	0.15	0.85	1.0
4	0.15	0.85	1.25
5	0.15	0.85	1.25
6	0.15	0.85	1.0
7	0.15	0.85	1.25
8	0.15	0.85	1.25
9	0.15	0.85	1.0
10	0.15	0.40	1.25
11	0.15	0.60	1.0
12	0.15	0.85	1.0

Table 8.2: Soil data used in the Waterval study.

segments	soil layer	layer thickness (mm)	soil group*	permeability (mm/h)	deep seepage (mm/h)
1 - 9	1	100	2	60	0.6
	2	150	2	60	0.6
	3	1000	2	60	0.6
10 - 12	1	250	7	2.3	0.6
	2	250	7	2.3	0.6
	3	1000	7	2.3	0.6

*soil groups: 2 = loamy sand
7 = clay loam

8.4. STORMFLOW MECHANISM AND ANTECEDENT MOISTURE CONDITIONS

Model simulations and site surveys quickly identified the primary mechanisms of stormflow production at Waterval. Hydrologically the catchment can be divided into three zones:

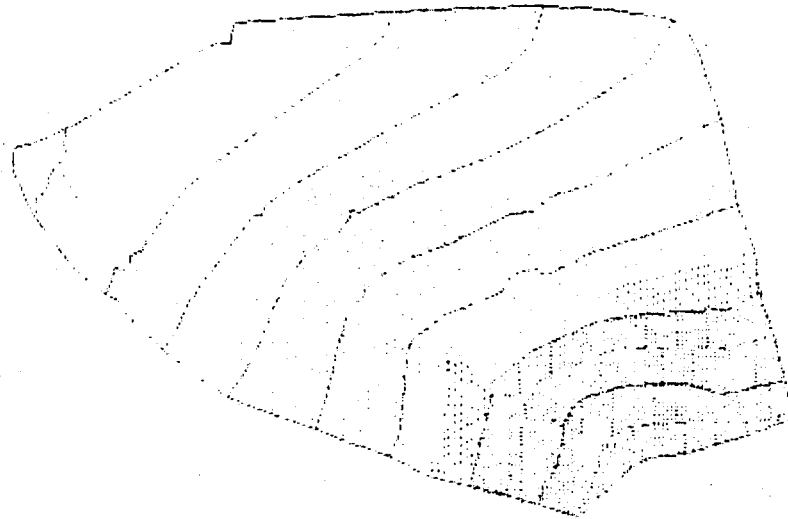
(i) *Upper catchment* (segments 1 to 3 in fig. 8.4): This area offers virtually no contribution to stormflow because of the sandy soils as well as low soil moistures resulting from downslope seepage between rain events.

(ii) *Mid portion* (segments 4 to 6): There is little runoff from this area because of moderate to high infiltration rates, also related to soil moisture.

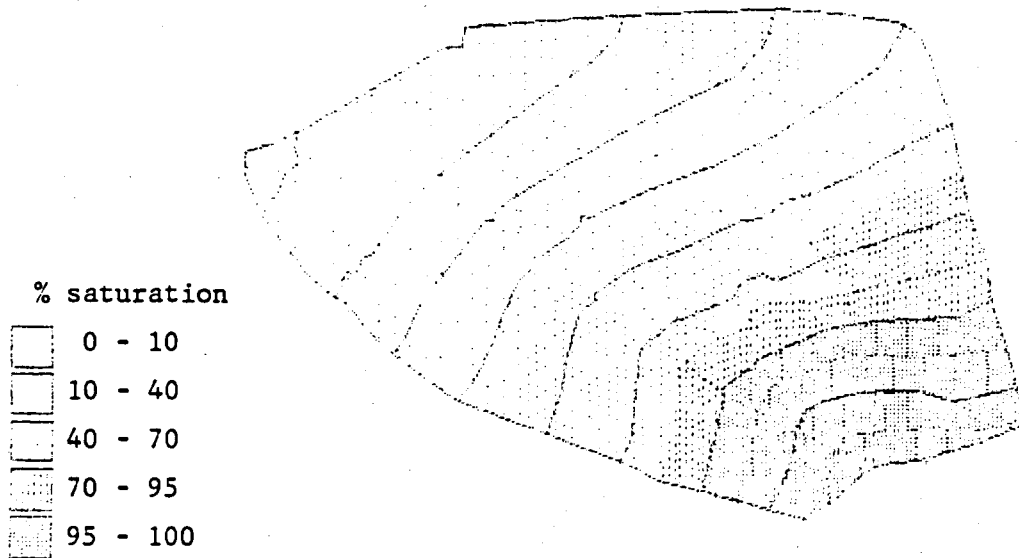
(iii) *Lower zone* (segments 7 to 12): This is the source area for storm runoff, because the clay region (segments 10, 11 and 12) has low infiltration rates, low permeability and high moisture retention, and blocks downslope soil moisture seepage from segments 7, 8 and 9, creating a zone of high soil moisture which acts as a primed source area for storm runoff. The presence of the clay region also results in exfiltration from segments 7, 8 and 9, since the downslope seepage of soil water after a storm is interrupted by the low-permeability clay and forced to the surface. Significant amounts of exfiltrating water have been observed shortly after a storm, apparently emerging from the ground at the approximate junction of segments 7, 8 and 9 with segments 10, 11 and 12.

Probably more than 90% of the storm runoff comes from area (iii), with a prolonged baseflow/interflow contribution resulting from exfiltration of soil water accumulated in areas (ii) and (iii).

As the present study follows an event-modelling approach, setting up the antecedent moisture conditions at the start of the simulation is of particular importance. Some rain had been recorded in the weeks preceding the event, suggesting damp soil conditions. A certain amount of trial with different antecedent moisture conditions was necessary. Using the information presented above on the stormflow mechanism as a guideline, antecedent soil moistures were finally assigned such that the source area was saturated and upslope soil moistures decreased according to the linear



(a) 15h35 on 26/9/1987 - start of storm (antecedent conditions)



(a) 16h15 on 26/9/1987 - end of storm

Figure 8.5: Soil moisture plots

variation of the ratio of upstream contributing area to local ground slope (a/s) as discussed in chapter 6 on subsurface processes. The resulting spatial variation in antecedent moistures is represented graphically in fig. 8.5(a) in which the intensity of shading represents the average moisture content in the topsoil (soil layers 1 and 2). Having set the antecedent moistures at the start of the simulation, they were not artificially re-set for any of the subsequent runoff peaks in the two-day simulation period, but the model was left to simulate continuously the above- and below-ground hydrological conditions for the full two-day period.

8.5. SIMULATION RESULTS

Simulation was started at 15:35 on 26/9/1987 at the start of a major storm, and terminated at 12:00 on 28/9/1987. The period modelled starts with a large storm followed by intermittent rain. The spatial distribution of rain was found to vary considerably despite the small size of the catchment. This is illustrated in table 8.3, taken from the first storm in the simulation. Shown here are the rainfall intensities allocated to each segment by the interpolation procedure of the model, interpolating between the four raingauges at each time step. It can be seen here that there are significant differences in rainfall between the top and bottom of the catchment. Furthermore on examination of this table the storm can be seen to be moving uphill over the catchment. For the first 20 minutes the highest intensities are at the bottom of the hillslope (segments 10 to 12), but this bias first equalises and then shifts somewhat to the top (segments 1 to 3) as the storm proceeds.

Changes in soil moisture during this storm are seen in fig. 8.5 showing soil moisture plots generated by the model before and after the first storm. Soil conditions at the end of the storm show a general increase in soil moisture over the catchment relative to the antecedent conditions, although the source area has remained relatively unchanged.

Fig. 8.6 was plotted using the hydrograph plotting facility "HYDRO" of the simulation program (described in Appendix A). Fig. 8.6(a) shows the runoff hydrograph generated by the simulation model for the input data

Table 8.3: Rainfall intensities (mm/h) interpolated by the simulation program from the raingauge data.

Segment	Time								
	15:40	15:45	15:50	15:55	16:00	16:05	16:10	16:15	16:20
1	0.9	6.9	21.4	44.8	62.8	64.1	43.5	24.7	1.2
2	2.0	8.8	17.7	50.9	77.2	53.6	35.9	7.6	1.2
3	1.1	8.7	18.3	51.6	75.0	65.8	43.0	12.9	1.2
4	0.3	5.5	23.2	41.2	54.7	68.8	47.1	34.0	1.1
5	0.1	3.4	22.0	39.4	52.1	69.2	47.6	36.6	1.2
6	0.9	14.6	25.5	52.6	72.8	70.0	45.8	16.2	0.9
7	1.8	28.4	38.5	57.9	77.4	67.5	44.2	11.3	0.5
8	2.0	31.2	40.4	59.9	80.1	67.5	43.9	8.7	0.4
9	2.2	35.4	43.3	63.1	84.4	67.4	43.5	4.3	0.3
10	2.3	36.8	44.5	63.8	85.1	67.2	43.3	3.7	0.3
11	2.4	38.2	45.5	64.7	86.2	67.2	43.2	2.6	0.2
12	2.4	38.1	45.3	64.6	86.2	67.2	43.2	2.6	0.2

and antecedent moisture conditions described above. A very good fit with the observed hydrograph is clearly evident on all except the last peak. The rainfall hyetograph is shown in this figure as a spatially average rainfall for the catchment. The input data was not calibrated in order to obtain this fit, apart from experimenting with different antecedent moisture conditions.

A better understanding of the runoff can be gained from looking at a plot of the flow depth over the weir, which is shown in fig. 8.6(b). Because of the V-portion of the measuring weir, low flows that are too small to be visible on the runoff hydrograph plot can be studied on the flow depth plot. Fig. 8.6(b) shows a prolonged baseflow lasting for a number of hours after every shower. This is caused by the interflow described previously, and as can be seen here the model has failed to predict it. Although this would appear to be a major omission on first glance, the

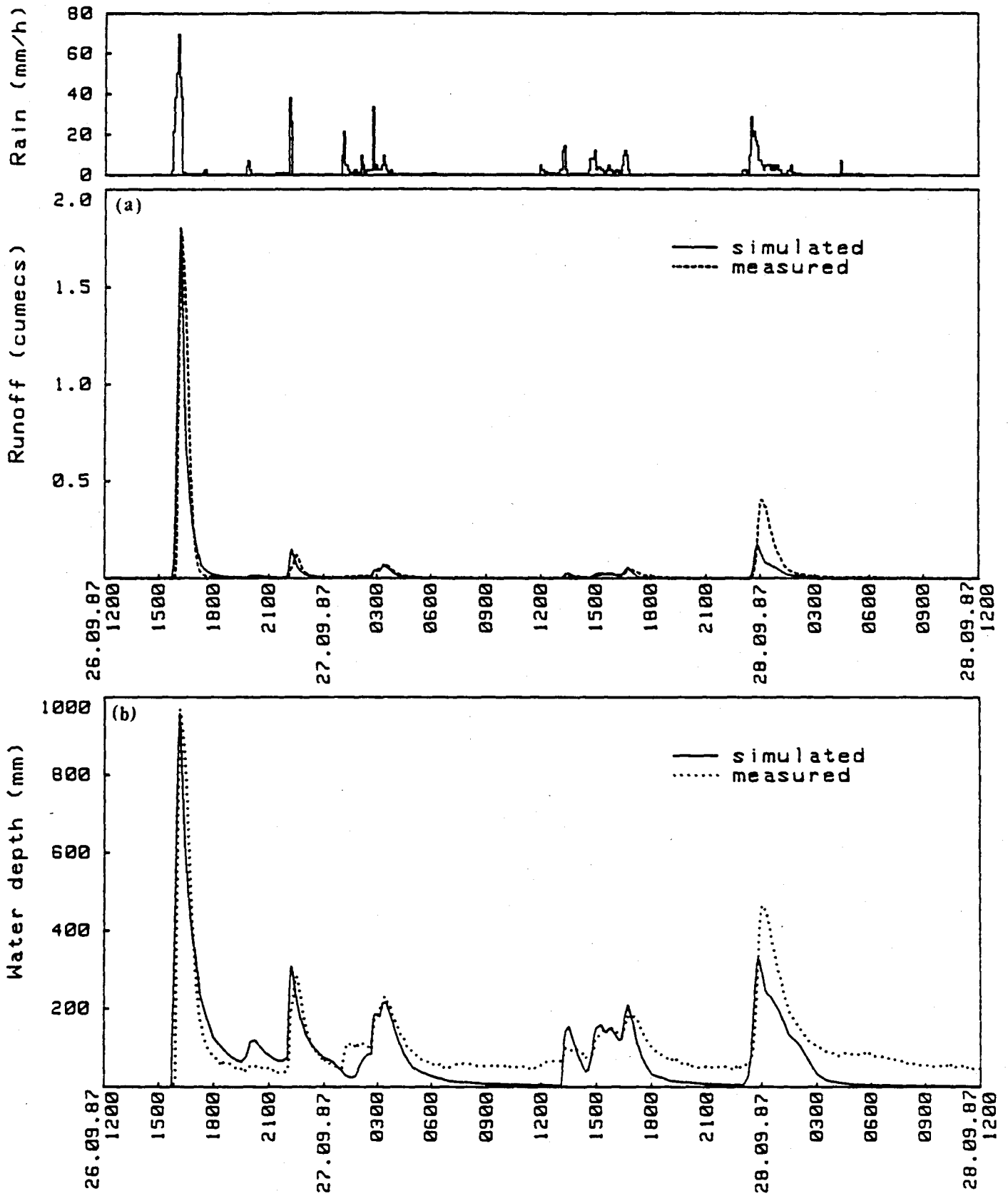


Figure 8.6: Simulation without interflow. (a) Runoff hydrograph. (b) Depth over weir.

magnitude of this baseflow is very low - about 50 mm over the weir which is approximately $0.0015 \text{ m}^3/\text{s}$.

The following procedure was employed for modelling the interflow component. Using the lower soil layer to model downslope seepage of water, exfiltration was forced at the junction of segments 7, 8 and 9 with segments 10, 11 and 12, where it has been observed to occur in the field. Then holding all other input parameters constant, the saturated conductivity of this soil layer was altered by trial until the correct interflow was simulated. The final solution is shown in fig. 8.7(b) with the corresponding runoff hydrograph in fig. 8.7(a), using a permeability of 900 mm/h for the lower soil layer and modifying the deep percolation from the clay region (segments 10 to 12) to 0.3 mm/h. No other changes were made to the input data and the same antecedent moisture conditions were used as previously. In fig. 8.7 it can be seen that the interflow has been successfully modelled. It should be noted that introducing interflow into the simulation is more complex than superimposing a baseflow onto the surface runoff, since exfiltrating water flows over the clay segments (10, 11 and 12) and hence is interactive with the overland routing.

The time increments used in this simulation are shown graphically in fig. 8.8, in which the time increment is plotted as a logarithmic ordinate. Small time increments of 5 minutes were used during moderate to high intensity rain, increasing to larger time increments for light rain and for modelling the recession limbs of surface runoff.

Statistical measures of fit for the simulated and recorded hydrographs were computed using equations given in Appendix C, and are shown in table 8.4. The coefficient of efficiency is a dimensionless measure of fit for hydrograph shape, and lies close to 1.0 for a good fit. The reduced error of estimate tends towards zero as a fit improves. Both of these statistics show good overall model results with slight improvement when the interflow is correctly simulated.

For comparison of the simulations with and without interflow, the sum of squared and log residuals were computed. These statistics can only be

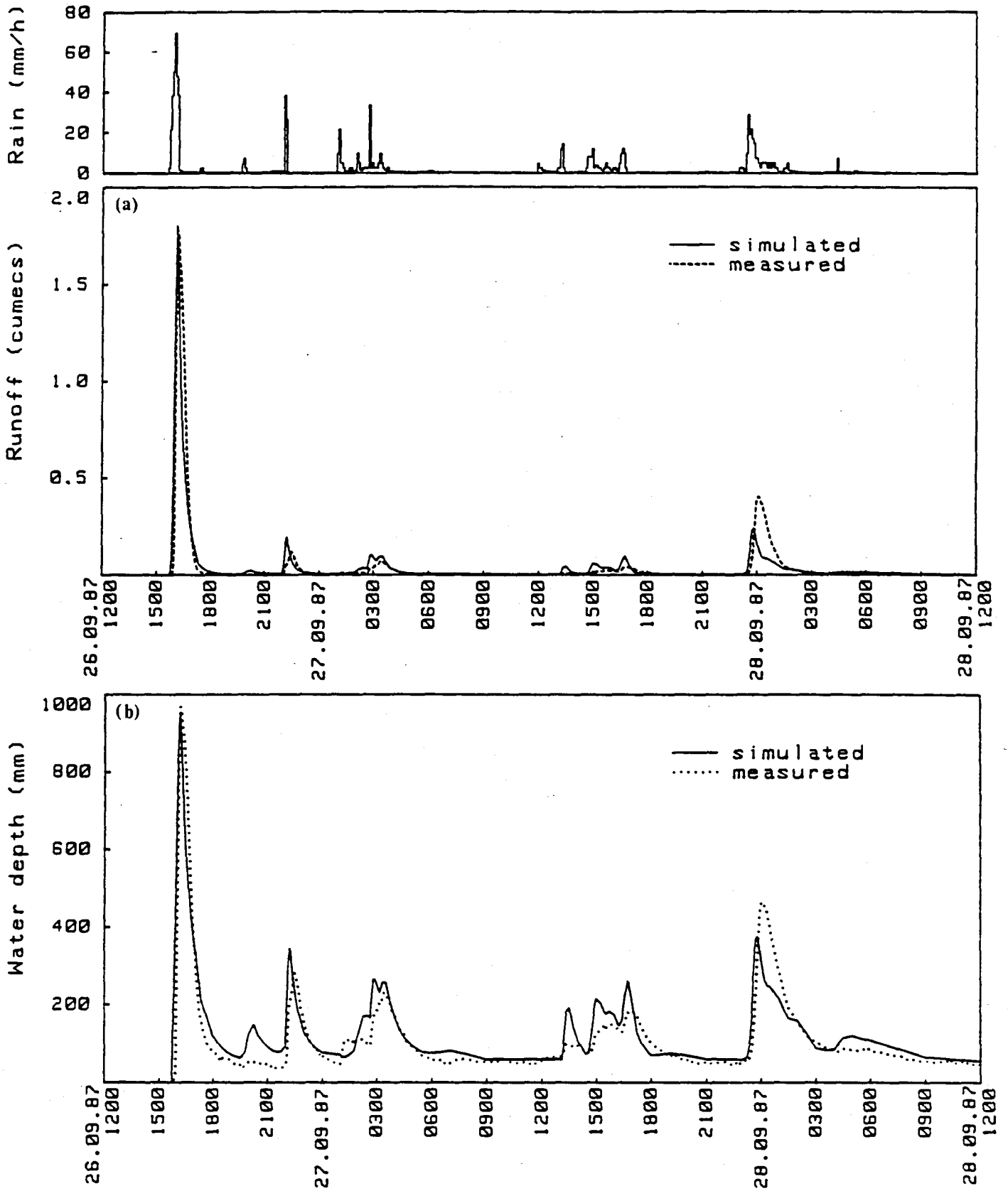


Figure 8.7: Simulation with interflow. (a) Runoff hydrograph. (b) Depth over weir.

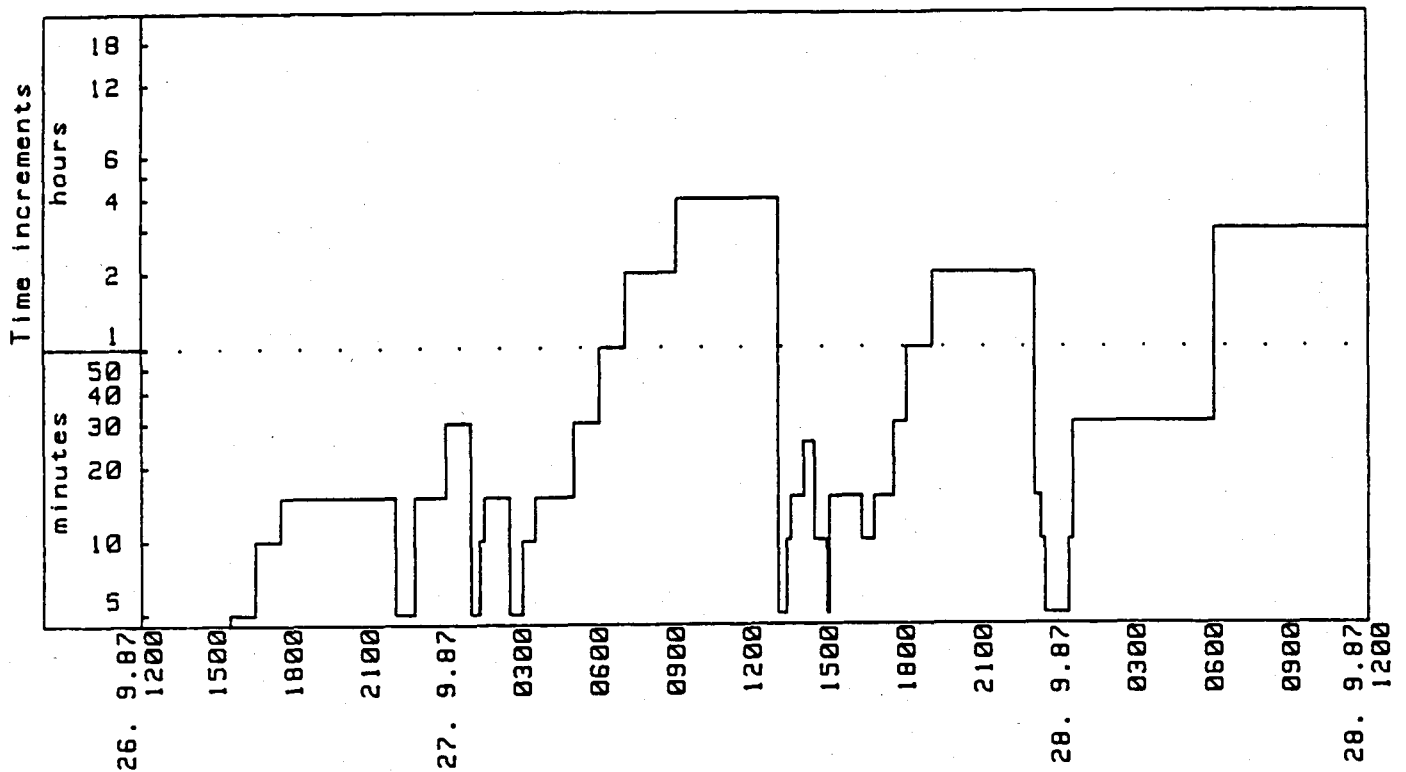


Figure 8.8: Graphical representation of time increments used in simulation.

used for comparative purposes since they are dimensional and depend on the length of record and number of ordinates used. The sum of squared residuals is biased towards large events and therefore shows only a slight improvement when the interflow component is modelled. The log residual is similar to the squared residual but incorporates the logarithms of simulated and recorded hydrograph ordinates, thus emphasising low flows. This statistic shows a dramatic improvement here when interflow is modelled.

8.6. DISCUSSION OF RESULTS

Good hydrograph fits for surface runoff have been presented above without any calibration of input data, using soil properties, overland and vegetation parameters assessed from site surveys and available information. However, calibration was required in order to model the interflow component because of unknowns in the subsurface environment, soil inhomogeneities and other features affecting interflow. Although the value of

Table 8.4: Statistics of hydrograph fit.

Statistic	Simulation without interflow	Simulation with interflow
Coefficient of efficiency	0.827	0.834
Reduced error of estimate	0.416	0.408
Sum of squared residuals (m ³ /s) ²	2.80	2.69
Sum of log residuals (log(m ³ /s)) ²	1533	104

900mm/h for permeability in the soil layer responsible for interflow is physically unrealistic, it has to account for unknown effects of factors that influence soil seepage, such as soil layering, piping and a hydraulic gradient that may differ from the ground slope. This study shows that on a small catchment where it is possible to collect detailed soil, vegetation and channel data, a distributed, physically-based model can reproduce surface runoffs well without having to calibrate sensitive parameters, although calibration may be required for unknown antecedent moisture conditions and for modelling delayed flows.

The Waterval study has illustrated a number of features of the simulation program developed in Section A, including the element discretization method, spatial variation of rainfall, the use of a variable time increment, the channelisation factor for rilling, the hydrograph plotting facility, and graphical representation of spatially variable parameters such as soil moistures. Model applications in which longer periods are simulated are presented in the following two chapters.

Chapter 9: THE ECCA CATCHMENT

The Ecça is a small, semi-arid research catchment on a tributary of the Ecça River in the Eastern Cape. The simulation model was used for a continuous simulation of a four-month period, focusing on two major storm events, and treating the runoff data as a split sample for calibration and verification. The results are compared with those of other models used in previous modelling studies of the Ecça. The role of model calibration brought up in the Waterval study is further discussed in this chapter. Features of particular interest in this study are the influence of geology on runoff, and the effect of spatial soil variations on runoff and source areas.

9.1. GENERAL DESCRIPTION OF THE ECCA BASIN

The location of the 9,1km² catchment is shown in fig. 9.1. Gorgens (1983) and Schultz (1988) provide information on the climate, vegetation and physical features of the area. The climate is harsh with extreme temperatures. The mean annual precipitation is about 480 mm, and mean annual evaporation from a free water surface is 1360 mm. Summer rainfall is generally caused by convection thunderstorms, whereas winter rain is associated with large-scale frontal systems. On average about 100 rain days occur per year, although many of the days produce no measurable runoff because of the dry soil conditions. All the streams are ephemeral with an average of three to four discrete runoff events per year.

The relief is characterised by steep hillslopes and narrow valley bottoms as seen in fig. 9.2. Slopes on the hillsides are up to 40% but are more gentle on the hilltops and the area surrounding the lower reaches of the main stream.

The vegetation in the Ecça region is Karoo Bushveld consisting of tall sub-succulent bush thinning to low succulent shrubs on the flatter areas. Dense thickets of succulent and thorny bushes are interspersed with low-growing shrubs and grass with a fair proportion of bare ground throughout



Figure 9.1: Location map of the Ecca catchment.

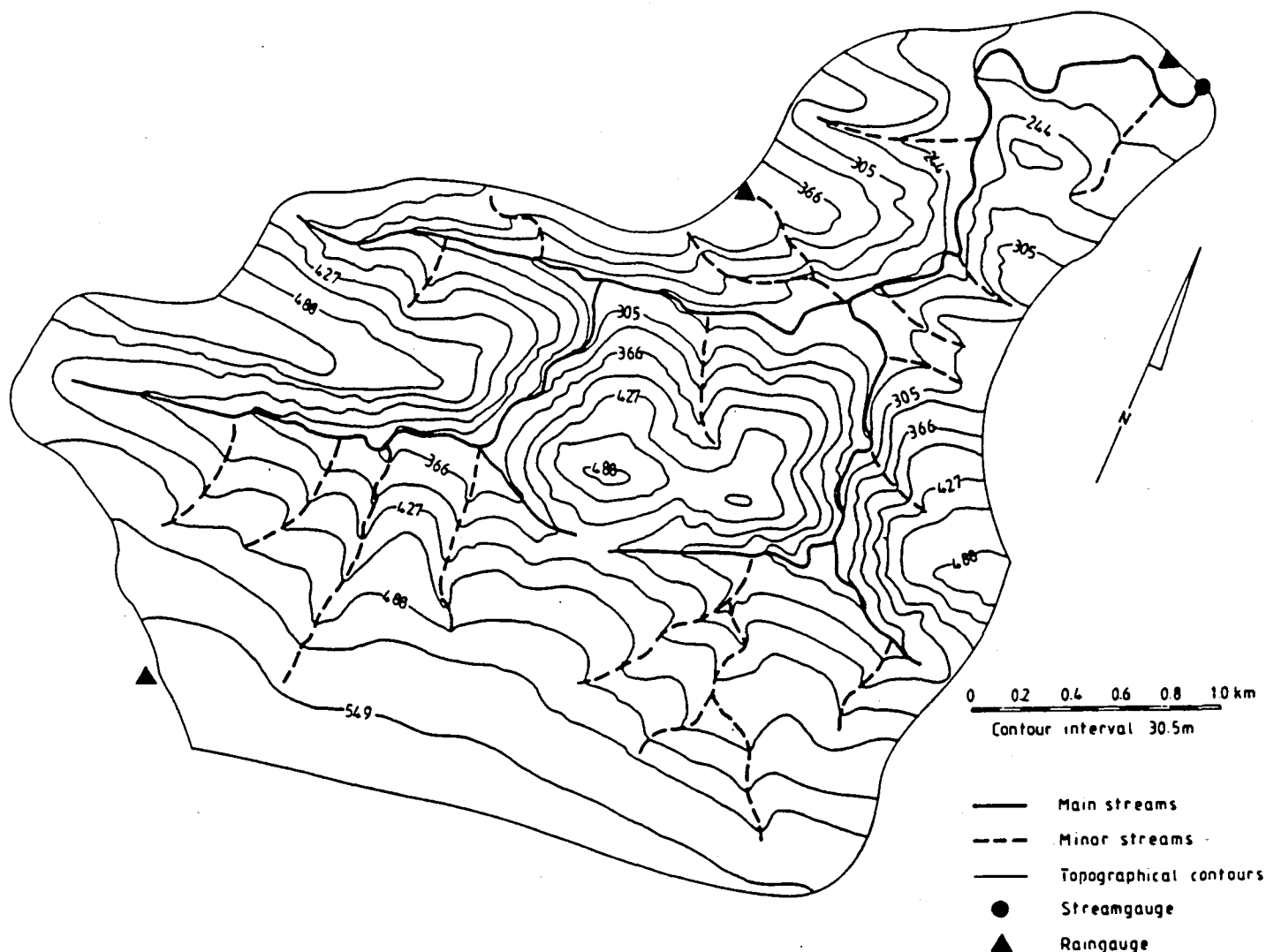


Figure 9.2: Relief map showing instrumentation.

the year. The only land use is small livestock farming which is practised in a stable manner. The vegetation is not very sensitive to grazing and does not undergo appreciable changes between seasons.

The geology consists of alternating bands of tillite, shale and sandstone dipping northward at about 40° . South facing hillsides therefore slope against the dip of the strata and form scarp slopes, while the opposite

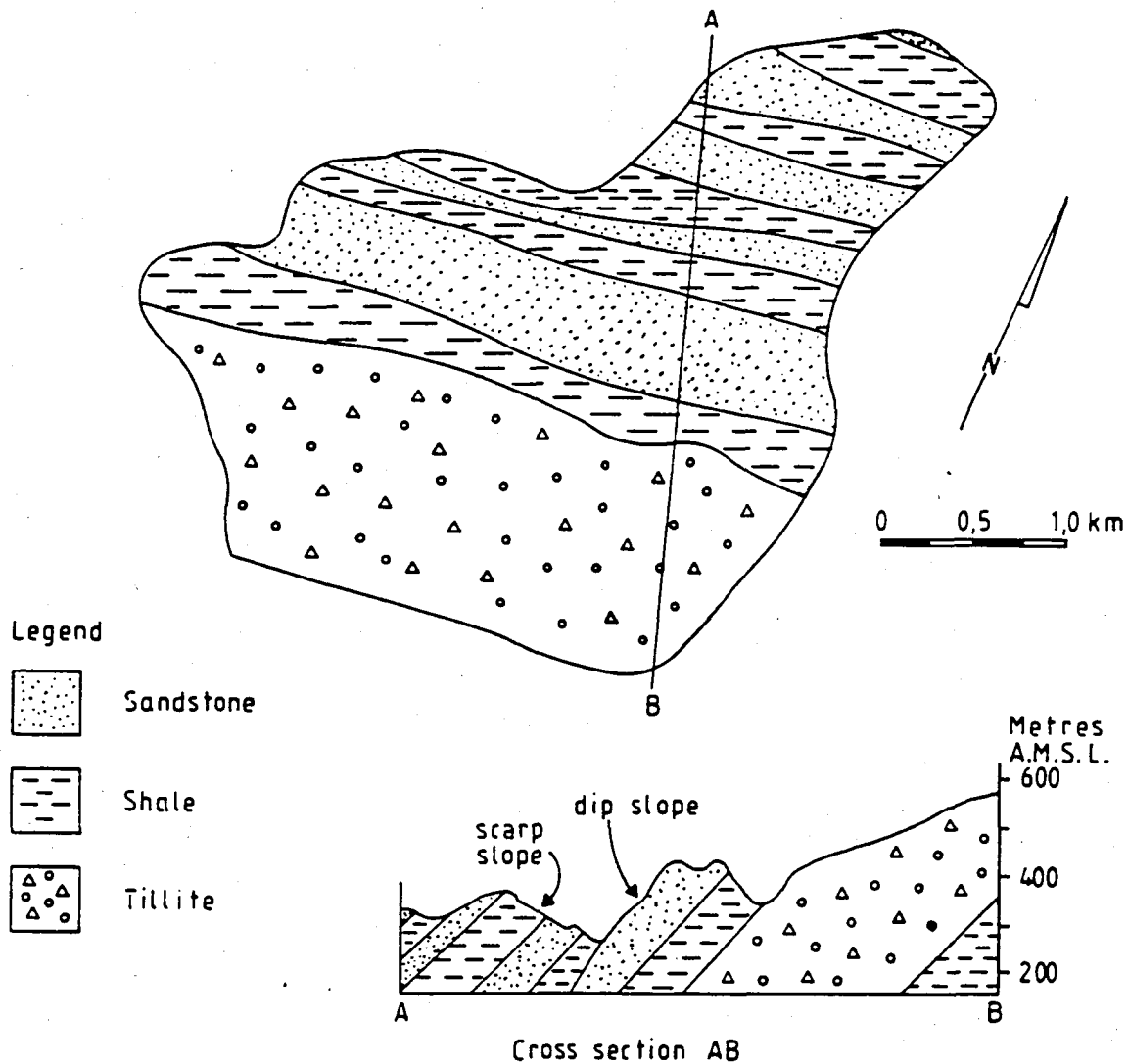


Figure 9.3: Geology map showing dip and scarp slopes (after Schultz, 1988).

hillsides slope with the strata (dip slopes). These features are illustrated in fig. 9.3. Soils are shallow, stony and of irregular depth, and rock outcrops are common. The soils in the valley bottoms near the main tributaries are of more alluvial origin.

Three autographic raingauges are located in this catchment as shown in fig. 9.2. Streamflow is measured by a multiple-notch, sharp-crested weir with continuous stage recording. Precipitation and streamflow are monitored by the Hydrological Research Unit at Rhodes University, who provided the data for this study.

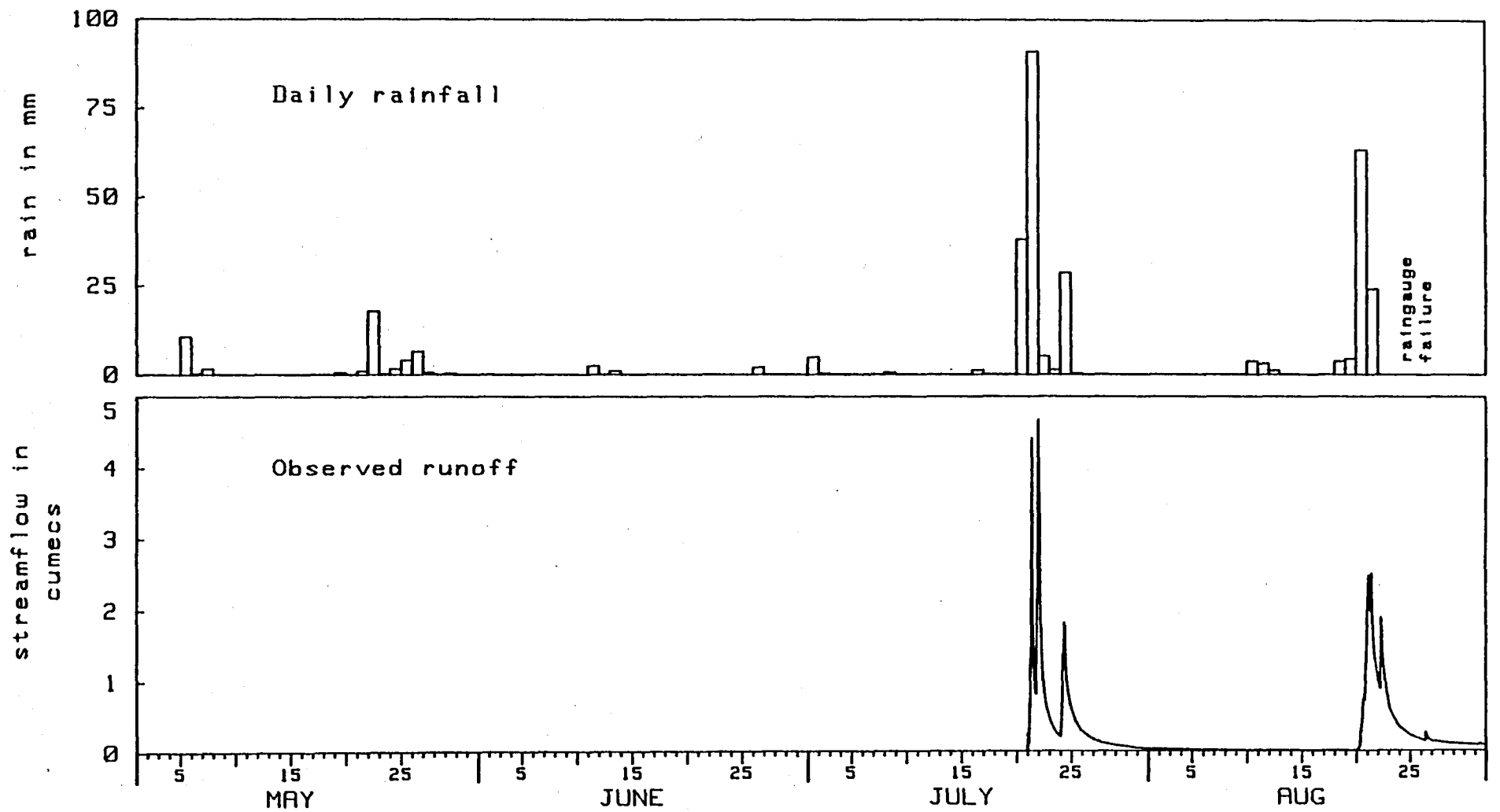


Figure 9.4: Recorded rainfall and runoff for period simulated (May to August 1979).

9.2. PERIOD SIMULATED

Two major runoff events in July and August 1979 dominate the runoff record of the catchment. Both of these events were caused by frontal storms lasting several days and producing multiple-peaked hydrographs. A four-month continuous simulation was run from May to August 1979 incorporating these two events. The rainfall and runoff data for the period simulated are shown in fig. 9.4. The first 2½ months served as a "warm up" period to set the antecedent moisture conditions for the July event. The remainder of the data was treated as a split sample. Those model parameters requiring calibration were calibrated on the July event, and then the calibration was checked on the August event. Although there is no runoff between the two events, the intervening period is very important for determining the soil moistures for the August event. The use of continuous simulation mode obviates the necessity of estimating antecedent moisture conditions for each event.

9.3. INPUT DATA

The data needed for model input was assembled from studies of the Ecca region by Roberts (1978), Gorgens (1983) and Schultz (1988), as well as additional information provided by the staff monitoring the catchment. The model parameters can be divided into two categories as shown in table 9.1, namely those that could be adequately defined from available data and those requiring calibration. Those in the first category were not adjusted at all during model runs whereas the calibrated parameters were adjusted using available data as guidelines. Sensitive parameters were defined separately for each element, but for less sensitive parameters, average values were assigned to each segment.

9.3.1. Catchment discretization

The discretization of the catchment into segments and elements is shown in fig. 9.5. Segment boundaries are positioned so as to separate dip and scarp hillslopes. The shaded elements in fig. 9.5 were shaped so as to enclose the flat alluvial areas adjacent to the major tributaries, since

Table 9.1: Calibrated and uncalibrated model parameters.

Un-calibrated parameters	Calibrated parameters
overland Manning's n channelisation factor ground slopes leaf area index proportion of roots interception capacity channel Manning's n channel widths channel bed slopes	soil depths soil permeability deep percolation

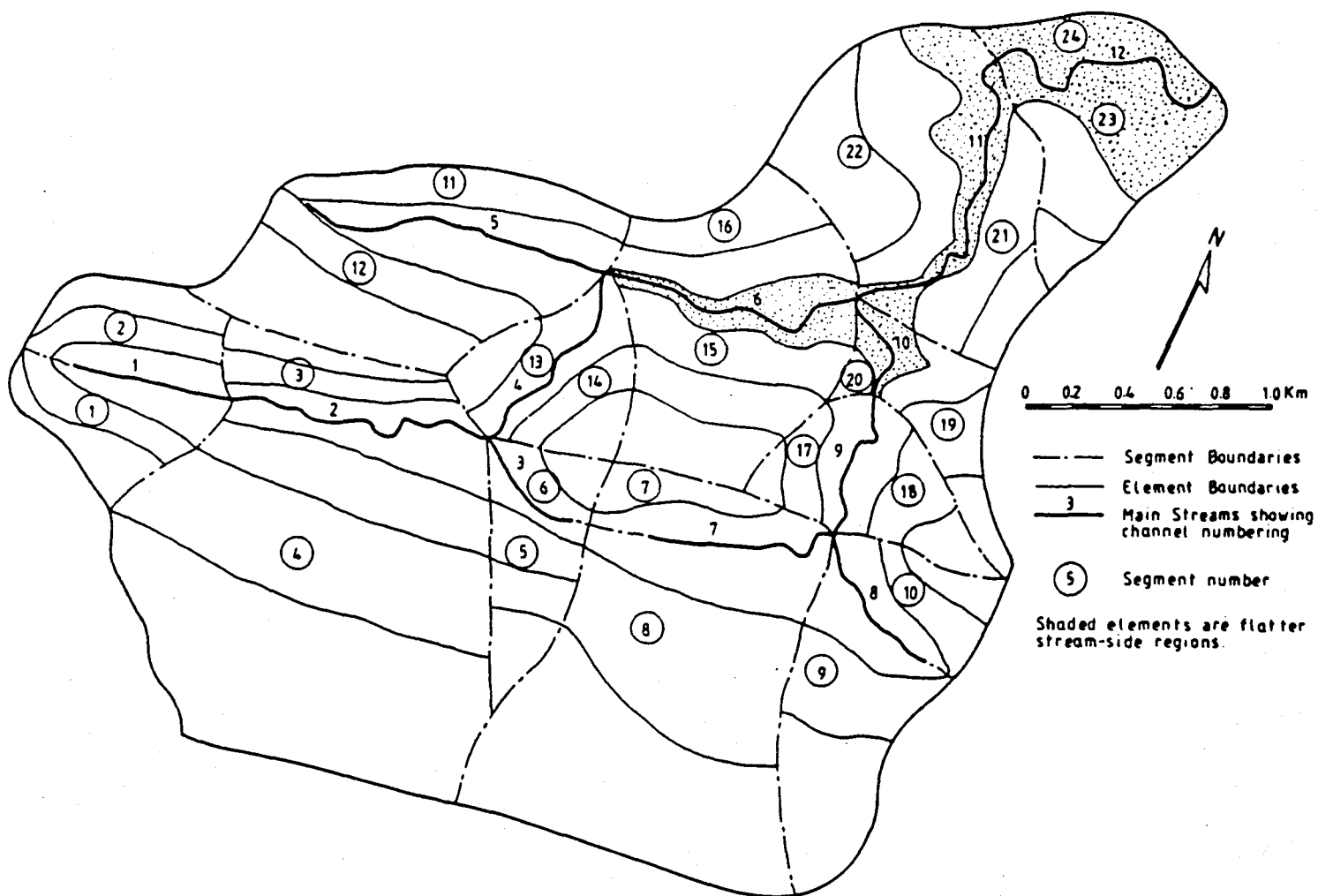


Figure 9.5: Discretization of catchment into segments and elements.

Table 9.2: Evaporation data (after Gorgens, 1983).

Month	A-pan evaporation (mm)	pan factor	potential evaporation (mm)
May 1979	91	0.74	67
June	83	0.74	61
July	86	0.74	64
August	92	0.72	66

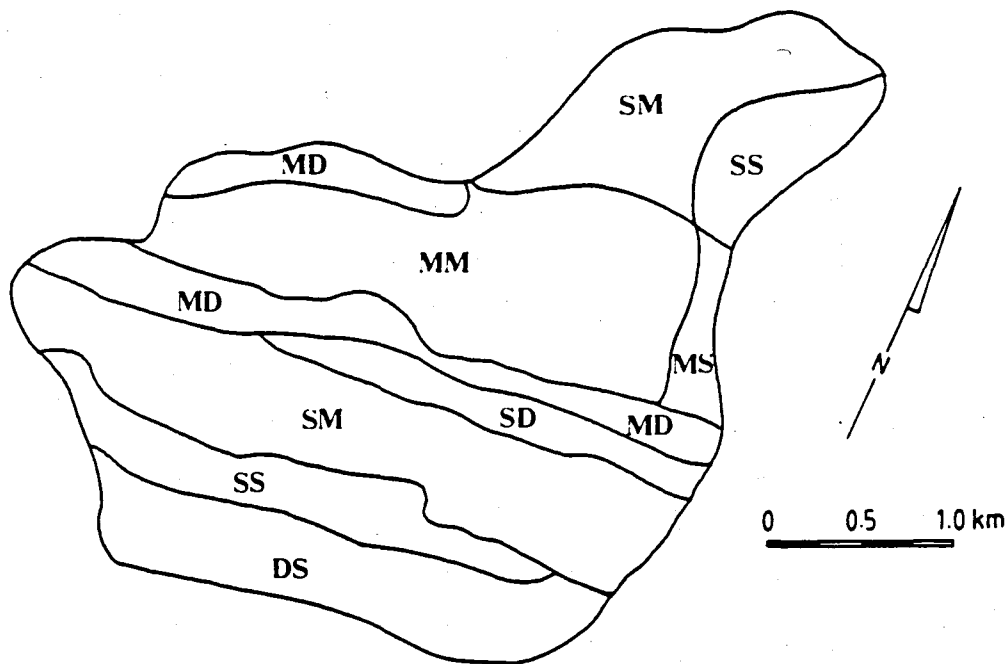


Figure 9.6: Vegetation density map (Roberts, 1978).

LEGEND

	GROUND	CANOPY	CODE
	S	S	SS
Sparse ----- S	S	M	SM
Medium ----- M	S	D	SD
Dense ----- D	M	S	MS
	M	M	MM
	M	D	MD
	D	S	DS
	D	M	DM
	D	D	DD

the soil properties in these these areas differ from those on the hillslopes.

9.3.2. Potential evaporation

Monthly A-pan evaporation values were taken from Gorgens (1983). Potential evaporation values for use in the simulation model were obtained by applying regional pan factors as shown in table 9.2.

9.3.3. Overland and vegetation parameters

Table 9.3 shows values of overland and vegetation parameters used in the simulation. The channelisation factors in the second column were assigned to each segment using the guidelines developed in the rill study (chapter 4). Their primary purpose here is to account for the streamlets and gullies that were not modelled as separate channels for the sake of computing economy. A Manning's coefficient of 0.35 was used for overland flow, based on the recommendation of Gorgens (1983) of 0.30 to 0.40 for the Ecca terrain.

The interception capacities and leaf area indices shown in table 9.3 were assessed using the vegetation density map shown in fig. 9.6 compiled by Roberts (1978). Vegetation densities are designated by two letters, the first referring to ground cover and the second to canopy. Following the approach of Schultz (1988), interception capacities (I_c) were calculated using a weighted average of the ground and canopy values, according to the equation:

$$W = 0.33G + 0.67C \quad (9.1)$$

where W = weighted interception capacity

G = interception capacity of ground cover

C = interception capacity of canopy.

Using values of 0.3, 1.2 and 2.0 mm for sparse, medium and dense conditions respectively, and averaging further when several densities occur in one segment, the values of I_c shown in table 9.3 were obtained.

Table 9.3: Overland and vegetation parameter values.

Segment	Channelisation factor	Manning's coefficient	I_c (mm)	LAI	Root distribution*
1	0.95	0.35	0.8	0.7	60/40
2	0.95	0.35	1.7	1.6	60/40
3	0.95	0.35	1.7	1.6	60/40
4	0.70	0.35	0.8	0.8	60/40
5	0.95	0.35	0.9	0.7	60/40
6	0.95	0.35	0.9	0.7	60/40
7	0.95	0.35	1.3	1.5	60/40
8	0.60	0.35	0.8	0.8	60/40
9	0.75	0.35	0.8	0.9	60/40
10	0.95	0.35	1.4	1.6	60/40
11	0.85	0.35	1.6	1.4	60/40
12	0.85	0.35	1.2	0.8	60/40
13	0.95	0.35	1.5	1.2	60/40
14	0.95	0.35	1.5	1.1	60/40
15	0.85	0.35	1.3	0.9	60/40
16	0.80	0.35	1.2	0.9	60/40
17	0.95	0.35	1.2	0.8	60/40
18	0.80	0.35	1.3	1.3	60/40
19	0.80	0.35	1.0	0.7	60/40
20	0.95	0.35	1.2	0.8	60/40
21	0.85	0.35	0.4	0.5	60/40
22	0.79	0.35	0.9	0.7	60/40
23	0.88	0.35	0.4	0.5	60/40
24	0.95	0.35	0.9	0.7	60/40

* Ratio of roots in the first and second soil layers.

The same procedure was used for assessing leaf area index. Values for sparse, medium and dense vegetation are suggested in the User's Manual (Appendix A). Since vegetation in the Ecce is adapted to semi-arid conditions with small leaves, thorns, succulent morphology and stunted

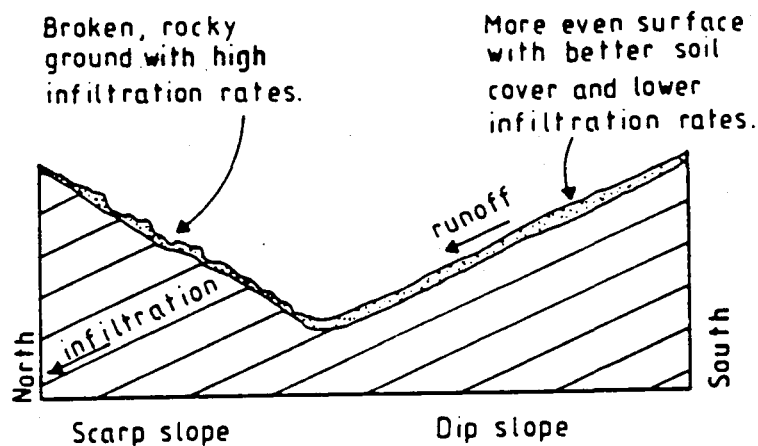


Figure 9.7: Schematic diagram of a valley cross section illustrating differences between the dip and scarp slopes.

growth (Schultz 1988), slightly reduced values of leaf area index were used as follows:

- sparse: 0.4
- medium: 0.8
- dense: 2.0

These values were used in an equation of the form of equation (9.1) to obtain the leaf area indices shown in table 9.3.

It was found that estimates of the root distribution in the soil based on recommendations of Schulze (1984) were similar for the different vegetation groups shown in fig. 9.6, so a representative distribution of 60% roots in the upper soil layer and 40% in the second layer was used for the whole catchment.

9.3.4. Soil properties

In the assessment of infiltration rates and soil conditions, the dip of the underlying rock is an important feature. On the scarp slopes the ground is broken by end-on outcrops of the sloping rock layers. Soil is very shallow on these slopes and infiltrating water is carried away rapidly by the fractured rock. Infiltration rates are therefore very high, and steady infiltration rates of up to 173 mm/h have been measured by Moolman (1985). The dip slopes on the other hand exhibit slightly deeper

soil with lower infiltration rates as a result of fine soil texture or surface sealing.

These features are illustrated in fig. 9.7. It has been observed that during storms the scarp slopes may not contribute at all to runoff, all the surface flow coming from the dip slopes (Hughes, 1990). A separation of the dip and scarp slopes is therefore very important when applying a distributed model to this catchment.

Most of the soils in the Eccca can be classified as Mispah, which is shallow soil on rock. Soil depths and textures are highly variable because of badly weathered rocks. Soil depths and properties must therefore of necessity be average values using field observations as a guideline. No detailed mapping of the Eccca soils has been carried out, and the following guidelines obtained from staff familiar with the catchment describe the general patterns of soil depths:

- o Scarp slopes: very shallow soil, less than 300 mm.
- o Hill tops: somewhat deeper soils, up to 600 mm in places, with a possible average of 400 mm.
- o Dip slopes and valley bottoms: Highly variable depth, 0 - 400 mm, typically 300 mm.

The soil permeability was found to be a sensitive parameter influencing infiltration rates and therefore peak runoffs. Because of the highly variable nature of the soils, combined with inaccessibility of many catchment areas because of the rough terrain, a detailed mapping of infiltration rates measured in the field is difficult. Table 9.4 is a summary of the trends discernible from soil samples collected over portions of the catchment by Schultz (1988). The permeability-ranges in column 3 are taken from the data of Rawls *et al* (1983) given in Appendix A.

In addition to the differentiation between dip and scarp slopes, further differentiation between hilltops, hillsides and valley bottoms is clearly important. Based on the soil depth and texture trends discussed above, four different soil zones were used in the model simulations, as shown

Table 9.4: Trends observed from soil samples collected by Schultz (1988).

Infiltration potential	Texture*	Permeability	Occurrence
low	SC/CL	1.0 - 3.3 mm/h	regions adjoining streams
medium	SL	20 - 40 mm/h	hillslopes
high	LS/SL	20 - 100 mm/h	hilltops & scarp slopes

* S = sand; C = clay; L = loam.

Table 9.5: Values of soil parameters used in Ecce simulation

parameter	zone 1 (scarp slopes)	zone 2 (hill tops)	zone 3 (dip slopes)	zone 4 (valley bottoms)
Thickness of 1st soil layer (mm)	100	200	<i>116</i>	<i>100</i>
Thickness of 2nd soil layer (mm)	100	200	<i>150</i>	<i>150</i>
Thickness of 3rd soil layer (mm)	1000	0	0	0
Soil group*	2	2	3	9
Permeability of topsoil (mm/h)	<i>60</i>	<i>60</i>	<i>30</i>	<i>3</i>
Permeability of 3rd layer (mm/h)	<i>5000</i>	-	-	-
Deep seepage, k_L (mm/h)	<i>0.001</i>	60	<i>0.27</i>	<i>0.01</i>

*soil groups: 2 = loamy sand

3 = sandy loam

9 = sandy clay

Values obtained by calibration are shown in *italics*.

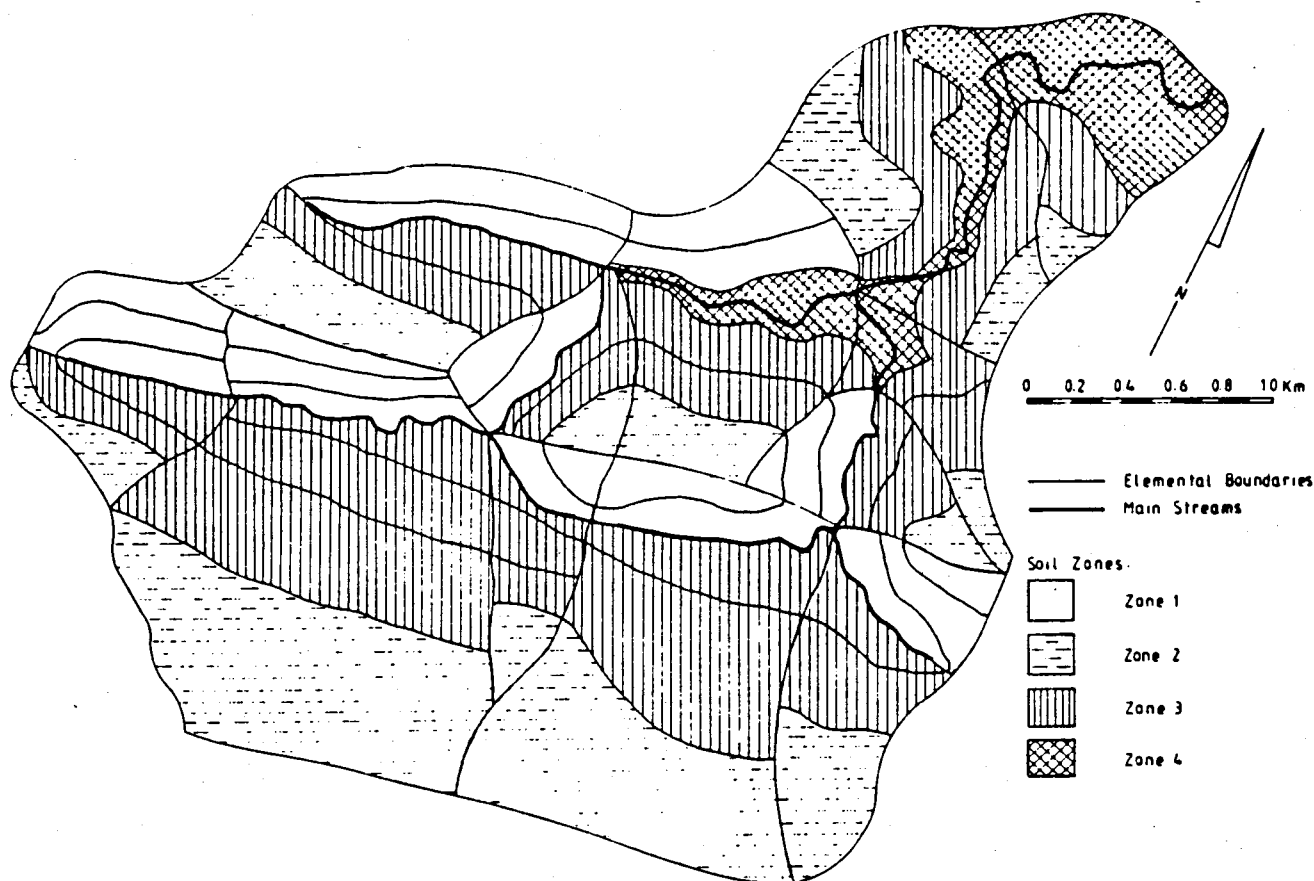


Figure 9.8: Soil zones in the Ecca study.

in fig. 9.8. Different sets of soil properties were assigned to each of the soil zones, and the values of the parameters including final values of calibrated parameters are shown in table 9.5. During model calibration the permeabilities were varied in the ranges shown in table 9.4, finally converging on the calibrated values given in table 9.5.

Long recession flows occur in the Ecca after major events. Areas of saturated alluvium seeping into the streams are very limited, and clearly the thin soils could not contribute significant seepage to streamflow. The probable cause of the recession flows is therefore thought to be the highly fractured rock and high relief of the catchment (Hughes, 1990). Infiltrated water seeping into the rock emerges lower down in the streams. Strictly speaking this is not ground water flow because it is not associated with a water table. However it could be modelled using any delay function with calibrated parameters, and in this study the third soil layer was used to model the source of recession flows. Only the scarp

Table 9.6: Channel properties

Channel	Manning's n	slope	base-width (mm)	bank slope	length (m)
1	0.047	0.083	300	45°	650
2	0.067	0.050	500	45°	1200
3	0.045	0.080	200	45°	500
4	0.072	0.072	900	60°	890
5	0.075	0.095	400	60°	1320
6	0.072	0.036	900	60°	1170
7	0.057	0.088	500	45°	1010
8	0.067	0.095	500	45°	700
9	0.072	0.067	900	60°	700
10	0.072	0.042	900	60°	560
11	0.063	0.025	1500	60°	1370
12	0.063	0.022	1500	60°	1200

slopes were used for this purpose since they are probably the main contributors to recession flows because of their geological structure and high infiltration rates. The calibrated permeability of 5000 mm/h in table 9.4 is unrealistically high for soils because it has to cater for water movement through fractured rock. The third soil layer was not used elsewhere in the catchment because of the thin soil mantle.

The deep percolation (k_L) values in table 9.5 were calibrated to drain the soil profile at a controlled rate governing the soil water retention. Calibration was necessary for some of the soil depths and deep percolation rates because these parameters determine the rate at which the soil fills and drains during a simulation, which in turn affects infiltration rates.

9.3.5. Channel properties

Channel flow parameters are shown in table 9.6, in which channel numbering is taken from fig. 9.5. Manning's roughness coefficient and stream width were taken from the channel survey conducted by Schultz (1988). Bed

slopes and channel lengths were obtained from a topographical map. Bank slopes of 45° and 60° were assumed for the small and large streams respectively, because the use of vertical banks was found to result in unreasonably high water depths.

9.3.6. Time increments

A time increment file was set up by consulting the rainfall and runoff records for the period simulated. Time increments of 10 to 15 minutes were used during rainy periods and over hydrograph peaks. This was increased to 30 minutes on the falling hydrograph limbs, and progressively increased up to 4 or 6 hours on the baseflow portions. Time increments from 1 to 5 days were used during dry periods.

9.4. SIMULATION RESULTS

The simulation results for the July and August events are shown in fig. 9.9. The calibrated flows (July events) show well-reproduced peaks. The runoff volume on the 24th of July is somewhat under-predicted, with a volumetric error of -27%. The second half of the split sample, namely the uncalibrated simulation of the August event, shows generally good agreement between measured and simulated hydrographs, although the peaks are somewhat over-estimated and the volume is again slightly underestimated. The simulation had to be terminated on the 22 August because of missing rain gauge data. Statistics of hydrograph fit will be discussed when comparing with other models.

The runoff mechanism of the basin can be described as follows:

- o Response to light rain comes mainly from the alluvial valley bottoms. During heavy rains these bottom lands also respond before the hillslopes do because of their lower infiltration rates.
- o During heavy rains, stormwater cascades down gullies on the steep valley sides of dip slopes.
- o The scarp slopes offer little or no contribution to runoff because of high infiltration rates. However, they are important for replenishing the sources of delayed flow.

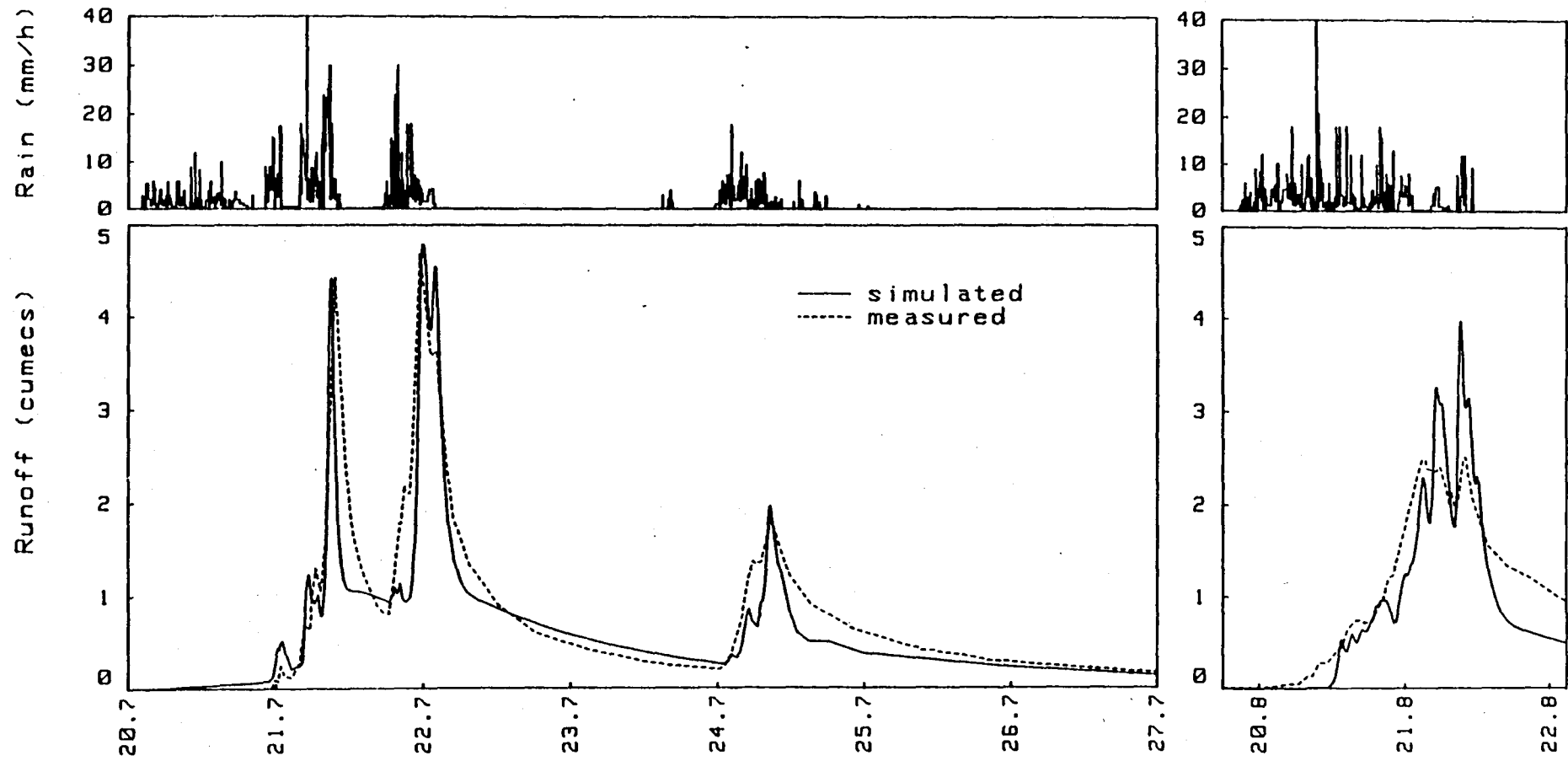


Figure 9.9: Comparison of measured and simulated streamflow hydrographs for July and August events.

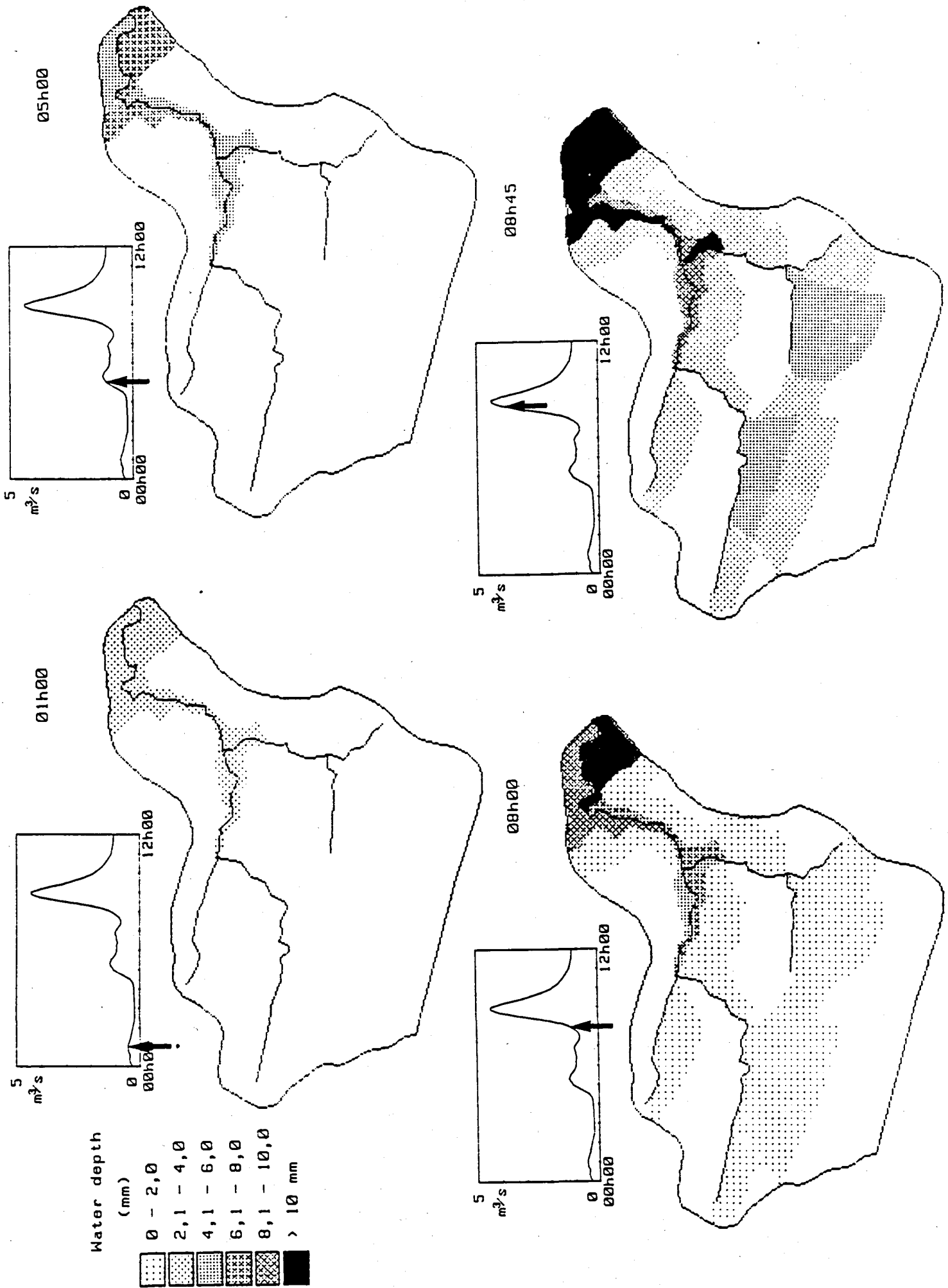


Figure 9.10: A time-lapse view of the Ecca basin showing plots of surface water generated by the model at various stages during the event on 21 July 1979.

These features are reflected in fig. 9.10 which shows sample plots of surface runoff at various stages during the simulation. These plots were generated by the simulation program using the facility to depict graphically the spatial distribution of a parameter by shading individual elements according to the relative magnitude of the specified parameter. Fig. 9.10 illustrates that the source area of a catchment is not only determined by antecedent moisture conditions but by the spatial distribution of soil properties as well.

9.5. COMPARISON WITH OTHER MODELS

Gorgens (1983) applied three hydrological models to the Ecca catchment. As in the present study, the models were calibrated on recorded streamflows in continuous simulation mode, so the results of the two studies are comparable.

The three models used by Gorgens (1983) were PITH, Pitr and the Stanford Watershed Model. PITH and Pitr are two derivatives of the Pitman model (Pitman, 1977; Pitman and Basson, 1979), which is a suite of programs that can operate on a monthly, daily or hourly basis. The original Pitman model is structured around 4 vertically aligned moisture stores, namely interception, depression storage, soil moisture and ground water. Empirical functions are used for soil moisture budgeting and computation of streamflows, with non-physically-based parameters that require calibration. It has been extensively used in Southern Africa for flood forecasting and water resource studies with considerable success.

PITH is a version of the hourly Pitman model with certain modifications described by Gorgens (1983), which essentially are improvements to the evaporation, soil moisture, runoff and interflow components. In addition, Pitr incorporates a re-infiltration of depression storage so as to allow for the infiltration of ponded water as well as incident rainfall during each time step. In the Ecca application, Gorgens used PITH and Pitr in conjunction with the daily Pitman model so that the hourly time step used for simulating storm events could be relaxed to daily time steps between events.

The Stanford Watershed Model (Crawford and Linsley, 1966) is a well established, versatile simulation model, and was chosen by Gorgens (1983) as a "base-line" with which to compare the performance of the modified Pitman models on the Eccca. It is more complex than the Pitman models, has a greater number of parameters, and is more physically-based in that Manning's equation is used for overland flow. The other hydrological processes are represented by conceptual moisture stores as in the Pitman approach. The model is thus a combination of physically-based components and empirical functions requiring calibration. In the Eccca application, the catchment was not divided into subareas but was treated by Gorgens (1983) as a lumped catchment for the Stanford Watershed and the Pitman models.

Gorgens (1983) presented his results as distinct runoff events, and for the purpose of comparison with this study, three events are defined:

- event 1: 20 - 22 July
- event 2: 24 - 25 July
- event 3: 20 - 21 August

The simulation results of the present study are compared with those of PITH, PITR and the Stanford Watershed Model in figs. 9.11 and 9.12. Statistics of fit for all 4 models are shown in table 9.7 for each event. On the first two events the present model shows excellent fits on the peaks, somewhat under-estimated volumes and a good coefficient of efficiency. For event 3 (the uncalibrated event) the errors on the peak and volume mentioned previously are quantified. The statistics for the present model generally compare favourably with those of the other 3 models. In terms of overall performance the present model performs best on peaks and coefficient of efficiency, followed closely by the PITR model. None of the models performs consistently well with respect to volumes.

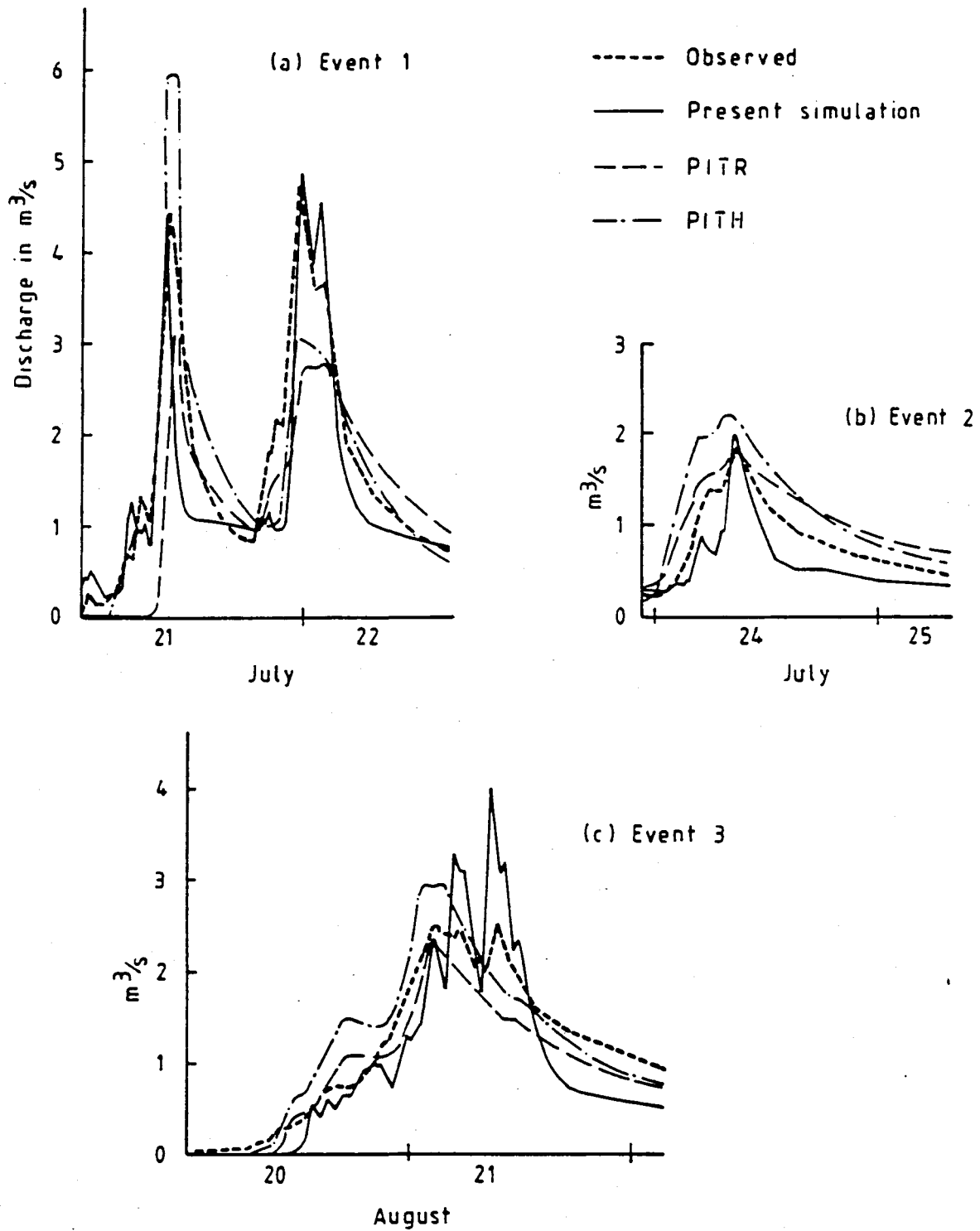


Figure 9.11: Comparison of present model with models PITR and PITH.

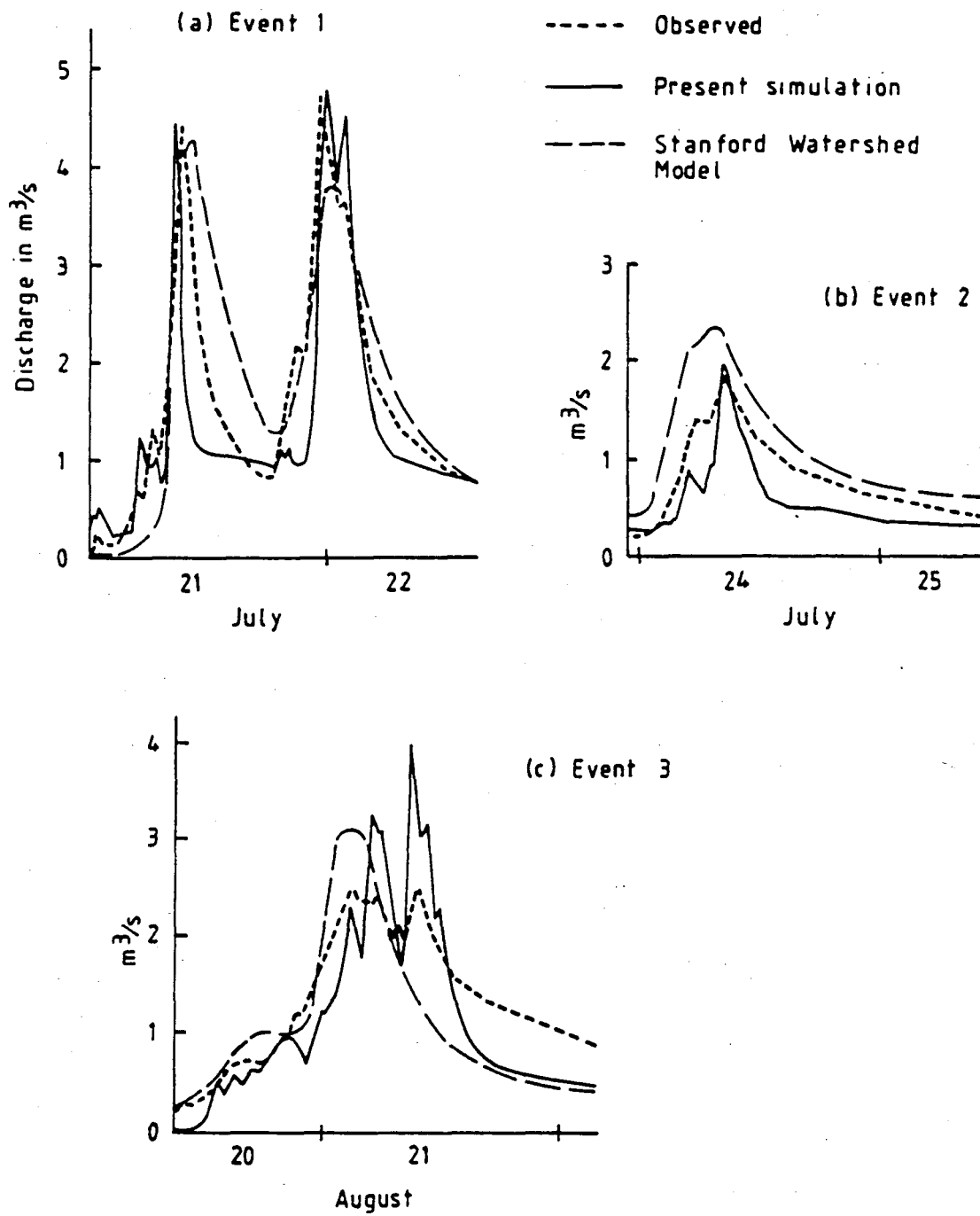


Figure 9.12: Comparison of the present model with the Stanford Watershed model.

Table 9.7: Statistics of fit between observed and simulated hydrographs.*

event	statistic	present model	PITR	PITH	SWM
1	peak error (%)	1	-29	32	-5
	volume error (%)	-8	-18	3	9
	HCE**	0.84	0.76	0.78	0.67
2	peak error (%)	8	-7	18	23
	volume error (%)	-27	32	40	31
	HCE	0.72	0.61	0.21	0.32
3	peak error (%)	29	19	68	67
	volume error (%)	-14	4	28	-8
	HCE	0.71	0.85	0.34	0.43

* Statistics are defined in Appendix C

** Hourly coefficient of efficiency

9.6. APPRAISAL OF THE ECCA STUDY

The comparison with three non-physically-based models reflects a definite although not appreciable improvement on simulated streamflows when using the present model. It therefore cannot be concluded from the results of this study that a physically-based model will necessarily give better streamflow simulations than a simpler, empirical model. However, this study illustrates a number of other advantages of a distributed, physically-based model over a lumped model with non-physically-based parameters. A physically-based model can provide more information about the flow processes within a catchment, such as the spatial distribution of surface runoff presented in this study (fig. 9.10). This can enhance the understanding of the runoff mechanism of a catchment. Other advantages are a large reduction in the number of parameters requiring calibration, as illustrated in table 9.1, and that the physical basis of the parameters facilitates estimation of their probable range.

Model calibration was used more in this study than for the Waterval catchment, where it was only required for the interflow component. Both surface and subsurface flows required calibration in the Ecca study. This is partly because of unknown soil characteristics and a greater degree of lumping than in the smaller Waterval catchment. It is also related to the interaction between soil parameters (which generally require calibration) and surface runoff in a continuous simulation. The soil parameters determine how quickly the soil saturates and drains, which in turn influences infiltration rates and hence surface runoff.

Despite the physical basis of this model, it was found that simulation results can be particularly sensitive to the soil parameters that require calibration. When soils are shallow as in the Ecca, results are especially sensitive to the soil depth and deep percolation rate, which determine the storage capacity and drainage rate of the soil respectively. These parameters are difficult to measure and may vary considerably within a small area. However, such parameters are not unique to the present model, for example the physically-based ANSWERS model (Beasley *et al*, 1977) uses an infiltration control zone depth, which determines the moisture storage capacity of the soil, and the Pitman model uses ST, the maximum soil moisture capacity, and FT, the maximum soil moisture percolation rate governing the drainage of the soil.

The Ecca catchment exhibits considerable spatial variations in soil conditions and ground slopes, with geology playing an important influential role. These features have a significant influence on the runoff characteristics of the catchment, and the distributed, physically-based approach of the present model is well-suited to this type of application.

Chapter 10: BETHLEHEM CATCHMENTS

The Bethlehem research catchments lie in the upper reaches of the Wilge River in a farming area near Bethlehem in the Orange Free State, as shown in fig. 10.1. The three nested catchments used in this study range from 83 km² to 372 km² in size, and are monitored by the Department of Water Affairs for rainfall and streamflow. Two 6-month summer seasons were studied here using the model to reproduce the recorded streamflows for each season. The 1981/82 season was used for model calibration, and the wetter 1980/81 season was reserved for verification.

A large number of farm dams and naturally occurring pans are interesting features of this study, and the effects of various hypothetical land use changes are considered.

10.1. CATCHMENT DESCRIPTION

The main sources of information about the Bethlehem catchments are the research reports of Mason-Williams (1984) and Kennedy (1981). The nested catchments are shown in fig. 10.2 and cover the following areas:

C8M12: 372 km²

C8M13: 251 km²

C8M25: 83 km²

The mean annual precipitation in the area is 676 mm, with about 80% falling in the summer months (October to March). The mean annual runoff at gauge C8M12 is 5 million m³.

The region is characterised by gently undulating topography with slopes generally less than 3% and rarely exceeding 12%. A river network with many deeply incised channels drains the area, with intermittent streamflow through most of the network. Geology consists of mudstones in the east, sandstones in the central regions and mudstones with sandstone bands in the western parts. The presence of dolerite dykes and

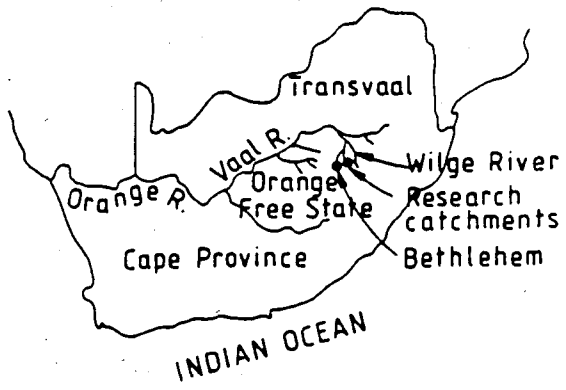


Figure 10.1: Locality map of Bethlehem catchments.

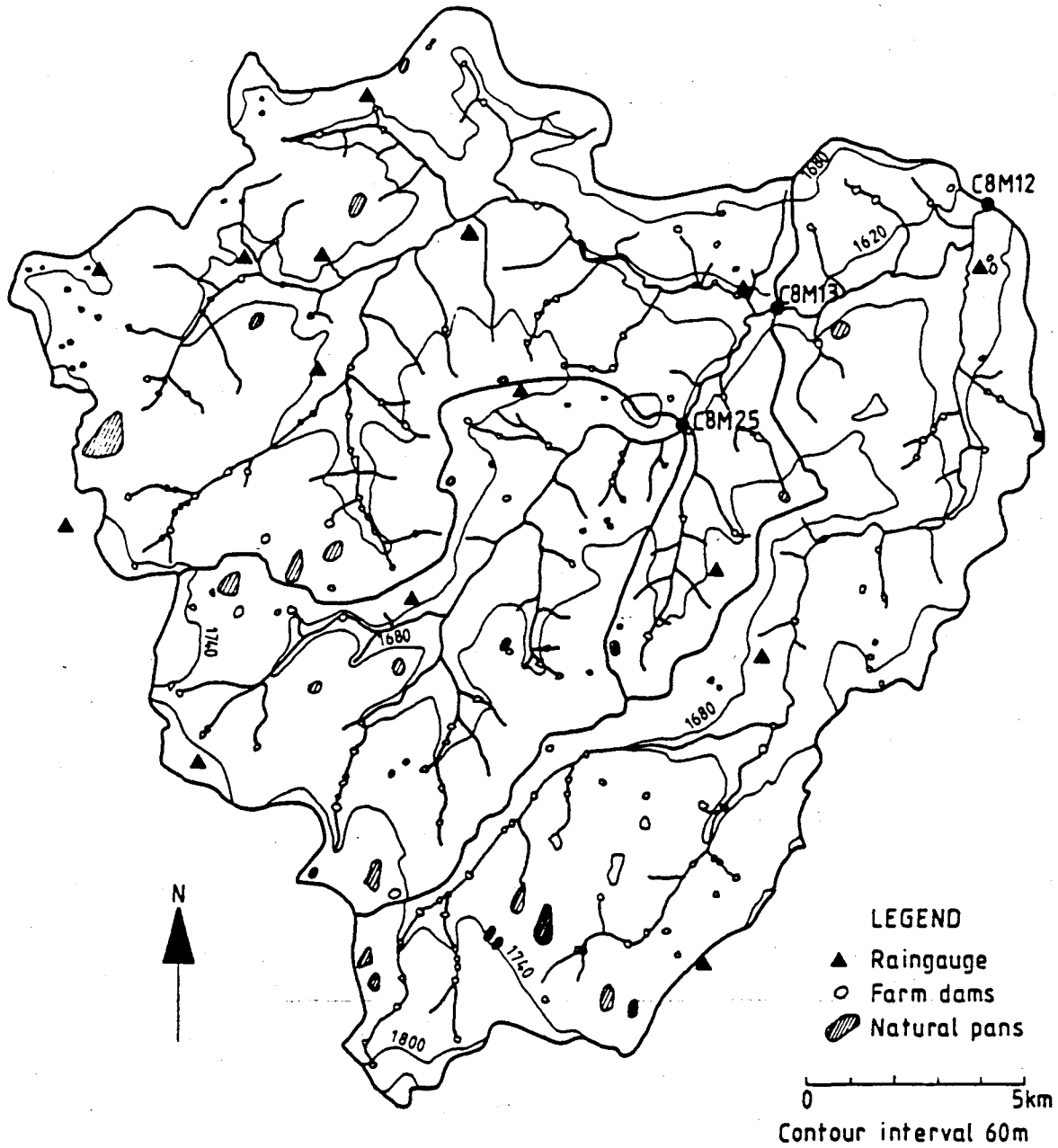


Figure 10.2: Nested Bethlehem catchments.

sills and sandstone bands in the impermeable mudstone, allows seepage to a deeper water table, although seepage from the sandstone outcrops reaches the rivers as delayed flow. Borehole data indicates that the subsurface drainage pattern is similar to the surface drainage pattern.

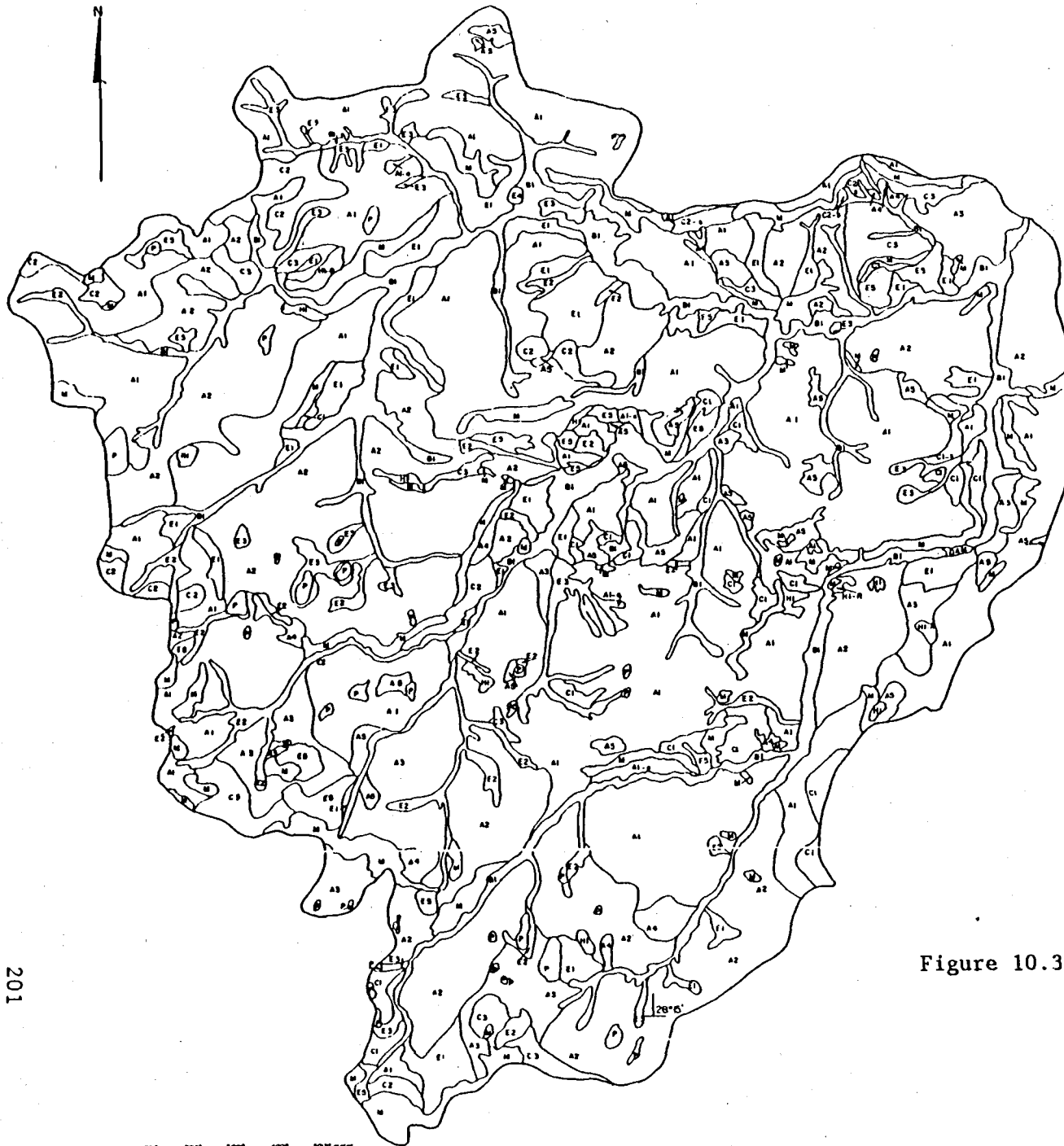
Soil types have been studied and mapped as shown in fig. 10.3. The uplands are dominated by light sandy soils consisting typically of a fine sandy topsoil overlying a fine sandy loam, merging into a zone of weathered bedrock. Along the major streams the soils are generally heavy, structured clays. In some of the concave lower-lying areas between the uplands and the major streams occur soils of the duplex class, consisting of sandy topsoil abruptly overlying clay. Soil depth is variable but on average the uplands have about 600 mm depth available for normal root development.

The land use of the catchments is agricultural, comprising cultivated crops, planted pastures and natural grazing land. The main crops are maize and wheat. A land use survey conducted in the 1979/80 season (Mason-Williams, 1984) showed the following proportions of crops and veld:

Table 10.1: Land use division of C8M12.

Land-use	% of total catchment area
maize (summer crop)	25.0
wheat (winter crop)	28.7
pasture	7.3
veld (grazing)	39.0

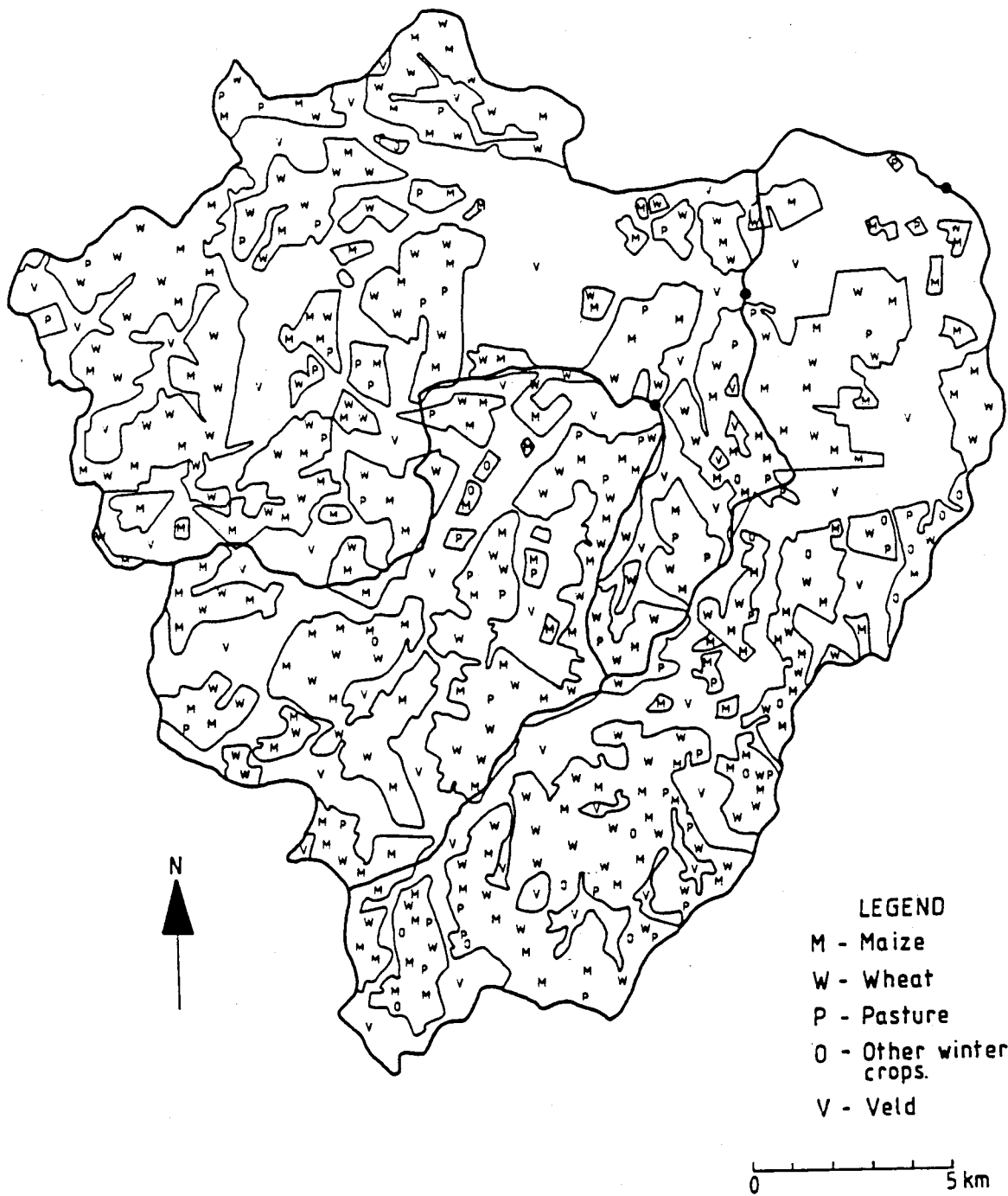
The distribution of crops in the 1979/80 survey is shown in fig. 10.4. Farming practices are variable, with ploughing up and down slopes being common practice, but contour ploughing and contour walls for soil conservation are becoming increasingly popular. Over-grazing and erosion of the natural veld occur to a certain extent.



LEGEND

MAP SYMBOL	SERIES COMPOSITION OF SOIL ASSOCIATION		
	DOMINANT	SUB DOMINANT	RARE
A1	BLEEK SAND	SOETMELK (-)	SOETMELK (+), RIETVLEI, BEATRIX, WAAISAND
A2	SOETMELK (-)	BLEEK SAND	SOETMELK (+), RIETVLEI, BEATRIX, WAAISAND
A3	SOETMELK (+)	BEZUIDENHOUT	RIETVLEI, KROONSTAD
A4	WAAISAND	BLEEK SAND	
A5	RIETVLEI	BLEEK SAND	SOETMELK
B1	VALSRIVIER		DOHNE, KATSPRUIT
C1	BLINKKLIP (-)	ANNANDALE BLEEK SAND	
C2	ANNANDALE	BLEEK SAND	BLINKKLIP (-)
C3	BLINKKLIP (+)		SHORROCKS
E1	KLERKSDORP	RIETVLEI, SOETMELK	KROONSTAD, VALSRIVIER
E2	DOHNE	VALSRIVIER	
E3	KROONSTAD		BLEEK SAND, WAAISAND
E4	KATSPRUIT		
E5	VALSRIVIER	RIETVLEI, KLERKSDORP	
H1	SHORROCKS		
UNDIFFERENTIATED LAND CLASSES			
M	LITHOLSOLS AND ROCKOUTCROPS		
P	PANS		
ADDITIONAL SYMBOLS			
-e = eroded phase			
-s = steep phase			
-R = rocky and/or stony			

Figure 10.3: Soil types of Bethlehem catchments (Mason-Williams, 1984).



LEGEND
 M - Maize
 W - Wheat
 P - Pasture
 O - Other winter crops.
 V - Veld

Figure 10.4: Land use map (after Mason-Williams, 1984).

A feature of hydrological significance is the large number of farm dams in the region, as indicated in fig. 10.2. There are more than 200 dams with capacities ranging from less than 100 m³ to over 100 000 m³. A study based on air photographs (Kennedy, 1981) indicated a total dam storage capacity of 640 000 m³ in 1976, and the number and size of dams is constantly increasing. The dams include those constructed across river channels as well as smaller embankments built on hillslopes. The majority are very shallow (less than 3 m deep), are prone to high evaporation losses, and are primarily used for livestock watering. Although most of the dams are small, collectively they are significant in the hydrology of the region because of their large number and extent of influence.

A number of natural pans occurring in the area are also shown in fig. 10.2. Their surface areas vary from less than a hectare to over 60 hectares, and they are generally shallow with depths less than 1.5 m and the deepest being 5.5 m. The total pan storage capacity is estimated as 6 million m³.

10.2. STREAMFLOW SIMULATION

10.2.1. Rainfall and runoff data

The catchments have been monitored by the Department of Water Affairs since the late 1970's. Streamflows are recorded using weirs and flumes equipped with continuous stage-recording instruments. Rainfall is measured in the summer months only, using a network of tipping-bucket raingauges linked to electronic data loggers.

Preparation of the raingauge files for the 1980/81 and 1981/82 seasons necessitated extensive processing and re-formatting of the data supplied by the Department of Water Affairs, as described in Appendix E. The raingauges used in this study are shown in fig. 10.2. Continuous streamflow data for the three streamgauges C8M12, C8M13 and C8M25 was also obtained and formatted for the present model.

10.2.2. Farm dams and natural pans

The division of the catchments into segments, elements and channel reaches for this study is shown in fig. 10.5. The large number of farm dams precluded modelling each one individually, and they were treated as follows.

Hillslope dams were catered for by combining all the dams in an element into a single equivalent dam with similar storage and flood attenuation properties. The model was modified such that a portion of the surface runoff from each element may be diverted into such a reservoir before flowing onto the downstream element or channel reach. An input parameter k_0 was introduced to quantify this, representing the fraction of an element forming catch areas for dams in that element. k_0 may take on different values for each element and lies between 0 and 1.0. Surface runoff computations for each element proceeded in the usual way, but k_0 times the runoff was routed to the equivalent dam, and $(1 - k_0)$ times the runoff was routed directly to the downslope element or channel. Flows were routed through each equivalent dam using the standard reservoir routing algorithm in the simulation program.

Dams built across the main streams were lumped into equivalent dams at the nodes of the channel network. Five such dams were used as indicated in fig. 10.5.

The equations representing reservoir geometry and outflow are

$$S = ah_w^b \quad (10.1)$$

$$A = abh_w^{b-1} \quad (10.2)$$

$$\text{and } Q = CL(h - h_w)^{3/2} \quad (10.3)$$

where S is dam storage capacity (m^3), A is the surface area (m^2), h and h_w are water level and wall height (m), a and b are constants, C is the spillway coefficient and L the length of the spillway (m). a , b , h_w and (CL) were used as input parameters for the equivalent dams. They were evaluated for each dam using the data compiled by Kennedy (1981), who conducted a survey of the dams in C8M12 and provided estimates of storage volumes, surface areas, maximum depths and embankment details for each dam.

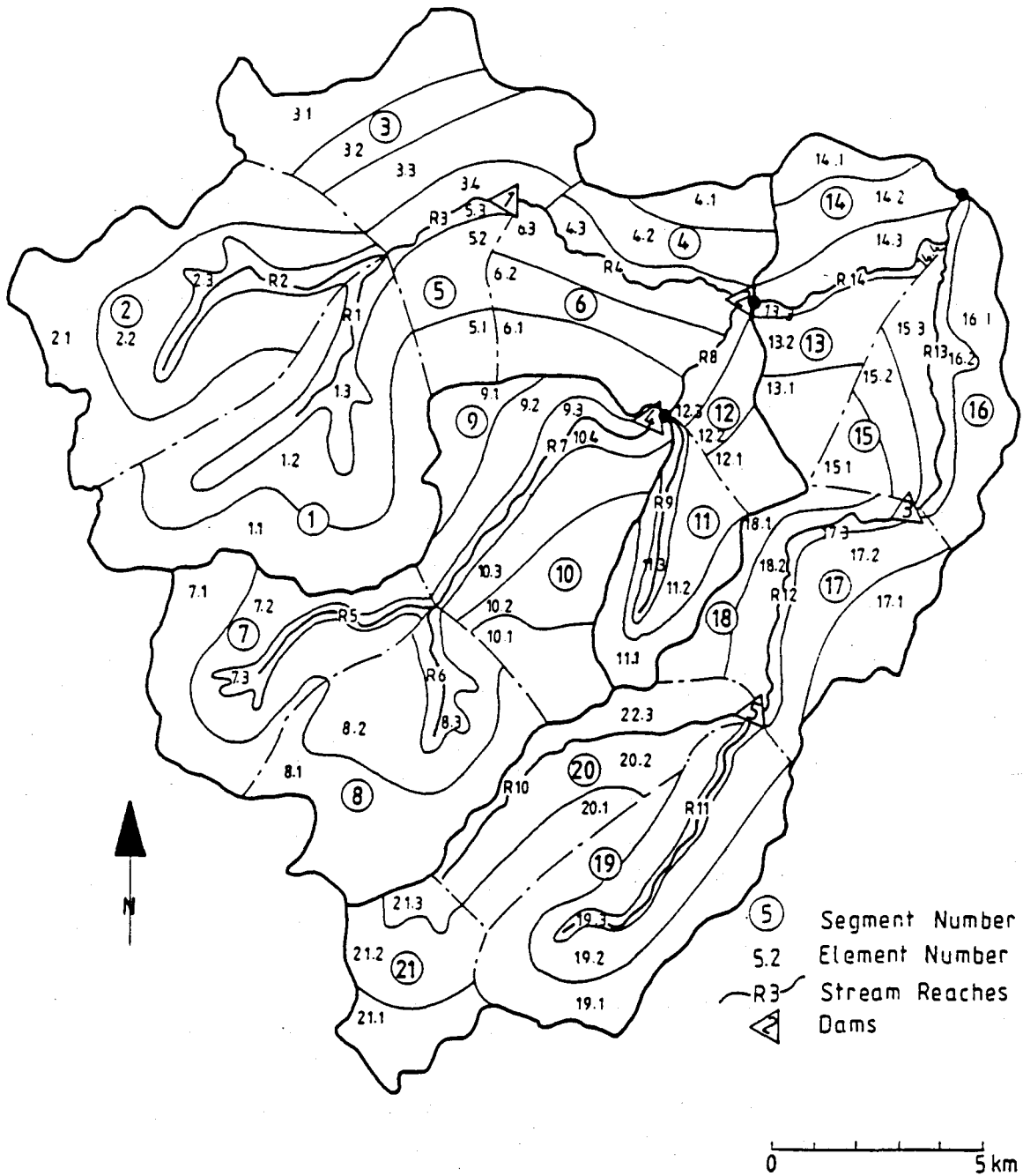


Figure 10.5: Catchment discretization for model simulations.

The survey showed that the dams typically have parabolic cross profiles, and a value of 2.0 was therefore used for the exponent b (after Hager and Sinniger, 1985). Using Kennedy's data, the total storage capacity and surface area of the dams in each element was ascertained and used to determine the wall height h_w and storage coefficient 'a' for the equivalent dam from equations (10.1) and (10.2). In this way the total capacity and surface area of the individual dams were preserved in the equivalent dams, with a view to achieving hydraulic similarity.

Outflow from the dams is either over the embankments or down uncontrolled grassed spillways. Values for the coefficient CL were obtained by combining Kennedy's (1981) information on embankment lengths with appropriate values of the crest coefficient C from Webber (1971). k_0 was determined for each element from a topographical map. The parameters for the channel dams were evaluated in the same way as for the hillslope dams. The hillslope and channel dam parameters used in model simulations are shown in tables 10.2 and 10.3.

The natural pans generally occur on flat upland areas near the watersheds between subcatchment boundaries. Those pans appearing to contribute to catchment runoff were treated in the same way as the farm dams and included in the determination of dam parameters in table 10.2. Those situated in hollows with no apparent outlet were treated as "dead" areas and omitted from the surface area of their respective elements.

10.2.3. Model parameters

A more relaxed policy of parameter calibration was permitted here than in the Waterval and Ecca studies, because of the size of the Bethlehem catchments and the correspondingly greater degree of lumping. Parameter values obtained from the literature and from Mason-Williams (1984) were adjusted where necessary to improve model output.

For potential evaporation, mean monthly values were taken from Mason-Williams (1984) as shown in table 10.4. The overland and vegetation data are shown in tables 10.5 and 10.6, and are based on the parameter-

evaluation guidelines in Appendix A. Values of the interception capacity I_c were assessed on a seasonal basis using information provided by de Villiers (1978), and an average value of 1.0 mm for the summer season was adopted. Similarly the root distribution represents a seasonal average. The more sensitive parameter LAI was assessed on a monthly basis using crop factors provided by Green (1985) weighted according to the distribution of crop types given in table 10.1.

The soil parameters were extensively calibrated because of their wide range of possible values and the sensitivity of model output to infiltration rates. Permeability values for the sandy uplands were varied between 40 and 120 mm/h, and for the clayey streamside areas between 1.0 and 10 mm/h. A certain amount of simplification of the soil distributions shown in fig. 10.3 was necessary in order to avoid an extremely complex element discretization. The streamside elements in fig. 10.5 were used to represent the clay source areas, and the upslope elements to represent the sandy midlands and uplands. The average upland soil depth of 600 mm was represented with two 300 mm thick soil layers in the upslope elements. In the low-permeability streamside elements, 100 mm thick soil layers were found to give better results, because otherwise the soil would drain too slowly and the smaller hydrograph peaks would be over-predicted. The spatial variation of infiltration parameters over the catchments was found to be vital for successful simulation results. Soil permeabilities in different elements were varied selectively using the spatial variations of rainfall to determine which parts of the catchment were the main sources of streamflow in each event. The final calibrated soil properties are shown in tables 10.7 and 10.8. Baseflows were modelled using a 2.0 m deep lower soil layer to prevent saturation to the surface, with calibrated permeabilities of 200 - 500 mm/h.

The channel data is shown in table 10.9. Slopes and lengths were obtained from a topographical map. Manning's coefficient was varied between 0.035 and 0.050 with the final values as shown in the table.

Model simulations for the 1981/82 season were run from 1 October to 30 March. The time increments employed ranged from 15 minutes to several days for wet and dry periods respectively. After a certain amount of

Table 10.2: Model parameters for hillslope dams.

Seg	Elem	k_s	CL ($m^{3/2}/s$)	h_w (m)	a (m)	Seg	Elem	k_s	CL ($m^{3/2}/s$)	h_w (m)	a (m)
1	1	0.6	600	0.60	11900	11	1	0.2	300	0.43	7750
	2	0.7	440	0.50	10700		2	0	-	-	-
	3	1.0	1500	0.40	22440		3	1.0	1300	1.46	32500
2	1	0.6	900	0.53	60160	12	1	0.2	50	0.40	520
	2	0.4	1100	0.51	142100		2	0.1	30	0.40	75
	3	1.0	1000	0.40	69700		3	0.8	450	0.90	3600
3	1	1.0	480	0.53	11400	13	1	0.25	200	0.57	2460
	2	1.0	100	0.55	1320		2	0.25	1400	2.00	25100
	3	0.2	230	0.40	5400		3	0	-	-	-
	4	0.5	630	0.77	11800	14	1	0	-	-	-
4	1	0.5	200	0.48	3500		2	0.3	650	0.82	11900
	2	0.5	440	0.57	8400		3	0.5	440	0.55	9450
	3	0	-	-	-	15	1	0	-	-	-
5	1	1.0	580	0.93	6600		2	0.5	190	0.50	2800
	2	0.5	40	0.32	390		3	0	-	-	-
	3	0	-	-	-	16	1	0.7	720	0.55	33100
6	1	0.8	540	0.58	13400		2	0.2	320	0.44	8500
	2	0.3	670	0.84	12000	17	1	0.6	580	0.50	22200
	3	0	-	-	-		2	0.35	500	0.51	14600
7	1	0.75	1500	1.50	76700		3	0.05	70	0.42	1130
	2	0.25	140	0.37	3200	18	1	0.4	220	0.40	220
	3	1.0	540	0.50	18800		2	0.3	110	0.44	2100
8	1	0.4	750	0.66	23300	19	1	0.3	470	0.46	16200
	2	0.5	300	0.48	6000		2	0.4	250	0.40	7000
	3	0.5	1150	1.00	44600		3	1.0	900	0.60	53200
9	1	0.7	240	0.40	6250	20	1	0.8	1300	0.50	300000
	2	0.5	400	0.70	8800		2	0.2	320	0.46	820
	3	0.6	580	1.00	30000		3	1.0	750	0.64	26600
10	1	1.0	720	0.82	15000	21	1	0.75	200	0.72	16650
	2	0.5	300	0.52	5300		2	0.5	620	0.57	21000
	3	0.5	180	0.52	2450		3	1.0	850	0.57	52300
	4	0.4	700	0.52	31800						

Table 10.3: Model parameters for channel dams.

Dam #	CL ($m^{3/2}/s$)	h_w (m)	a (m)
1	50	1.0	4000
2	50	1.0	22800
3	50	3.5	14000
4	50	1.0	10000
5	50	1.0	10000

Table 10.4: Potential evaporation (mm/day).

Oct	Nov	Dec	Jan	Feb	Mar
5.2	5.4	6.0	5.7	5.0	4.0

Table 10.5: Overland and vegetation parameters.

Manning's coefficient	0.20
Rill ratio	0.65
Interception capacity (mm)	1.0
% roots in upper soil layer	60

Table 10.6: Monthly values of LAI.

Oct	Nov	Dec	Jan	Feb	Mar
0.84	0.86	0.93	0.79	0.66	0.47

Table 10.7: Soil parameters for upper two soil layers.

Seg	Upslope elements			Streamside elements		
	Layer thickness (mm)	Soil group	Permeability (mm/h)	Layer thickness (mm)	Soil group	Permeability (mm/h)
1	300	LS	40	100	SC	4
2	300	LS	40	100	SC	4
3	300	LS	100	100	SC	7
4	300	LS	40	100	SC	10
5	300	LS	40	100	SC	4
6	300	LS	40	300	LS	40
7	300	LS	60	100	LS/SC	60/5*
8	300	LS	60	100	LS/SC	60/5*
9	300	LS	120	100	SC	4
10	300	LS	60	100	SC	4
11	300	LS	100	100	SC	10
12	300	LS	60	100	SC	5
13	300	LS	120	100	SC	10
14	300	LS	120	100	SC	10
15	300	LS	60	300	LS	60
16	300	LS	60	100	SC	5
17	300	LS	60	300	LS	60
18	300	LS	60	100	SC	5
19	300	LS	40	100	SC	4
20	300	LS	40	100	SC	4
21	300	LS	40	100	SC	4

LS = loamy sand; SC = sandy clay

* Double value indicates separate parameter values for first and second soil layers.

Table 10.8: Soil parameters for lower soil layer.

Segments	Deep seepage k_L (mm/h)	Layer thickness (mm)	Soil group	Permeability (mm/h)
7 - 10	0.025	2.0	sand	200
1-6; 11-21	0.035	2.0	sand	500

Table 10.9: Channel data.

Reach	Manning's coefficient	Slope	Width (m)	Length (m)
1	0.04	0.0080	2	5720
2	0.04	0.0100	2	7380
3	0.04	0.0037	4	4500
4	0.04	0.0015	5	7300
5	0.04	0.0070	2	5230
6	0.04	0.0100	2	3610
7	0.04	0.0041	4	8630
8	0.04	0.0014	5	4280
9	0.04	0.0130	2	4980
10	0.04	0.0100	2	9770
11	0.04	0.0100	2	7460
12	0.04	0.0049	5	7930
13	0.04	0.0025	6	8020
14	0.05	0.0020	8	6600

Table 10.10: Initial dam levels.

Dam	h/h_w
hillslope dams	0.33
channel dam 1	0.50
channel dam 2	1.003
channel dam 3	0.57
channel dam 4	0.40
channel dam 5	0.50

trial, antecedent moisture conditions for the start of the simulation were set at 0.3 (i.e. 30% saturated) in soil layers 1 and 2. Initial perched water table levels were finalised at 60 mm in catchment C8M25 and 150 mm in the other catchments. Initial dam levels are given in table 10.10.

10.2.4. Simulation results

The simulation results are shown in fig. 10.6 for the 1981/82 season on which the parameters were calibrated. The results are presented as double hydrograph plots with the lower portion magnifying the low flows that would not be visible if a single scale was used. Some of the hydrograph peaks are over- or under-predicted and the delayed flows after each event are poorly reproduced, although the low baseflows are generally present in the simulated record. The daily coefficients of efficiency shown in table 10.11 are poor for streamgauges C8M12 and C8M13, but improve for C8M25. The coefficient of determination is greater than the coefficient of efficiency for all three streamgauges, indicating a systematic error. The equations used for computing these statistics are given in Appendix C.

Table 10.11: Daily coefficients of efficiency and determination for 1981/82 season.

Streamgauge	Coeff. of efficiency	Coeff. of determination
C8M12	0.20	0.32
C8M13	0.28	0.37
C8M25	0.82	0.86

The results are further analysed by considering flow peaks, time lags and runoff volumes. A scatter diagram of simulated versus observed peaks is shown in fig. 10.7, using logarithmic axes so that the small peaks can be seen. There is generally better agreement on the high peaks than the small peaks, as it is easier to calibrate major events than the small

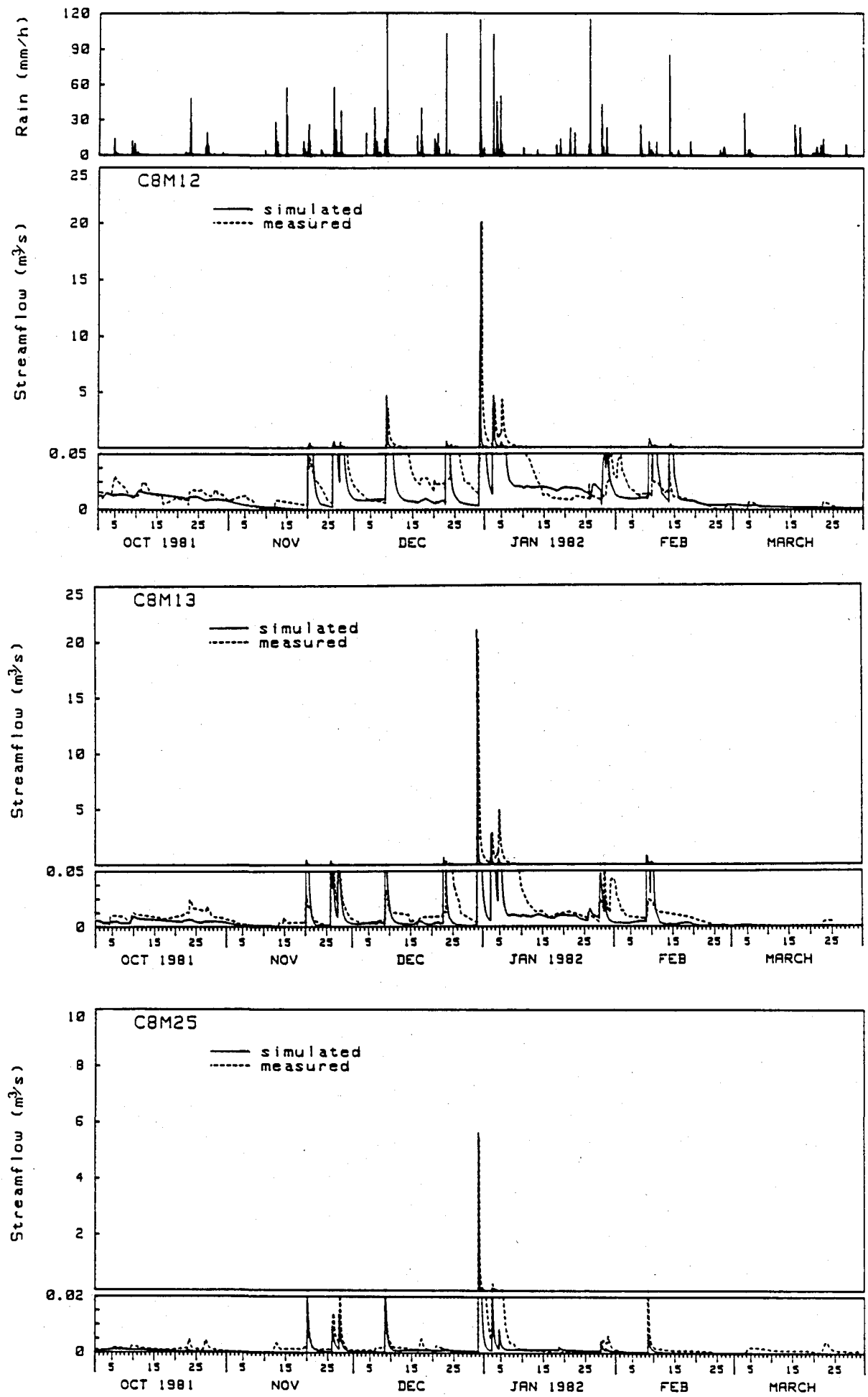


Figure 10.6: Model simulations for 1981/82 season
(calibration data set).

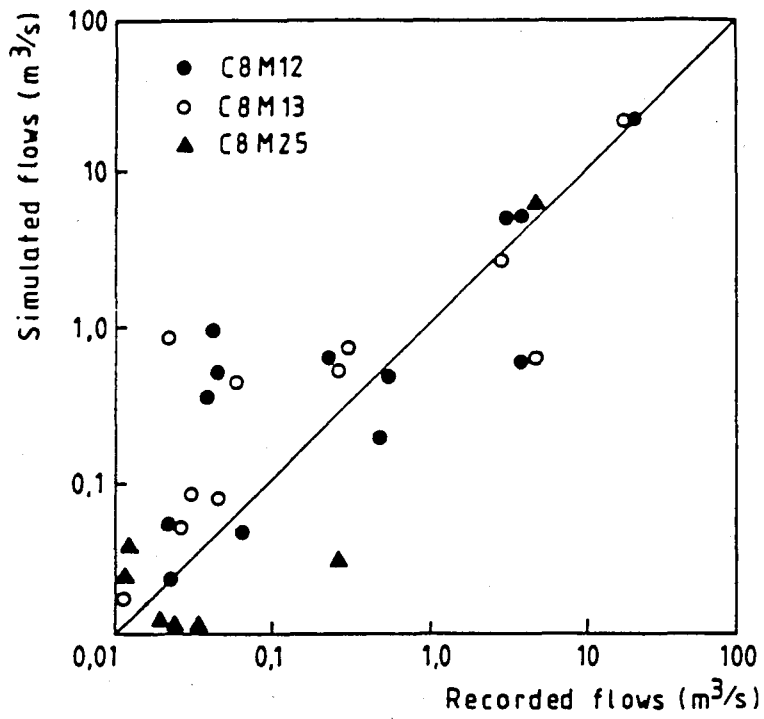


Figure 10.7: Scatter diagram for simulated and observed hydrograph peaks for 1981/82 season.

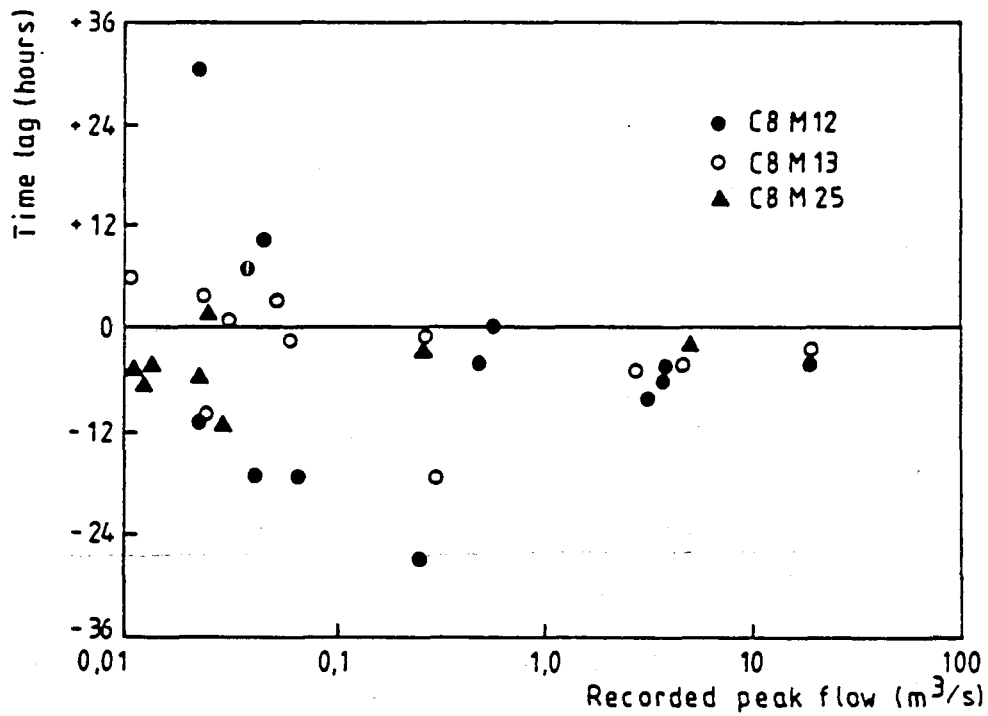


Figure 10.8: Scatter diagram of hydrograph lags for 1981/82 season.

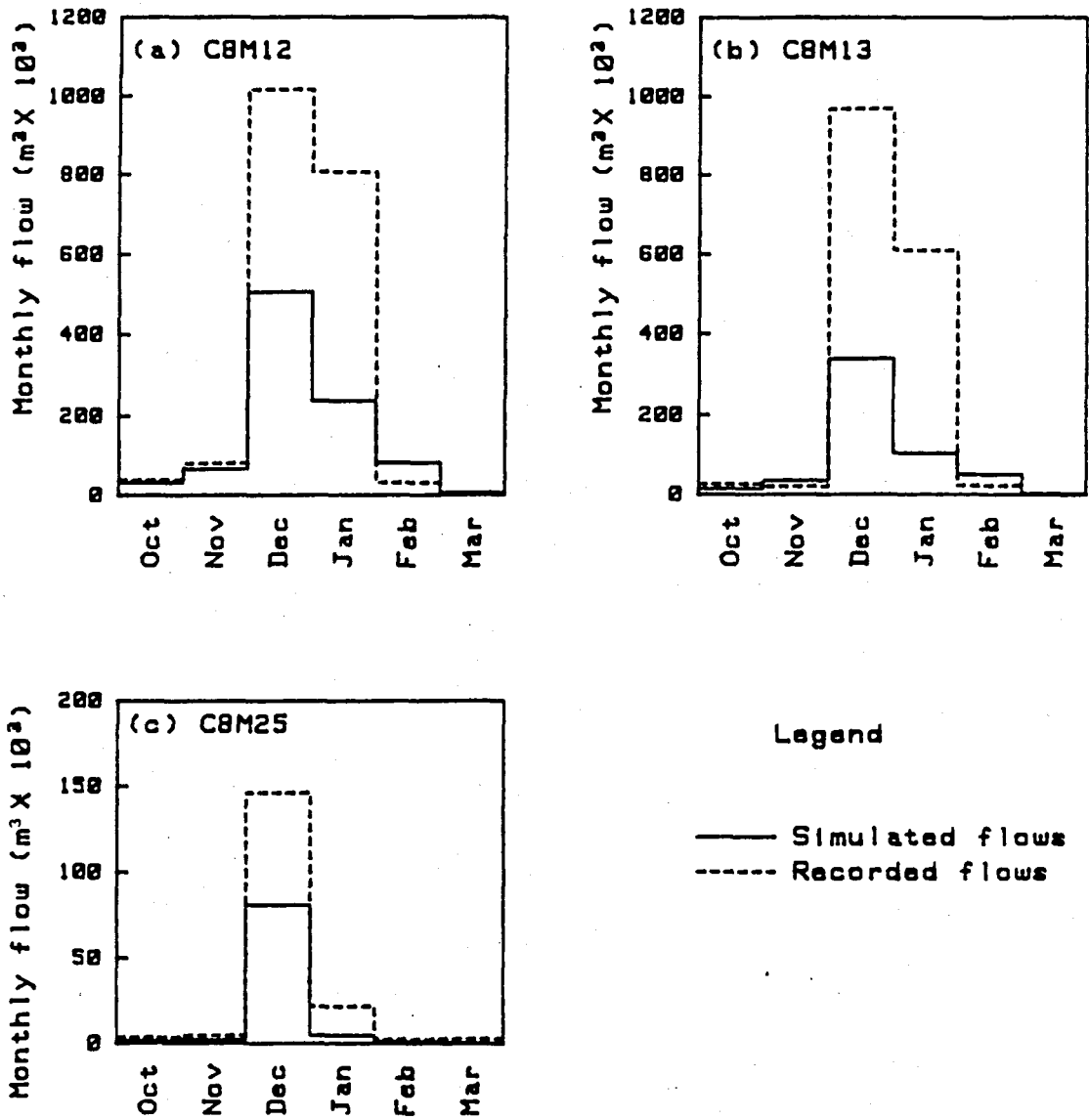


Figure 10.9: Total monthly flows for 1981/82 season.

details of minor events. The high peaks are all well predicted except for the event of 4 January 1982.

A scatter diagram of time lags is shown in fig. 10.8, in which the lag between the simulated and recorded peak for each event is plotted as a function of the peak flow, representing the magnitude of the event. A positive lag indicates that the simulated peak comes later than the recorded one, and a negative lag indicates that the simulated peak comes earlier. Again there is more scatter for the smaller events than the larger ones. Apart from some of the very low peaks less than $0.1 \text{ m}^3/\text{s}$,

the lags are generally negative, i.e. the simulated peaks tend to arrive at the streamgauges too soon. This may be caused by insufficient lag through the equivalent dams, or by flow paths being too short because of lumping the clay source areas in the streamside elements. The large lag errors are a major factor responsible for the low coefficient of efficiency for streamgauges C8M12 and C8M13.

The other factor contributing to the low coefficients of efficiency is the general under-prediction of volumes, as illustrated in fig. 10.9. Simulated and recorded monthly streamflows are plotted showing volumes greatly under-predicted by the model. Reasons for this are the failure of the model to adequately reproduce the delayed flows after each event, and the simulated hydrograph peaks being too "narrow" or peaky.

Although every effort was made to improve the model predictions it was not possible within the time constraints of this project to better these results. The simulation results for the uncalibrated 1980/81 season are shown in fig. 10.10 for C8M12. The recorded streamflows are poorly reproduced and no statistical measures of fit were generated for this season.

In general, discrepancies between recorded and simulated streamflows can be attributed to shortcomings in catchment discretization, input data or the model itself. In the Bethlehem study a number of possible reasons that may have contributed to the disappointing results can be identified:

1. Possible errors in the recorded streamflow and rainfall data sets. In particular, the spatially variable nature of rainfall and missing patches of data may have introduced errors into this study.
2. The effect of the large numbers of farm dams and natural pans on runoff can be difficult to quantify. The lumping into equivalent dams may introduce a certain amount of error, and errors in dam parameters are possible because of the construction of new dams and the unknown occurrence of dam breakages. The delayed flows that the model failed to reproduce may consist partly of seepage from dams, which was not accounted for by the model.

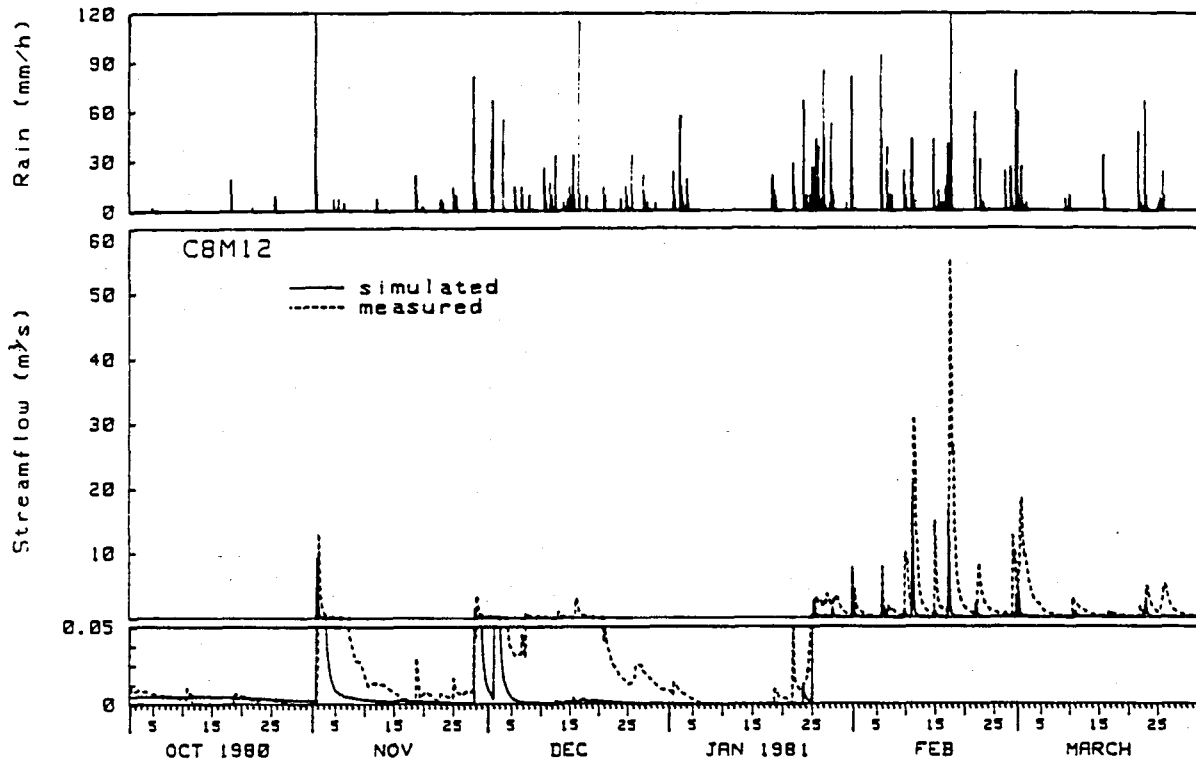


Figure 10.10: Model simulations for 1980/81 season
(verification data set).

3. While the lower soil layer was able to reproduce the low baseflow portion of the hydrograph, it did not simultaneously model shorter term interflow which probably contributes to the delayed flows after each event. This is a possible shortcoming in the model which should be addressed in future research.
4. Insufficient knowledge of the spatial variations of sensitive parameters such as infiltration rates.
5. Inaccurate lag times brought about by lumping clay source areas near the main streams.

10.3. LAND USE CHANGES

According to the Department of Water Affairs (1986), evaluating the effects of land use changes on runoff is an area requiring urgent attention so as to promote optimal management of water resources. Research is required to evaluate the effects of changes in cultivation, grazing, soil erosion, soil conservation and farm dam construction.

The present model was used to predict the affects of different land use management practices on the runoff from catchment C8M12 for the 1981/82 season. Although the model was seen above to under-predict recorded streamflow volumes in this catchment, inferences can be made concerning the *relative* changes in streamflow volume as a result of various changes in land use. The following practices were considered:

1. *Poor agricultural practices* such as ploughing with the slope, heavy over-grazing and neglecting to use any erosion controlled measures.
2. *Good agricultural practices* including contour ploughing, controlled grazing and the use of contour walls for erosion control.
3. *Present state of the catchment*. This includes a combination of good and poor practices.

The effects of these practices were considered assuming no changes in the types of crops presently grown. Using the calibrated model parameters in tables 10.2 to 10.10 to represent the present state, the deviations in land use were represented by adjusting pertinent parameters as shown in table 10.12. Low values of Manning's coefficient and the rill ratio are associated with the presence of rills and gullies, well-eroded lands, and fields ploughed with the slope. Conversely larger values are applicable where greater tillage roughness and flow obstacles such as contour walls are present, increasing attenuation and overland travel times. Over-grazing results in a reduction of vegetation density, with lower values of interception capacity and leaf area index as shown in the table. A shallower root system was assumed for sparse vegetation and lands in poor condition. The changes in leaf area index and infiltration rates were represented by a multiplication factor applied to the parameter values used in the above model simulations. Infiltration rates were reduced by 20% for poor agricultural practices to allow for hard, rain-packed earth in areas such as over-grazed lands, and increased to allow for the maintenance of soil permeabilities by good practices. The dam parameters were left unadjusted as their effect is considered separately below.

Table 10.12: Parameters used in catchment management simulations.

Parameters	Poor practices	Present state	Good practices
Manning's coefficient (overland flow)	0.15	0.20	0.30
Rill ratio	0.55	0.65	0.75
I_c (mm)	0.7	1.0	1.0
LAI*	0.7	1.0	1.0
Root distribution**	80	60	60
Soil permeability*	0.8	1.0	1.2

* Multiplication factor applied to model parameters.

** Percentage roots in upper soil layer.

The effects of the different practices on the total streamflow volume for the 1981/82 season are shown in fig. 10.11(a). The lands in poor condition show an 81% increase in runoff, while the maintenance of good practises shows a potential 42% decrease. This is a benefit in terms of reduced soil erosion and better retention of moisture for crops, but must be weighed up against the decrease in catchment yield for major dams fed by the basin.

The effect on hydrograph peaks is shown in fig. 10.11(b) in which the change in peak is plotted versus the simulated flow peaks for the present land use. With poor practices the smaller peaks are increased up to 400% and the larger peaks up to 200%. For good practices most of the peaks are decreased to less than 50% of their original values. There is generally wide scatter and no definite trends are discernible.

The influence of farm dams on streamflow was studied by considering the effect on the simulated output of changing the total capacity and coverage of dams. The storage coefficients ('a' in eqn. 10.1) for all the dams were altered from zero to double their present values, and the parameters CL and k_0 adjusted proportionally. The effects on total streamflow volume for the season are shown in fig. 10.12, in which the total dam capacity of the basin is represented on the horizontal axis relative to the present

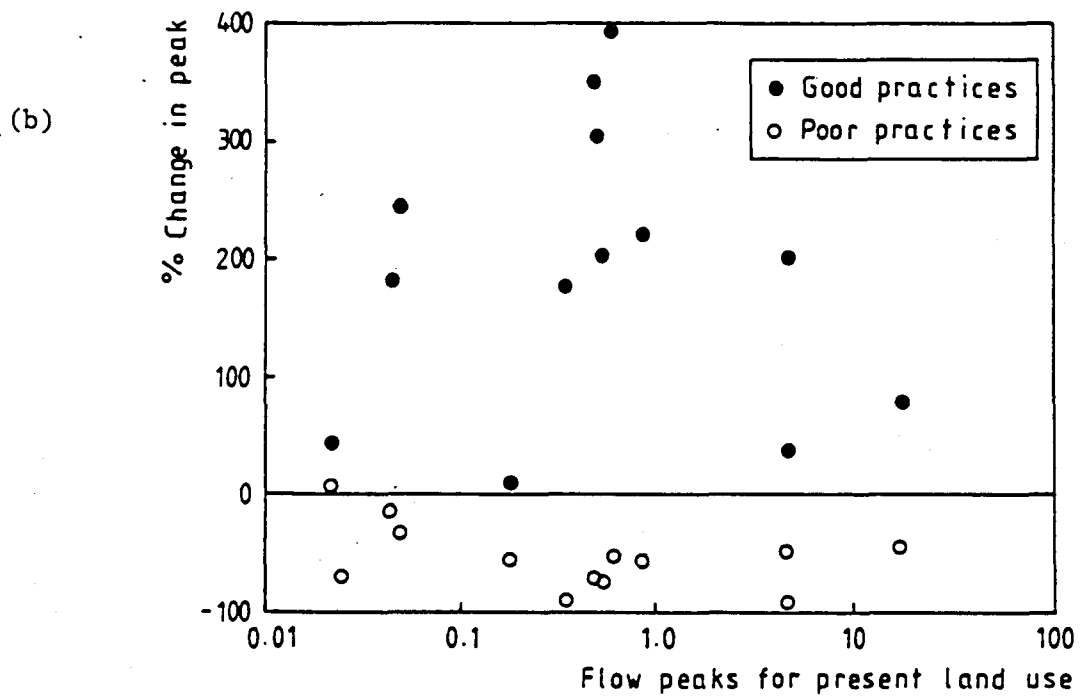
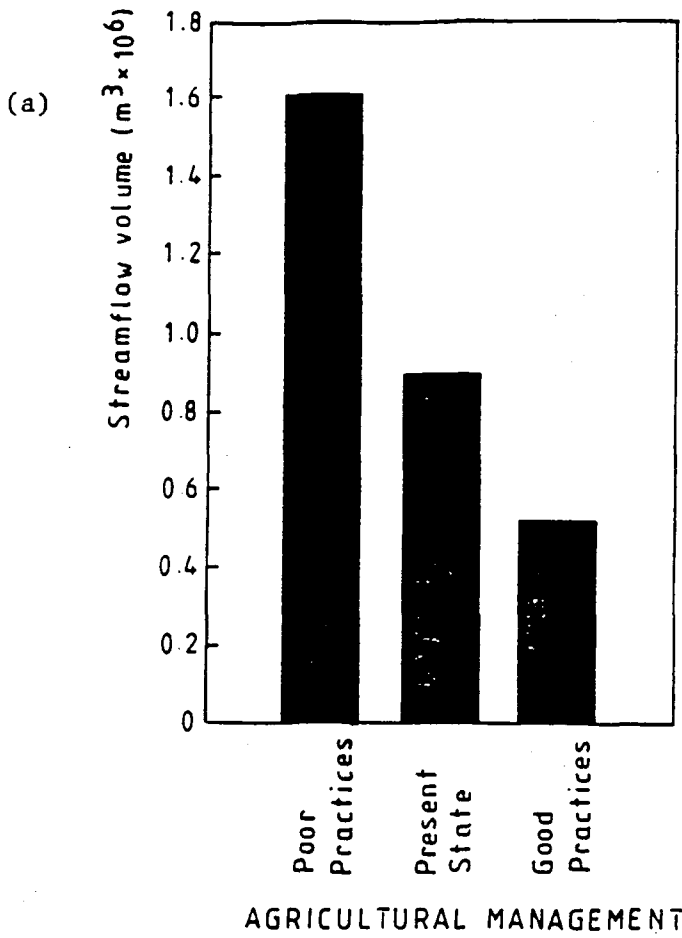


Figure 10.11: Effects of changes in agricultural practices on (a) volumes and (b) peak flows.

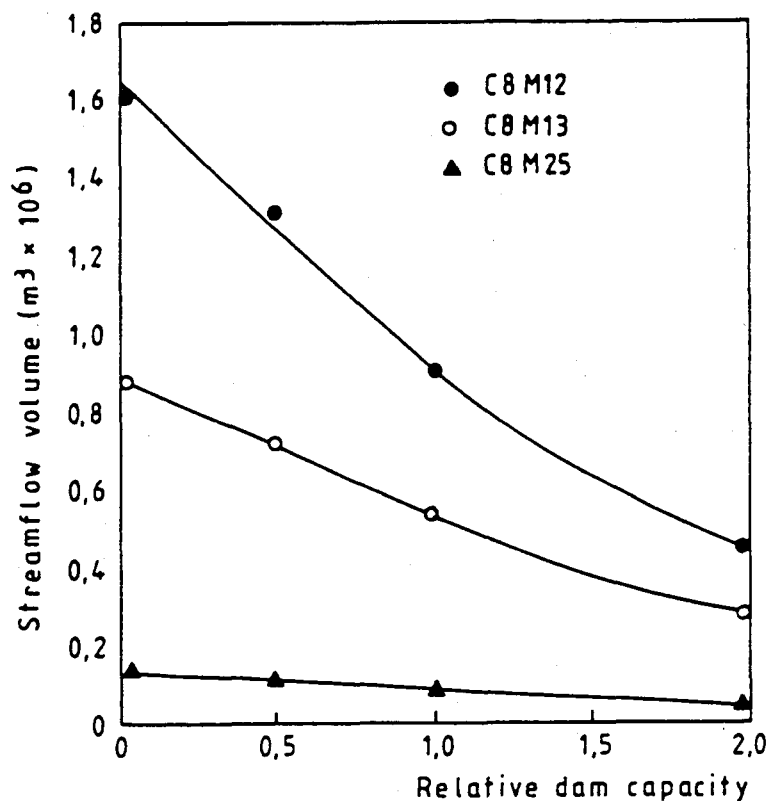


Figure 10.12: Effects of dam capacity on streamflow.

state. The curves show a steady decrease in simulated runoff with increasing dam capacity, illustrating the significant effect of a large number of small dams on runoff. Catchment C8M25 shows the least change because it has a lower density of dams than the rest of the basin. The model predictions for streamgauge C8M12 decrease from about 1.6 million m³ with no dams to 0.9 million m³ with the present density of dams. This indicates a decrease of some 43% in potential runoff because of the presence of the dams in the catchment. This compares well with long-term observations of about 40% reduction in seasonal streamflows in tributaries of the Orange and Upper Brude Rivers as a result of the construction of farm dams (Department of Water Affairs, 1986).

10.4. CONCLUSIONS

The Bethlehem study is more rigorous than the Waterval and Ecca studies because of the longer period simulated and the greater number of streamgauges. Although the correspondence between simulated and recorded streamflows was generally disappointing, a number of valuable conclusions may be drawn from the study. It was found that reproducing the spatial rainfall patterns of this large basin was important, as well as the spatial variations of soil properties. A larger number of input parameters required calibration than in the Waterval and Ecca studies because of more uncertainties in parameter values and a greater degree of lumping in the larger Bethlehem basin. Attention should be given to improving the soil component of the model to reproduce delayed flows where baseflow and shorter-term interflow occur together. Future simulations of the Bethlehem catchments should consider seepage from the dams, improved modelling of the delayed flows, and finer discretization of the catchments.

Effects of hypothetical changes in agricultural practices on streamflow volumes and runoff peaks were studied, as well as the influence of farm dams on seasonal runoff. The results are in agreement with known trends, and this kind of land use study shows potential for catchment management exercises.

The development of the simulation model in this study incorporates research into numerical methods and work on developing the individual model components. Catchment applications were used for verifying the model and investigating certain aspects of physically-based modelling. The main points are presented below with discussion on their relevance to hydrological modelling.

11.1. NUMERICAL METHODS

The numerical methods used for component hydrological processes in the simulation model were based on extensive research into the properties of finite difference methods. Finite difference formulations for the kinematic equations were studied using a generalised Preissmann formulation of the continuity equation with various values of the temporal and spatial weighting coefficients θ and ϕ . Criteria governing numerical stability and diffusion were studied and their dependence on the weighting coefficients and on grid spacing was clarified. It was found that numerical diffusion is only controlled by introducing a variable coefficient θ into the formulation. Since numerical schemes generally use a constant θ , the accuracy of the numerical solution is dependent on grid spacing, a problem that has been discussed elsewhere but apparently not solved.

It was shown that a hillslope should be divided into a number of elements for modelling overland flow, since a numerical solution converges on the true solution as Δx decreases. The practise of setting Δx equal to the overland flow length in watershed models can therefore lead to erroneous results. However, it was found that subdividing a flow plane onto a number of Δx -increments introduces parasitic waves into the solution.

A finite difference formulation for the kinematic equations using the Muskingum-Cunge approach of Cunge (1969) was also studied, and found not to suffer from the problem of parasitic waves. The approach was also shown to have other advantages. It has been previously shown that Muskingum-Cunge routing models attenuation by matching numerical and physical diffusion, constituting a second order approximation to diffusion routing (Ponce, 1986). In the present study, it was further shown

that the scheme can be improved by re-defining the routing coefficients based on a value of the spatial weighting coefficient ϕ equal to zero. This ensures unconditional numerical stability at low grid spacings.

Conventional finite difference methods for solving the kinematic equations become implicit when $\phi = 0$, requiring iterative solution. A computationally simpler, explicit solution can be used, based on $\phi = 1.0$, but at the expense of numerical instability at low grid spacings (Courant criterion). In the past, much attention has been given to judiciously selecting values of Δx and Δt so as to avoid numerical instability and minimise numerical diffusion (for example Constantinides, 1982, and Green, 1984). The Muskingum-Cunge finite difference scheme with $\phi = 0$ avoids both of these problems. It was shown here that the grid spacing does not affect the accuracy of the solution through numerical diffusion, and furthermore, an *explicit* formulation at $\phi = 0$ is possible, with savings in computational time and effort.

This modified Muskingum-Cunge approach was used for the overland and channel routing components of the simulation model. Finite difference schemes for other component processes in the model were also based on $\phi = 0$ for numerical stability, namely reservoir routing, the interception equations and the soil sub-model. Further research is still required in developing improved finite difference methods, as shown by the tendency of the Muskingum-Cunge approach to generate negative flows under certain conditions.

11.2. DEVELOPMENT OF SIMULATION MODEL

11.2.1. Catchment discretization

The simulation model was based on an element approach to catchment discretization in which subcatchments are subdivided into strips normal to the flow direction. The approach was based on that of Jayawardena and White (1979), but was adapted by employing larger elements with less formidable data entry requirements, and streamlining the data entry process using digitising techniques.

This element discretization can be seen as an intermediate approach relative to the more commonly-used subcatchment and grid approaches. Discretization by means of subcatchments may provide too coarse a framework for hydraulic routing of stormflows, as well as not allowing for variations in soil moistures, soil properties and source areas over a hillslope. The grid approach is therefore often used, making use of two-dimensional solutions of the surface and subsurface flow equations. The use of elements in the present study facilitates a simpler one-dimensional solution of the routing equations, while providing a finer discretization than with the subcatchment approach.

The element discretization was shown here to be more flexible than the grid approach, since elements can be shaped to realistically represent the physical features of a catchment, and varied in size to suit local conditions. This results in computational and data storage savings, fewer elements being necessary than with a rectangular grid. The element discretization was found to be well suited to representing spatial variations of soil moistures and soil properties and the occurrence of source areas. It also proved to be a useful tool for graphically representing soil and surface water conditions. In future research the approach could be made more powerful by developing a means by which the simulation program automatically defines the element boundaries from digital terrain data.

11.2.2. Continuous simulation with variable time increments

Continuous simulation has the advantages of regenerating antecedent moisture conditions for each storm, and of being able to model short-term stormflows as well as long-term responses of a catchment to rainfall. It is also of use for simulating seasonal or annual streamflows for applications such as catchment management, land use and water resource studies, as illustrated in the present work.

In order to make simulations over long periods computationally feasible, efficient choice of simulation time steps is essential, especially in distributed, physically-based models in which many computations are carried out at each time step, and many short time increments are required

during rapidly changing flow conditions encountered during storms. As a refinement of dual time increment systems, the concept of a constantly-varying time increment was investigated here, in which time steps vary between a few minutes and several hours or days. This was implemented by means of user-defined time increment files, and found to be successful for selecting appropriate time steps throughout a simulation and for ensuring optimum computational and output-storage efficiency. As a further development of this concept, a means of automation should be sought whereby a program automatically selects appropriate time increments according to rainfall and streamflow conditions.

11.2.3. Model components

Work was done on the effect of rilling on surface runoff, and a channelisation factor was incorporated in the overland flow routing algorithm of the simulation model. The Muskingum-Cunge algorithm developed for channel routing included both looped and single-valued rating relationships so as to make the model more versatile. A modified storage-indication reservoir routing algorithm was incorporated, with improved numerical stability characteristics obtained by re-deriving the equations with the weighting coefficient ϕ set equal to zero. The soil sub-model was based on a three-layer approach with vertical and downslope soil moisture seepage.

The interception and evapotranspiration components of the model were based on a dynamic interception store and leaf area index respectively. The interception component is necessary for a rural catchment model and the evapotranspiration for continuous simulations, but they were not tested independently using measured soil moisture and interception data.

Spatial variations of rainfall were accounted for by interpolating between a number of raingauges in a catchment. Spatial rainfall patterns were found to be important in both small and large catchments, emphasising the importance of using a number of raingauges with a distributed model.

11.3. MODEL APPLICATIONS

The simulation model was applied to a number of rural catchments with a range of sizes and climates. Good agreement between simulated and recorded streamflows was achieved in the Waterval and Ecca studies, indicating the basic integrity of a physically-based approach with measured parameters. The model also performed well in comparison with the Pitman and Stanford Watershed models in the Ecca study. Less successful results for the Bethlehem catchments were attributed to unknown factors related to the modelling of the farm dams, as well as simplifications adopted in the discretization of the catchment and possible inadequate modelling of delayed flows.

The study of land use changes in the Bethlehem catchments enabled predictions to be made concerning the effects of various management practices on seasonal streamflows. The other catchment studies provided valuable information enabling the main stormflow-producing mechanisms to be identified, such as the location of source areas and the relative roles of quick flow and delayed flow. This is an advantage of using a distributed, physically-based model, although there is a need for variables such as soil moistures and the extent of source areas to be monitored in the field and compared with simulated model output.

11.3.1. Modelling delayed flows

Physically-based modelling of subsurface flows presents particular problems because of the difficulties of modelling the complex subsurface environment and of collecting detailed soil data. Considerable attention was given to this component in the present study, and the three-layer soil sub-model was successfully used to model delayed flows (interflow and baseflow).

Experience with the soil model showed that the upper two soil layers were best for representing infiltration, vertical downward soil moisture seepage and evapotranspiration losses in the root zone. Downslope saturated flow in the third soil layer was successfully used to model interflow and baseflow in the Ecca and Waterval catchment simulations, with

good agreement between simulated and recorded flows. It was found that calibration of the parameters in the lower soil layer was necessary in order to compensate for the unknown effects of soil layering, pebble markers, piping, rock strata and variable soil permeabilities on delayed flows. When treated in this way the lower soil layer becomes a conceptual layer rather than a physical zone. This suggests that any empirical or conceptual delayed flow function could be used for this component of the simulation model, not necessarily a physically-based function.

A number of areas can be identified where the soil model could be improved. Model output was sometimes sensitive to the thickness chosen for the soil layers, since this determines the average moisture content for a given volume of soil moisture and hence the drainage rate of the soil. This could be rectified by introducing a separate parameter to determine the drainage rate of the upper two soil layers. The simulation of interflow and baseflow is also open to improvement. Although interflow and baseflow occurring separately were well reproduced in the Waterval and Ecca studies, their occurrence together in the Bethlehem catchment was not as successfully modelled. Accommodating interflow and baseflow simultaneously could either involve modifying the delayed flow function or introducing an additional soil layer for saturated downslope flow. The model also tends to under-predict streamflow volumes, probably because the delayed flow contribution is too small.

Parameters such as soil depth and permeability can be subject to considerable spatial variation in the field. When modelling the subsurface environment, average parameter values are used to represent highly variable quantities, and there is a "quantum leap" of applying theory developed for point-processes to larger areas of land (Beven, 1989). This is a short-coming of present modelling approaches which needs to be addressed in future research. One way of addressing this would be to make use of a fine grid with soil properties and depths assigned to each grid cell by means of a statistical distribution with user-defined mean and standard deviation.

11.3.2. Parameter calibration

Particular attention was given to the issue of calibration of parameters in the model studies. Beven (1989) contended against the indiscriminate use of calibration in physically-based models because the parameters are intended to be measurable quantities. However, a certain amount of calibration is generally carried out in physically-based modelling, and some possible reasons for this being necessary are suggested below:

- o A lack of detailed catchment data.
- o The need to compensate for errors introduced through approximations and simplifying assumptions made in model development.
- o Lumping of land areas into pseudo "homogeneous" areas with equivalent, average values of model parameters.
- o Uncertainties in quantities such as soil properties that are highly variable in the field and costly to measure in detail.

In the present study, calibration of parameters was minimised as much as possible. From the model studies in this work the following conclusions may be drawn:

1. It is possible to obtain good results without calibration for surface runoff on small catchments where large-scale lumping is not employed and detailed soil, vegetation and stream data can be collected.
2. Calibration of parameters representing interflow and ground water flow against recorded streamflows appears to be unavoidable. This can be attributed to the heterogeneous nature of soils, the expense of collecting detailed soil data in the field, and the use of a simplified representation of the complex subsurface environment.
3. The amount of calibration of surface and subsurface parameters and the number of parameters requiring calibration tend to increase with increasing catchment size, because of the increasing cost of data collection and the greater degree of lumping.
4. Although it is not always possible to avoid calibration, an advantage of physically-based modelling is that the physical basis of parameters results in a known range in which they can be adjusted.

Based on the results of the present study, it is suggested that the parameters of a physically-based model can be divided into three categories as represented in table 11.1, namely those that always need to be calibrated, those requiring calibration under certain circumstances, and those not requiring calibration at all. The sensitivity classification of certain parameters in this table is related to the present model, but may differ depending on the application.

Table 11.1: Role of calibration in physically-based modelling.

PARAMETERS NOT RE-QUIRING CALIBRATION	PARAMETERS SOMETIMES REQUIRING CALIBRATION	PARAMETERS HAVING TO BE CALIBRATED
Obtained from topographical maps and aerial photographs.	These parameters are measurable or may be estimated from known field conditions or published data, but may need calibration because of uncertainties in their exact value, lumping, etc.	Generally require calibration against recorded streamflows.
Areas, slopes & channel lengths.	<p><i>Sensitive parameters:</i> Hydraulic roughness coefficients, infiltration capacities, soil depths, rill ratio.</p> <p><i>Less sensitive parameters:</i> Interception and evapotranspiration parameters; channel dimensions.</p>	Parameters representing soil moisture seepage and delayed flows.

11.3.3. Advantages of physically-based modelling

A distributed, physically-based model will not necessarily produce better streamflow predictions than an empirical or entirely calibrated model. However, certain advantages of a physically-based approach were highlighted in this study:

1. Calibration requirements of a physically-based model should be less extensive than for other types of models.
2. Physically-based simulations provide not only streamflow output, but information on conditions within a catchment such as dam water levels, soil moistures and source areas. Graphical representation of the spatial variation of catchment parameters is facilitated by a distributed approach.
3. The physical basis facilitates a better understanding of hydrologic processes occurring within a catchment, and assists the modeller in identifying the streamflow-producing mechanisms.
4. The effects of proposed or hypothetical land use changes on streamflows can be assessed for catchment planning and management purposes.

11.4. DEVELOPMENTS AND FURTHER RESEARCH

The developments made in the present study can be summarised as follows:

- o The development of a continuous simulation model capable of simulating a comprehensive range of catchment processes, and of reproducing the quick flow as well as delayed flow components of streamflows.
- o An element approach to catchment discretization was adapted and shown to be a viable basis for a distributed model.
- o Current understanding of numerical methods for the kinematic equations was enhanced, and the Muskingum-Cunge approach was improved and used for developing flow routing algorithms.
- o Various improvements to standard modelling techniques were incorporated in the component processes of the simulation model.

- o A variable time increment was successfully used as an improvement on less flexible single- or dual-time increment systems, with savings in computation time and output storage requirements.
- o Certain aspects of the role of calibration in physically-based modelling were clarified.
- o Advantages of physically-based modelling were highlighted with respect to parameter calibration, land use changes and the use of physically-based models to facilitate a better understanding of catchment processes and streamflow mechanisms.
- o Guidelines were compiled to assist in assessing model parameter values. These guidelines are of wider application than just the present model.

Some areas in need of further research have been identified as follows:

- o Automating the setting up of discretization elements from DTM data, and of time increments from rainfall data and catchment conditions.
- o Further refinement of Muskingum-Cunge routing and further research in finite difference methods.
- o Modelling the subsurface environment is a wide field for research, including refinement of methods for modelling subsurface seepage and delayed flows; employing statistical variations of soil properties; and bridging the gap between field-scale processes and equations for point-processes.
- o Assessment of distributed model output such as soil moistures, dam water levels and source areas by comparing with field data, in order to improve confidence in model output.

Hydrological modelling is a field of ongoing research, incorporating both basic research and the development of computer models. Although the present work is far from being the final word on physically-based modelling, it is hoped that it will answer certain questions, provide improved methods for specific aspects of catchment modelling, and stimulate further research, and it is in this spirit that it is offered.

Abbot, M.B., Bathurst, J.C., Cunge, J.A., O'Connell, P.E. and Rasmussen, J. (1986a): "An introduction to the European hydrological system - Systeme Hydrologique Europeen, 'SHE'. 1: History and philosophy of a physically-based, distributed modelling system." Journal of Hydrology, vol. 87, pp. 45 - 59.

Abbot, M.B., Bathurst, J.C., Cunge, J.A., O'Connell, P.E. and Rasmussen, J. (1986b): "An introduction to the European hydrological system - Systeme Hydrologique Europeen, 'SHE'. 2: Structure of a physically-based, distributed modelling system." Journal of Hydrology, vol. 87, pp. 61 - 77.

Ackers, P., White, W.R., Perkins, J.A. and Herison, A.J.M. (1978): "Weirs and flumes for flow measurement." Published by Wiley.

Al-Soufi, R. (1987): "A physically-based model for the agrohydrologic processes." Journal of Hydrology, vol. 93, pp. 199 - 219.

Amerman, C.R. and Naney, J.W. (1982): "Subsurface flow and ground water systems." In: "Hydrological modelling of small watersheds," Haan (ed.), American Society of Agricultural Engineers, Monograph no. 5.

Antoine, L.A.G. (1989): "Geophysical investigation of the Waterval catchment." Internal report, Civil Engineering Department, University of the Witwatersrand.

ASCE (1985): "Evaluation of hydrologic models used to quantify major land-use change effects." ASCE, Journal of Irrigation and Drainage Engineering, vol. 111, no. 1, pp. 1 - 17.

Bathala, C.T., Spooner, J.A. and Rao, A.R. (1976): "Regional aquifer evaluation studies with stochastic inputs." Purdue University, Water Resources Center, Technical Report 72, West Lafayette, IN.

Bathurst, J.C. (1986): "Physically-based distributed modelling of an upland catchment using the Systeme Hydrologique Europeen." Journal of Hydrology, vol. 87, pp. 79 - 102.

Beasley, D.B., Monke, E.J. and Huggins, L.F. (1977): "The ANSWERS model: a planning tool for watershed research." Proceedings, ASAE, paper 77/2532.

Bernier, P.Y. (1985): "Variable source area and storm-flow generation: an update of the concept and a simulation effort." Journal of Hydrology, vol. 79, pp. 195 - 213.

Betson, R.P. (1964): "What is watershed runoff?" Journal of Geophysics Research, vol. 69, pp. 1541 - 1552.

Beven, K. (1981): "Kinematic subsurface stormflow." Water Resources Research, vol. 17, no. 5, pp. 1419 - 1424.

Beven, K. (1982): "On subsurface stormflow: Predictions with simple kinematic theory for saturated and unsaturated flows." Water Resources Research, vol. 18, no. 6, pp. 1627 - 1633.

Beven, K. (1989): "Changing ideas in hydrology - the case of physically-based models." Journal of Hydrology, vol. 105, pp. 157 - 172.

Beven, K. and Kirkby, M.J. (1979): "A physically-based variable contributing area model of basin hydrology." Hydrological Science Bulletin, vol. 24, pp. 43 - 69.

Beven, K. and Wood, E.F. (1983): "Catchment geomorphology and the dynamics of runoff contributing areas." Journal of Hydrology, vol. 65, pp. 139 - 158.

Blake, G.J. (1975): "The Interception Process." In: "Prediction in Catchment Hydrology," National Symposium on Hydrology, Australian Academy of Science, Chapman and Dunin (ed).

Blaney, H.F. and Criddle, W.D. (1966): "Determining consumptive use for water developments." ASCE, Proceedings of Irrigation and Drainage Spec. Conf., pp. 1 - 34.

Bloemen, G.W. (1980): "Calculation of hydraulic conductivities of soils from texture and organic matter content." Zeitschr. Pflanzenernaerung Bodenkunde, vol. 143, pp. 581 - 605.

Bodman, G.B. and Coleman, E.A. (1944): "Moisture and energy conditions during downward entry of water into soils." Proceedings, Soil Science Society, vol. 8, pp. 116 - 122.

Bouwer, H. (1969): "Infiltration of water into non-uniform soil." Proceedings, ASCE, Journal of the Irrigation and Drainage Division, vol. 95, pp. 451 - 462.

Brakensiek, D.L. (1967): "Kinematic flood routing." Transactions, ASAE, vol. 10, part 3, pp. 340 - 343.

Brendecke, C.M., Laiho, D.R. and Holden, D.C. (1985): "Comparison of two daily streamflow simulation models of an alpine watershed." Journal of Hydrology, vol. 77, pp. 171 - 186.

Brooks, R.H. and Corey, A.T. (1966): "Properties of porous media affecting fluid flow." Proceedings, ASCE, Journal of the Irrigation and Drainage Division, vol. 72, IR2, pp. 61 - 88.

Burt, T.P. and Butcher, D.P. (1984): "A BASIC hillslope runoff model for use in undergraduate teaching." Huddersfield Polytechnicon, Department of Geography, Occasional Paper no. 11.

Campbell, G.S. (1974): "A simple method for determining unsaturated hydraulic conductivity from moisture retention data." Soil Science, vol. 117, pp. 311 - 314.

Campbell, G.S. (1985): "Soil physics with BASIC." Developments in Soil Science 14, Elsevier Science Publishers, Amsterdam, The Netherlands.

Carrigan, P.H. (1973): "Calibration of U.S. Geological Survey Rainfall-Runoff Model for Peak Flow Synthesis - natural basins." U.S. Geological

Survey Computer Report, U.S. Department of Commerce, National Technical Information Service.

Chen, C.L. (1976): "Flow resistance in broad shallow channels." Proceedings, ASCE, Journal of the Hydraulics Division, vol. 102, HY3, pp. 307 - 322.

Childs, E.C. (1969): "An introduction to the physical basis of soil water phenomena." Publ. Wiley and Sons Ltd, London.

Childs, E.C. and Collis-George, N. (1950): "The permeability of porous materials." Proceedings, Royal Society of London, A201, pp. 392 - 405.

Chow, V.T. (1964): "Handbook of Applied Hydrology." Publ. McGraw-Hill Book Co., New York.

Clarke, R.T. (1973): "A review of some mathematical models used in hydrology, with observations on their calibration and use." Journal of Hydrology, vol. 19, pp. 1 - 20.

Constantinides, C.A. (1982): "Two-dimensional kinematic modelling of the rainfall-runoff process." University of the Witwatersrand, Department of Civil Engineering, Water Systems Research Programme, Report no. 1/1982.

Constantinides, C.A. (1983): "Comparison of kinematic and time shift routing in closed conduits." University of the Witwatersrand, Department of Civil Engineering, Water Systems Research Programme, Report no. 3/1983.

Cook, H.L. (1946): "The infiltration approach to the calculation of surface runoff." Transactions, American Geophysics Union, vol. 27, pp. 726 - 743.

Courant, R., Friedrichs, K.O. and Lewy, H. (1928): "Über die partiellen Differentialgleichungen der Mathematischen Physik." Math. Ann, 100.

Crawford, N.H. and Linsley, R.K. (1966): "Digital simulation in hydrology: Stanford Watershed Model IV." Department of Civil Engineering, Stanford University, Stanford, California, Technical Report no. 39, 210 pp.

Crawford, N.H., Linsley, R.K. and Franz, D.D. (1976): "Hydrocomp Simulation Programming Operations Manual." Hydrocomp Inc., Palo Alto, California.

Cunge, J. (1969): "On the subject of a flood propagation computation method (Muskingum Method)." Journal of Hydraulic Research, vol. 7, no. 2, pp. 205 - 230.

Davidoff, B. and Selim, H.M. (1986): "Goodness of fit for eight water infiltration models." Soil Science Society Journal, vol. 50, no. 3, pp. 759 - 764.

De Jager, J.M. and Van Zyl, W.H. (1989): "Atmospheric evaporative demand and evaporation coefficient concepts." Water S.A., vol. 15, no. 2.

De Villiers, G. du T. (1975): "Reenvalonderskeppingsverliese in die Republiek van Suid-Afrika - 'n Streekstudie." Unpublished PhD thesis, University of the Orange Free State, Bloemfontein, 219 pp.

De Villiers, G. du T. (1978): "Grondreëval en onderskeppingsverliese by landbougewasse." Crop Production, vol. VII, pp. 153 - 157.

De Villiers, G. du T. (1982): "Predictive models for estimating net rainfall and interception loss in savanna vegetation." Water S.A., vol. 8, pp. 208 - 212.

Department of Water Affairs (1986): "Management of the Water Resources of South Africa." Publ. CTP Book Printers, Cape Town.

Diskin, M.H. (1984): "CELMOD - A semi-distributed cell model for conversion of rainfall into runoff." First draft of a report submitted to

Southwest Rangeland Watershed Research Centre, U.S. Department of Agriculture, Tuscon, Arisona.

Diskin, M.H. and Green, I.R.A. (1985): "A case of delayed subsurface flow in an urban catchment." *Water S.A.*, vol. 11, no. 3.

Doorenbos, J. and Kassam, A.H. (1979): "Yield response to water." *FAO Irrigation Drainage Paper 33*, 193 pp.

Dunne, T. (1978): "Field studies of hillslope flow processes." In "Hillslope Hydrology," Kirkby (ed.), Publ. Wiley.

Eeles, C.W.O. (1978): "A conceptual model for the estimation of historic flows." *Institute of Hydrology Report no. 55*, Wallingford, U.K.

England, C.B. (1975): "Soil moisture accounting component of the USDAHL-74 model of watershed hydrology." *Water Resources Bulletin* 11, no. 3, pp. 559 - 567.

Engman, E.T. (1986): "Roughness coefficients for routing surface runoff." *ASCE, Journal of Irrigation and Drainage Engineering*, vol. 112, no. 1, pp 39 - 53.

Fiering, M.B. and Jackson, B.B. (1971): "Synthetic streamflows." *American Geophysical Union, Water Resources Monograph 1*, pp. 1 - 98.

Fleming, G. (1975): "Computer simulation techniques in hydrology." *Elsevier Environmental Science Series*, American Elsevier Publishing Co., New York.

Foster, G.R. (1982): "Modelling the erosion process." In: "Hydrological modelling of small watersheds", Haan (ed.), *American Society of Agricultural Engineers, Monograph no. 5*.

Foster, G.R., Huggins, L.F. and Meyer, L.D. (1968): "Simulation of overland flow on short field plots." *Water Resources Research*, vol. 4, no. 6, pp. 1179 - 1187.

Freeze, R.A. (1971): "Three-dimensional, transient, saturated-unsaturated flow in a ground water basin." *Water Resources Research*, vol. 7, no. 2, pp. 347 - 366.

Freeze, R.A. (1980): "A stochastic-conceptual analysis of rainfall runoff process on a hillslope." *Water Resources Research*, vol. 16, pp. 391 - 408.

Gash, J.H. (1979): "An analytical model of interception by forests." *Quarterly Journal of R. Met. Soc.*, vol. 105, pp. 43 - 55.

Germann, P.F. and Beven, K. (1985): "Kinematic wave approximation to infiltration into soils with sorbing macropores." *Water Resources Research*, vol. 21, no. 7, pp. 990 - 996.

Gorgens, A.H.M. (1978): "Precipitation-runoff relationship." Lecture notes, Pretoria Hydrology Course, University of Pretoria, S.A.

Gorgens, A.H.M. (1983): "Conceptual modelling of the rainfall-runoff process in semi-arid catchments." Hydrological Research Unit, Rhodes University, Report no. 1/83.

Green, G.C. (1985): "Estimated irrigation requirements of crops in South Africa." *Memoirs on the Agricultural Natural Resources of South Africa*, Soil and Irrigation Research Institute, Department of Agriculture and Water Supply, Pretoria.

Green, I.R.A. (1984): "WITWAT stormwater drainage program - version II." University of the Witwatersrand, Department of Civil Engineering, Water Systems Research Programme, Water Research Commission Report no. 115/2/84.

Green, W.H. and Ampt, G.A. (1911): "Studies on soil physics. 1: The flow of air and water through soils." *Journal Agric. Soils*, vol. 4, pp. 1 - 24.

Grijzen, J.G. (1986): "River flow simulation." In: "River flow modelling and forecasting," Kraijenhoff and Moll (ed.), Water Science and Technology Library, Reidel Publishers.

Haan, C.J., Johnson, H.P. and Brakensiek, D.L. (1982): "Hydrological modelling of small watersheds." American Society of Agricultural Engineers, Michigan, Monograph no. 5.

Hager, W.H. and Sinniger, R. (1985): "Flood storage in reservoirs." ASCE, Journal of Irrigation and Drainage Engineering, vol. 111, no. 1, pp. 76 - 85.

Hawkins, R.H. (1978): "Runoff curve numbers with varying site moisture." Proceedings, ASCE, Journal of Irrigation and Drainage Division, vol. 104, IR4, pp. 389 - 398.

Henderson, F.M. (1966): "Open channel flow." MacMillan Publishing Co., New York.

Henderson, F.M. and Wooding, R.A. (1964): "Overland flow and interflow from limited rainfall of finite duration." Journal of Geophysics Research, vol. 69, no. 8, p. 1531.

Hewlett, J.D. (1961): "Watershed management." U.S. Department of Agriculture, Forest Ser. Southeastern Forest Experiment Station, Asheville, North Carolina, Report for 1961, pp. 61 - 66.

Hillel, D. and Hornberger, G.M. (1979): "Physical model of the hydrology of sloping heterogeneous fields." Soil Science Society Journal, vol. 43, no. 3, pp. 434 - 439.

Hjelmfelt (Jr), A.T. (1981): "Overland flow from time-distributed rainfall." Proceedings, ASCE, Journal of the Hydraulics Division, vol. 107, HY2, pp. 227 - 238.

Hjelmfelt (Jr), A.T. (1985): "Negative outflows from Muskingum flood routing." ASCE, Journal of Hydraulic Engineering, vol. 111, no. 6, pp. 1010 - 1014.

Holden, A.P. and Stephenson, D. (1988): "Improved four-point solution of the kinematic equations." Journal of Hydraulic Research, vol. 26, no. 4, pp. 413 - 423.

Holtan, H.N. (1961): "A concept for infiltration estimates in watershed engineering." US Department of Agriculture, ARS Bulletin 41-51, 25 pp.

Holtan, H.N., Stiltner, G.J., Henson, W.H. and Lopez, N.C. (1975): "USDAHL-74 model of watershed hydrology." US Department of Agriculture, ARS Technical Bulletin 1518.

Horton, R.E. (1919): "Rainfall interception." Monthly Weather Review, vol. 47, pp. 603 - 623.

Horton, R.E. (1933): "The role of infiltration in the hydrological cycle." Transactions, American Geophysics Union, vol. 14, pp. 446 - 460.

Hromadka, T.V., McCuen, R.H. and Yen, C.C. (1987): "Comparison of overland flow hydrograph models." ASCE, Journal of Hydraulic Engineering, vol. 113, no. 11, pp. 1422 - 1440.

Huang, Y.H. (1978): "Channel routing by finite difference method." Proceedings, ASCE, Journal of the Hydraulics Division, vol. 104, HY10, pp. 1379 - 1393.

Huber, W.C., Heaney, J.P., Nix, S.J., Dickenson, R.E. and Polman, D.J. (1982): "Stormwater Management Model, User's Manual." Department of Environmental Engineering Science, University of Florida, Gainesville, Florida.

Hughes, D. (1990): Personal communication. Professor of Hydrology, Geography Department, Rhodes University, Grahamstown.

Institute of Hydrology (1984): Research Report 1981-84, Galliard Printers, U.K.

Jackson, I.J. (1975): "Relationships between rainfall parameters and interception by tropical forest." Journal of Hydrology, vol. 24, pp. 215 - 238.

Jacob, C.E. (1950): "Flow of ground water." In: "Engineering hydraulics," Rouse and Hunter (ed), Publ. Wiley and Sons, New York.

James, W. and Robinson, M.A. (1981): "Standard terms of reference to ensure satisfactory computer-based urban drainage design studies." Canadian Journal of Civil Engineering, vol. 8, no. 3, pp. 294 - 303.

Jayawardena, A.W. and White, J.K. (1979): "A finite element distributed catchment model, II: Application to real catchments." Journal of Hydrology, vol. 42, pp. 231 - 249.

Johanson, R.C., Imhoff, J.C., Kittle, J.L. and Donigian, A.S. (1984): "Hydrological Simulation Program - Fortran (HSPF): User's Manual." U.S. Environmental Protection Agency, Georgia.

Keefer, T.N. and McQuivey, R.S. (1974): "Multiple linearization flow routing model." Proceedings, ASCE, Journal of the Hydraulics Division, vol. 100, HY7, pp. 1031 - 1046.

Kennedy, P.J. (1981): "A hydrological study of agricultural dams and natural pans in a research catchment in South Africa." Unpublished BSc thesis, University College of Swansea.

Kirkby, M.J. (1978): "Hillslope Hydrology." Published by Wiley.

Kirkby, M.J. and Chorley, R.J. (1967): "Throughflow, overland flow and erosion." Bulletin, Int. Assoc. Sci. Hydrol., vol. 12, no. 3, pp. 5 - 21.

Knisel, W.G. (1980): "CREAMS: A field scale model for chemical, runoff and erosion from agricultural management systems." U.S. Department of Agriculture, Science and Education Administration, Conservation Research Report 26, 643 pp.

Kolovopoulos, P. (1988): "Free surface water level computation." Unpublished PhD thesis, Department of Civil Engineering, University of the Witwatersrand, Johannesburg.

Kostiakov, A.N. (1932): "On the dynamics of the coefficient of water-percolation in soils and on the necessity for studying it from a dynamic point of view for purposes of amelioration." Transactions, 6th Comm. Intern. Soil Sciences Soc., Russian Part A, pp. 17 - 21.

Koussis, A. (1976): "An approximate dynamic flood routing method." Proceedings, International Symposium on Unsteady Flow in Open Channels, Paper L1, Newcastle-Upon-Tyre, England.

Kouwen, N. and Li, R. (1980): "Biomechanics of vegetative channel linings." Proceedings, ASCE, Journal of the Hydraulics Division, vol. 106, HY6, pp. 1085 - 1103.

Kristensen, K.J. (1974): "Actual evaporation in relation to leaf area." Nordic Hydrol., vol. 5, pp. 173 - 182.

Kuichling, E. (1889): "The relation between the rainfall and the discharge of sewers in populous districts." Transactions, ASCE, vol. 20, pp. 1 - 56.

Lambourne, J.J. and Stephenson, D. (1986): "Factors affecting storm runoff in South Africa. II: Water losses." University of the Witwatersrand, Department of Civil Engineering, Water Systems Research Programme, Report no. 3/86.

Lighthill, M.J. and Whitham, G.B. (1955): "On kinematic waves. 1: Flood movement in long rivers." Proceedings, the Royal Society of London, series A, vol. 229, pp. 281 - 316.

Linacre, E.T. (1977): "A simple formula for estimating evaporation rates in various climates using temperature data alone." *Agricultural Meteorology*, vol. 18, pp. 409 - 424.

Linsley, R.K., Kohler, M.A. and Paulhus, J.L.H. (1949): "Applied hydrology." McGraw-Hill Publishers, New York.

Lyn, D.A. and Goodwin, P. (1987): "Stability of a general Preissmann scheme." *ASCE, Journal of Hydraulic Engineering*, vol. 113, no. 1, pp. 16 - 28.

Maaren, H. (1978): "Estimating potential total evapotranspiration with the Penman equation for different vegetation covers for use in catchment management models." Hydrological Research Institute, Department of Environmental Affairs, Technical Report 83.

Marshall, T.J. (1958): "A relation between permeability and size distribution of pores." *Journal of Soil Science*, vol. 9, pp. 1 - 8.

Mason-Williams, S. (1984): "The Bethlehem run-off augmentation research project: past, present and future." Hydrological Research Institute, Department of Environmental Affairs, Technical Report 118.

Meadows, M.E. (1984): "Introduction and modelling concepts" and "Infiltration models," Short Course on Kinematic Hydrology, Department of Civil Engineering, University of the Witwatersrand, Johannesburg.

Mein, R.G. and Larson, C.L. (1973): "Modelling infiltration during a steady rain." *Water Resources Research*, vol. 9, no. 2, pp. 384 - 394.

Meyer, W.S. and Green, G.C. (1980): "Water use by wheat and plant indicators of available water." *Agronomy Journal*, vol. 72, pp. 253 - 256.

Middleton, B.J., Lorentz, S.A., Pitman, W.V. and Midgley, D.C. (1981): "Surface Water Resources of South Africa." University of the Witwatersrand, Hydrological Research Unit Report no. 12/81.

Monsi, M. and Saeki, T. (1953): "Über den Lichtfaktor in den Pflanzengesellschaften und seine Bedeutung für die Stoffproduktion." Japanese Journal of Botany, vol. 14, pp. 22 - 52.

Monteith, J.L. (1965): "Evapotranspiration and environment." In: "The state and movement of water in living organisms," Fogy (ed.), Academic Press, New York, pp. 205 - 234.

Moolman, J.H. (1985): "Data collection for the study of runoff, solute and sediment generating processes in a semi-arid catchment." Rhodes University, Hydrological Research Unit, Water Research Commission Report no. 100/1/85.

Moor, I.D., Coltharp, G.B. and Sloan, P.G. (1983): "Predicting runoff from small Appalachian watersheds." Transactions K. Acad. Sci., vol. 44(3-4), pp. 135 - 145.

Morel-Seytoux, H.J. (1984): "Some recent developments in physically-based rainfall-runoff modelling." Frontiers in Hydrology, Maxwell and Beard (ed.), Water Resources Publications, Fort Collins, CO, pp. 37 - 51.

Morgali, J.R. (1970): "Laminar and turbulent overland flow hydrographs." Proceedings, ASCE, Journal of the Hydraulics Division, vol. 96, HY2, pp. 441 - 460.

Morris, E.M. and Woolhiser, D.A. (1980): "Unsteady one-dimensional flow over a plane: partial equilibrium and recession hydrographs." Water Resources Research, vol. 16, no. 2, pp. 355 - 360.

Nash, J.E. (1957): "The form of the instantaneous unit hydrograph." Proceedings, Gen. Assembly Toronto, Intern. Assoc. Scien. Hydrol. 3, pp. 114 - 121.

NERC (1975): "Flood Studies Report, volume 1: Hydrological Studies." Natural Environmental Research Council, London.

Overton, D.E. (1971): "Mechanics of surface runoff on hillslopes." Proceedings, Third International Seminar for Hydrology Professors on Biological Effects in the Hydrological Cycle, Purdue University, West Lafayette, IN, pp. 186 - 210.

Overton, D.E. and Meadows, M.E. (1976): "Storm Water Modelling." Academic Press, New York.

Patrick, N. (1988): "The effects of storm patterns on runoff." Unpublished Masters thesis, Department of Civil Engineering, University of the Witwatersrand, Johannesburg.

Penman, H.L. (1948): "Natural evaporation from open water, bare soil and grass." Proceedings, the Royal Society of London, Series A, vol. 193, pp. 120 - 146.

Philip, J.P. (1957): "The theory of infiltration: 4. Sorptivity and algebraic infiltration equations." Soil Science, vol. 84, pp. 257 - 264.

Pingoud, K. (1982): "A lumped parameter model for infiltration." Journal of Hydrology, vol. 57, pp. 175 - 185.

Pitman, W.V. (1977): "Flow generation by catchment models of differing complexity - a comparison of performance." University of the Witwatersrand, Department of Civil Engineering, Hydrological Research Unit Report no. 1/77.

Pitman, W.V. and Basson, M.S. (1979): "Flood forecasting for reservoir operation." University of the Witwatersrand, Department of Civil Engineering, Hydrological Research Unit, Report no. 1/79.

Podmore, T.H. and Huggins, L.F. (1980): "Surface roughness effects on overland flow." Transactions, ASAE, vol. 23, no. 6, pp. 1434 - 1439.

Ponce, V.M. (1979): "Simplified Muskingum routing equation." Proceedings, ASCE, Journal of the Hydraulics Division, vol. 105, HY1, pp. 85 - 91.

Ponce, V.M. (1986): "Diffusion wave modelling of catchment dynamics." ASCE, Journal of Hydraulic Engineering, vol. 112, no. 8, pp. 716 - 727.

Ponce, V.M., Chen, V.H. and Simons, D.B. (1979): "Unconditional stability in convection computations." Proceedings, ASCE, Journal of the Hydraulics Division, vol. 105, HY9, pp. 1079 - 1086.

Ponce, V.M., Li, R.M. and Simons, D.B. (1978): "Applicability of kinematic and diffusion models." Proceedings, ASCE, Journal of the Hydraulics Division, vol. 104, HY3, pp. 353 - 360.

Ponce, V.M. and Theurer, F.D. (1982): "Accuracy criteria in diffusion routing." Proceedings, ASCE, Journal of the Hydraulics Division, vol. 108, HY6, pp. 747 - 757.

Ponce, V.M. and Yevjevich, V. (1978): "Muskingum-Cunge method with variable parameters." Proceedings, ASCE, Journal of the Hydraulics Division, vol. 104, HY12, pp. 1663 - 1667.

Preissmann, A. (1961): "Propogation des intumescences dans les canaux et les Rivieres." 1'e Congres de l'Association Francaise de Culcule, Grenoble, France, pp. 433 - 442.

Price, R.K. (1978): "A river catchment flood model." Proceedings, Institution of Civil Engineers, London, part 2, vol. 65, pp. 655 - 668.

Rajendran, R. and Mein, R.G. (1986): "Determination of rainfall excess on spatially variable catchments." Journal of Hydrology, vol. 83, pp. 67 - 89.

Rawls, W.J., Brakensiek, D.L. and Miller, N. (1983): "Green-Ampt infiltration parameters from soils data." ASCE, Journal of Hydraulic Engineering, vol. 109, no. 1, pp. 62 - 70.

Rawls, W.J., Brakensiek, D.L. and Saxton, K.E. (1981): "Soil water characteristics." ASAE, St Josephs, Michigan, Paper 81-2510.

Ritchie, J.T. and Burnett, E. (1971): "Dryland evaporative flux in a subhumid climate. 2: Plant influences." *Agronomy Journal*, vol. 63, pp. 56 - 62.

Richards, L.A. (1931): "Capillary conduction of liquids through porous media." *Physics 1*, pp. 318 - 333.

Roberts, P.J.T. (1978): "A comparison of the performance of selected conceptual models of the rainfall-runoff process on semi-arid catchments near Grahamstown." Rhodes University, Hydrological Research Unit, Report no. 1/78.

Rockwood, D.M. (1975): "SSARR, Streamflow Synthesis and Reservoir Regulation Model." U.S. Army Corps of Engineers, North Pacific Division, Portland, OR.

Ross, B.B., Contractor, D.N. and Shanholtz, V.O. (1979): "A finite element model of overland and channel flow for assessing the hydrologic impact of land use change." *Journal of Hydrology*, vol. 41, pp. 11 - 30.

Rovey, C.E.K. and Richardson, E.V. (1975): "Mathematical model of flow in a stream-aquifer system." *Proceedings, Second Annual Symposium on Model Technology*, San Francisco, Publ. ASCE, New York, pp. 439 - 457.

Rovey, E.W., Woolhiser, D.A. and Smith, R.E. (1977): "A distributed kinematic model of upland watersheds." Colorado State University, Fort Collins, CO, Hydrology Paper 93, 52 pp.

Rutter, A.J., Kershaw, K.A., Robins, P.C. and Morton, A.J. (1971): "A predictive model of rainfall interception in forests. 1: Derivation of the model from observations in a plantation of Corsican Pine." *Agric. Meteorol.*, vol. 9, pp. 367 - 383.

Saxton, K.E. and McGuinness, J.L. (1982): "Evapotranspiration" in "Hydrological modelling of small watersheds," Haan (ed.), American Society of Agricultural Engineers, Monograph no. 5.

Saxton, K.E., Johnson, H.P. and Shaw, R.H. (1974): "Modelling evapotranspiration and soil moisture." Transactions, ASAE, vol. 17, no. 4, pp. 673 - 677.

Scheidegger, A.E. (1960): "Physics of flow through porous media." McMillan publ., New York.

Scholes, B. (1989): Personal communication. Botany Department, University of the Witwatersrand, Johannesburg.

Schultz, C.B. (1988): "Integrated studies of the generation of runoff, solutes and sediment in tributary catchments of the Great Fish River." Rhodes University, Hydrological Research Unit, Water Research Commission Report no. 100/1/88.

Schulze, R.E. (1983): "Hydrological processes: concepts and thoughts, with reference to Southern Africa." In Proceedings of South African National Hydrological Symposium, Pretoria, Technical Report no. 119, Department of Environmental Affairs, pp. 18 - 67.

Schulze, R.E. (1984): "Hydrological models for application to small rural catchments in Southern Africa: Refinements and Development." Water Research Commission Report no. 63/2/84.

Schulze, R.E., Scott-Shaw, C.R. and Nanni, U.W. (1978): "Interception by Pinus Patula in relation to rainfall parameters." Journal of Hydrology, vol. 36, pp. 393 - 396.

Sherman, V.T. (1932): "The relation of hydrographs of runoff to size and character of drainage basins." Transactions, American Geophysics Union, pp. 332 - 339.

Slabbers, P.J. (1980): "Practical prediction of actual evapotranspiration." Irrigation Science, vol. 1, pp. 185 - 196.

Slack, D.C. (1978): "Predicting ponding under moving irrigation systems." Proceedings, ASCE, Journal of the Irrigation and Drainage Division, vol. 104, IR4, pp. 446 - 451.

Smith, R.E. and Hebbert, R.H.B. (1983): "Mathematical simulation of interdependent surface and subsurface hydrologic processes." Water Resources Research, vol. 19, no. 4, pp. 987 - 1001.

Soil Conservation Service (1972): "Soil Conservation Service National Engineering Handbook." Section 4, Hydrology, U.S. Department of Agriculture, Washington, D.C.

Soil Conservation Service (1975): "Agriculture Handbook No 436." Soil Taxonomy, Soil Survey Staff, U.S. Department of Agriculture, Washington, DC.

Stephenson, D. (1981): "Storm water hydrology and drainage." Developments in Water Science, no. 14, Elsevier Science Publishers, Amsterdam.

Stephenson, D. (1989a): "A modular model for simulating continuous or event runoff." New Directions for Surface Water Modelling, IAHS, Publication no. 181.

Stephenson, D. (1989b): "Selection of stormwater model parameters." ASCE, Journal of Environmental Engineering, vol. 115, no. 1, pp. 210 - 220.

Stephenson, D. and Meadows, M.E. (1986): "Kinematic hydrology and modeling." Developments in Water Science, no. 26, Elsevier Science Publishers, Amsterdam.

Terstriep, M.L. and Stall, J.B. (1974): "The Illinois Urban Drainage Area Simulator, ILLUDAS." Illinois State Water Survey, Urbana, Bulletin 58.

Tischendorf, W.G. (1969): "Tracing stormflow to varying source area in small forested watersheds in the Southeastern Piedmont." PhD dissertation, University of Georgia, 114 pp.

Tolikas, P.K., Tolikas, D.K. and Tzimopoulos, C.D. (1983): "Vertical infiltration of water into unsaturated soils with variable diffusivity and conductivity." *Journal of Hydrology*, vol. 62, pp. 321 - 332.

U.S. Army Corps of Engineers (1973): "HEC-1 flood hydrograph package." User's and programmer's manuals, Hydraulic Engineering Centre, Program 723-X6-L2010.

Viessman, W., Knapp, J.W., Lewis, G.L. and Harbaugh, T.E. (1977): "Introduction to hydrology." Publ. Harper and Row Inc.

Villeneuve, J.P., Houle, S. and Isabel, D. (1986): "A distributed hydrological model adapted to the automatic calibration of parameters." *Journal of Hydrology*, vol. 87, pp. 1 - 8.

Webber, N.B. (1971): "Fluid mechanics for Civil Engineers." Publ. Chapman and Hall, London.

Weinmann, P.E. and Laurenson, E.M. (1979): "Approximate flood routing methods: a review." *Proceedings, ASCE, Journal of the Hydraulics Division*, vol. 105, HY12, pp. 1521 - 1536.

Williams, J.R. (1975): "HYMO flood routing." *Journal of Hydrology*, vol. 26, pp. 17 - 27.

Williams, J.R. and Hann, R.W. (1973): "HYMO: Problem-orientated computer language for hydrological modelling." U.S. Department of Agriculture, Agriculture Research Service, 76 pp.

Woolhiser, D.A. and Liggett, J.A. (1967): "Unsteady, one-dimensional flow over a plane - the rising hydrograph." *Water Resources Research*, vol. 3, no. 3, pp. 753 - 771.

Zaslavsky, D. and Sinai, G. (1981a): "Surface hydrology. 1: Explanation of phenomena." *Proceedings, ASCE, Journal of the Hydraulics Division*, vol. 107, HY1, pp. 1 - 16.

Zaslavsky, D. and Sinai, G. (1981b): "Surface hydrology. 4: Flow in sloping, layered soil." Proceedings, ASCE, Journal of the Hydraulics Division, vol. 107, HY1, pp. 53 - 64.

Zinke, P.J. (1967): "Forest interception studies on the United States." In International Symposium on Forest Hydrology, Sopper and Lull (ed.), Pergamon, Oxford, pp. 137 - 161.